Isoform-specific Ras expression and signalling.

Thesis submitted in accordance with
the requirements of the University of Liverpool
for the degree of

Doctor in Philosophy

by Anna Urszula Newlaczyl, MSci, MRes

September 2015

Abstract

Isoform-specific Ras expression and signalling.

Anna Urszula Newlaczyl

Ras proteins are GTPases that are molecular central hubs for propagation of intracellular signals that are involved in diverse processes, including cell differentiation and proliferation. The four main Ras isoforms, HRas, NRas and the two KRas splice variants, KRasA and KRasB, are highly homologous and conserved proto-oncogenes that constitute a paradigm of cellular transformation. While all *RAS* genes are commonly mutated in human cancers, different isoforms couple to distinct tumours and the mutations in *KRAS* constitute the majority (~86%) of all *RAS* mutations. Intriguingly, KRasB is the only Ras isoform essential for normal embryonic growth in the mouse.

Such discrepancy of Ras isoform contribution to different cancers and the uniquely essential role of KRasB in normal development may stem from the distinct spatiotemporal expression of Ras isoforms and their differential coupling to downstream effectors. However, to date there has been no comprehensive quantitative comparison of Ras isoform expression across various tissues throughout development. Moreover, there are no studies that compared Ras isoform-specific signalling in an endogenous context. Therefore, this thesis aims to provide the first complete map of Ras isoform expression during development and the first comparison of endogenous Ras isoform-specific signalling.

In the first part of this work, quantitative real-time RT-PCR was used to measure Ras isoform transcript levels in mouse embryonic stem cells (ESCs) and in a panel of embryonic, postnatal and adult mouse tissues. KRasB was found to be the most highly expressed isoform, whereas KRasA was shown to be the most dynamically regulated. Transcript copy number does not necessarily

correlate with protein copy number; therefore, protein standard absolute quantitation mass spectrometry was used to accurately measure tissue Ras protein levels. In contrast to the qRT-PCR data where KRasB was 5-10-fold higher expressed than any of the other isoforms, protein abundance levels were found to be similar for the Ras isoforms. The mechanistic basis for this and the implications for models of isoform-specific Ras association with specific cancers are discussed.

In the second part of this thesis, isogenic SW48 human colorectal cancer cell lines identical except for the presence of an activating G12V mutation in each of the three *RAS* gene loci were utilised to study endogenous Ras signalling. The results revealed isoform-specific coupling to canonical Ras effector pathways for example, HRas was the most potent activator of downstream MAPK and PI3K pathways. These data represent the basis for planned network biology studies to model Ras isoform-specific signalling.

Together, this study provides the first most complete approaches for studying baseline Ras isoform expression and signalling in an endogenous context. The results guide our understanding of Ras isoform-specific network biology, coupling to distinct human cancers and involvement in normal development.

Table of Contents

List of Figures

List of Tables

Abbreviations

ΔG – Gibbs free energy

A – adenine

aa – amino acid

ATP – adenosine triphosphate

BM – basement membrane

bp – base pair

C – cysteine

cDNA – complementary DNA

CDS – coding DNA sequence

cds – coding sequence

DEPC – diethyl pyrocarbonate

DMEM – Dulbecco's modified eagle medium

DNA – deoxyribonucleic acid

dsDNA – double stranded DNA

DTT – dithiothreitol

E – embryonic day

%E – percent efficiency

EB – embryoid body

EDTA – ethylenediaminetetraacetic acid

EGF – epidermal growth factor

EGFR – EGF receptor

ER – endoplasmic reticulum

ERK – extracellular signal-regulated kinase

ESC – embryonic stem cells

FBS – foetal bovine serum

fg – femtogram

G – guanine

GDP – guanosine diphosphate

GTP – guanosine triphosphate

hESC – human embryonic stem cells

HGF – hepatocyte growth factor

HVR – hypervariable region

IAA – iodoacetamide

IGF – insulin-like growth factor

IGFR – IGF receptor

IMDM – Iscove's modified Dulbecco's medium

ITS – insulin transferrin selenium

KI – knock-in

KO – knock-out

LIF – leukemia inhibitory factor

MDA – modular response analysis

MEK – mitogen-activated protein kinase kinase

mESC – mouse embryonic stem cells

mg – milligram

min – minute/minutes

mRNA – messenger RNA

MTG – monothioglycerol

ng – nanogram

nt – nucleotide

P – postnatal day

PBS – phosphate buffer saline

PCR – polymerase chain reaction

PDGF – platelet-derived growth factor

PDGFR – PDGF receptor

pg – picogram

PI3K – phosphoinositide 3-kinase

PM – plasma membrane

POL2RE – RNA polymerase II, polypeptide E

qRT-PCR – quantitative reverse transcription PCR

RNA – ribonucleic acid

rRNA – ribosomal RNA

RTK – receptor tyrosine kinase

SD – standard deviation

SDS-PAGE – sodium dodecyl sulfate polyacrylamide

SEM – standard error of the mean

siRNA – small interfering RNA

ssDNA – single stranded DNA

T – thymine

Ta – annealing temperature

TFA – trifluoroacetic acid

Tm – melting temperature

UTR – untranslated region

wt – wild type

µg – microgram

Acknowledgements

"It always seems impossible until it's done."

- Nelson Mandela

First of all, I would like to thank my supervisors Prof Ian Prior and Dr Judy Coulson for their continuous support, guidance and invaluable remarks, and especially for sharing their experience and optimism.

Many thanks go to my PhD mentors Prof Alan Morgan, Prof Chris Sanderson and Dr Tobias Zech, for their support and encouragement. I would like to thank Prof Sylvié Urbe and Prof Michael Clague for their discussions during laboratory meetings and beyond. I am much obliged to Dr Craig Mageean for his help with mass spectrometry and Dr Fiona Hood for her help with SW48 cell line culture. A big thank you to all past and present members of our lab: Dr Yvonne Tang, Dr Claire Heride (for her help with microscopy), Dr Amos Liang, Dr Emma Rusiłowicz, Dr Ewan MacDonald, Dr Han Liu, Dr Jia Lih Wong, Dr Monica Faronato, Dr Yasminka Omerovic, Dr Dora Pedroso, Dr Veronica Aran, Dr Maria Hernandez-Valladares, Rebecca Eccles, Dr Monika Chojnowska, Dr Viktor Malec, Alice Howarth, Alison Beckett, Dr Simon Oliver (for providing NRasG12V SW48 cell line), Arnold Salvais, Dr Jenna Kenyani, Sarah Darling, Matthew Concannon, Zohra Butt (for her help with statistical analysis), Dr Andrew Fielding, Dr Joseph Sacco, Carolyn Levene and Michelle Nelson, not only for your help around the lab, but also for being very good friends and colleagues.

A big thank you to Dr Patricia Murray and her lab members, Dr Aleksandra Rak-Raszewska, Dr Virginie Mournetas, Dr Sofia Pereira and Dr Arthur Taylor, for providing mouse embryonic stem cells and training in SC culture. A special thank you goes to Dr Bettina Wilm for her invaluable help in mouse dissections. I would like to thank the employees of APEX building for their assistance with animal work and Prof Mark Caddick and Jean Wood for providing PowerLyzer

for tissues homogenisation. Many thanks go to Dr Pryank Patel for his help with data analysis and Dr Rosalind Jenkins for processing mass spectrometry samples. I would like to express my gratitude to the Wellcome Trust for funding this project [092791/Z/10/Z].

I would also like to thank my boyfriend Dominik, who has always been a constant support for me. Lastly, this work would not be possible without the love and never-ending care of my Parents throughout my education. For them I want to dedicate my thesis and there are no words to describe how grateful I am to have them.

Chapter 1

Introduction

1.1 Importance of Ras in normal tissues

1.1.1 Ras superfamily of GTPases

Ras proteins are part of a superfamily of small GTPases, which comprise over 100 molecules, sized 20 to 25 kDa (Colicelli, 2004, Karnoub and Weinberg, 2008, Rojas et al., 2012). The superfamily is divided, among the others, into Ras, Rab, Ran, Rho and Arf families, which all share a common intrinsic guanosine triphosphate (GTP) hydrolysis mechanism (Fig 1.1) and are highly conserved across different species.

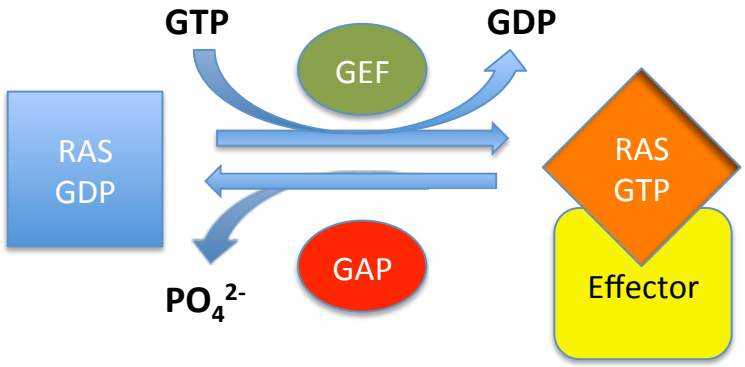

Fig. 1.1 GTPase cycle in Ras proteins. Members of Ras superfamily of small GTPases share a common mechanism for binding and hydrolysis of GTP. As an example, Ras is illustrated in the inactive, GDP-bound state on the left, and its activated form bound to GTP is shown on the right. The exchange of GDP to GTP is facilitated with a guanosine exchange factor (GEF), which then results in a conformational change in Ras and binding of downstream effectors. The intrinsic GTPase activity of Ras is enhanced via a GTPase activating protein (GAP), which leads to GTP hydrolysis and return of Ras to its inactive conformation.

The GTPase cycle switches Ras proteins between active GTP (guanosine triphosphate)-bound and inactive GDP (guanosine diphosphate)-bound states. Upon extracellular stimulation by growth factors (Campisi et al., 1984) or cytokines (Emanoil-Ravier et al., 1985, Samid et al., 1985), guanine nucleotide-exchange factors (GEFs) (e.g. son of sevenless – SOS) promote the exchange of GDP for GTP in the Ras nucleotide binding pocket. This brings about conformational changes of switch I and II regions of Ras that result in the formation of an interface for downstream effector proteins (Fig. 1) (Hall et al., 2002, Karnoub and Weinberg, 2008, Shima et al., 2010, Vetter and Wittinghofer, 2001, Wittinghofer and Herrmann, 1995). The signals transduced are involved in a plethora of cellular processes, including proliferation and differentiation (Crespo and Leon, 2000, Traverse et al., 1992). While intrinsic GTPase activity of Ras is relatively weak (Gibbs et al., 1984, Manne et al., 1985, McGrath et al., 1984, Sweet et al., 1984), a myriad of GTPase activating proteins (GAPs), such as EIF5, NF1 or RasGAP (Boguski and McCormick, 1993, Bos et al., 2007, Pamonsinlapatham et al., 2009) facilitate hydrolysis of GTP and, hence, lead to the inactivation of Ras (Trahey and McCormick, 1987).

The Ras family of GTPases is further subdivided into subfamilies, including Rit, Rap, Ral, MRas, RRas and Ras, on the basis of their protein sequence similarity (Fig. 1.2) (Crespo and Leon, 2000, Karnoub and Weinberg, 2008). The family also includes ERas, which was discovered in mouse embryonic stem cells (ESCs) (Takahashi et al., 2003) and is more distantly related to the other subfamilies. There is evidence that the functional protein of ERas is not expressed in normal human tissues (Kameda and Thomson, 2005), although it could be found in human gastric cancer (Yashiro et al., 2009). The extended Ras family also encompasses proteins with lower sequence homology than ERas, including Rheb, Rem and RasD (Fig. 1.2). The study of this thesis focuses on the Ras subfamily, but also on ERas in mouse ESCs.

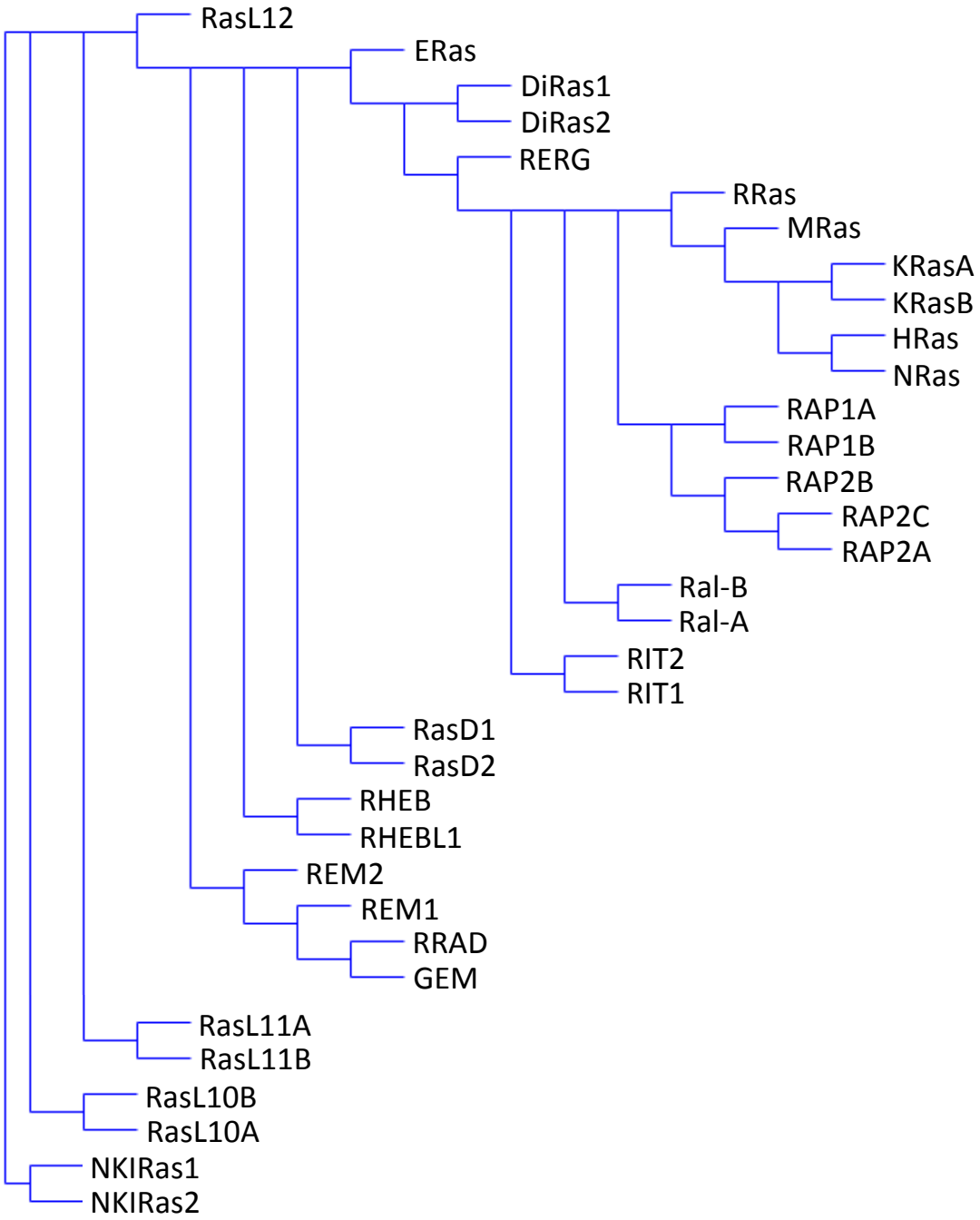

Fig. 1.2 Phylogenetic tree of the extended Ras family members in *Mus musculus* (house mouse) based on protein sequence similarity. The dendrogram was generated using VECTOR NTI Advance (v11.5.2) and includes ERas, which is expressed only in undifferentiated embryonic stem cells (Takahashi et al., 2003).

1.1.2 Ras subfamily

The key members of Ras subfamily of small GTPases are highly related HRAS, KRAS and NRAS, and all play crucial role in human carcinogenesis. Since their discovery in viral sequences and their cellular counterparts, substantial research has focused on biochemical properties and delineation of function and signalling of these Ras isoforms (Cox and Der, 2010, Malumbres and Barbacid, 2003). Essential discoveries in this field are summarised in Fig. 1.3 and are described in detail in this and further sections.

The founding studies that paved the way into extensive Ras research took place in the 1960s, when for the first time oncogenic Harvey and Kirsten murine sarcoma viruses (Ha-MSV and Ki-MSV) were isolated by two independent groups and were named after their discoverers (Harvey, 1964, Kirsten and Mayer, 1967). In early 1970s, the Ha-MSV and Ki-MSV genomes were found to contain normal rat gene sequences that lead to transforming properties of the viruses (Scolnick and Parks, 1974, Scolnick et al., 1973). Further work ascertained that these viral *ras* genes, named for causing ***ra***t ***s***arcomas, produce 21 kDa protein products (p21) (Shih et al., 1979), which bind guanine nucleotides (Scolnick et al., 1979) and localise to the plasma membrane (PM) (Willingham et al., 1980). The cellular homologues of the viral genes were soon discovered in rat and human genomes, as well as in other vertebrate species, including mouse and chicken (Chang et al., 1982b, DeFeo et al., 1981, Ellis et al., 1982, Ellis et al., 1981).

The protein products of cellular *ras* genes were also identified in vertebrate cells (Langbeheim et al., 1980) and were shown to associate with GDP and GTP and attach to the PM, similarly to their viral equivalents (Papageorge et al., 1982). Notably, high levels of normal cellular Ras proteins were shown to elicit oncogenic transformation (Chang et al., 1982a), which required a GTP-bound state of Ras (Gibbs et al., 1984, Scolnick et al., 1979). Transforming activation of endogenous *ras* was also found to be due to single point mutations, which were also present in the viral *ras* (Capon et al., 1983, Reddy et al., 1982, Tabin et al., 1982, Taparowsky et al., 1982).

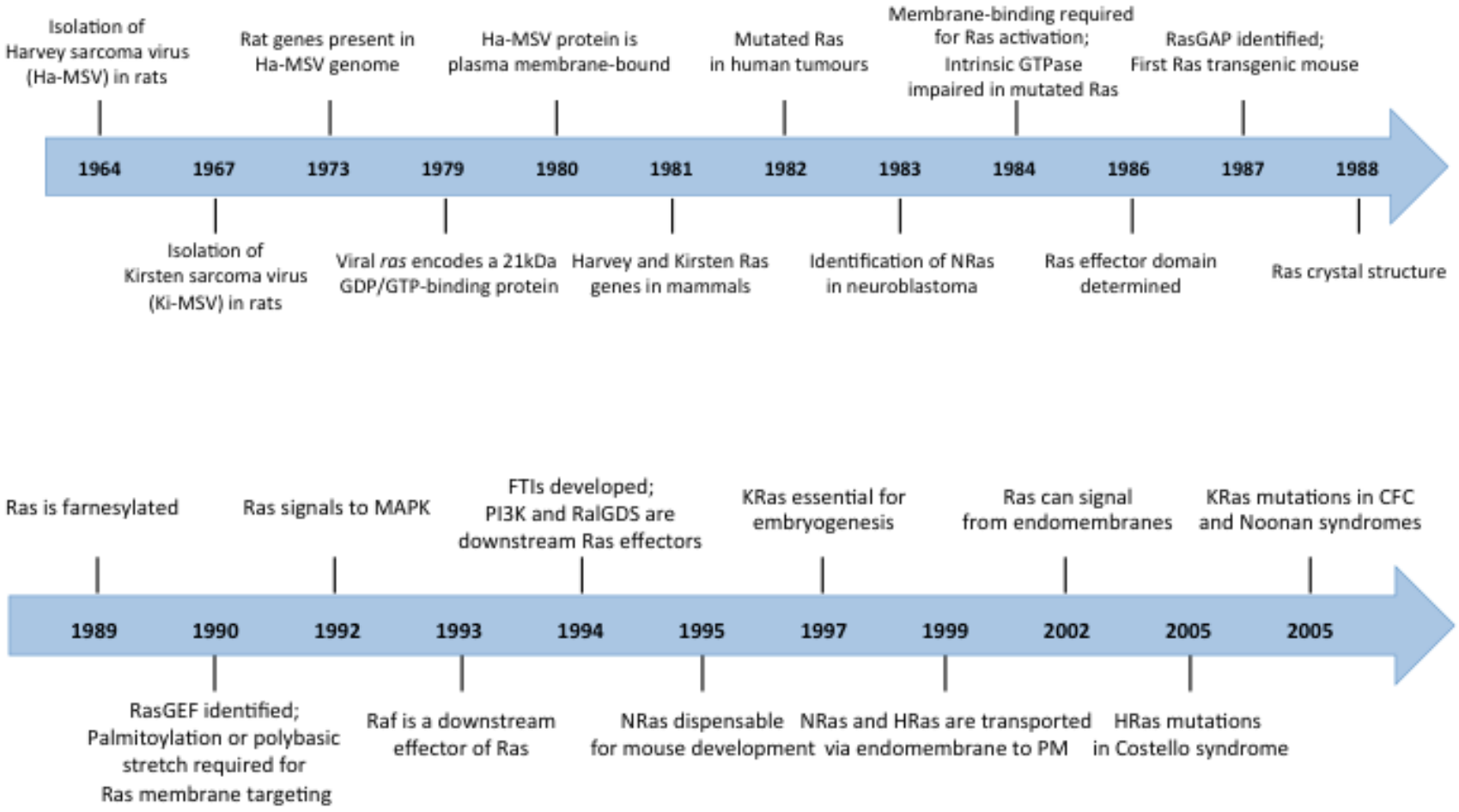

Fig. 1.3 Key milestones in Ras research. The timeline depicts some of the key discoveries in the Ras research field in the first five decades. Adapted from (Karnoub, 2008, Cox, 2010).

Activated Ras oncogenes have since been found in numerous human cancer cell lines and human tumours (Der et al., 1982, Parada et al., 1982, Santos et al., 1984, Santos et al., 1982, Cox et al., 2014, Feig et al., 1984, Prior et al., 2012). The genes were labelled *HRAS* and *KRAS*, and the corresponding protein products HRas and KRas. The third *ras* gene was discovered in human neuroblastoma and leukaemia cell lines and was termed *NRAS*, for **n**euroblastoma-ras (Hall et al., 1983, Murray et al., 1983, Shimizu et al., 1983, Taparowsky et al., 1983).

Remarkably, *KRAS* gene expresses two alternative splice variants – KRas-4A (or KRasA) and KRas-4B (KRasB), which differ only in their fourth terminal exon (Capon et al., 1983, McGrath et al., 1983). All Ras isoforms, HRas, NRas and the two KRas splice variants, are highly homologous and comprise 189 residues, or 188 for KRasB. The sequence similarity is around 82-90% among the isoforms and all proteins are identical in the first 164 residues, which contain the G domain responsible for binding and hydrolysis of guanine nucleotides (Fig. 1.4).

The G domain is highly conserved not only across the main Ras isoforms, but also across Ras superfamily members and heterotrimeric G proteins (Vetter and Wittinghofer, 2001). It is around 20 kDa and contains a six-stranded β- sheet, five α-helices and ten interconnecting loops. The three-dimensional structure of Ras proteins was solved by X-ray crystallography and it provided detail on the differences between GTP- and GDP-bound states of Ras and on their mutants (Brunger et al., 1990, Krengel et al., 1990, Milburn et al., 1990, Pai et al., 1989, Schlichting et al., 1990, Tong et al., 1989).

The G domain consists of five conserved motifs placed on the loop regions that take part in nucleotide binding and GTP hydrolysis (Fig. 1.4) (Vetter and Wittinghofer, 2001, Karnoub and Weinberg, 2008). The nucleotide base binds mainly to the N/TKxD motif, whereas the β, γ-phosphates interacts with the phosphate-binding loop (P-loop) that comprises the GxxxxGKS/T motif (Saraste et al., 1990). The guanine binding specificity arises from the side of the

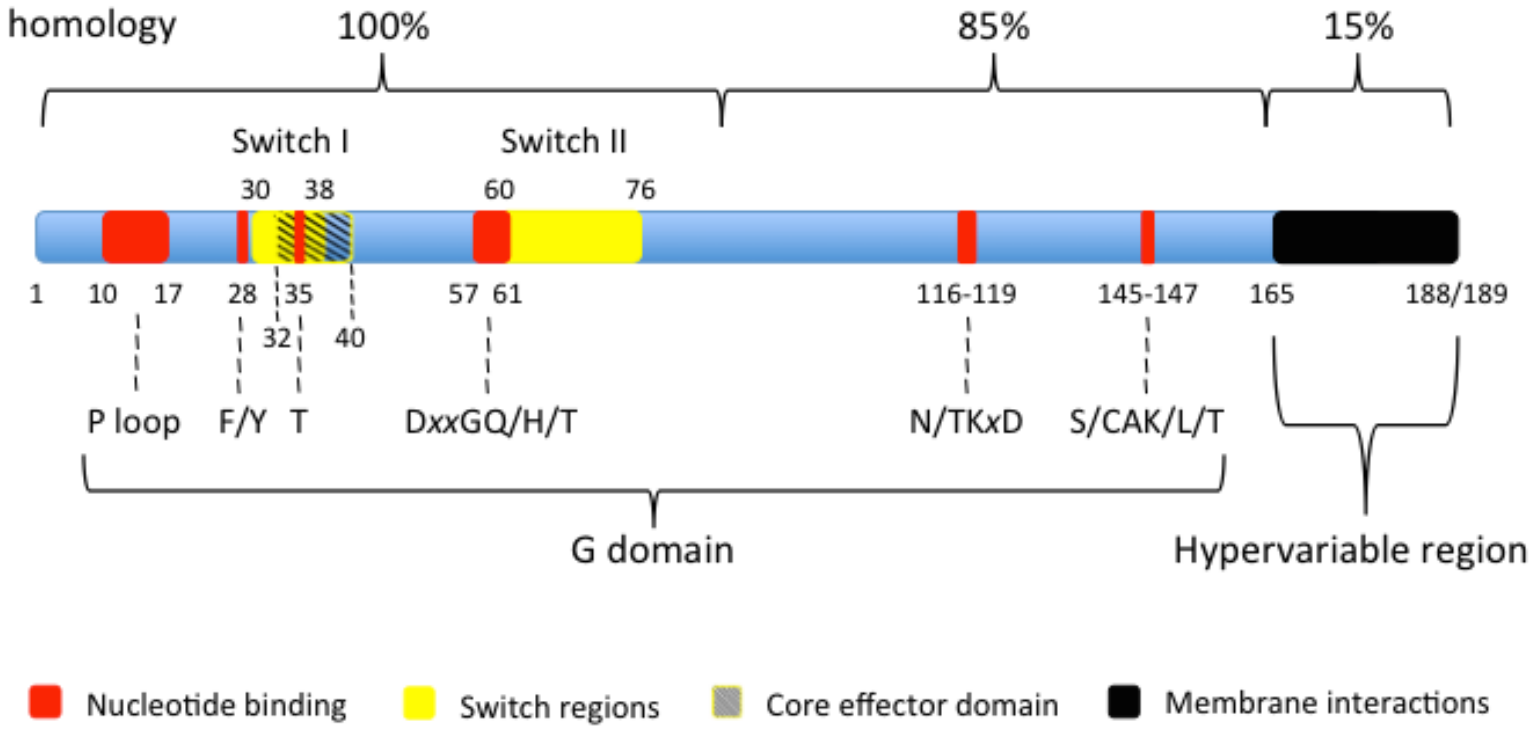

Fig. 1.4 Ras domain structure. Ras proteins share a conserved G domain, which consists of 4-5 motifs that take part in guanine nucleotide binding and hydrolysis. Ras proteins possess two switch regions, which change their conformation upon GTP binding and lead to exposure of effector domain to downstream signalling molecules. The C-terminal hypervariable region is least conserved across Ras isoforms and is responsible for membrane interactions. Adapted from (Cox and Der, 2010).

conserved aspartate residue situated in the DxxG motif and the main chain of the alanine (Ala146) residue from the SAK motif.

The G domain also contains two so-called "switch regions" that change conformation upon GTP binding and take part in interactions of Ras with its upstream regulators, such as GAPs and GEFs, as well as downstream targets by exposing effector binding domain (Milburn et al., 1990, Schlichting et al., 1990, Vetter and Wittinghofer, 2001). In the GTP-bound state, the γ-phosphate forms two hydrogen bonds with the threonine (Thr35, which also binds Mg^{2+}) residue in switch I (amino acids 30-38) and with glycine (Gly60) residue in switch II region (amino acids 60-76) (Cox and Der, 2010). Following GTP hydrolysis, the two switch regions go back to the relaxed GDP-bound conformation.

Ras proteins are highly conserved across different species, as depicted in Fig. 1.5, which compares all three main Ras protein sequences and their isoforms based on protein sequences from model organisms representing major eukaryotic kingdoms and phyla. Although there are no direct homologs of Ras in plant genomes, the flowering plant *Arabidopsis thaliana*, as shown in the figure, expresses a Ras-related RABD2A protein, which is related more to RAB family member RAB1A (part of Ras superfamily). However, homologous Ras proteins have been studied in species such as amoeba *Dictyostelium discoideum* (Reymond et al., 1984), yeast *Saccharomyces cerevisiae* (Dhar et al., 1984, Powers et al., 1984), nematode *Caenorhabditis elegans* (Beitel et al., 1990, Han and Sternberg, 1990), arthropods, such as common fruit fly *Drosophila melanogaster* (Neuman-Silberberg et al., 1984), amphibians such as African clawed frog *Xenopus laevis* (Andeol et al., 1990, Baum and Bebernitz, 1990) and zebrafish *Danio rerio* (Cheng et al., 1997, Liu et al., 2008).

Mouse and human Ras proteins are highly related with 97-100% identity, depending on the isoform. Similarly, their mRNA sequence is highly conserved, showing 88-95% identity. Fig. 1.6 depicts mRNA coding sequence alignment for KRASA, which shows the highest sequence homology between mouse and human.

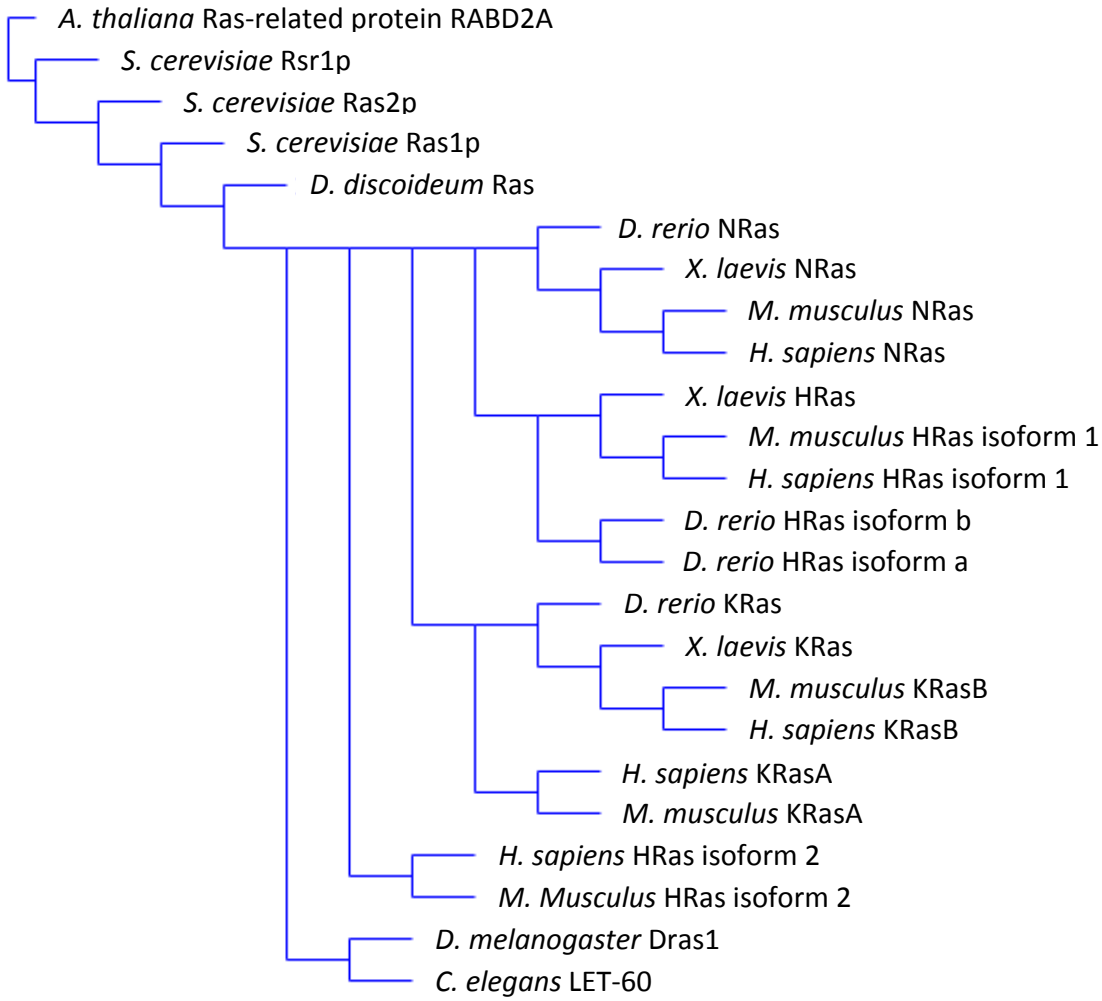

Fig. 1.5 Ras isoform conservation across species. Phylogenetic tree of main Ras subfamily members and their isoforms in model organisms and human (*Saccharomyces cerevisiae*, *Dictyostelium discoideum*, *Caenorhabditis elegans*, *Drosophila melanogaster*, *Xenopus laevis*, *Danio rerio*, *Mus musculus* and *Homo sapiens*), based on protein sequence similarity. In plants (*Arabidopsis thaliana*), the most closely related protein to Ras is RABD2A (homologue of RAB family member RAB1A). The dendrogram was generated using VECTOR NTI Advance (v11.5.2).

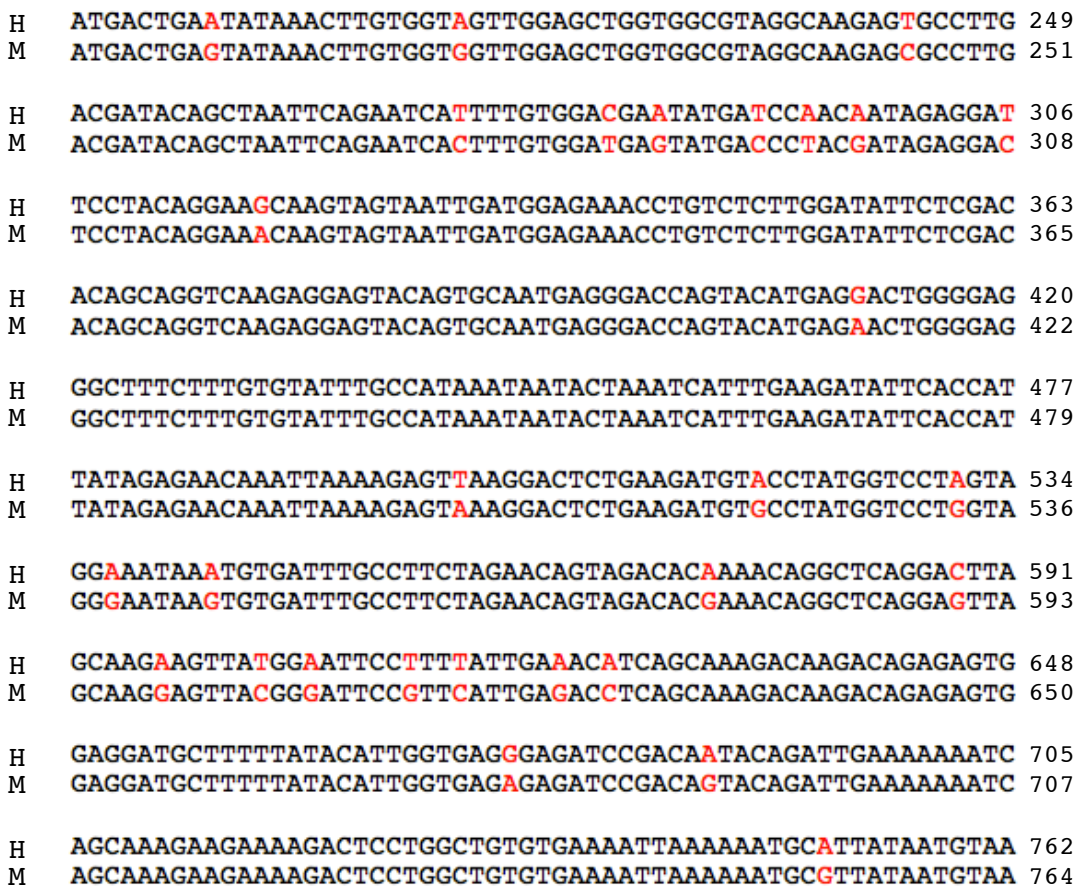

Fig. 1.6 Conservation of mRNA protein coding sequences of KRasA isoform between human and mouse. Alignment of mRNA coding sequence for KRasA in human (H) and mouse (M) show high identity (95%) between the two species. Numbers on the right indicate nucleotide number in mRNA sequence.

1.1.3 Cellular dynamics and signalling differences between Ras isoforms

Although highly conserved in mRNA and protein sequence, Ras isoforms are non-redundant in their cellular functions. Table 1.1 summarises the main functional differences between the four main Ras isoforms that are discussed in the next sections.

1.1.3.1 Ras signalling pathways

1.1.3.1.1 Upstream activators of Ras

Ras proteins are molecular central hubs, on which a plethora of intracellular signals converge and diverge (Fig 1.8). Epidermal growth factor receptor

Table 1.1 Main functional and cellular differences between the four main Ras isoforms. For references please refer to text. PM – plasma membrane; ESCs – embryonic stem cells, IL-3 – interleukin-3, CSF-1 – colony-stimulating factor 1, EGF – epidermal growth factor, AML – acute myelogenous leukaemia, HNSCC – neck squamous cell carcinoma

Property	Ras isoform			
	HRas	**KRasB**	**KRasA**	**NRas**
PM attachment	Farnesylation + double palmitoylation	Farnesylation + polybasic lysine stretch	Farnesylation + monopalmitoyl -ation	Farnesylation + monopalmitoyl -ation
Upstream activators	Ras-GRF1, Sos1 strongest	RasGRP2, Sos1 weakest, calmodulin,		RasGRP2, Sos1 medium
		preferential: IL-3, CSF-1 and EGF		
MAPK/PI3K association	Weakest activator of Raf-1	Best activator of Raf-1	Second-best activator of Raf-1	Weak activator of Raf-1
	Better activator of PI3K	Better activator of Rac		Better activator of PI3K
Downstream effectors	NF-κB	RASSF2		
Intracellular localisation and signalling	Golgi stacks; ER; endosomes; lipid rafts and bulk membrane of PM	Bulk membrane of PM	PM	Noncaveolar lipid rafts of PM, *trans* Golgi, ER
mRNA expression	Lowly abundant	Highly abundant, ubiquitous	Not ubiquitous, minor KRas isoform	Moderately abundant
Protein expression	Lowly abundant	Highly abundant; impaired translation	Lowly abundant	Moderately abundant
Function in development	Dispensable for mouse development; supports differentiation and growth arrest	Essential for mouse development; specific for cardiovascular homeostasis;	Dispensable for mouse development;	Dispensable for mouse development
		supports proliferation and self-renewal		
Involvement in congenital disorders	Costello and Noonan syndromes	Noonan syndrome		
Function in cancer	3% of Ras mutations, prevalent in HNSCC, bladder cancer	86% of Ras mutations, prevalent in pancreatic and lung cancers, multiple myeloma, endometrial, stomach and colorectal cancers		11% of Ras mutations, prevalent in melanoma, AML, thyroid cancer

(EGFR) was the first receptor discovered responsible for conveying signals upstream of Ras (Kamata and Feramisco, 1984). Stimulation of EGFR, as well as another receptor tyrosine kinase (RTK) platelet-derived growth factor (PDGF) receptor (PDGFR) by receptor-specific ligands was shown to augment activated Ras (GTP-bound) (Gibbs et al., 1990, Satoh et al., 1990a, Satoh et al., 1990b). Further work determined that Grb2 is an adaptor protein that links upstream RTKs with Ras (Lowenstein et al., 1992) through its association with GEF Sos1 (Buday and Downward, 1993, Chardin et al., 1993, Egan et al., 1993, Gale et al., 1993, Li et al., 1993, Olivier et al., 1993, Quilliam et al., 1994, Rozakis-Adcock et al., 1993, Simon et al., 1993). Further research demonstrated that Grb2 could connect Ras with other adaptors, such as Shc, leading to association of Ras with many different RTKs (Giubellino et al., 2008, Margolis and Skolnik, 1994, Yonezawa et al., 1994).

Subsequent work showed that Ras proteins can be stimulated by a variety of upstream receptors, including G protein-coupled receptors (GPCR), such as bradykinin B_2 or adrenergic receptors via activation of phospholipase C β (PLCβ) (Blaukat et al., 2000, Della Rocca et al., 1997, Dikic et al., 1996, Dorsam and Gutkind, 2007), and integrin receptors (Schlaepfer et al., 1994, Yoon et al., 2006). Nonetheless, the level of activation by upstream signalling is not uniform among Ras isoforms. Ras-GRF1, a GEF, activates *in vivo* HRas, but not KRas or NRas (Jones and Jackson, 1998, Matallanas et al., 2003). In contrast, RasGRP2, a GEF that is stimulated by calcium and diacylgrycerol (DAG), activates only NRas and KRas (Clyde-Smith et al., 2000). Sos1, in turn, activates Ras isoforms with the following efficiency: HRas > NRas > KRas (Jaumot et al., 2002). Further differences between Ras isoform coupling and activation include preferential binding of calmodulin to KRas, which inhibits downstream ERK1/2 (Villalonga et al., 2001), covalent binding of the cyclopentenone 15-deoxy-delta 12,14-prostaglandin J2 to HRas, which leads to cell proliferation (Oliva et al., 2003) and preferential activation of KRasB by the growth factors interleukin-3, colony-stimulating factor 1 and epidermal growth factor (EGF) (Ehrhardt et al., 2004).

1.1.3.1.2 Downstream Ras effectors

The canonical signalling pathways that diverge from activated Ras are mitogen-activated protein kinase (MAPK) and phosphoinositide 3-kinase (PI3K) pathways (Fig. 1.7). The first identified mammalian Ras effector was the serine/threonine protein kinase Raf (Van Aelst et al., 1993, Warne et al., 1993, Zhang et al., 1993), which was known to activate downstream MAPK kinase 1 and 2 (MEK1 and MEK2), as well as MAPK, also known as extracellular signal-regulated kinase 1 and 2 (ERK1 and ERK2) (Dent et al., 1992, Howe et al., 1992, Kyriakis et al., 1992, Moodie et al., 1993). In this way, the prototypical Ras-Raf-MEK-ERK pathway (MAPK cascade) was delineated and it was ascertained that homologous pathways are present in a range of species (Dickson et al., 1992, Masuda et al., 1995, Han et al., 1993). To propagate signals down the pathway, the effectors utilise activating phosphorylation events on their downstream targets. In mammals, the pathway is essential for a myriad of cellular functions, including proliferation, differentiation and gene expression (Chang and Karin, 2001, Imajo et al., 2006, Nishida and Gotoh, 1993, Pearson et al., 2001).

The second Ras effector to be discovered was PI3K, a lipid kinase that consists of the p110 catalytic and p85 regulatory subunits (Rodriguez-Viciana et al., 1994, Rodriguez-Viciana et al., 1996, Sjolander et al., 1991). Activated PI3K generates phosphatidylinositol-3,4,5-triphosphate (PIP_3), which acts as a second messenger and translocates protein kinase B (PKB, also called Akt) to the PM (Scheid and Woodgett, 2001). Akt, in turn, is phosphorylated and activated by phosphoinositide dependent kinase 1 (PDK1). Akt regulates a range of downstream effectors, such as mammalian target of rapamycin (mTOR) and glycogen synthase kinase-3 (GSK-3), which are key for regulating cell cycle, cell proliferation and survival (Cross et al., 1995, Nave et al., 1999, Osaki et al., 2004, Sekulic et al., 2000).

Importantly, each Ras effector possesses a Ras binding domain (RBD), which allows them to specifically associate with activated GTP-bound Ras through its effector domain (Spaargaren and Bischoff, 1994, Vojtek et al., 1993). Apart from

Raf and PI3K, Ras propagates signals to a plethora of other downstream effectors. RalGDS (ral GDP dissociation stimulator), a GEF for Ras-related proteins (RalA and RalB), is the third main downstream target of Ras (Hinoi et al., 1996, Kikuchi and Williams, 1996, Urano et al., 1996). It interacts with Ras via its Ras association (RA) domain (Hofer et al., 1994, Kikuchi et al., 1994, Spaargaren and Bischoff, 1994) and transmits signals to downstream phospholipase D (PLD) and Ral-interacting protein 1(RIP1), to name a few, that are responsible for cell migration, actin organisation, as well as regulation of endocytosis and exocytosis (Cantor et al., 1995, Feig, 2003, Jullien-Flores et al., 1995, Luo et al., 1998, Rosse et al., 2006).

The remaining Ras effectors include Rac-specific GEF – T lymphoma invasion and metastasis protein 1 (Tiam1) (Lambert et al., 2002), which takes part in cell migration (Yamauchi et al., 2005a, Yamauchi et al., 2005b), PLCε (Kelley et al., 2001, Lopez et al., 2001, Song et al., 2002), which is involved in cell growth and differentiation (Wu et al., 2003, Yun et al., 2008) and RAS association domain family proteins (e.g. Rassf1) (Tommasi et al., 2002, Vos et al., 2003b) that control apoptosis (Allen et al., 2007, Eckfeld et al., 2004, Khokhlatchev et al., 2002, Vos et al., 2000, Vos et al., 2003a).

Nonetheless, different Ras isoforms differ in their quantitative ability to activate downstream effectors. KRas recruits Raf-1 more efficiently to the plasma membrane and is its more potent activator than HRas, which, in turn, is a better activator of PI3K (Yan et al., 1998). Yet, recent work has shown that Ras alone cannot activate PI3K, but for this it requires stimulation by GFs (Mendoza et al., 2011, Toettcher et al., 2013). Moreover, all four Ras isoforms differ in their abilities to activate Raf-1, with the following order: KRasB > KRasA >>> NRas > HRas (Voice et al., 1999). The extent of G domain reorientation towards the PM is thought to affect such preferential coupling of isoforms to downstream effectors (Abankwa et al., 2010, Abankwa et al., 2008).

The activation of the Rac pathway by oncogenic KRasG12V is 2-fold greater than that by HRasG12V, which is demonstrated by higher surface area of membrane

ruffles, higher number of pinocytic vesicles, enhanced cell migration in a wound healing assay and Pak-binding activity of Rac, which is a measure of activated Rac (Walsh and Bar-Sagi, 2001). There are also several Ras isoform-specific effectors, which include pro-apoptotic RASSF2 – a KRas-specific effector (Vos et al., 2003a) – and downstream NF-κB, which is preferentially activated by HRas (Millan et al., 2003). As a result, differential effector coupling of Ras isoforms leads to isoform-specific signalling, differences in transforming potency and it affects cell motility and induction of apoptosis.

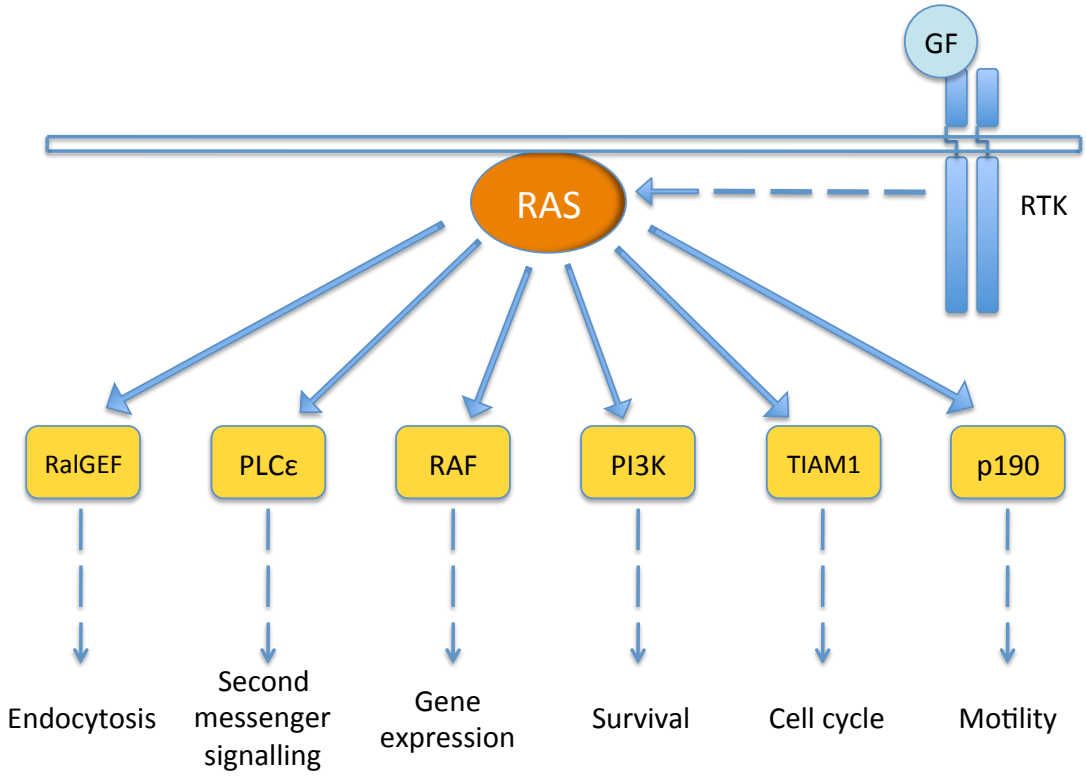

Fig. 1.7 Ras signalling pathways. A growth factor (GF) binds and activates receptor tyrosine kinase (RTK), which then propagates the signal through adapter proteins and guanosine exchange factors (GEFs) (not shown) to a membrane-bound Ras. As a central signalling hub, Ras disseminates activating signals to a plethora of downstream effectors, which stimulate signalling cascades involved in all major cellular processes, including cell cycle and survival.

1.1.3.2 Ras trafficking and posttranslational modifications

Effector binding and growth factor activation differences may stem from distinct plasma membrane and cellular localisations of Ras isoforms. Ras proteins traffic to the plasma membrane via alternative pathways due to differential lipid post-translational modifications that are necessary for membrane association (Apolloni et al., 2000, Hancock et al., 1990). These distinct modifications result from amino acid differences at the hypervariable region (HVR) located at the C-terminal region (Fig. 1.8).

In the cytosol, the cysteine residue of the CAAX motif of all Ras isoforms is targeted for the addition of a farnesyl moiety by the farnesyl transferase enzyme (Hancock et al., 1989, Lowy and Willumsen, 1989). Subsequent proteolysis and methylation of the C-terminus take place on the ER (Casey et al., 1989, Hancock et al., 1989). Farnesylated KRasB is directly transported into high-buoyant density domains in the PM, which contain activated receptors and GEFs (Ehrhardt et al., 2004). Such location may privilege KRasB for better activation by GFs compared to other Ras isoforms. Ras requires a second membrane-targeting signal, which for KRasB comprises an intrinsic polybasic stretch of six lysine residues (Hancock et al., 1990). For the other isoforms, KRasA, HRas and NRas, the second signal involves palmitoylation of cysteine residues and this lipid modification directs trafficking to the PM via the exocytic pathway (Apolloni et al., 2000, Choy et al., 1999, Laude and Prior, 2008, Rocks et al., 2005). HRas is palmitoylated on two cysteine residues, whereas KRasA and NRas are monopalmitoylated (Roy et al., 2005). The continuous de/repalmitoylation cycle allows dynamic shuttling of Ras between the PM and the Golgi (Lorentzen et al., 2010).

Interestingly, Ras isoforms also differ in segregation to distinct plasma membrane microdomains. HRas resides in caveolar and noncaveolar lipid rafts and in the bulk membrane, whereas KRas is only found in the latter (Prior and Hancock, 2001, Prior et al., 2003). All three Ras isoforms are dynamically associating with distinct signalling nanoclusters; whilst HRas leaves lipid rafts when activated, NRas travels in the opposite direction (Omerovic and Prior, 2009).

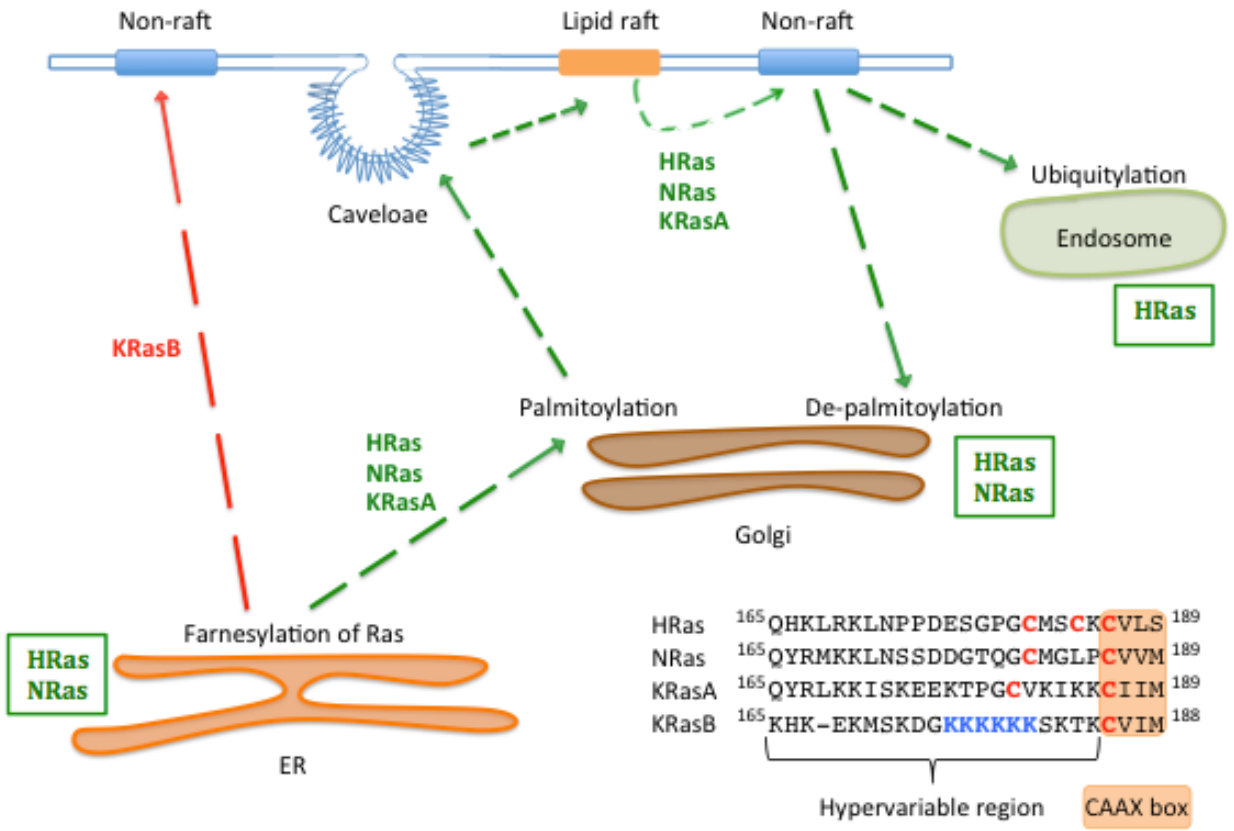

Fig. 1.8 Ras isoform post-translational modifications and subcellular localisations. To allow membrane targeting, Ras proteins are post-translationally modified at the hypervariable C-terminal region that comprises the CAAX box (bottom right). The cysteine residues (C in red) in the CAAX box are farnesylated at the endoplasmic reticulum (ER). KRasB possesses a poly-lysine stretch (K in blue) and is directly transported to the non-raft domains of plasma membrane (PM). KRasA, HRas and NRas are further modified by the addition of palmitate in the Golgi (red cysteines outside the CAAX box). They can traffic to the caveloae, lipid rafts and non-raft domains of the PM, and then cycle back to the Golgi, where they are de-palmitoylated, or to the endosomes, where they become ubiquitylated. Green boxes denote Ras isoforms that accumulate on and signal from endomembranes (Golgi, ER and endosomes) is. The figure was adapted from (Karnoub et al., 2008).

Until recently, it has been postulated that Ras activation and Ras-dependent signalling originates exclusively from the PM (Quilliam et al., 1995). However, latest research provides evidence for Ras signalling from distinct subcellular compartments: the ER, the Golgi complex and the endosomes (Fig. 1.8) (Chiu et al., 2002, Perez de Castro et al., 2004, Roy et al., 2002). Constitutively active HRas has been shown to recruit RBD of Raf-1 on the PM, the Golgi and the ER, and constitutively active NRas – on the PM and the Golgi (Chiu et al., 2002, Philips, 2005). Another study has demonstrated that HRas dynamically shuttles from the PM to the recycling endosomes, where it also binds to the downstream RBD of Raf-1 (Gomez and Daniotti, 2005). Oncogenic H-Ras, when artificially anchored to the ER, activates ERK, c-Jun N-terminal kinase (JNK) and PI3K. However, when tethered to the Golgi, H-RasG12V may activate ERK or RalGDS (Matallanas et al., 2006). While HRas is evenly distributed on the Golgi, NRas is present mainly on the *cis* Golgi sub-compartment (Lynch et al., 2015). RasGRP1, a Ras GEF, has been shown to specifically activate Ras on the Golgi (Caloca et al., 2003). On the other hand, endogenous NRas is selectively activated by endothelial nitric oxide synthase (eNOS) on the Golgi in response to antigen stimulation of T cells (Ibiza et al., 2008).

The different Ras subcellular localisations can be also affected by various factors: the deubiquitinating enzyme USP17 disrupts NRas localisation on the PM, but not on the Golgi or ER (de la Vega et al., 2010), BRaf inhibitors specifically enhance nanoclustering of KRas and NRas on the PM and decrease PI3K signalling (Cho et al., 2012), whereas high intracellular oxygen leads to accumulation of HRas on the Golgi and PM (Kim et al., 2015). What is more, Ras isoforms can also localise to the mitochondria and the nucleus. KRas that is anchored to the plasma membrane can induce transformation, while KRas associated with Bcl-Xl on the mitochondria can induce apoptosis (Bivona et al., 2006). Both KRas and NRas have also been shown to regulate normal mitochondrial biology (Wolfman et al., 2006). Moreover, transcriptional profiling of compartment-specific Ras signalling revealed distinct gene signatures (Agudo-Ibanez et al., 2007). Yet, other studies argue that endogenous activation of Ras could only be visualised at the PM (Augsten et al., 2006). In light of these discrepancies between results, the possibility of Ras activation at

different subcellular compartments and the possibility of differential activation of Ras isoforms and diverse signalling outcomes remain to be resolved.

1.1.4 Ras function in development

1.1.4.1 Functions of Ras isoforms in self-renewal and differentiation

Various *in vitro* studies utilised exogenous Ras to study isoform-dependent signalling in a context of cellular differentiation and self-renewal of stem cells (SCs). Distinct Ras isoforms have been shown to differentially engage in these developmental processes (discussed in section 4.1.2). In general, activated HRas was associated with differentiation and growth arrest (Quinlan et al., 2008, Quinlan and Settleman, 2008, Yoshida-Koide et al., 2004), whereas KRas supported proliferation and self-renewal of SCs (Luo et al., 2007, Quinlan et al., 2008, Quinlan and Settleman, 2008). On the other hand, the Ras isoform ERas, which is expressed only in mouse embryonic SCs (ESCs), was shown to contribute to oncogenic properties of undifferentiated cells (Kameda and Thomson, 2005, Takahashi et al., 2003). Such disparity in Ras involvement in cellular processes may be a reflection of Ras isoform-specific coupling to downstream effectors, intracellular localisation or Ras expression levels (Castellano and Santos, 2011).

1.1.4.2 Mouse models to study Ras during development

1.1.4.2.1 Normal mouse development

Mouse models are often utilised to study cellular signalling at different stages of development by gene knock-in (KI) or knock out (KO) techniques. However, to appreciate the phenotypic outcomes of such models, it is imperative to clearly understand the physiological changes that take place during normal mouse development. The following paragraphs describe prenatal and postnatal mouse development with particular emphasis on the major organs that were examined in this study – brain, intestine, stomach, liver, skeletal muscle, heart, kidney and lung.

Around 4 days post-conception (E4.5), the mouse embryo is a blastocyst and begins implantation, i.e. adhering to the uterine wall (Theiler, 1989). At embryonic day 6 (E6), differentiation of embryonic and extraembryonic endoderm and ectoderm begins, while mesoderm starts to form around E7. At E7.5 the neural plate is more distinct and the head process starts to develop. Mouse organogenesis begins at E8, during which the gut pocket, pronephric duct and cardiac crescent appear and the brain plate rapidly develops (Theiler, 1989, Davidson, 2008, Mitiku and Baker, 2007, Kaufman, 1992). Also, the first somite pairs appear, which are lumps of mesenchymal cells derived from paraxial mesoderm of segmented animals and subsequently differentiate into vertebrae, ribs, skeletal muscle and the dermis (Tam, 1981, Gilbert, 2010). Mouse embryos reach over 60 pairs of somites at E15 (up to 65 pairs) (Kaufman, 1992, Tam, 1981).

At E8.5 the mouse embryo rotates resulting in a major change in shape (Theiler, 1989). The first organ buds start to form from the foregut and hindgut around E9–10.5 and give rise to lung, liver, stomach, pancreas and intestine (Crawford et al., 2010, Maeda et al., 2007, Wells and Melton, 1999). By E9, the heart sustains primitive circulation with regular heartbeat, while both the ventricular and atrial chambers are being developed (Savolainen et al., 2009, Theiler, 1989). Proper kidney development starts at E10.5 with the formation of the uretic bud from the pronephric duct (Davidson, 2008). By the same time, brain development has substantially advanced (Gilbert, 2010, Kaufman, 1992, Theiler, 1989). The neural tube closed completely as the neural folds joined together and the cranial blood vessels rapidly developed. Differentiating neural crest gave rise to peripheral nervous system ganglia. The hindbrain portion of the brain, which later develops into the pons, medulla oblongata and cerebellum, enlarged substantially. Cranial motor nuclei and inferior olivary nucleus, which are involved in motor control, show peak in neurogenesis at E9 and E10, respectively (Finlay et al., 1995). By E11 mouse sex cannot be determined (Theiler, 1989).

At E11.5 the limb buds start to differentiate, while the arterial system is now more mature (Kaufman, 1992, Theiler, 1989). The heart is still developing – the

atrium is almost partitioned, but the ventricle remains unpaired and the aorta is differentiating. The liver shows hematopoietic foci and, together with stomach, it enlarged substantially as compared to E10.5 (Theiler, 1989). In the lung, the branching of the major bronchi takes place (Metzger et al., 2008, Warburton, 2008). At this stage, kidney development progresses with the formation of metanephros as a result of branching of the uretic bud (Davidson, 2008). The brain has grown and matured substantially and the forebrain part, which will form the thalamus and hypothalamus, is more distinct (Gilbert, 2010, Theiler, 1989). The embryo is around 6-7 mm long and has now 43-48 pairs of somites (Kaufman, 1992, Theiler, 1989).

At E12 the mouse embryo has the first signs of developing fingers (Theiler, 1989). The aorta and the pulmonary artery are formed through the division of an arterial trunk (Gilbert, 2010, Theiler, 1989). The rudiments of the tongue and teeth start to develop and the lung buds have now tertiary bronchi. The epithelium of the stomach shows regional differentiation, while the liver starts producing megakaryocytes, which are responsible for the production of platelets. At this stage sexual differentiation may be apparent (Theiler, 1989). In the brain, the pineal gland starts to form, while the lens of the eye is differentiating.

By E13 the length of the embryo is around 9-11 mm and the outer ear is rapidly developing (Theiler, 1989). In the heart, the valves have formed, while in the lungs, the branching of the bronchi has advanced. The liver development progresses substantially and both hepatocytes and biliary epithelial cells start to differentiate (Zorn, 2008). By E13.5 the liver is divided into four main lobes (Crawford et al., 2010). The kidneys also rapidly develop, while sexual differentiation begins (Theiler, 1989). In the brain, the development of choroid plexus, which produces cerebrospinal fluid, is complete (Gilbert, 2010, Theiler, 1989).

By E15 the mouse embryo is around 11.5-14 mm and the toes of its hindlimbs are well separated (Theiler, 1989). The final prenatal circulation, as well as the

shape of the heart are established. The four main heart valves are developed and the ventricles are separated (Gilbert, 2010, Theiler, 1989). In the small and large intestine, the villi and the crypts are forming, respectively (Theiler, 1989). The two parts of the stomach – the glandular and nonglandular – can be distinguished. In the developing lung, the major bronchi subsequently form secondary and tertiary branches that proliferate until E16 (Metzger et al., 2008, Warburton, 2008). This process is accompanied by innervation and vasculogenesis (Maeda et al., 2007). In the forebrain, the primary cortex is formed and the cranial nerves, as well as ganglia are more distinct.

By E16 the embryo's heart achieved the definitive prenatal configuration, apart form the coronary artery and atrioventricular valve leaflets (Savolainen et al., 2009, Theiler, 1989). The intestinal tract is still developing – the villi of the small intestine, the crypts of the large intestine and the epithelium of the stomach are forming and rapidly growing (Theiler, 1989). The liver achieved its final external appearance and is increasing the production of blood cells. The glomeruli of the kidney are being formed, but the nephrons are still not developed (Theiler, 1989). In the foetal brain, the pituitary and pineal glands are still differentiating and the primary cerebral cortex is expanding.

At E17 mouse foetus is around 16.5-20 mm, its eyelids are fused and the skin is thickened (Theiler, 1989). At this stage, the major changes include the developing epithelium in the aveolar ducts of the lungs. By E17.5 pulmonary acinus becomes organised and the respiratory epithelium starts to differentiate, which will continue until around postnatal day 5 (P5) (Maeda et al., 2007). Between E17 and birth, the intrahepatic bile ducts are forming in the liver, while hepatocytes become more epithelial and mature (Zorn, 2008).

Around E18 the mouse measures between 18-23 mm and has long whiskers. By this time, large alveolar ducts and primitive alveoli markedly developed in the lungs (Theiler, 1989). The liver is still the site of haemopoiesis and the stomach is subdivided into two parts: glandular, which contains gastric glands, and non-glandular, which stores and digests the food (Kararli, 1995). In the brain, the

pineal and pituitary glands and the olfactory lobe are now developed (Theiler, 1989).

At birth (postnatal day 0 – P0), the newborn mouse measures around 23-27 mm and its eyes and ears are closed. By this time, histological development is still ongoing and the neonates are considered histologically immature (Theiler, 1989). In the heart, the foramen ovale, which is a foetal cardiac shunt that allows the blood to flow from the right to the left atrium, is no longer functional (Gilbert, 2010, Theiler, 1989). The liver is still the site of haemopoiesis, while the stomach starts active enzyme secretion to aid in the digestion of milk. The kidneys are growing in size and more ossification centres are present in the vertebral column.

During postnatal period, the mouse grows in size and fully matures at least until P30 (Holder and Blaustein, 2014, Theiler, 1989). Postnatal development of the lungs is demonstrated by the formation and growth of alveoli and maturation of the vasculature until P28 (Maeda et al., 2007). For the liver, its size rapidly increases until P21 and the final remodelling of the bile duct and organisation of hepatocytes takes place (Crawford et al., 2010). In the brain, some major changes in the formation of layer V in the cerebral cortex and in the whisker sensory area occur until P5. Also by the same time, the internal ear is still differentiating, but the ears open and a fine fur appears (Theiler, 1989). By P10, more ossification centres are present in the bone and by P15 both ears and eyes are open and fully developed. Weaning starts around P20 and may continue until P30 (Curley et al., 2009). By this time, mice should show firs signs of sexual maturation – for CD1 mice, vaginal opening occurs approximately at P30 (Holder and Blaustein, 2014). The first oestrus cycle occurs around 7-20 days after the vaginal opening (Holder and Blaustein, 2014) and the first mating when the mouse is around 2-3 months old (Theiler, 1989).

1.1.4.2.2 Ras mouse models

Several mouse models demonstrated that only KRasB is essential for mouse embryo development (discussed in section 5.1.1) (Koera et al., 1997, Johnson et al., 1997, Plowman et al., 2003, Umanoff et al., 1995, Esteban et al., 2001). *KRASB* KO mice had increased embryonic lethality due to anaemia, liver defects, thin heart ventricular walls and increased motoneuron cell death. However, subsequent studies demonstrated that replacement of KRas with HRas, which was knocked into the *KRAS* locus, resulted in normal embryonic development, but induced dilated cardiomyopathy during adulthood (Potenza et al., 2005). This suggests that HRas could functionally replace KRas during early development, when its expression pattern in mouse tissues mimics that of KRas. However, HRas may not compensate for KRas-specific function in adult cardiovascular homeostasis. Yet, the ability of HRas to substitute KRas in certain physiological context could mean that Ras isoforms share many cellular functions and the isoform-specific differences in signalling are the result of disparity in timing of their gene expression and in tissue/lineage-specific expression pattern (Castellano and Santos, 2011).

To date, only a few studies have provided semi-quantitative data on Ras expression across different tissues and developmental stages in the mouse and human (further discussed in section 5.1.2) (Leon et al., 1987, Pells et al., 1997, Plowman et al., 2006, Plowman et al., 2003). More work is needed to quantitatively measure Ras abundance, which will inform models of the mechanistic basis of Ras isoform functional overlap.

1.2 Ras in pathogenesis

1.2.1 Ras in developmental disorders

The role of isoform-specific function in early development could be better understood by studying rasopathies – distinct congenital disorders caused by germline mutations in *RAS* genes or in other components of Ras signalling pathways (Denayer et al., 2008, Schubbert et al., 2006, Tartaglia and Gelb, 2010,

Tidyman and Rauen, 2008, Tidyman and Rauen, 2009). Rasopathies share many phenotypic features and are collectively referred to as neuro-cardio-faciocutaneous (NCFC) developmental syndromes, characterised by mental retardation, developmental delay, cardiomyopathies, as well as musculoskeletal and craniofacial abnormalities.

Costello syndrome (CS) is a rare autosomal dominant disease predominantly caused by germline *HRAS* mutations, especially G12S (Aoki et al., 2008, Rauen, 2007, Tidyman and Rauen, 2009). Patients with CS are predisposed to developing tumours, such as bladder carcinoma or ganglioneuroblastoma (Roberts et al., 2006a). Noonan syndrome (NS), in turn, is a common disorder (1/2000 births) caused by various germline mutations in the MAPK pathway, where Ras mutations, especially in *KRAS*, constitute less than 2% of all cases (Cirstea et al., 2010, Roberts et al., 2007, Tartaglia and Gelb, 2010). NS is characterised by webbed neck and rotated ears and cancer is uncommon in patients, but some can develop acute lymphoblastic leukaemia. Scarce *RAS* mutations have also been reported in cardio-facio-cutaneous syndrome and autoimmune lymphoproliferative syndrome (Oliveira et al., 2007, Tidyman and Rauen, 2008).

RAS mutations involved in NCFC syndromes affect various codons and are usually milder than those found in cancers (Fernandez-Medarde and Santos, 2011, Schubbert et al., 2006, Seeburg et al., 1984). Mouse models have been developed for many of these mutations, which allows investigating molecular mechanisms that lead to distinct phenotypic changes in NCFC syndromes.

1.2.2 Ras in cancer

Ras proteins constitute a paradigm of cellular transformation by being some of the most commonly mutated proto-oncogenes in human cancer (Cox et al., 2014, Forbes et al., 2015, Prior et al., 2012). Although HRas, NRas and both KRas splice variants share high sequence homology and many cellular functions, each

isoform presents a distinct spectrum of mutations (Fig. 1.9), as well as shows unique pattern of coupling to different cancer types (discussed in section 5.1.1).

The most common Ras mutations found in cancers affect residues G12, G13 and Q61 in the protein sequence, all of which are part of the Ras active site for intrinsic GTP hydrolysis (Franken et al., 1993, Gremer et al., 2008, Krengel et al., 1990, Pai et al., 1990). While HRas shows equal mutation frequency of all three codons, KRas is most often mutated at residue G12 and NRas at residue Q61 (Fig. 1.9) (Forbes et al., 2015). The extensively studied G12V mutation, which substitutes the glycine residue into a more bulky valine residue at position 12, is the second most common Ras mutation across all human cancers (over 20%) and is most prevalent in KRas (23% of all KRas mutations, Fig. 1.9) (Forbes et al., 2015, Prior et al., 2012). The mutation decreases the intrinsic GTPase activity of Ras to around 10% of that of the wild type, as well reduces the affinity of GAPs (Al-Mulla et al., 1999, John et al., 1988). This causes a constitutively active GTP-bound state and activation of Ras, resulting in increased propagation of the signal to downstream effectors.

KRas mutations comprise around 86% of all Ras mutations in human cancer, while HRas mutations are uncommon and constitute around 3% of all Ras mutations (Forbes et al., 2015). The disparity in mutation frequency, residues that are mutated and the affected tissues of cancer origin across Ras isoforms may arise from differences in isoform subcellular location and coupling to downstream effectors (Chiu et al., 2002, Perez de Castro et al., 2004, Roy et al., 2002, Voice et al., 1999, Yan et al., 1998). A recent study also suggested that the high mutation frequency of KRas could be the result of its lower expression at protein level due to the presence of rare codons in its sequence (Lampson et al., 2013). Strikingly, lower expression of a Ras oncogene is linked to cellular proliferation, whereas higher expression leads to a senescent phenotype (Collado and Serrano, 2010, Sarkisian et al., 2007). This correlation means that KRas mutations may accumulate more readily due to less cellular senescence.

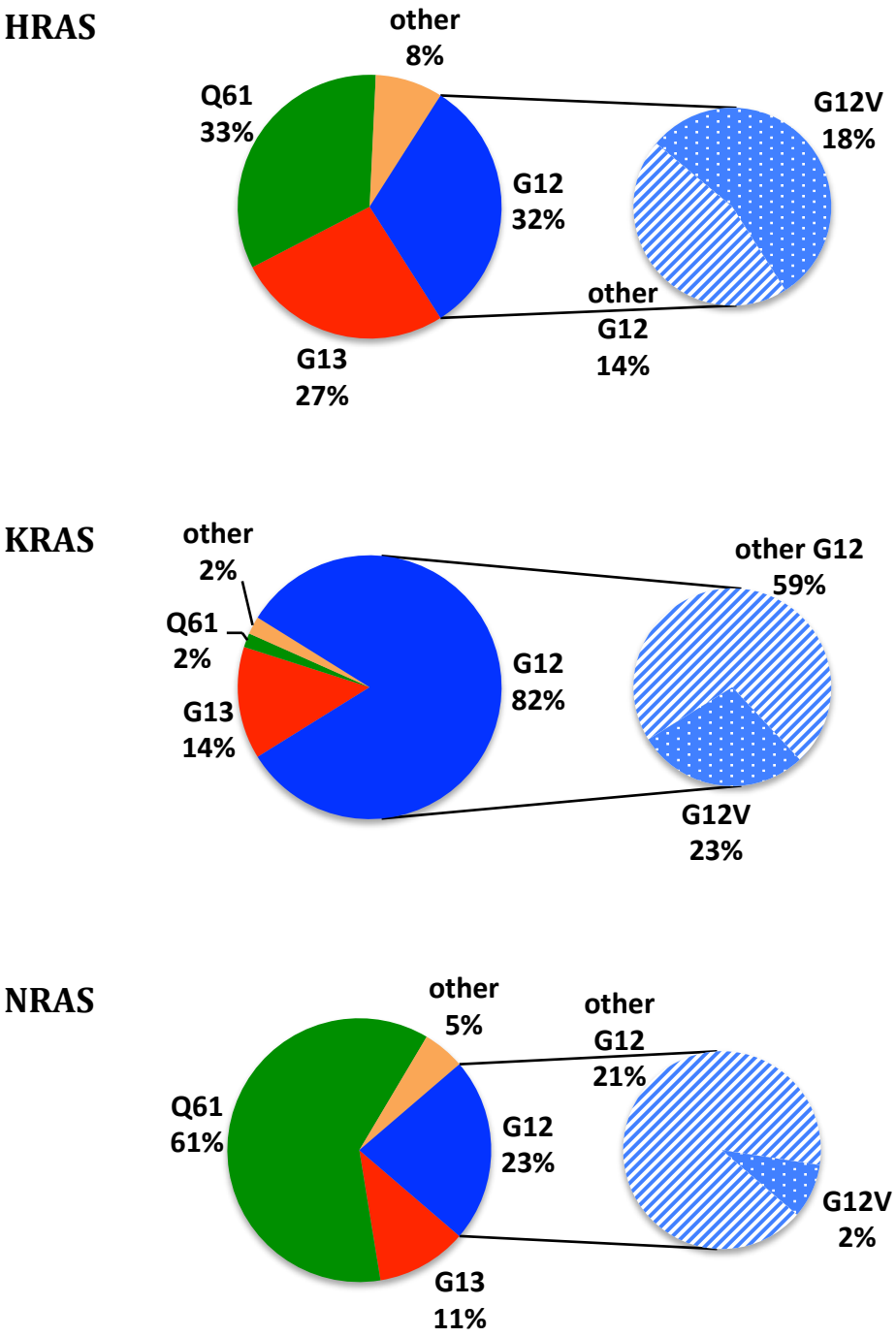

Fig. 1.9 Mutation pattern for Ras isoforms across all human cancers. HRas, KRas and NRas mutations not only couple to different cancers, but also the distribution of their different mutations across human tumour samples is not uniform. The predominant mutation site for KRas is G12 (82% of all KRas mutations), while for NRas it is Q61 (61% of NRas mutations). HRas mutations are equally distributed among G12, G13 and Q61 residues. Among all Ras mutations, the G12 residue is the most frequently mutated. The data used to generate mutation distribution pies is based on COSMIC database (v72) (Forbes et al., 2015).

There has been little progress in the development of anti-Ras therapies. Farnesyltransferase inhibitors (FTIs) that target post-translational farnesylation of Ras proteins and therefore their membrane recruitment, proved largely unsuccessful due to alternative geranylgeranylation of Ras and off-target effects (Zhu et al., 2003). So far little advancement in targeting Ras-driven cancers was achieved by using anti-Ras ribozymes (Kijima et al., 2004) and small interfering RNA (siRNA) (Fleming et al., 2005). A recently developed treatment against activated Ras shows a more specific and promising approach by allosterically targeting KRas G12C mutation, often found in lung tumours (non-small cell lung carcinoma – NSCLC) (Fiala et al., 2013, Ostrem et al., 2013). The inhibitor disrupts the conformational state of Ras and blocks the interaction with downstream Raf effector. Nevertheless, this approach still awaits further validation *in vitro* and future clinical trials. More research into key differences between Ras mutations, as well as Ras isoform-dependent signalling is needed to elucidate specific mechanisms as targets for possible Ras-targeted therapies.

1.3 Aims of this study

While there has been substantial research into Ras function in pathological context of cancer, still little is known about Ras isoform-specific biological functions in normal non-cancerous tissues and during development. Research into normal physiological processes and endogenous levels of expression of Ras isoforms could lead into clues in answering questions about KRasB predominance in the regulation of normal mouse development and the prevalence of KRas-driven tumours. Yet, there is no single study that would provide a comprehensive quantitative method for measuring expression levels across all Ras isoforms and across various tissue types throughout development. Based on this, the following hypothesis can be formulated:

Hypothesis 1: The expression levels can explain Ras isoform functional non-redundancy during development.

To test this hypothesis, one of the aims of this study is to use a quantitative method that would measure the absolute number of transcripts (absolute quantification) of all Ras isoforms across a range of normal mouse tissues throughout development. The early developmental stages will be measured in mouse ESCs. This study will provide the first most complete comparison of the spatiotemporal distribution of Ras isoform expression in absolute copy number.

Another aspect of Ras biology, which is not fully understood, is the preferential coupling of Ras isoforms to their downstream effectors. Importantly, previous work did not provide a comprehensive analysis of all Ras isoforms in an endogenous context and, hence I would like to test the following hypothesis:

Hypothesis 2: Endogenous Ras isoforms signal differently from each other.

Thus, the next objective of this project is to compare the endogenous levels of Ras isoform-specific pathway activation using isogenic cell lines. This model will provide the first comprehensive comparison of Ras isoform-dependent signalling at endogenous levels.

In summary, this project is divided into three main research areas, in which I:

1. develop a method for absolute quantification (non semi-quantitative) for measuring Ras isoform transcript levels based on real time polymerase chain reaction (RT-PCR) (Chapter 3);

2. measure and compare Ras isoform transcript abundance in mouse ESCs (Chapter 4) and across different mouse tissues throughout normal development by qRT-PCR method developed earlier and also at protein level by mass spectrometry (MS) (Chapter 5);

3. quantitatively measure Ras isoform downstream signalling in an endogenous context using isogenic cell lines and Western blotting (Chapter 6).

Chapter 2

Materials and Methods

2.1 Materials

All tissue culture plasticware was from Corning (Corning B.V. Life Sciences, Fogostraat 12, 1060 LJ Amsterdam, the Netherlands), unless otherwise stated. Mouse-specific Ras plasmids (pCR4-TOPO-ERas (IMAGE ID: 8734026), pCR-Blunt II-TOPO-KRas-4A (IMAGE ID: 40052024) and pCMV-SPORT6-KRas4B (IMAGE ID: 3158212)) were purchased from Source BioScience (William James house, Cowley Road, Cambridge, CB4 0WU, UK).

All chemicals were ordered from Sigma (Sigma-Aldrich Company Ltd., The Old Brickyard, New Road, Gillingham, Dorset, SP8 4XT), unless otherwise stated. Absolute ethanol and methanol were obtained from the Chemistry Department, University of Liverpool.

In this work the following laboratory equipment was used: benchtop microcentrifuges: #022621807, 5417R, Eppendorf AG; #13-100-676, accuSpin Micro 17R, Fisher Scientific and #5453 000.011, MiniSpin plus, Eppendorf AG; Jouan CR4i centrifuge, Thermo Electron Corporation; tissue culture centrifuge #5804 000.013, 5804, Eppendorf AG; thermomixer compact, Eppendorf AG; microplate reader Multiskan Spectrum no. 1500, Thermo Lab Systems.

2.2 Cell lines

2.2.1 SW48 Ras isogenic cell lines

The SW48 cell line was originally derived from Duke's type C, grade IV, colorectal adenocarcinoma from an 82-year-old female by A. Leibovitz at Scott and White Clinic, Temple, Texas, USA (Leibovitz et al., 1976). For this study parental (wild type Ras), HRasG12V and KRasG12V SW48 cell lines (#HD 103-034 and HD 103-007) were purchased from Horizon Discovery (7100

Cambridge Research Park, Waterbeach, Cambridge, CB25 9TL, UK), whereas NRasG12V SW48 cell line was made in house by Dr Simon Oliver using AAV technology (Vasileva and Jessberger, 2005), at the University of Liverpool, UK. In all Ras isoform isogenic cell lines, only one allele was targeted.

2.2.2 STO mouse fibroblasts

The STO cell line was originally derived from a continuous cell line of SIM (Sandos Inbred Mice) mouse embryonic fibroblasts by A. Bernstein at Ontario Cancer Institute, Toronto, Canada (Martin and Evans, 1975). For this study the cell line was kindly provided by Dr Patricia Murray, University of Liverpool, UK.

2.2.3 R1 mouse Embryonic Stem Cells (mESCs)

The R1 cell line was originally derived from inner cell mass of a 3.5 day male blastocyst by crossing two mouse 129 substrains (129S1/SvlmJ and 129X1/SvJ) in 1991 by Andras Nagy in Toronto, Canada (Nagy et al., 1993). For this study the cell line was kindly provided by Dr Patricia Murray, University of Liverpool, UK.

2.3 Routine cell culture

As a part of routine cell culture, all cell lines were verified by STR (short tandem repeat) DNA profiling and were regularly tested for mycoplasma. All cell lines were cultured at 37˚C in a humidified 5% (v/v) CO_2 atmosphere.

2.3.1 Routine SW48 Ras isogenic cell lines culture

SW48 cell lines were routinely cultured in McCoy's medium (#S6600-021, Gibco) containing 10% (v/v) Foetal Bovine Serum (FBS) (#10270-106, Gibco) and 1% (v/v) Penicillin/Streptomycin (stock 10,000 U/ml Pen, 10,000 µg/ml

Strep, 29.2 mg/ml L-Glutamine, #10378-016, Gibco) on 10 cm dishes and were passaged after achieving 80% confluence. First, cells were washed once with 0.01M (1 x) Phosphate Buffered Saline (PBS) (#P5493) and then incubated in 1 ml of 0.05% (1 x) trypsin-EDTA (#15400-054, Gibco) at 37˚C for 5-10 mins. The trypsin reaction was stopped by adding 4 ml of 10% FBS McCoy's medium and cells were typically split 1 in 3 to 1 in 5 (Table 2.1) into another 10 cm dish. Typical seeding densities, depending on the plate used, are summarised in Table 2.2

Table 2.1 A list of cell lines used in this study and splitting densities.

Cell line	Splitting ratio
SW48 parental	1 in 5
SW48 HRasG12V	1 in 4
SW48 KRasG12V	1 in 4
SW48 NRasG12V	1 in 3
STO mouse fibroblasts	1 in 3
R1 mouse embryonic stem cells	1 in 3

Table 2.2 Standard seeding densities for SW48 Ras isogenic cell lines.

SW48 cell line	10 cm dish	6-well plate	24-well plate
Parental	2.3 x 10^6 cells	4.0 x 10^5 cells/well	3.5 x 10^5 cells/well
HRasG12V	2.3 x 10^6 cells	4.0 x 10^5 cells/well	3.5 x 10^5 cells/well
KRasG12V	3.0 x 10^6 cells	5.3 x 10^5 cells/well	4.64 x 10^5 cells/well
NRasG12V	3.0 x 10^6 cells	5.3 x 10^5 cells/well	4.64 x 10^5 cells/well
RIPA buffer (V)	300 µl	100 µl per well	20-40 µl per well

2.3.2 Embryonic stem cell culture

2.3.2.1 Plate coating protocols

To allow cell attachment of STOs and ESCs, cell culture dishes were first coated with sterile 0.1% (w/v) gelatin by incubation at room temperature for 10 mins. 7 ml or 2 ml of gelatin solution was added to 10 cm or 3.5 cm dishes, respectively. Gelatin solution was then aspirated and dishes were washed 3 times for 5 mins with warm 1 x PBS.

For the suspension differentiation protocol, 3.5 cm non-adherent petri dishes (Sarsted) were treated with 2 ml of 0.01% (w/v) Pluronic F-127 (#P6867, Invitrogen) in 1 x PBS for at least 15 mins and then washed 3 times with 1 x PBS.

2.3.2.2 STO culture as a feeder layer

STOs were routinely cultured in Dulbecco's Modified Eagle medium (DMEM) high glucose (2500 mg/L, #D6546) containing 10% FBS, 1% L-Glutamine (#25030-081, Gibco), 0.1 mM Non Essential Amino Acids (NEAA) (#11140-050, Gibco), 1% Penicillin/ Streptomycin and 0.01% (5 µM) β-mercaptoethanol (stock 50 mM, #31350-010 Gibco), hereafter referred to as STO medium (Table 2.3), on gelatin-coated 10 cm dishes. When cells were about 90% confluent, 50 µl of 2 mg/ml mitomycin C (20 µg/ml, #M4287) was added to 5 ml of STO medium to stop cell proliferation. Cells were washed twice in 1 x PBS and incubated in 5 ml of 1 x trypsin for 5 mins at 37˚C. 7 ml of 10% FBS DMEM (stop medium) was added to the cells to stop trypsinisation. Cells were centrifuged at 200 x g for 3 mins, the medium was aspirated and 12 ml of STO medium was added and mixed with the cells. 1 ml of cells was added to each of the twelve 3.5 cm dishes already containing 1 ml of STO medium. STO cells were then ready to be used as a feeder layer for mESC culture.

Table 2.3 A list of cell culture media used for the culture of STO feeder layer and embryonic stem cells (ESC). DMEM - Dulbecco's Modified Eagle medium, IMDM - Iscove's modified Dulbecco's medium, FBS - Foetal Bovine Serum, NEAA - Non Essential Amino Acids, MTG – monothioglycerol, LIF - leukaemia inhibitory factor, ITS - insulin transferrin selenium

STO	**ESC**				
	Undifferentiated	**Endoderm differentiation**		**Mesoderm differentiation**	
STO medium	**R1 ESC medium**	**ENDO ESC/EB medium**	**ENDO EB medium**	**MESO ESC/EB medium**	**MESO EB medium**
- DMEM high glucose - 10% FBS - 1% L-Glutamine -0.1 mM NEAA - 1% Penicillin/ Streptomycin - 0.01% β-mercaptoethanol	- DMEM high glucose - 15% FBS - 1% L-glutamine - 0.1 mM NEAA - 1% Penicillin/ Streptomycin - 0.01% β-mercaptoethanol - 260 U/ml LIF		- DMEM high glucose - 15% FBS - 1% L-glutamine - 0.1 mM NEAA - 1% Penicillin/ Streptomycin - 0.01% β-mercaptoethanol	- IMDM - 10% FBS - 1% L-glutamine - 0.15% MTG - 1% Penicillin/ Streptomycin - 1,000 U/ml LIF	- IMDM - 15% FBS - 1% L-glutamine - 0.45% MTG - 1% Penicillin/ Streptomycin - 1% ITS - 0.1% ascorbic acid

2.3.2.3 Routine ESCs culture

R1 embryonic stem cells were cultured on a feeder layer of STOs (2.3.2.2) on 3.5 cm cell culture dishes using the following protocol (Fig. 2.1 A, derived from (Xiong et al., 1998)). Cells were grown in filtered R1 ESC medium (DMEM high glucose (#D6546) containing 15% FBS, 1% L-glutamine, 0.1 mM NEAA, 1% Penicillin/Streptomycin, 0.01% (5 μM) β-mercaptoethanol and 260 U/ml leukemia inhibitory factor (LIF) (10^7 U/ml #ESG1107, lot #JBC1872217, Chemicon, Millipore)) (Table 2.3) and split when they were around 90% confluent. Cells were trypsinised and after centrifugation the medium was aspirated and the cells were re-suspended in 3 ml of R1 ESC medium. 1 ml of cells was transferred to each of the 3 gelatinised 3.5 cm dishes with STO feeder layer, which already contained 1 ml of R1 ESC medium.

2.3.3 Cell freezing protocols

To freeze SW48 cell lines, cells grown in 75 cm^2 flasks that were at least 80% confluent were first washed once with 1 x PBS and incubated in 1.5 ml of 1 x trypsin/EDTA for 5-10 mins at 37˚C. 8.5 ml of 10% FBS McCoy's medium was added to stop the reaction and the cells were centrifuged at 200 x g for 5 mins. The medium was aspirated and 4 ml of freezing medium (50% FBS, 45% McCoy's medium, 5% dimethyl sulfoxide (DMSO #sc-358801, Santa Cruz Biotechnology)) was added to the cells and mixed gently. 1 ml of the cells was then transferred into cryovials (#BR114840).

To freeze R1 ESCs, cells grown on a feeder layer on 3.5 cm gelatinised dishes that were at least 90% confluent were washed twice with 1 x PBS and incubated in 1.5 ml of 1 x trypsin/EDTA for 3-5 mins at 37˚C. To terminate the trypsin reaction, 2 ml of stop medium was added to the dish and the cells were then transferred to 15 ml Falcon tubes already containing 2 ml stop medium. The cells were centrifuged at 200 x g for 3 mins and the medium was aspirated. The cells were re-suspended in 3 ml of Recovery™ Cell Culture Freezing

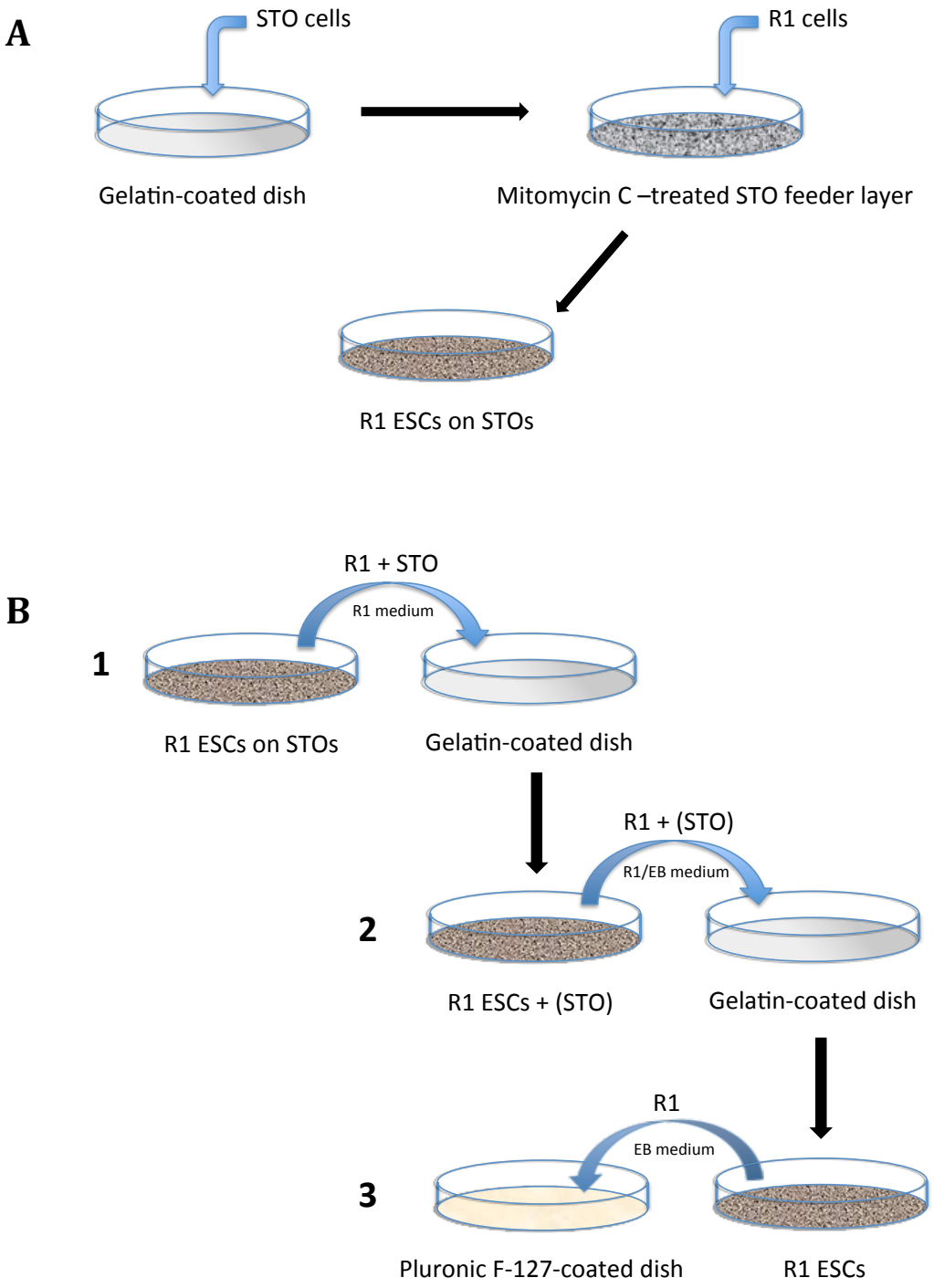

Fig. 2.1 Schematic illustrations of cell culture conditions for undifferentiated and differentiating R1 mouse embryonic stem cells ESCs. **A** Undifferentiated ESCs culture on STO feeder layer. STO mouse fibroblasts were cultured on a gelatin-coated dish and, when confluent, their growth was inhibited with mitomycin C. R1 ESCs were then seeded onto STO feeder layer. **B** Separation of ESCs from feeder layer for embryoid body (EB) differentiation protocol. ESCs cultured on STO feeder layer were passaged onto gelatinised dish in R1 medium several times to deplete STOs (1). ESCs were passaged in R1/EB medium to deplete the remaining STOs (2). ESCs were seeded onto Pluronic F-127-coated Petri dish in EB medium to initiate cell differentiation (3).

Medium (#12648-010, Gibco) and 1 ml transferred into individual cryovials (#BR114840).

Cryovials for all cell lines were placed into a freezing chamber containing isopropanol and left in -80˚C freezer overnight to allow slow freezing by 1˚C per hour. The next day, cells were transferred into a liquid nitrogen tank for long-term storage.

2.3.4 Cell thawing protocols

All cell lines were first thawed in a water bath at 37˚C. SW48 Ras isogenic cell lines were gently mixed by pipetting and then transferred to 25 cm^2 flasks containing 9 ml of 10% FBS McCoy medium. Once thawed, 1 ml of stop medium was added. Cells were gently mixed, transferred to 15 ml Falcon tubes containing 3 ml stop medium and centrifuged at 200 x g for 3 mins and the medium was aspirated. For STO cells, 10 ml of STO medium was added for subsequent routine cell culture on 10 cm gelatinised tissue culture dishes. For R1 mESCs, 2 ml of R1 ESC medium was added, mixed and pipetted gently onto 3.5 cm tissue culture dish with STO feeder layer, from which STO medium was aspirated.

2.3.5 Cell counting

Cells were trypsinised and transferred to 15 ml Falcon tubes. 10 µl of cell suspension was pipetted onto a Hausser Scientific haemocytometer and cells were observed under the microscope (Leica DM IL Microsystems Type 090-135.001) using 10 x objective lens. Viable cells that appeared round and healthy were counted in four squares and the average number of cells was multiplied by a chamber factor of 10^4, which gave the cell number per 1 ml of cell suspension. The required number of cells was then calculated and diluted in the appropriate amount of medium for seeding.

2.3.6 Separation of R1 ESCs from STO feeder layer

To extract RNA and protein from undifferentiated R1 ESCs, these cells had to be first separated from the STO feeder layer. In order to do this, cells were first trypsinised as described before (section 2.3.2.3). After the centrifugation step, the medium was aspirated and the cells were re-suspended in 5ml of R1 ESC medium, and then transferred onto gelatinised 10 cm dishes containing 5 ml of R1 ESC medium. The dish was left at 37˚C for at least 20 mins to allow STOs to attach to the plate. As the rate of attachment to the gelatinised plate is faster for STOs than R1 ESCs, separation of the two cell lines was possible. The cells were observed under the microscope to see whether STO attachment to the plate was complete. 10 ml of the R1 ESCs suspension in the medium was then transferred to a Falcon tube and centrifuged at 200 x g for 3 mins. Cells were then either counted using a haemocytometer (section 2.3.5) and split onto a gelatinised dish for imaging, or re-suspended in RNA lysis buffer for RNA and protein extraction (section 2.7.8 and 2.8.2).

2.4 Suspension differentiation protocols

R1 mESCs were grown in suspension to form embryoid bodies (EB) as a model to study cell differentiation, according to an established protocol (Fig. 2.1 B, derived from (Murray and Edgar, 2000, Rak-Raszewska et al., 2012)). First, cells were cultured on an STO feeder layer on 3.5 cm dishes in R1 ESC medium, as described in section 2.3.2.3, and then passaged several times onto gelatinised 6 cm dishes without the feeder layer in 5 ml of R1 ESC medium to deplete STOs from the culture. When cells were 90% confluent, they were split 1 in 6 onto gelatinised 6 cm dishes (Thermo Scientific, Nunc™) in 5 ml of R1 ESC medium for endoderm differentiation or in 5 ml of MESO ESC/EB medium (10% FBS, 1% L-glutamine, 1% Penicillin/Streptomycin, 0.15% monothioglycerol (MTG, 100mM stock, #M6145), 1,000 U/ml LIF in IMDM (#13390, Iscove's modified Dulbecco's medium)) for mesoderm differentiation (ESC/EB medium, Table 2.3). When the cells achieved 90% confluence, they were trypsinised and counted for seeding on Pluronic F-127-coated dishes (section 2.3.2.1).

For endoderm differentiation, 50,000 cell/ml were seeded onto the Pluronic F-127-treated dishes in 2 ml of ENDO EB medium (R1 ESC medium without LIF, Table 2.3). For mesoderm differentiation, 30,000 cells/ml were seeded onto the dishes in 2 ml of MESO EB medium (15% FBS, 1% L-glutamine, 0.45% MTG, 1% ITS (insulin transferrin selenium, #25-800-CI, Mediatech), 1% Penicillin/ Streptomycin, 0.1% ascorbic acid (500mM stock) in IMDM, Table 2.3). The embryoid bodies that started to form were cultured for a maximum of 20 days and the EB media were changed every 2 days.

2.5 Phenotypic assays

2.5.1 Microscopy

To take bright-field images, SW48 cells were placed in a chamber at 37 ˚C and viewed under Nikon Ti-E microscope using a 20 x objective lens. STOs, undifferentiated R1 ESCs and embryoid bodies were viewed under a Leica DFC420C microscope using 10 x and 20 x objective lenses to take bright-field images.

2.5.2 Cell viability assay

CellTiter-Glo® Luminescent Cell Viability Assay (#G7571, Promega) was used according to manufacturer's instructions to measure cell viability by quantifying the amount of ATP produced by metabolically active cells. SW48 Ras isogenic cell lines were seeded in 5 technical replicates at specified densities (250-5000 cells/well) onto 96-well plates and cultured in 10% FBS McCoy's medium for 1-5 days. As a control for background luminescence, 5 wells contained medium only. Before the assay, cells were taken out of the incubator and equilibrated at room temperature for 30 mins. 100 µl of CellTiter-Glo® Reagent (CellTiter-Glo® Buffer mixed with CellTiter-Glo® Substrate) was then added per well and the plate was shaken at 250 rpm on an orbital plate shaker (Rotamax 120, Heidolph) for 2 mins to induce cell lysis and left at room temperature for a

further 10 mins away from the light to stabilise the luminescent signal. Luminescence was recorded using a GloMAX®-Multi+ Microplate Multimode Reader with Instinct® software (Promega) with integration time of 1 sec per well. The background luminescence of control wells with media only was subtracted from the raw data.

2.5.3 Growth factor and inhibitor assays

SW48 cell lines were seeded on 10 cm dishes or 6- or 24-well plates using appropriate seeding densities (Table 2.2). Once cells achieved 70-80% confluence (after 1-3 days), they were serum-starved for 24 hours (0% FBS media) and treated with varying concentrations of inhibitors or with DMSO as a control for the indicated length of time (1 hour up to 16 hours). The following inhibitors were used in this study (Table 2.4): AZD6244 (selumetinib) (#606143-52-6/S1008, Selleck, Lot #S100823), Sorafenib (#S-8502, LC Labs; Lot #BSF-106), LY294002 (#BML-ST420-0005, Enzo Life Sciences), Rapamycin (#S1039, Selleck, Lot #S103908) and AZ628 (#4836, Tocris). Following serum-starvation, cells were stimulated with specific growth factors or 20% FBS in media that also contained the inhibitor, where appropriate, at 37˚C typically for either 5 or 20 mins. The following growth factors were used at varying concentrations: EGF (#AF-100-15, Preprotech), HGF (#100-39, Preprotech, Lot #0410S201-3) and IGF-1 (#100-11, Preprotech, Lot #11201). After stimulation, cells were lysed (section 2.8.1) or visualised (section 2.5.1).

Table 2.4 Inhibitors used in this study with the corresponding cellular targets and IC_{50} values.

Inhibitor	Target	IC_{50}	Reference
AZD6244	MEK1 ERK1/2	14 nM 10 nM	(Garon et al., 2010, Huynh et al., 2007)
Sorafenib	c-Raf-1 BRAF (wt) $BRAF^{V600E}$	6 nM 22 nM 38 nM	(Wilhelm et al., 2004)
LY294002	PI(3)K Pim-1 kinase	1.4 uM 4.0 uM	(Mena et al., 2014, Wu et al., 2014)
Rapamycin	mTOR	~0.1 nM	(Edwards and Wandless, 2007)

2.6 Preparation of murine tissues

2.6.1 Organ dissection and tissue harvesting

Adult CD1 mice (Charles River) were sacrificed by increasing CO_2 concentration in CO_2 chamber and by cervical dislocation as stated in Schedule 1 procedure of Home Office Regulations. Mouse embryos were dissected from time-mated mice at embryonic days (E) 11.5, 13.5 and 16.5. First, the uterine horns were removed from mothers at room temperature and then placed in ice cold 1x PBS (Invitrogen). Next, embryos were removed from extraembryonic membranes and decapitated according to Schedule 1 procedure of Home Office Regulations. Organs were dissected using a stereoscopic microscope (Leica MZ6) starting from the limbs/skeletal muscle, the heart and the lungs, followed by the liver, stomach, intestine, kidney rudiments/kidney and finally the brain. Neonates at postnatal days (P) 0, 5, 10, 15, 20, 25 and 30, as well as adult mice, were sacrificed and dissected accordingly. Dissected organs and tissues were placed in 1.5 ml microcentrifuge tubes (#3621, Costar™), immediately snap-frozen in liquid nitrogen and stored at -80 ˚C before tissue homogenisation.

2.6.2 Tissue homogenisation

Frozen mouse tissues were placed in 1.5 ml microcentrifuge tubes on dry ice. Small pieces of tissue were cut with a curved surgical blade (Sterile Blade No. 12, Swann-Morton), transferred to pre-weighed 2 ml tubes (#UC-13119-500, Cambio) containing 6 x 2.8 mm ceramic beads (#13114-325, Cambio) and weighed on milligram digital balance (AVI14C Adventurer® Pro, OHAUS). For RNA extraction, 300 µl of RNA Lysis Buffer (#17215, Lot #582484, Norgen Biotek Corp; XI-0718 Geneflow) containing 1% (v/v) β-mercaptoethanol was added per 10 mg of tissue and the tissues were homogenised using a PowerLyzer® 24 (#13155, MO BIO Laboratories) using the following protocol (based on manufacturer's recommended settings for RNA isolation from animal tissues): 3,500 rpm (~5.7 m/sec), 2 x 45 sec., 30 sec. dwell time. For protein extraction, 100 µl of RIPA buffer (10 mM TrisHCl pH 7.5, 150 mM NaCl, 1% (w/v) Triton-X, 0.1% (w/v) SDS, 1% (w/v) sodium deoxycalate) containing mammalian Protease Inhibitor Cocktail (#P8340) was used per 10 mg of tissues. The lysates were transferred to RNase-free microcentrifuge tubes (#3621, Costar) and centrifuged for 2 minutes at 18,000 x g to pellet any cell debris. 600 µl of the supernatant was transferred to fresh microcentrifuge tubes, snap frozen in liquid nitrogen and stored at -80˚C before RNA and protein extraction (section 2.7.8 and 2.8.2).

2.7 Molecular Biology

2.7.1 Agarose gel electrophoresis

Agarose gel electrophoresis was run to check the size of DNA products amplified in PCR reactions (section 2.7.11) and restriction digests (section 2.7.7), and to check the quality of RNA samples (section 2.7.8). 1.2 – 2% agarose gels were made by boiling agarose powder (#161-3101EDU, Bio-Rad) in 1 x TBE (Tris/Borate/EDTA) buffer (89 mM Tris-borate, 2 mM EDTA, pH 8.3, #T3913) and adding ethidium bromide to a final concentration of 0.5 µg/ml. Gels were set in gel tanks (Bio-Rad) and 1 x TBE running buffer was added. The DNA or RNA samples were prepared in 1 x sample buffer (0.5% w/v glycerol,

0.01 mM EDTA, 0.004% bromophenol blue) and electrophoresed at 120 V for 1.5 – 2 hours, along with HyperLadder IV (#BIO-33029, Bioline), HyperLadder VI (#BIO-33033, Bioline) or MassRuler (#SM0403, Life Technologies) molecular weight markers. DNA and RNA bands were visualised by ultraviolet light using GeneFlash gel documentation system (Syngene). For RNA samples, all buffers and solutions were made in nuclease-free water treated with diethyl pyrocarbonate (DEPC) and all equipment was treated with RNaseZAP (#R2020) before use.

2.7.2 Gel extraction of DNA fragments

Following agarose gel electrophoresis, appropriate DNA fragments were excised and weighed on a milligram digital balance (AVI14C Adventure™ Pro, OHAUS). DNA was extracted using QIAquick gel extraction kit (#28704, QIAGEN) and a microcentrifuge, according to manufacturer's instructions. Briefly, one volume of agarose gel was dissolved in 3 volumes of Buffer QG at 50°C, and one gel volume of isopropanol was added and mixed. The sample was then added onto the QIAquick column and centrifuged for 1 min at 10,000 x g to bind DNA. The column was washed with 0.75 ml Buffer PE and the extracted DNA was eluted in a final volume of 30 µl of Elution Buffer (10 mM Tris-Cl, pH 8.5). DNA concentrations were determined using a NanoDrop Spectrophotometer ND-1000 (Thermo Scientific) based on absorbance at a wavelength of 260 nm. The eluted DNA fragments were subsequently used for subcloning (section 2.7.3) or were sent for sequencing to DNA Sequencing & Services (MRC PPU MSI/WTB/JBC Complex, College of Life Sciences, University of Dundee, Dundee, Scotland, DD1 5EH, UK).

2.7.3 TOPO cloning

Gel-purified DNA fragments were subcloned into pCR4®Blunt-TOPO vector using TOPO technology (Invitrogen). A typical TOPO ligation mixture is detailed in Table 2.5. The reaction was left at room temperature (RT) for 15 mins and then put on ice just before bacterial transformation (secton 2.7.4).

Table 2.5 TOPO-cloning reaction mixture.

Reagent	Volume
pCR4®Blunt-TOPO vector (10 ng/µl)	1 µl
Salt solution (200 mM NaCl, 10 mM $MgCl_2$)	1 µl
Extracted PCR product (~10 ng)	4 µl
Total	6 µl

2.7.4 Bacterial transformation

50 µl of TOP10 chemically competent *E. coli* cells (#C4040, Invitrogen) were thawed on ice and briefly spun down to collect the cells at the bottom of the tube. 6 µl of TOPO ligation reaction (section 2.7.3) was added to the cells, which were then left on ice for 20 mins. To transform the cells, the bacteria were heat-shocked at 42˚C for 60 sec and then left on ice for about 2 minutes. 200 µl of Lysogeny broth (LB) (1% (w/v) tryptone, 0.5% (w/v) yeast extract, 170 mM NaCl) was added to the cells, which were then incubated at 37˚C for 50-60 mins in a thermoshaker at 180 rpm. After incubation, the cell suspension was spread onto LB/agar plates with appropriate antibiotic (100 µg/ml Ampicillin or 50 µg/ml Kanamycin), which were left to dry for about 10 mins and then inverted and incubated at 37˚C overnight.

The next day single bacterial colonies were picked and inoculated into 5-8 ml LB with the appropriate antibiotic. The bacterial cultures were grown overnight and the following day the DNA was purified by QIAGEN MiniPrep Kit (section 2.7.6).

2.7.5 Glycerol stock

To make glycerol stocks, 800 µl of overnight bacterial culture, which was grown from a single bacterial colony, was gently mixed with 200 µl of sterile glycerol and left on ice for 30mins. Glycerol stocks were then stored at -80˚C.

2.7.6 Plasmid preparation (miniprep)

5 ml of overnight LB culture from a single bacterial colony was pelleted and used for plasmid preparation using QIAprep Spin Miniprep Kit (#27104, QIAGEN) and a microcentrifuge according to manufacturer's instructions. Briefly, the bacterial pellet was resuspended in 250 µl Buffer P1 and mixed first with 250 µl Buffer P2 and then with 350 µl Buffer N3 in a microcentrifuge tube. The sample was centrifuged for 10 min at 17,900 x g and the supernatant was transferred onto QIAprep spin column and centrifuged for 1 min to bind DNA. The column was washed with 0.75 ml Buffer PE and the purified plasmid DNA was eluted in a final volume of 40 µl of Elution Buffer (10 mM Tris-Cl, pH 8.5). DNA concentration was checked using a NanoDrop, as described in section 2.7.2.

2.7.7 Restriction digestion

Restriction digests were set up to screen for correct inserts of TOPO cloning (section 2.7.3) and to make linearised plasmid standards for qRT-PCR (section 2.7.12). Typically, 1-2 µg of plasmid DNA was used per restriction digest reaction and an appropriate restriction enzyme was chosen together with its incubation buffer (NEB, New England Biolabs, 75-77 Knowl Piece, Wilbury Way, Hitchin, Herts SG4 0TY). A typical restriction digest reaction is shown in Table 2.6 and all restriction enzymes used in this study are listed in Table 2.7. The restriction digestion reactions were incubated at 37˚C for 2 hours and the digest products were analysed on 1.2% agarose gels.

Table 2.6 Restriction digest reaction mixture.

Reagent	Volume/amount
Restriction enzyme	1 µl
10 x NEB buffer	2 µl
10 x BSA (if required)	2 µl
DNA	1-2 µg (~15 µl)
water	up to 20 µl
Total	20 µl

Table 2.7 List of restriction enzymes used for restriction digestion.

Restriction enzyme	NEB buffer used
*Bgl*II	NEB3
*Eco*RI	NEB4
*Nco*I	NEB3
*Xcm*I	NEB2
*Xho*I	NEB3 + BSA

2.7.8 RNA extraction and purification

Total RNA was extracted from tissues or cell lysates using an RNA/Protein Purification Kit in a 96-well format (#37900, Norgen; Geneflow code: P4-0085, cat #582782) or columns (#23000, Norgen; Geneflow lot no #581790), by a centrifugation procedure according to the manufacturer's instructions. In short, the protocol was as follows: 600 µl of tissue lysate (section 2.6.2) or 350 µl of cultured cell lysate was combined with an equal volume of 70% ethanol or with 150 µl of isopropanol (#I9516), respectively, and vortexed for 10 seconds. Next, this mix was applied onto the column, 600 µl at a time, and centrifuged for 1 min at 14,000 x g. The flow-through was retained for protein extraction. 400 µl of Nucleic Acid Wash Solution was applied per column and centrifuged for 1

min. To eliminate genomic DNA contamination, 100 µl of Enzyme Incubation Buffer (40 mM Tris-HCl, pH 8.0, 10 mM $MgSO_4$, 1 mM $CaCl_2$) mix containing 25 U of DNase I (RQ1 RNase-Free DNase #M6101, Promega) was added to the column and centrifuged for 1 min. To ensure maximum DNA removal and RNA yield, the flow through was re-applied to the column and incubated at RT for 15 mins before washing the column with 400 µl of Nucleic Acid Wash Solution and drying for 2 mins at 14,000 x g. The column was placed into a fresh 1.7 ml elution tube and RNA was eluted by adding 50 µl of Nucleic Acid Elution Solution and centrifuging for 2 mins at 200 x g, followed by 1 min at 14,000 x g. The columns were retained for the protein purification step (section 2.8.2) and eluted RNA was stored at -80˚C.

For the 96-well format, 300 µl of tissue lysate (section 2.6.2) was combined with 120 µl of isopropanol, mixed and applied onto the well. The plate was centrifuged for 2 mins at 3,000 x g and the flow through was retained for protein purification (section 2.8.2). 400 µl of Nucleic Acid Wash Solution was applied per well and centrifuged for 2 mins. 75 µl of RQ1 DNase Reaction Buffer mix containing 18.75 U of DNase I was added per well, centrifuged for 30 sec, pipetted back onto the wells and incubated for 15 mins. The wells were washed twice with 400 µl of Nucleic Acid Wash Solution and dried for 5 mins at 3,000 x g. The 96-well filter plate was placed on top of the Elution Plate and RNA was eluted by adding 75 µl of Nucleic Acid Elution Solution and centrifuging for 2 mins. at 3,000 x g. The 96-well filter plate was retained for protein purification and RNA was stored at -80˚C.

RNA integrity was assessed by running agarose gel electrophoresis (section 2.7.1). The presence of two distinct bands of 28S and 18S rRNA subunits and lack of smears indicated intact RNA. RNA concentration was determined by measuring absorbance at 260nm using a NonaDrop, as described for DNA in section 2.7.2. In addition, RNA quality was determined from the 260nm/280nm and and 260nm/280nm ratios, which respectively indicate protein or chemical contamination.

2.7.9 Reverse transcription (RT)

Extracted mRNA was reverse transcribed. Either 0.5 µg or 1 µg of RNA was used as a template for cDNA synthesis and in a parallel "-RT" control reaction, to which no reverse transcriptase enzyme was added. The volume of RNA was adjusted to 10 µl with nuclease-free water (#W4502) and 1 µl of Oligo(dT)$_{15}$ Primer (500 µg/ml, #C1101, Promega) was added, which hybridises to the poly(A) tail of mRNA. The reaction mixture was incubated at 70˚C for 5 minutes, then snap-cooled on ice and 8 µl of the RT buffer mixture (Table 2.8) was added. The reactions were incubated at 37˚C whilst adding 1 µl of M-MuLV Reverse Transcriptase (200U, #EPO451, Thermo Fisher Scientific). No reverse transcriptase was added to the negative "-RT" tubes. All reactions were incubated at 42˚C for 1 hour and then at 70˚C for 10 mins to heat inactivate the reverse transcriptase. cDNA and "-RT" samples were snap-cooled on ice for 5 mins, diluted 5 x with 80 µl of nuclease-free water to the final volume of 100 µl and stored at -20˚C.

Table 2.8 Reverse transcription buffer mixture.

5 x Reverse Transcription Buffer (MBI-Fermentas)	4 µl
PCR Nucleotide Mix, 10mM (#C1145, Promega)	2 µl
RNasin(R) Plus RNase Inhibitor (#N2615, Promega)	0.5 µl
Nuclease-free deionised water	1.5 µl
Total volume	8 µl

2.7.10 PCR primers

Primer sequences were individually designed to amplify the different Ras isoform transcripts (Chapter 3) and were ordered from Eurofins MWG Operon in an amount of 0.025 µmol. Primers were dissolved in nuclease-free water up to a stock concentration of 100 µM and stored at -20˚C. For working concentrations, primers were further diluted to 20 µM or 10 µM. Details of all

PCR primer sequences used in this study are shown in Table 2.9. The amplified PCR products were sequence verified in both directions by DNA Sequencing & Services (Dundee) using M13 primers (Table 2.10).

Table 2.9 Primer sequences used for end-point PCR and quantitative real time (qRT) PCR.

Primer pair name	Primer sequences	Amplicon size
ERas	F: 5' GGTCAGATCCGCCTACTGCC 3'	230 bp
	R: 5' CACCACCACTGCCTTGTACTCG 3'	
HRas	F: 5' GCTGTAGAAGCTATGACAGAATAC 3'	188 bp
	R: 5' GCTGTGTCTAAGATGTCCAGTAG 3'	
KRas-4A	F: 5' AGATGTGCCTATGGTCCTGGTAG 3'	184 bp
	R: 5' CAATCTGTACTGTCGGATCTCTCTC 3'	
KRas-4B	F: 5' GATGTGCCTATGGTCCTGGTAG 3'	142 bp
	R: 5' CATCGTCAACACCCTGTCTTG 3'	
NRas	F: 5' CAAGGACAGTTGACACAAAGC 3'	213 bp
	R: 5' TGTCTTACTACATCAGCACACAG 3'	
POL2RE	F: 5' CCGGAAGCTTACCATGGAAC 3'	278 bp
	R: 5' TGTCTGTCTGAGGTAAGTGC 3'	
18SrRNA	F: 5' TTGACGGAAGGGCACCACCAG 3'	131 bp
	R: 5' GCACCACCACCCACGGAATCG 3'	

Table 2.10 Sequencing primers.

Target	**Primer name**	**Primer Sequences**
pCR4-TOPO	M13	F: 5' CTGGCCGTCTTTTAC 3'
		R: 5' CAGGAAACAGCTATGAC 3'

2.7.11 Polymerase Chain Reaction (PCR)

End-point PCR (Mullis et al., 1986) was used to amplify DNA fragments for subcloning into TOPO vectors and to check for correct insertion of a DNA fragment into a vector, as well as to test primer specificity and optimise the annealing temperatures for primer pairs to be used in RT-PCR. For subcloning (section 2.7.3), DNA was amplified using PfuUltra Hotstart Polymerase (#600390, Strategene) and a typical reaction mixture and reaction protocols are shown in Table 2.11 and Table 2.12, respectively. For all other PCR reactions, Taq DNA polymerase (#BIO-21040, Bioline) was used with a typical reaction mixture detailed in Table 2.13 and PCR protocol in Table 2.14. All PCR reactions were performed in 0.5 ml PCR tubes (#I1405-8200, StarLab) on a PCR Express Thermal Cycler (Px2, Thermo Hybaid).

Table 2.11 PfuUltra Hotstart DNA Polymerase reaction mixtures for end-point PCR.

Reagents	**Volume**
cDNA	4 µl
Forward Primer (20µM)	0.625 µl
Reverse Primer (20µM)	0.625 µl
PfuUltra HF Reaction Buffer (10X)	5 µl
PfuUltra HS DNA Polymerase (2.5U/µl)	1 µl
dNTPs (100mM)	0.5 µl
Water	38.25 µl
Total Volume	50 µl

Table 2.12 PfuUltra Hotstart DNA polymerase protocol.

Step	No. of cycles	Temperature	Time Duration
Initial denaturation	1	95˚C	5 min
Denaturation	40	95˚C	45 sec
Annealing		T_m/gradient	45 sec
Extension		68˚C	45 sec
Final extension	1	68˚C	10 min

Table 2.13 Taq DNA Polymerase reaction mixtures for end-point PCR.

Reagents	**Volume**
cDNA	2 µl
Forward Primer (10µM)	1.5 µl
Reverse Primer (10µM)	1.5 µl
Hostart Taq Mastermix	15 µl
Water	10 µl
Total Volume	30 µl

Table 2.14 Taq DNA polymerase protocol.

Step	No. of cycles	Temperature	Time Duration
Initial denaturation	1	95˚C	5 min
Denaturation	35-40	94˚C	30 sec
Annealing		60-62˚C	30 sec
Extension		72˚C	30 sec
Final extension	1	72˚C	5 min

2.7.12 Quantitative Reverse Transcription-Polymerase Chain Reaction (qRT-PCR)

Real time qRT-PCR (Higuchi et al., 1992) was used to measure the absolute levels of Ras isoform transcripts in RNA extracted from mouse embryonic stem cells and mouse tissues. First, cDNA (section 2.7.1) was diluted 1:4 in nuclease-free water, from which 4 µl was used in 10 µl reaction in 96-well plates (#HSS9601, Bio-Rad). The protocol was based on the manufacturer's instructions for the SYBR® Green qPCR kit (Bio-Rad), and is detailed in Table 2.15. The PCR primers were designed in-house (as described in Chapter 3), and are listed in Table 2.8.

Table 2.15 qRT-PCR reaction mixture.

cDNA	4 µl
2 x SYBR Mastermix	5 µl
Nuclease-free deionised water	0.7 µl
Forward Primer 10µM	0.15 µl
Reverse Primer 10µM	0.15 µl
Total volume per well	10 µl

PCR products were amplified using a CFX Connect™ Real-Time PCR Detection System (Bio-Rad) and a protocol based on the manufacturer's instructions that are detailed in Table 2.16.

Table 2.16 qRT-PCR protocol.

Step	No. of Cycles	Temperature	Time Duration
Initial denaturation	1	95˚C	3 mins
Denaturation	40	94˚C	30 sec.
Annealing		62˚C	30 sec.
Extension		72˚C	30 sec.
Melting curve	41	55˚C to 95˚C	30 sec. for every 0.5 ˚C

Fluorescence was measured in real time after each extension step of the 40 cycles. To be able to compare between different qPCR plates, cDNA synthesised from RNA of undifferentiated R1 mESCs was used as an on-plate internal control. Standard curves based on a 5-fold dilution series of linearised Ras isoform-specific plasmids (section 2.7.7) were used to calculate the absolute transcript copy numbers in the mRNA of interest. An example of the standard curve concentrations and corresponding copy numbers for the KRasB plasmid is shown in Table 2.17. Each sample was analysed in duplicate or triplicate (as on-plate technical repeats). To calculate statistical significance, at least 3 biological replicates experiments were analysed.

As a standard quality control measure, melt curves (run after qRT-PCR protocol in 0.5˚C increments) were assessed for evidence of primer-dimer formation or non-specific amplicons. Furthermore, to control for non-specific PCR product formation (e.g. from genomic DNA), negative "-RT" controls (section 2.7.9) and water blanks were run alongside qPCR reactions with cDNA.

Table 2.17 5-fold dilution series of KRasB plasmid standard curve with corresponding concentrations and copy numbers per qPCR reaction.

Standard no	Concentration	4µl per well contains	Copy number
1	0.2 ng/ul	0.8ng	1.2×10^8
2	0.04 ng/ul	0.16ng	2.4×10^7
3	8 pg/ul	32pg	48×10^5
4	1.6 pg/ul	6.4pg	9.6×10^5
5	0.32 pg/ul	1.28pg	1.92×10^5
6	64 fg/ul	256fg	3.84×10^4
7	12.8 fg/ul	51.2fg	7,680
8	2.56 fg/ul	10.24fg	1,536
9	0.512 fg/ul	2.048fg	307.2
10	0.1024 fg/ul	0.4096fg	61.44
11	0.02048 fg/ul	0.08192fg	12.288
12	4.096 ag/ul	0.016384fg	2.4576

2.8 Protein Biochemistry

2.8.1 Cell lysis and harvesting

After drug treatment and/or stimulation SW48 cells were placed on a metal tray on ice and washed 3 times with ice-cold 1 x PBS. Depending on the dish size, an appropriate amount of RIPA buffer containing mammalian Protease Inhibitor Cocktail and 1 PhosStop Phosphatase Inhibitor Cocktail tablet (#04906837001, Roche) was added on the cells (for amount of lysis buffer used per dish – see Table 2.2). Cells were lysed for 30 mins on ice with gentle shaking. Cell lysis was assessed under a microscope (Invertoscope ID 03, Zeiss) with phase–contrast to determine the extent of cell membrane disruption and cellular debris. The lysates were then transferred to Eppendorf microcentrifuge tubes and centrifuged at 18,000 x g for 15 mins at 4˚C. The supernatants were transferred to fresh eppendorf tubes and vortexed before measuring protein concentration using the BCA assay (section 2.8.3) and storage at -20 ˚C.

2.8.2 Protein purification

To extract protein from mouse tissues or cell lines, the flow-through retained from the Norgen RNA extraction step (section 2.7.8) was processed according to the manufacturer's instructions for RNA/Protein Purification Kit in a 96-well plate format (#37900, Norgen; Geneflow code: P4-0085, cat #582782) or using spin columns (#23000, Norgen; Geneflow lot no #581790). When using columns, up to 100 µl of flow-through was adjusted to 575 µl with Molecular Biology Grade Water (#W4502) and 24 µl of pH Binding Buffer was added and mixed. 600 µl of the pH-adjusted protein sample was applied at a time onto the column and centrifuged for 2 mins at 5,200 x g. The column was washed with 500 µl of Protein Wash Buffer by centrifuging for 2 mins at 5,200 x g. Then 9.3 µl of Neutralizer (containing 45 mM citric acid and 45 mM phosphoric acid) was added to a fresh 1.7 ml elution tube and protein was eluted in 100 µl of Protein Elution Buffer (10 mM sodium phosphate, pH 12.5) by centrifuging for 2 mins at 5,200 x g. Purified protein samples were stored at -80˚C.

For the 96-well format, 100 µl of flow through was adjusted to 400 µl with Molecular Biology Grade Water and 16 µl of pH Binding Buffer was added and mixed. The pH-adjusted protein samples were applied into the wells of the 96-Well Filter Plate and centrifuged for 2 mins at 3,000 x g. The plate was washed with 400 µl of Protein Wash Buffer by centrifuging for 2 mins at 3,000 x g. Then 9.3 µl of Neutralizer was added per well into a new 96-Well Elution Plate and protein was eluted in 100 µl of Protein Elution Buffer by centrifuging for 2 mins at 3,000 x g.

2.8.3 Bicinchoninic acid (BCA) protein assay

The Pierce® BCA Protein Assay Kit (#23225, Thermo Scientific) was used to measure protein concentration in cell (section 2.8.1) and tissue lysates (section 2.8.2). 2 mg/ml bovine IgG solution (#I5506) was used to generate a standard curve for calculating absolute protein concentrations up to 2,000 µg/ml. 1-5 µl of protein sample was assayed in duplicate. A Multiskan Spectrum plate spectrophotometer (Thermo Labsystems) was used to measure absorbance at

595 nm. The background absorbance was subtracted from the raw data prior to calculation of sample protein concentrations.

2.8.4 Sodium dodecyl sulfate-polyacrylamide gel electrophoresis (SDS-PAGE)

Lysates were prepared in 1 x Laemmli sample buffer (2% SDS, 10% glycerol, 5% 2-mercaptoethanol, 0.002% bromphenol blue and 62.5 mM Tris HCl, pH 6.8) and boiled at 98˚C for 5 mins. Lysate concentrations were adjusted to allow loading of equal volumes and protein amounts per lane. 10-25 µg of lysate was loaded per well on a 10% polyacrylamide gel (National Diagnostics) or a precast 4-12% Bis-Tris NuPAGE gel (Novex®, Life Technologies). The recipes for the 10% resolving and 4% stacking gel solutions are shown in Table 2.18. Standard SDS-PAGE gels were run in BioRad tanks in 1x running buffer (1% SDS, 24.8 mM Tris Base, 192 mM glycine), whereas NuPAGE gradient gels were run in Invitrogen tanks in 1 x MES (2-(*N*-morpholino)ethanesulfonic acid) buffer (50 mM MES, 50 mM Tris Base, 0.1% SDS, 1 mM EDTA, pH 7.3, #NP0002-02, NuPAGE, Invitrogen). The gels were run first at 100 V for 10 mins and then at 150-180 V until the dye front reached the bottom of the gel. Full-range rainbow marker (#RPN800E, GE Healthcare Life Sciences) was used to determine the protein sizes.

Table 2.18 Recipes for 10% resolving and 4% stacking gel solutions for SDS-PAGE. ProtoGel (#EC-890; 30% (w/v) acrylamide: 0.8% (w/v) Bis-Acrylamide Stock solution (37:5:1)), ProtoGel Stacking Buffer (#EC-893; 0.5 M Tris-HCl, 0.4% SDS pH 6.8) and ProtoGel Resolving Buffer (#EC-892; 4x: 1.5 M Tris-HCl, 0.4% SDS pH 8.8) were from National Diagnostics. APS - ammonium persulfate.

	Volume per Resolving gel	**Volume per Stacking gel**
ProtoGel	3.35 ml	0.65 ml
Resolving/Stacking buffer	2.6 ml	1.25 ml
Deionised water	3.95 ml	3.05 ml
10% APS	75 µl	25 µl
TEMED	7.5 µl	5 µl
Total	10 ml	5 ml

2.8.5 Western Blotting

Following SDS-PAGE, the gel was removed from plates, trimmed and briefly rinsed in transfer buffer (25 mM Tris, 192 mM glycine, 20% (v/v) methanol). Next, the gel was transferred into a Genie blotter tank, which was assembled in the following order: 2 grids ridged side up, cathode plate, 1 grid ridged side down, pad, Whatman paper, gel, nitrocellulose membrane (#10600001, GE Healthcare Life Sciences, Amersham Protran, 0.2 µm pore size), Whatman paper, pads up to top (3-4), grid ridged side up, anode plate, plastic cover. The pads, paper and membrane were previously immersed in transfer buffer and care was taken to remove all bubbles as transfer buffer was poured into the assembly. The container was then put into Genie blotter tank and the whole assembly was run for 1 hour at constant current of 0.5 A (around 30 V) (Burnette, 1981).

The Genie blotter was disassembled and the membrane was briefly rinsed in Ponceau-S to stain the transferred proteins. If necessary, the membrane was cut with a stainless steel surgical blade (Sterile Blade No. 11, Swann-Morton) for blotting of differently sized proteins with more than one antibody. The membrane was washed in 1 x TBST (Tris buffered saline plus Tween-20; 12 mM Tris, 137 mM NaCl, pH 7.6, 0.1% w/v Tween-20) to de-stain Ponceau-S and then incubated for 1 hr at room temperature in the appropriate blocking buffer (Table 2.19), corresponding to the primary antibody, using gentle rocking. All blocking buffers and primary antibodies were prepared in 1 x TBST. Following blocking, the membrane was transferred to the appropriate primary antibody solution and incubated overnight at 4˚C with gentle rocking. Following incubation, the membrane was washed 3 times for 5-10 mins in 1 x TBST before incubating in the appropriate secondary antibody (Table 2.20) for 1 hr at room temperature. All incubations were in the same blocking buffer as for primary antibody incubations (Table 2.19). The membrane was again washed 3 times in 1 x TBST and placed on the LICOR Odyssey for scanning at 84 μm resolution with high intensity. The bands were quantified using ImageJ (1.47v).

Table 2.19 Primary antibody list for Western blotting. Primary antibody names listed with manufacturers (#product code), followed by species of antibody: m – mouse, r – rabbit, g – goat, molecular weight (MW) of the detected protein, dilution factor of the antibody used, as well as blocking and antibody buffers. BSA – bovine serum albumin

protein/primary antibody name	Manufacturer (code)	MW [kDa]	Dilution	blocking buffer	antibody buffer
Akt	CST (#9272), r	60	1/1000	5 % Marvel	5 % Marvel
Beta-actin	Abcam (#Ab6276), m	42	1/10000	5% BSA/Marvel	5% BSA/Marvel
Cleaved PARP (Asp214) (19F4)	CST (#9546), m	89, 116	1/2000	2.5% BSA	2.5% BSA
Phospho-Akt (Ser473)(D9E)	CST (#4060), r	60	1/2000	5% Marvel	5% Marvel
EGFR (1005)	santa cruz (#sc-03-G), g	175	1/200	5 % Marvel	5 % BSA
Phospho-EGF Receptor (Tyr1068)	CST (#2234), r	175	1/1000	5 % Marvel	5 % BSA
p44/42 MAPK (ERK1/2)(137F5)	CST (#4695), r	42,44	1/1000	5 % Marvel	5 % Marvel
Phospho-p44/42 MAPK (Erk1/2) (Thr202/Tyr204) (D13.14.4E)	CST (#4370), r	42,44	1/2000	5% Marvel	5% Marvel
H-Ras (C-20)	santa cruz (#sc-520), r	21	1/300	5 % Marvel	5 % Marvel
IGF-1 Receptor β	CST (#3027), r	95	1/1000	5 % BSA	5 % BSA
Phospho-IGF-1 Receptor β (Tyr1135/1136)/ Insulin Receptor β (Tyr1150/1151) (19H7)	CST (#3024), r	95	1/500	5 % BSA	5 % BSA
K-Ras-2B (C-19)	santa cruz (#sc-521), r	21	1/500	5 % Marvel	2 % Marvel
MEK1/2	CST (#9122), r	45	1/1000	5 % BSA	5 % BSA
Phospho-MEK1/2 (Ser217/221) (41G9)	CST (#9154), r	45	1/1000	5 % BSA	5 % BSA
Met (25H2)	CST (#3127), m	145, 170	1/1000	5% Marvel	5% BSA
Phospho-Met (Tyr1230/1234/1235)	Life Tech (#44-888G), r	145	1/1000	5 % Marvel	5 % BSA
N-Ras (F155)	santa cruz (#sc-31), m	21	1/300	5 % Marvel	5 % Marvel
p70 S6 Kinase	CST (#9202), r	70, 85	1/1000	5 % BSA	5 % BSA
Phospho-p70 S6 Kinase (Thr389)	CST (#9205), r	70, 85	1/1000	5 % BSA	5 % BSA
Ras (EP1125Y)	Epitomics (#1819-1), r	21	1/1000	5% Marvel	5% Marvel

Table 2.20 Secondary antibody list for Western blotting.

Secondary antibody name	Manufacturer (code)	Dilution
Donkey anti-mouse IRDye 800CW	LICOR Biosciences (926-32212)	1/15000
Donkey anti-mouse IRDye 680CW	LICOR Biosciences (926-32222)	1/15000
Donkey anti-rabbit IRDye 800CW	LICOR Biosciences (926-32213)	1/15000
Donkey anti-goat IRDye 800CW	LICOR Biosciences (926-32214)	1/15000

2.9 Proteomics

2.9.1 Ras standards

The Ras standards were kindly provided by Dr Craig Mageean (Prior Laboratory, University of Liverpool, UK) (Mageean et al., 2015). In brief, the standards were 27kDa, his-tagged, full-length Ras proteins, labelled with Arg10 and Lys8 and grown in auxotrophic AT713 *E. coli* bacteria that do not generate their own arginine or lysine (obtained from The Coli Genetic Stock Center, Yale). The standards were purified through his-tag pull down using a metal-affinity column and then gel filtration through Superdex 200(GE Healthcare). The standards were over 98% labelled with heavy isotopes of arginine and lysine. To measure the concentration of the standards, a known quantity of light KRasB reference protein was used in a mix with heavy labelled Ras proteins. The light KRasB protein was accurately quantified using BCA assay, as well as Nanodrop 1000, using an absorbance at 280 nm (Mageean et al., 2015). For quality control, standards were run on a 12-4% Bis-Tris NuPAGE gel and stained using Colloidal Blue Staining Kit (#LC6025, Invitrogen) according to manufacturer's instructions, which showed minimal contamination with non-specific proteins.

The standards were stored in standard buffer (20mM Tris (pH 7.4), 150 mM NaCl, 2mM DTT, 5mM $MgCl_2$) in 1.5 ml Protein LoBind tubes (#0030 108.116, Eppendorf) that were pre-treated with 2% BSA for 2 hours at RT, before all the BSA was removed and any remaining liquid was allowed to evaporate in a tissue culture hood for over 3 hours. All dilutions of the standards were performed in standard buffer plus 0.1% BSA. Stock solutions were stored at -80˚C and final standard concentrations were freshly prepared for use in quantitative proteomics experiments. The standards were always thawed on ice and flicked gently to mix. They were stored at -80˚C and flash-frozen in liquid nitrogen after use (up to 3 times). 10 ng of KRas-4B and 5 ng of each H-Ras and N-Ras standards were used per 50 μg of protein lysate.

2.9.2 In-gel digest protocol

The Ras-specific in-gel digest protocol was optimised by Dr Craig Mageean (Prior Laboratory, University of Liverpool, UK). In brief, 45-50 μg of protein lysates in Laemmli sample buffer (section 2.8.4) were spiked with Ras standards and run on 10-well, 1.5mm, 12-4% Bis-Tris NuPAGE gel in 1 x MES buffer at 50V for 10 mins and then at 150V until the samples had migrated halfway down the gel. The gel was fixed in 10% acetic acid, 40% HPLC water, 50% HPLC methanol for 15 mins using gentle shaking and then washed twice with HPLC grade water (# 97063-722, VWR Chemicals).

The gel was transferred to a laminar flow cabinet and placed in non-tissue culture treated 15 cm polystyrene Petri dish (#P5981-100EA). The gel pieces were excised between the 31 kDa and 17 kDa markers. The gel pieces were then diced into cubes 1 mm in diameter, carefully transferred to 1.5 ml LoBind Eppendorf tubes in their entirety and then briefly centrifuged for 15 sec.

150 μl of 50 mM ammonium bicarbonate/ 50% (w/w) acetonitrile was added to the gel pieces and incubated at 37°C for 15 mins in a thermoshaker at 900 rpm.

The supernatant was discarded using a gel loading tip and the gel pieces were washed again in the same solution and the solution was discarded.

150 μl of 10 mM dithiothreitol (DTT) was added and the gel pieces were incubated at 37°C for 30 mins in a thermoshaker at 900 rpm. The supernatant was discarded and the gel pieces were cooled for 5 mins at room temperature. 150 μl of 55 mM iodoacetamide (IAA) was added and incubated at room temperature in the dark for 30 mins. The solution was discarded and the gel pieces were washed twice in the following order: with 200 μl of 100% acetonitrile in a thermoshaker at 37°C for 10 minutes and then with HPLC water in thermoshaker for 5 minutes. Water was removed, the gel pieces were dehydrated with 200 μL of 100% acetonitrile at 37°C for 15 min in a thermoshaker and then left at room temperature for 10 mins to allow the solvent to evaporate.

250 μl of Dilute Trypsin Gold (Promega) in reaction buffer (40 mM ammonium bicarbonate, 9% (v/v) acetonitrile) was added to gel pieces, using 200 ng of trypsin per every 50 μg of lysate. The reaction was incubated overnight at 37˚C (>16 hours).

The supernatant obtained from the overnight reaction was transferred to fresh LoBind tubes and 0.1% of formic acid was added. 200 μl of acetonitrile was added to the gel pieces and incubated for 10 min at room temperature at 900 rpm. The supernatant was transferred again to the same LoBind tubes containing formic acid and centrifuged for 15 min at 13,000 x g. Most of the supernatant was transferred to fresh LoBind eppendorf tubes, leaving behind around 3-5 μl to avoid gel debris. The samples were dried in SpeedDry vaccum concentrator (RVC 2-25, CHRIST with cooling trap CT02-50) at 60°C until all liquid had evaporated and the protein pellets were stored at -20˚C.

2.9.3 Mass spectrometry

The protein pellets were re-suspended with 25 µl 0.1% trifluoroacetic acid (TFA), vortexed thoroughly and centrifuged at 18,000 x g for 15 mins at 4 ˚C in a bench-top centrifuge. 25 µl was transferred into a glass vial and 5 µl was loaded onto the 5500 QTRAP (AB SCIEX) to measure diagnostic peptides and transitions (Mageean, 2014) in Pharmacology Mass Spectrometry Facility, University of Liverpool (measured by Dr Rosalind Jenkins).

2.10 Bioinformatics and statistical analysis

The following software packages were used in this study: NetPrimer Premier Biosoft v1.10 and Primer-BLAST (Ye et al., 2012) was used for primer design; Basic Local Alignment Search Tool (BLAST) (Altschul et al., 1990) to compare nucleotide and protein sequences; MultiExperiment Viewer MeV v4.8.1 for generation of heat maps; VECTOR NTI Advance v11.5.2 for dendrograms of Ras family and Ras isoforms; SerialCloner 2-5 for generating plasmid vector maps.

The mean, standard deviation (SD) and the standard error of the mean (SEM) were calculated for triplicate biological experiments. For statistical analysis, the data was analysed by unpaired student *t*-test and one or two-way ANOVA with Fisher's LSD or Tukey's post-hoc test using PRISM v6.0c. Means were considered to be significantly different if $p<0.05$ (two-tailed P value). EC_{50} and IC_{50} values were calculated for the normalised response also using PRISM v6.0c.

When curating data from literature to compare relative Ras isoform abundance, data was normalised to the highest value within a study (100%), and all Ras isoform abundance values were assigned a number 1-4, depending on the quartile into which they fell: 1 – 0 - 25%, 2 – 25%< - 50%, 3 – 50%< - 75%, 4 – 75%< - 100%.

Chapter 3

Establishing Reagents for qRT-PCR

3.1 Introduction

This chapter describes the design, optimisation and performance of quantitative reverse transcription-polymerase chain reaction (qRT-PCR) assays used to investigate the abundance of Ras isoforms at transcripts by SYBR® Green assays in mouse embryonic stem cell line and in mouse tissues. As described in detail below, many variables must be taken into account to design specific and sensitive assays.

PCR primers were individually designed that were specific for each Ras isoform using the BLAST online tool (Altschul et al., 1990, Ye et al., 2012) and Net primer software (PREMIER Biosoft International). As different assays would be run on the same plates, a common optimal annealing temperature was chosen. The primers were then tested for specificity between Ras isoforms and their efficiency in product amplification. The Ras primers described in this thesis met all the criteria for primer design and RT-PCR reaction optimisation (Bio-Rad Laboratories, 2006, Degen et al., 2006).

Different quantification methods were also evaluated. Plasmids encoding the Ras isoforms were subcloned and linearised to generate standard curves for absolute quantification of Ras transcripts in qRT-PCR reactions. In addition, the use of a reference transcript that might be applicable across tissues and through development was considered for relative quantification.

3.1.1 qRT-PCR as a method for accurate quantification of transcript abundance

In qRT-PCR the amount of amplified product is measured in real time as the reaction proceeds (Higuchi et al., 1992, VanGuilder et al., 2008). qRT-PCR requires a set of target-specific primers, a template DNA, a heat-stable Taq

polymerase (Chien et al., 1976, Saiki et al., 1988, Eckert and Kunkel, 1990) and a fluorescent dye to monitor the product accumulation (Kubista et al., 2006). qRT-PCR has many advantages over other nucleic acid quantitative techniques, including wide dynamic range, high accuracy and cost effectiveness of the detection of defined sets of transcripts (Schmittgen et al., 2000, Heid et al., 1996). A variety of qRT-PCR strategies are available, including the use of FRET probes such as Taqman, or sequence-independent intercalators, such as SYBR green (Kubista et al., 2006, McPherson and Møller, 2006).

A common feature of qRT-PCR assay is that accumulation of the PCR product with each PCR cycle is directly proportional to detection of a fluorescent dye (Nolan et al., 2006, VanGuilder et al., 2008). These raw data are used to determine the cycle threshold (C_T) value for each reaction, that is the number of cycles required to achieve a defined fluorescence signal above noise. Thresholds are set in the exponential phase of the PCR reaction, where product doubles with each cycle, so there is linear relationship between the C_T value and the logarithm (base 2) of the initial amount of template (Higuchi et al., 1993).

In this study, qRT-PCR was based on SYBR® Green I (Ponchel et al., 2003), a fluorescent dye that binds to the double-stranded DNA (dsDNA) (Vitzthum et al., 1999, Morrison et al., 1998, Bengtsson et al., 2003). Interaction of SYBR Green I with single-stranded DNA (ssDNA) is about 11-fold weaker than intercalation to dsDNA (Zipper et al., 2004), which enhances its fluorescence more than 1,000-fold (Dragan et al., 2012). This fluorescence is recorded by qRT-PCR thermocyclers after each cycle as the when double-stranded amplicons are generated. Overall, SYBR Green I is a very good DNA intercalating dye, which is routinely used in RT-PCR experiments, due to its thermal stability and ability to detect any dsDNA sequence. Because of this, however, there are some caveats. SYBR Green I binds to non-specific amplification products and to primer-dimers, which can lead to false positive signals in non-optimal qRT-PCR reactions (McPherson and Møller, 2006).

For this reason, qPCR instruments can characterise the final PCR reaction components by melt curve analysis (Ririe et al., 1997, Wilhelm and Pingoud,

2003). The DNA is slowly denatured, by incremental temperature increases and the loss of fluorescence signal is monitored. When the temperature reaches the melting temperature (T_m) of an amplicon, the fluorescence decreases abruptly as the dsDNA melts (Nygren et al., 1998, Kubista et al., 2006). This shift in fluorescence can be plotted as a peak on a negative derivative melt curve graph. As specific and non-specific amplicons such as primer-dimers have distinct T_m they are easily distinguished as separate peaks on melt curves.

3.1.2 Considerations for the design and optimisation of qRT-PCR

The design of Ras isoform-specific primers and optimisation of qRT-PCR assays were based on generally accepted guidelines described in the Bio-Rad Real-Time PCR Applications Guide (Bio-Rad Laboratories, 2006), Roche PCR Applications Manual (Degen et al., 2006), PREMIER Biosoft (http://www.premierbiosoft.com) and key reviews (Kubista et al., 2006, Bustin, 2000, Lutfalla and Uze, 2006, McPherson and Møller, 2006, Kramer and Coen, 2006).

3.1.2.1 Primer design

The efficiency of the amplification reaction depends on the amplicon size, which should be between 75 to 200 base pairs (bp). Longer amplicons lead to less efficient reactions and potentially saturating fluorescence signal. However, very short amplicons may not be distinguishable from primer-dimers. It is also important to consider the properties of primer pairs (Williams, 1989, Wu et al., 1991). The length of primer pairs should be similar and within the range of 18-30 bases, which is sufficient for target specificity, even within complex human genomic DNA. Primers that are too short may bind non-specifically, whereas longer primers can reduce PCR efficiency through slow hybridisation rate and hence decrease the yield.

The balance of nucleotides within a primer is also important. For a given primer pair, the T_m should be similar and allow annealing to the template at 55 to 65˚C. The T_m is defined as the temperature at which 50% of the primer-template duplexes melts and becomes single-stranded. The T_m reflects the stability of the

primer-template complex and is dependent on the percentage of G and C nucleotides (GC%). As G-C hydrogen bonding provides higher stability than A-T bonding, it contributes to a higher T_m (Wu et al., 1991). Ideally, the overall %GC for each primer should be 40-60%. Primer should also be designed with a G or C at the 3' end, referred to as a GC clamp, to aid in the correct priming from the template. However, GC runs exceeding three bases should be avoided at the 3' end, as this can lead to mispriming of GC-rich regions and can contribute to primer-dimer formation. Long GC runs can also lead to non-Watson-Crick base pairing within a primer, which can impede primer-template binding or result in mispriming. Di-nucleotide repeats should also be avoided, as repeats of more than four (e.g. TATATATA), can also cause mispriming.

Primer design should avoid sequences that may form stable secondary structures, as these hinder primer annealing to the template and lead to low product yield (Wang and Seed, 2003, Hoebeeck et al., 2005). Intramolecular hybridisation occurs due to internal complementarity within a primer and can lead to stable formation of a hairpin. Predicted 3' end hairpins with Gibbs free energy G (ΔG) of -2 kcal/mol and internal hairpins with ΔG of -3 kcal/mol are generally acceptable.

Secondary structure can also arise from intermolecular interactions that lead to the formation of primer-dimers: either homo-dimers due to self-complementarity, or hetero- dimers that can form by complementarity between forward and reverse primers. 3' end primer-dimers with ΔG = -5 kcal/mol and internal primer-dimers with ΔG = -6 kcal/mol are generally accepted. Primer-dimer formation often leads to misquantification in qRT-PCR experiments and therefore any base-pairing at the 3' ends of primer sequences should be avoided (Wang and Seed, 2003). Primer-dimer formation can be monitored by melt curve analysis as described in section 3.1.1.

3.1.2.2 Annealing temperature

The annealing temperature (T_a) used during the PCR reaction is critical for the specificity and efficiency, as primer-template hybridisation is temperature-

dependent (Williams, 1989, Rychlik et al., 1990). If the T_a is too high, this causes dissociation of the template and the primers, leading to reduced yield of PCR product (Don et al., 1991). On the other hand, if the T_a is too low, this allows partial hybridisation decreasing the specificity of priming. Therefore, an optimal T_a should yield minimal amount of non-specific PCR products and maximise the correct amplicon.

For optimal stringency, the T_a should be within 5°C of the T_m of primers (Rychlik et al., 1990). Sufficient annealing of the primers to the template already occurs at the primer T_m (von Ahsen et al., 2001), but the maximum specificity of the PCR assay is achieved using the highest T_a, at which amplification of the correct PCR product still occurs (Wu et al., 1991). Although theoretical calculation of optimal T_a is possible (Rychlik et al., 1990), each primer pair should be tested empirically using a range of T_a to optimise product specificity and reaction efficiency .

3.1.2.3 Primer efficiency

The final aspect to consider in PCR optimisation is the reaction efficiency for a given primer set. During the exponential phase of amplification, the reaction is 100% efficient if the amount of the amplicon doubles every cycle (Higuchi et al., 1993). However, reaction efficiency is often limited by a number of factors, including primer secondary structures, self-complementarity of the DNA template sequences (Wang and Seed, 2003) and non-optimal T_a (Rychlik et al., 1990, Chou et al., 1992). Therefore, it is important to empirically determine the reaction efficiency for each primer pair. The equation $Q = q_0 2^n$ denotes how the amount of PCR product Q correlates to the number of cycles n with a starting amount of DNA template q_0 if the reaction is 100% efficient.

Typically serial dilution of a DNA template is used to determine reaction efficiency. Recorded C_T values are plotted against the logarithm (base dilution factor) of starting quantity of the template for regression analysis. Accurate calculation of reaction efficiency depends on the number of dilution points and the dilution factor used (Hellemans et al., 2007). Based on the previous

equation, calculation of efficiency of the reaction *E* uses the formula $E = 2^{(m1/m2)}$, where *m1* denotes the perfect gradient and *m2* – the gradient of the regression line. In case of a 2-fold dilution series, the perfect gradient *m1* would be -1 and the reaction efficiency would be 2. To calculate the percentage efficiency of the reaction %E, the equation $\%E = (E-1) \cdot 100\%$ is used. Ideally, %E should be between 90-105%, as low values indicate poor optimisation of the reaction conditions or primer design. Values that are too high usually imply pipetting errors or amplification of primer-dimers.

3.1.2.4 Quantification of qRT-PCR

In general, there are two methods that can be employed to quantify the qRT-PCR results: the absolute quantification method using a template standard curve and the relative quantitation using a reference gene.

For absolute quantitation, C_T values obtained from the qRT-PCR data are converted to copy number using standard curves generated by a serial dilution of the template, for example cloned into a plasmid. However, the C_T values of the chosen dilutions must reflect the range of C_T values obtained from the test samples, so that any calculated data could be interpolated, not extrapolated, from the standard curve. The calculated data can be normalised to unit mass, for example data may be expressed as copy number per pg of RNA.

The alternative method of quantifying transcripts by qRT-PCR relies on relative quantification. In essence, this is a method of normalising the expression level of a target gene to those of a reference gene (Karge et al., 1998). In brief, the C_T values of a target gene are subtracted from the C_T values of a reference gene in each test sample, using the equation ΔC_T (relative expression) $= 2^{CT(reference) - CT(target)}$ to determine the target/reference gene expression ratio. Thus, relative expression of the target gene can be compared to across samples. The data may be further normalised to a calibrator, e.g. a control sample within the experiment.

One benefit of such ΔC_T method that normalised expression of a target gene to a reference gene is reduction of experimental noise arising from technical

variations between test samples, such as differences in input RNA amount or reverse transcription efficiency (Karge et al., 1998, Derveaux et al., 2010). However, choosing a reliable reference gene is crucial. First, the efficiency of amplification for the reference gene and target gene should be similar to ensure that the ΔC_T equation is valid (Kozera and Rapacz, 2013). Secondly, a reference gene must be ubiquitously and stably expressed across all test samples.

3.1.2.5 Selection of reference genes for relative quantitation in qRT-PCR

To enable relative quantitation, the expression levels of a reference gene must be constant across all test samples, regardless of developmental stage, tissue type or treatment method. In some cases it is not possible to find a single candidate gene that would fulfil these criteria (Carnahan et al., 2013), as expression levels of all genes are tightly regulated and depend on different physiological states (Kraemer et al., 2012). Hence, several reference genes should be independently assessed for any given experimental context. Although it is recommend to normalise qRT-PCR data to more than one reference gene to achieve better accuracy (Kozera and Rapacz, 2013, Nicot et al., 2005), the use of a single optimised reference gene might be sufficient (Willems et al., 2006, Thellin et al., 1999).

Among the most commonly used reference genes in qRT-PCR are so-called housekeeping genes. These are essential metabolic or structural genes, and were the first to be considered as reference genes (Thellin et al., 1999, Kozera and Rapacz, 2013). One example is cytoskeletal β–actin, for which expression levels have been shown to be stable in various samples under different treatments (Giulietti et al., 2001). However, certain conditions can affect β–actin mRNA levels, e.g. hypoxia (Suzuki et al., 2000). Another housekeeping gene, glyceraldehyde-3-phosphate dehydrogenase (GAPDH), is also widely used for normalisation of qRT-PCR data (McPherson and Møller, 2006). It is an enzyme primarily involved in glycolysis, but also in a number of non-metabolic processes. Although its expression is ubiquitous and generally stable across cell

types, levels can be affected by certain treatments, such as programmed neuronal cell death (Suzuki et al., 2000, Ke et al., 2000).

An alternative reference gene commonly used in qRT-PCR is the ribosomal RNA (rRNA) subunit 18S (Kozera and Rapacz, 2013). There are, however, several pitfalls associated with its use for normalisation. First, this iRNA is synthesised by RNA polymerase I, independently to mRNA synthesis by RNA polymerase II (Radonic et al., 2004). The 18S expression level is also much higher than that of many mRNAs (Paolacci et al., 2009), and the rRNA:mRNA ratios can also significantly differ between test samples (Vandesompele et al., 2002), making 18S rRNA unsuitable for normalisation of lower abundance transcripts. What is more, rRNA is more stable than mRNA (Paolacci et al., 2009), meaning that normalisation to 18S would not account for differences in mRNA degradation in the test samples. 18S rRNA expression can also be affected by certain treatments (Nicot et al., 2005). Overall, 18S it is not a good representation of the mRNA population within a cell (Suzuki et al., 2000).

Another reference gene to consider is RNA polymerase II (POL2RE). As mentioned above, it is involved in the transcription of all mRNA and is reported to be the most stably expressed reference gene across different tissue types (Radonic et al., 2004). POL2RE levels have also been shown to remain constant throughout mouse ESCs differention (Kraemer et al., 2012). Taken together, among all reference genes considered, POL2RE is most likely to reflect mRNA levels in murine test samples examined in this study.

3.2 Results

3.2.1 Primer design

Based on the general recommendations for primer design (section 3.1.2.1), Ras primers were designed to generate amplicons of approximately 200 bp that met the GC content criteria. The Ras isoform primers, together with their properties, are listed in Table 3.1. Primer sequence positions within the Ras isoform transcripts are illustrated in Fig. 3.1 – 3.4, based on AceView sequence representation (http://www.ncbi.nlm.nih.gov/IEB/Research/Acembly/) (Thierry-Mieg and Thierry-Mieg, 2006, Durbin and Thierry-Mieg, 1994) and BLAST (Altschul et al., 1990).

To avoid the detection and amplification of any contaminating genomic DNA, primers that span exon-exon boundaries or flank introns were designed (McPherson and Møller, 2006, Degen et al., 2006, Huang et al., 1996, Wang and Seed, 2003). For the former, at least one primer within each pair was designed to span an intron, so that it would partially hybridise to the first exon and partially to the following exon. Hence, such primers would not amplify any contaminating genomic DNA, which contains the intron. This method of primer design was used for primer pairs that specifically amplify KRas-4B (Fig. 3.3) and NRas (Fig. 3.4) transcripts. The design of primers on exon-exon boundaries aided in the specific amplification of alternatively spliced KRas isoforms (Fig. 3.3).

The other option was to design primers that flank introns, so that the forward and reverse primer anneal entirely to different exons separated by at least one intron. Thus, genomic DNA templates would be longer than intron-less cDNA templates and unlikely to be amplified during the qRT-PCR reaction cycles. If genomic amplicons were produced, these could be distinguished by melt curve analysis (section 3.2.2) or by performing an end-point PCR reaction and running the PCR products on an agarose gel. Primer pairs flanking an intron were designed for specific amplification of ERas (Fig. 3.1), HRas (Fig. 3.2) and KRas-

4A (Fig. 3.3) transcripts. For ERas, the forward primer annealed to the non-coding exon 0, comprising the 5' untranslated region (UTR).

These methods of primer design were an extra precaution, as all RNA samples were treated with DNase to remove genomic DNA. Also, representative samples were compared along with their "-RT" controls (RNA samples without reverse transcriptase in the reverse transcription reaction) using end-point PCR and qRT-PCR to exclude any false positives due to genomic DNA amplification.

Each primer pair was tested *in silico* using NetPrimer v1.10 (PREMIER Biosoft International) for the formation of any secondary structures, including hairpins and primer-dimers, GC content and T_m. Primers with GC content of 50-65%, and with free energy higher than ΔG = -0.7kcal/mol for hairpin formation, ΔG = -5kcal/mol for self-dimer and ΔG = -5.5kcal/mol for cross-dimer, as well as with a T_m of around 60°C were chosen and further verified by Primer-BLAST (Ye et al., 2012) for gene specificity. Several to dozens of primer pairs were tested for each Ras isoform *in silico* before the most optimal primers were chosen for laboratory evaluation.

Table 3.1 Properties of Ras isoform and reference gene primer pairs. A list of qRT-PCR primers used in this study, including the generated amplicon size in base pairs (bp), primer length in nucleotides (nt), GC content (GC%), melting temperature (T_m) and the Gibbs Free Energy (ΔG) for hairpin, self-dimer and cross-dimer formation stability.

Primer pair name	Amplicon size	Primer sequence	Length (nt)	T_m (°C)	GC%	ΔG (kcal/mol)		
						Hairpin	Self-dimer	Cross-dimer
ERas	230 bp	F: 5' GGTCAGATCCGCCTACTGCC 3'	20	61.77	65.00	-0.35	-4.62	-
		R: 5' CACCACCACTGCCTTGTACTCG 3'	22	62.82	59.09	-	-4.65	
HRas	188 bp	F: 5' GCTGTAGAAGCTATGACAGAATAC 3'	24	53.23	41.67	-0.59	-4.89	-4.89
		R: 5' GCTGTGTCTAAGATGTCCAGTAG 3'	23	53.79	47.83	-	-4.55	
KRas-4A	184 bp	F: 5' AGATGTGCCTATGGTCCTGGTAG 3'	23	60.04	52.17	-	-3.56	-4.65
		R: 5' CAATCTGTACTGTCGGATCTCTCTC 3'	25	59.20	48.00	-	-4.62	
KRas-4B	142 bp	F: 5' GATGTGCCTATGGTCCTGGTAG 3'	22	58.74	54.55	-	-3.56	-5.41
		R: 5' CATCGTCAACACCCTGTCTTG 3'	21	58.49	52.38	-0.7	-4.90	
NRas	213 bp	F: 5' CAAGGACAGTTGACACAAAGC 3'	21	55.55	47.62	-	-4.9	-4.87
		R: 5' TGTCTTACTACATCAGCACACAG 3'	23	53.20	43.48	-	-4.3	
POL2RE	278 bp	F: 5' CCGGAAGCTTACCATGGAAC 3'	20	59.57	55.00	-	-12.52	-9.92
		R: 5' TGTCTGTCTGAGGTAAGTGC 3'	20	50.05	50.00	-	-	

A. Gene overview

B. Transcript NM_181548.2

C. qRT-PCR primer positions in mRNA sequence of NM_181548.2

ggtcagatccgcctactgcccctcatcagactgctactcctgggagcacagcacctgct
ctttacacctcttccttgagctgctggggaATGGCTTTGCCTACAAAGTCTAGCATCTT
GGACCTGAGCTCCGGCACCCCATGCACCAGATCTCCAGAGGAAAGTCACGAGGCTTGGG
CACAGTGCAAAGATGCTGGCAGGCAGCTACCCGAGTACAAGGCAGTGGTGGTGGGTGCA
AGTGGTGTTGGTAAAAGTGCTCTCACCATCCAGATGACTCACCAATGCTTCGTGAAAGA
CCATGACCCCACTATCCAAGATTCCTACTGGAAGGAAGTGGCCAGGGACAACGGAGGCT
ACATTCTAAATGTTCTGGATACATCTGGGCAGGATATTCACCGGGCTCTGCGTGACCAG
TGCTTGGCATCTGGTGATGGTGTGCTGGGCGTCTTTGCTCTTGACGACCCCTCGTCTCT
GGACCAGTTGCAGCAGATATGGTCCACCTGGACCCCTCACCACAAGCAGCCTCTGGTAC
TAGTGGGCAACAAGTGTGACCTGGTGACCACTGCTGGAGATGCTCATGCTGCCGCAGCC
CTCCTTGCTCACAAGTTGGGGGCCCCCTTGGTGAAGACCTCAGCCAAGACGCGGCAAGG
TGTGGAGGAAGCCTTTGCCCTGCTTGTCCATGAGATTCAGAGGGCCCAGGAGGCTGTGG
CCGAATCAAGCAAGAAGACCCGACACCAGAAAGCCGTGTGTAGCTGTGGCTGCTCTGTA
GCCTGAagatctttgtctagcaaattgacccttgtctcatgtcaaggtgacaattctct
tgtaataagatttccctctccgaccaagttaccacagacatcttttattgtcatttgg
tgagaagttacgtggtaacatgggacatccctcattgactgtgttttatgaaactctat
gcaaaattaaataaatgttctcaggattcaaagcttcctttatac

Fig. 3.1 ERas sequence and position of qRT-PCR primers. A A schematic gene overview with exons (boxes) and introns (lines) and the corresponding lengths in base pairs (bp). **B.** Transcript variant showing coding (blue) and non-coding sequence (black) in exons with aligned qRT-PCR primers (arrows). **C.** mRNA coding sequence with primer positions (red arrows and underlined sequences). Non-coding sequence is depicted in lower case, coding sequence is depicted in blue.

A. Gene overview

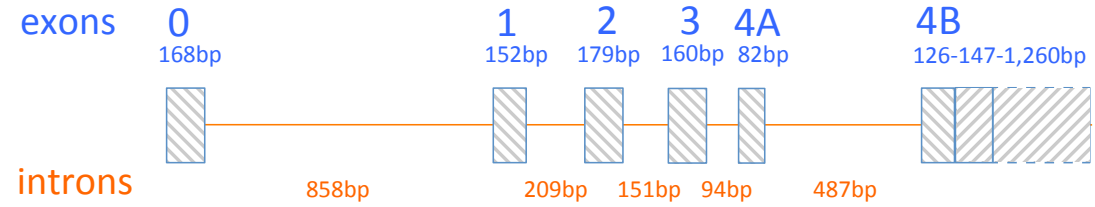

B. Transcript variants

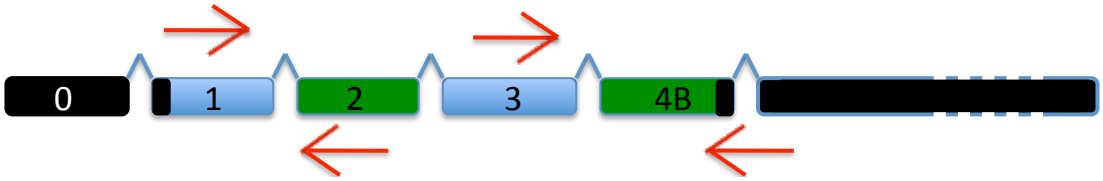

NM_008284.2

NM_001130444.1

NM_001130443.1

C. qRT-PCR primer positions in mRNA sequence of NM_008284.2

gctgtagaagctATGACAGAATACAAGCTTGTGGTGGTGGGCGCTGGAGGCGTGGGAAAGAG
TGCCCTGACCATCCAGCTGATCCAGAACCACTTTGTGGACGAGTATGATCCCACTATAGAGG
ACTCCTACCGGAAACAGGTGGTCATTGATGGGGAGACATGTCTACTGGACATCTTAGACACA
GCAGGTCAAGAAGAGTATAGTGCCATGCGGGACCAGTACATGCGCACAGGGGAGGGCTTCCT
CTGTGTATTTGCCATCAACAACACCAAGTCCTTCGAGGACATCCATCAGTACAGGGAGCAGA
TCAAGCGGGTGAAAGATTCAGATGATGTGCCAATGGTGCTGGTGGGCAACAAGTGTGACCTG
GCTGCTCGCACTGTTGAGTCTCGGCAGGCCCAGGACCTTGCTCGCAGCTATGGCATCCCCTA
CATTGAAACATCAGCCAAGACCCGGCAGGGCGTGGAGGATGCCTTCTATACACTAGTCCGTG
AGATTCGGCAGCATAAATTGCGGAAACTGAACCCACCCGATGAGAGTGGTCCTGGCTGCATG
AGCTGCAAATGTGTGCTGTCCTGAcaccaggctcaggacatgg

Fig. 3.2 HRas sequence and position of qRT-PCR primers. A A schematic gene overview with exons (boxes) and introns (lines) and the corresponding lengths in base pairs (bp). **B.** Transcript variants showing coding (alternating blue and green; alternative exon in orange) and non-coding sequences (black) in exons with aligned qRT-PCR primers (arrows). **C.** mRNA sequence with primer positions (red arrows and underlined sequences). Non-coding sequence is depicted in lower case, coding exons in alternating blue and green.

A. Gene overview

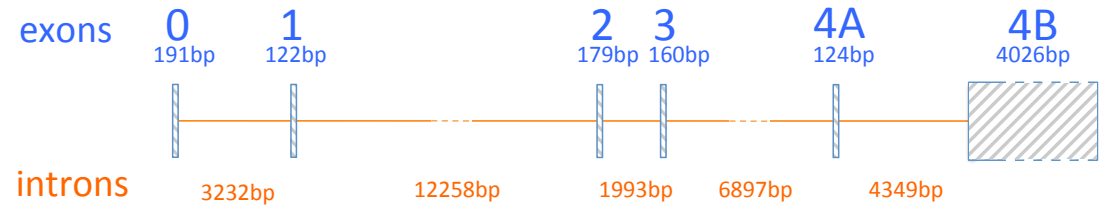

B. Transcript variants

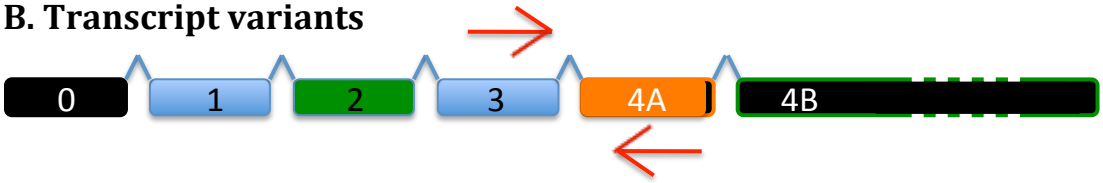

BC119495.1 KRasA

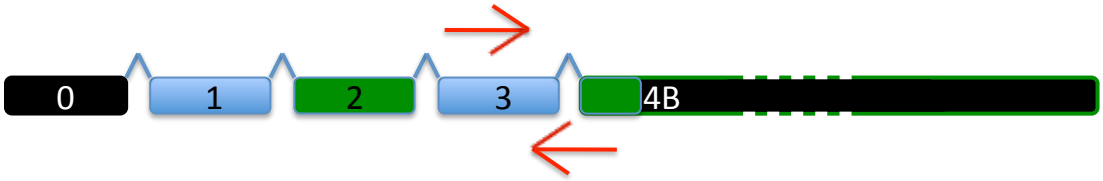

NM_021284.6 KRasB

C. qRT-PCR primer positions in KRasA mRNA BC119495.1

ATGACTGAGTATAAACTTGTGGTGGTTGGAGCTGGTGGCGTAGGCAAGAGCGCCTTGACGATACAGCT
AATTCAGAATCACTTTGTGGATGAGTATGACCCTACGATAGAGGACTCCTACAGGAAACAAGTAGTAA
TTGATGGAGAAACCTGTCTCTTGGATATTCTCGACACAGCAGGTCAAGAGGAGTACAGTGCAATGAGG
GACCAGTACATGAGAACTGGGGAGGGCTTTCTTTGTGTATTTGCCATAAATAATACTAAATCATTTGA
AGATATTCACCATTATAGAGAACAAATTAAAAGAGTAAAGGACTCTGAAGATGTGCCTATGGTCCTGG
TACGGAATAAGTGTGATTTGCCTTCTAGAACAGTAGACACGAAACAGGCTCAGGAGTTAGCAAGGAGT
TACGGGATTCCGTTCATTGAGACCTCAGCAAAGACAAGACAGAGAGTGGAGGATGCTTTTTATACATT
GGTGGAGAGAGATCCGACAGTACAGATTGAAAAAAATCAGCAAAGAAGAAAAGACTCCTGGCTGTGTGA
AAATTAAAAAATGCGTTATAATGTAAtctggtgttgacgatg

D. qRT-PCR primer positions in KRasB mRNA NM_021284.6

ATGACTGAGTATAAACTTGTGGTGGTTGGAGCTGGTGGCGTAGGCAAGAGCGCCTTGACGATACAGCT
AATTCAGAATCACTTTGTGGATGAGTATGACCCTACGATAGAGGACTCCTACAGGAAACAAGTAGTAA
TTGATGGAGAAACCTGTCTCTTGGATATTCTCGACACAGCAGGTCAAGAGGAGTACAGTGCAATGAGG
GACCAGTACATGAGAACTGGGGAGGGCTTTCTTTGTGTATTTGCCATAAATAATACTAAATCATTTGA
AGATATTCACCATTATAGAGAACAAATTAAAAGAGTAAAGGACTCTGAAGATGTGCCTATGGTCCTGG
TACGGAATAAGTGTGATTTGCCTTCTAGAACAGTAGACACGAAACAGGCTCAGGAGTTAGCAAGGAGT
TACGGGATTCCGTTCATTGAGACCTCAGCAAAGACAAGACAGGGTGTTGACGATGCCTTCTATACATT
AGTCCGAGAAATTCGAAAACATAAAGAAAAGATGAGCAAAGATGGGAAGAAGAAGAAGAAGAAGTCAA
GGACAAGGTGTACAGTTATGTGA

Fig. 3.3 KRas sequence and position of qRT-PCR primers. A A schematic gene overview with exons (boxes) and introns (lines) and the corresponding lengths in base pairs (bp). **B.** Transcript variants showing coding (alternating blue and green; alternative exon in orange) and non-coding sequences (black) in exons with aligned qRT-PCR primers (arrows). **C. and D.** mRNA sequence with primer positions (red arrows and underlined sequences). Non-coding sequence is depicted in lower case, coding exons in alternating blue and green and alternative exon in orange.

A. Gene overview

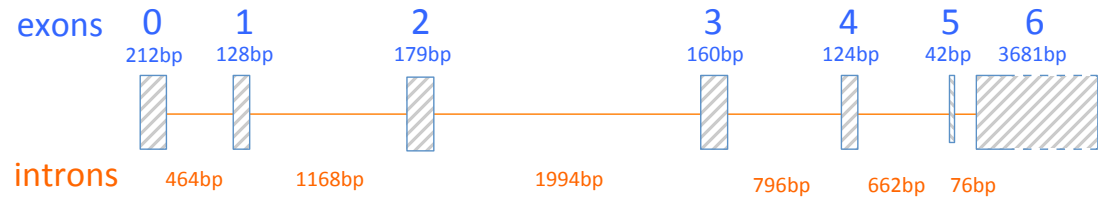

B. Transcript NM_010937

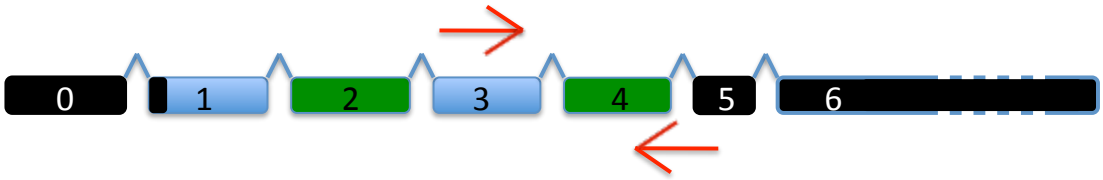

C. qRT-PCR primer positions in mRNA sequence of NM_010937

ATGACTGAGTACAAACTGGTGGTGGTTGGAGCAGGTGGTGTTGGGAAAAGCGCCTTGAC
GATCCAGCTAATCCAGAACCACTTTGTGGATGAATATGATCCCACCATAGAGGATTCTT
ACCGAAAGCAAGTGGTGATTGATGGTGAGACCTGCCTGCTGGACATACTGGACACAGCT
GGACAAGAGGAGTACAGTGCCATGAGAGACCAGTACATGAGGACAGGCGAAGGGTTCCT
CTGTGTATTTGCCATCAATAATAGCAAATCATTTGCAGATATTAACCTCTACAGGGAGC
AAATTAAGCGTGTGAAAGATTCTGATGATGTCCCCATGGTGCTGGTAGGCAACAAGTGT
GACTTGCCAACAAGGACAGTTGACACAAAGCAAGCCCACGAACTGGCCAAGAGTTACGG
AATTCCATTCATTGAGACCTCAGCCAAGACCCGACAGGGTGTGGAGGATGCCTTTTACA
CACTGGTAAGGGAGATACGCCAGTACCGAATGAAAAAGCTCAACAGCAGTGACGATGGC
ACTCAAGGTTGTATGGGGCTGCCTTGTGTGCTGATGTAGtaagaca

Fig. 3.4 NRas sequence and position of qRT-PCR primers. A A schematic gene overview with exons (boxes) and introns (lines) and the corresponding lengths in base pairs (bp). **B.** Transcript variant showing coding (alternating blue and green) and non-coding sequences (black) in exons with aligned qRT-PCR primers (arrows). **C.** mRNA coding sequence with primer positions (red arrows and underlined sequences). Non-coding sequence is depicted in lower case, coding exons are depicted in alternating blue and green.

3.2.2 Optimisation of qRT-PCR

Each step of the RT-PCR reaction (extension, denaturation and annealing) utilising SYBR Green I, as well as primers used in the assay, require further optimisation (McPherson and Møller, 2006, Bio-Rad Laboratories, 2006). The qRT-PCR reaction cycles were based on previous assays established in the lab and are described in Chapter 2. The primers selected in section 3.2.1 were tested empirically. Subsequent sections will describe annealing temperature optimisation (section 3.2.2.2), testing of primer specificity (section 3.2.2.3) and efficiency (section 3.2.2.4), as well as generation of standard curves to assess RT-PCR reaction performance (section 3.2.2.5). Section 3.2.2.1 describes the generation of Ras isoform-specific plasmids for use as control templates and the final section 3.2.2.6 addresses selection of a reference gene for qRT-PCR data normalisation.

3.2.2.1 Generation of plasmids

Plasmids encoding murine Ras isoforms were used to test the Ras primer specificity (section 3.2.2.3) and to generate standard curves for absolute quantification of Ras isoforms in qRT-PCR reactions (section 3.2.2.5). Mouse ERas, KRasA and KRasB plasmids were purchased from Source Bioscience. Mouse HRas and NRas fragments were cloned from undifferentiated R1 mouse ESCs cDNA for TOPO cloning (vector maps are shown in Appendix Fig. A3.1-A3.2).

For HRas, the whole coding DNA sequence (CDS), as well as a small non-coding DNA fragment from exon 1 (Fig. 3.2), were amplified from the cDNA using previously designed HRas forward primer (Table 3.1, F: 5' GCTGTAGAAGCTATGACAGAATAC 3') and a cloning reverse primer (R: 5' ACCTCGAGATCAGGACAGCAC 3') that recognised the 3' end of the CDS (exon 4B of all transcript variants, Fig. 3.2). The properties of the forward and reverse primers are summarised in Table 3.2. Although NetPrimer predicted the formation of a cross-dimer and a self-dimer for the reverse primer (ΔG was lower than 6 kcal/mol), any non-specific products would be unlikely to prevent

amplification of the required product. Primer-BLAST confirmed that the specific amplicon would be 582 bp long, whereas any amplification of genomic DNA would yield an amplicon longer than 3,000 bp, which would be easily distinguished on an agarose gel. Primer-BLAST also predicted amplification of additional sequences, which included a 664 bp product from HRas transcript 1 variant X4 (XM_006536160.1).

Table 3.2 Properties of HRas cloning primers. Primers were used for amplifying mouse HRas transcript 1 coding DNA sequence and a short non-coding fragment for subsequent TOPO cloning. Nt – nucleotides, T_m – melting temperature, GC% - percentage of G and C bases, ΔG – Gibbs free energy.

Primer	Length (nt)	T_m (˚C)	GC%	ΔG (kcal/mol)		
				Hairpin	Self-dimer	Cross-dimer
Forward	24	53.23	41.67	-0.59	-4.89	-9.03
Reverse	21	58.84	57.14	-0.57	-9.96	

The PCR reactions were performed using annealing temperature gradient and PfuUltra Hotstart polymerase that has a proofreading ability (Lundberg et al., 1991) (section 2.7.12). PCR products were run on a 2% agarose gel and visualised by UV transilluminator (Fig. 3.5). The reaction revealed an additional band at a molecular weight (MW) above 600 bp (Fig 3.5, red asterisk), which might have been the predicted HRas transcript 1 amplicon.

For NRas cloning, the PCR primers designed for RT-PCR (Table 3.1) were used to amplify a 213 bp fragment from the CDS and 3'UTR of NRas (Fig. 3.4). The PCR products were run on a 2% agarose gel (Fig. 3.5). The Ras sequences were gel-purified and subcloned into pCR4-TOPO and transformed into competent *E. coli* TOPO bacteria. Glycerol stocks and minipreps were made from overnight bacterial cultures and minipreps were tested for the correct fragment insertion by *Eco*RI restriction digest and sequencing.

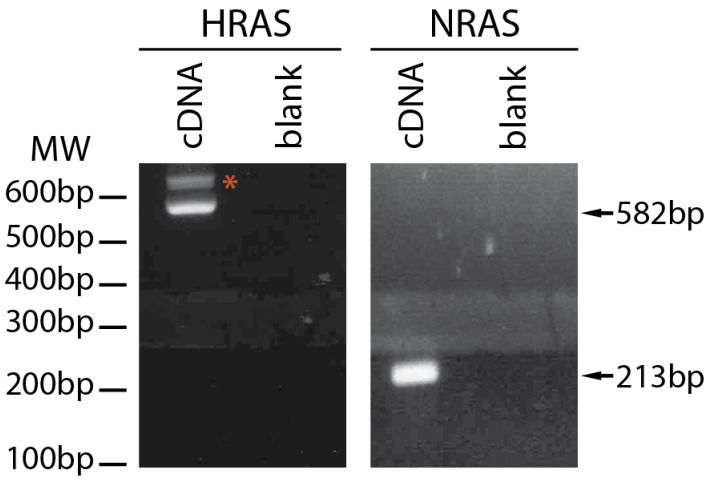

Fig. 3.5 Generation of mouse isoform-specific Ras fragments for subcloning into pCR4-TOPO plasmid. End-point PCR reactions were performed with 40 ng of cDNA from undifferentiated R1 ESCs p.19 using mouse HRas- or NRas-specific primers, including blanks with water instead of cDNA used as a negative control. PCR reactions were using proofreading Pfu polymerase and annealing temperature (T_a) gradient. The PCR products were run on 2 % agarose gels (T_a = 52.1˚C, for HRas; T_a = 52.3˚C, for NRas) and the correct amplified gene fragments (shown by arrows with length in bp) were excised and purified for subsequent subcloning into the pCR4-TOPO plasmid. Red asterisk corresponds to an unspecific amplification product for HRAS primers. MW – molecular weight marker, bp – base pair.

3.2.2.2 Annealing temperature optimisation

First, all Ras-isoform primer pairs were amplified at T_a = 60˚C for 40 cycles using cDNA from undifferentiated R1 ESCs as a template (Fig. 3.6 A). Negative controls with "-RT" and with nuclease-free water were included in each primer set. The PCR products of all reactions were run on 2% agarose gels to reveal correct amplification products for each Ras isoform-specific primers. However, primer-dimer product formation was present in all negative control reactions for all primer pairs and in reactions with cDNA for ERAS, HRAS and KRASA primers. Although no other unspecific amplicons were present, formation of primer-dimer products alone meant that the PCR conditions were not fully optimised.

Next, an annealing temperature gradient was used in end-point PCR for a series of PCR assays with T_a below and above the T_m of each Ras isoform-specific primer pair. A negative control (blank) with nuclease-free water instead of cDNA was included for each primer set and the PCR products were run on 2% agarose gels (Fig. 3.6B). For HRas, two different primer pairs were tested initially – HRAS1, specific only for HRAS transcript 1, and HRAS, specific for all HRAS transcripts. Both primer pairs amplified the desired PCR products of 171 bp and 188 bp for the HRAS1 and HRAS primer pairs, respectively. However, PCR reactions with the HRAS1 primer pair led to primer-dimer products at lower annealing temperatures (55.1-57.8˚C) and in the reaction with no template cDNA (blank). Thus, this primer set was not ideal for qRT-PCR as primer-dimer formation depletes primers from binding to the DNA template and reduces reaction efficiency (Chou et al., 1992). No non-specific product formation was seen for HRAS primer pair, hence, these were chosen for further optimisation.

For the remaining Ras isoform-specific primer pairs, all PCR reactions yielded products of the desired length, suggesting correct amplification of the PCR product within the range of tested T_a (Fig. 3.6B). However, higher T_a during the PCR resulted in less PCR product. For KRASB primer pair at T_a = 56.7˚C there

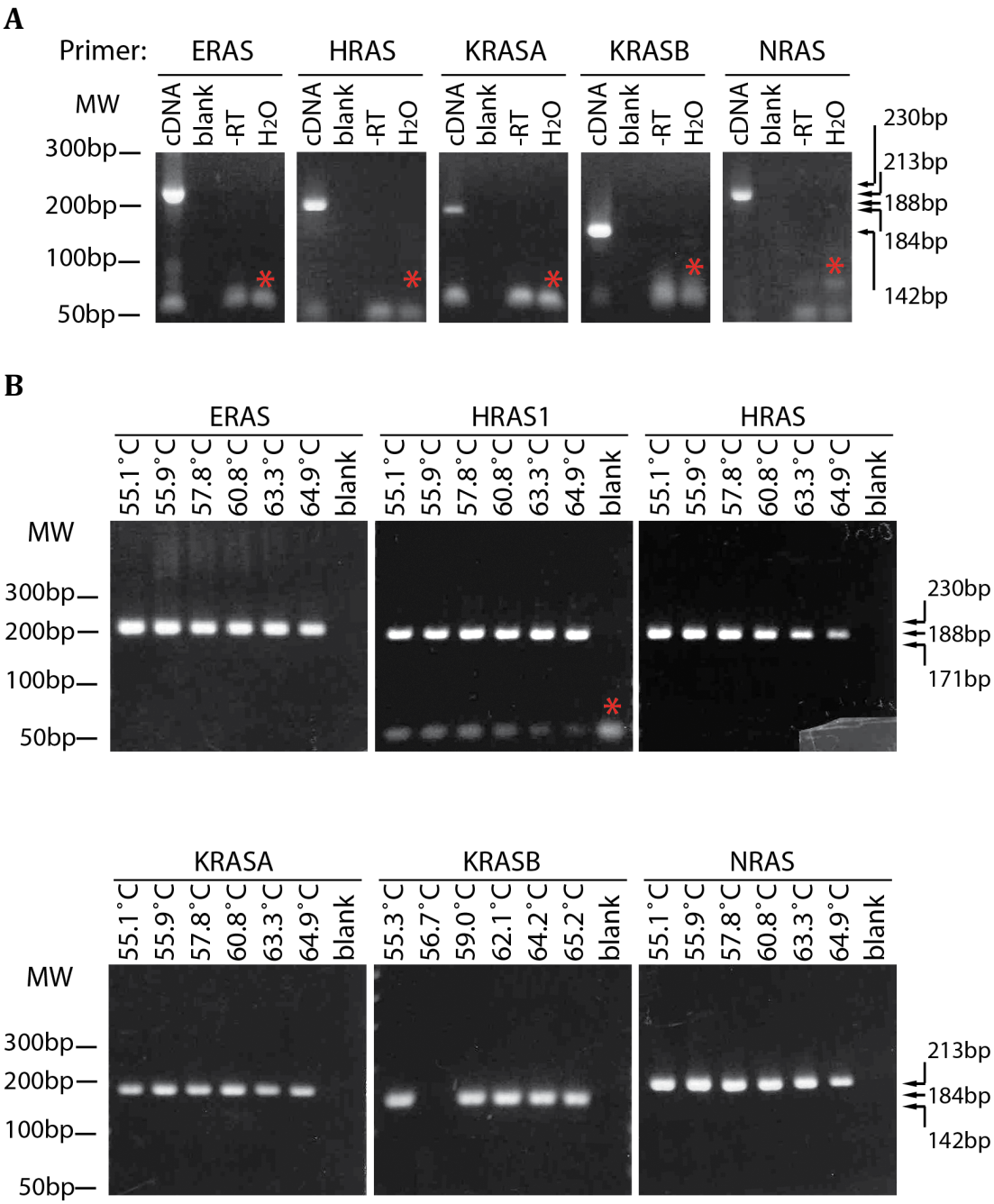

Fig. 3.6 Optimising annealing temperature (T_a) for Ras isoform primers. Ras isoform-specific primers were used to amplify 20 ng of cDNA from undifferentiated R1 ESCs. "-RT" and nuclease-free water were used in reactions as negative controls. Reaction products were run on 2% agarose gels. **A** PCR conditions: 95˚C for 5 mins, 94˚C for 30sec, 60˚C for 30 sec, 72˚C for 30 sec, 40 cycles; blank – no reaction. **B** PCR conditions: 95˚C for 5 min, 94˚C for 30 sec, T_a (gradient 55-65˚C) for 30 sec, 72˚C for 20 sec; 35 cycles. Blanks represent PCR with no cDNA (T_a = 60.9˚C for KRASB, T_a = 59.0˚C for other primers). Specific amplicons for Ras isoforms: ERAS – 230bp, HRAS transcript 1 – 171 bp, HRAS (all transcripts) – 188 bp, KRASA – 184 bp, KRASB – 142 bp, NRAS – 213 bp. Red asterisks indicate primer-dimer.

was no PCR product, possibly because of mispipetting of one of the PCR constituents. Negative controls (blanks) did not show formation of primer-dimer products. Representative bands from each primer pair reaction were excised, purified and sequence-verified (Dundee Sequencing Services). As higher T_a contributes to better primer-template specificity, a T_a of 62˚C was chosen for the subsequent PCR reactions for all primer pairs.

3.2.2.3 Primer specificity

Primer specificity depends on the T_a (Wu et al., 1991, Don et al., 1991), as discussed in section 3.1.2, and is also highly sensitive to other PCR parameters (Wang and Seed, 2003). Ras isoform-specific primers were shown to amplify the correct PCR products (Fig. 3.6), which complemented *in silico* primer specificity testing by Primer-BLAST (section 3.2.1). However, the specificity between Ras isoforms under the selected PCR condition also needs to be verified empirically.

Ras isoform plasmids (Section 3.2.2.1) were used as DNA templates in PCR reactions for each Ras isoform primer pair (Fig. 3.7). All primers revealed high specificity for the correct Ras isoform by amplifying the desired DNA fragments only in the reactions with the corresponding Ras plasmids. Most importantly, Ras primers did not cross-amplify from the other Ras isoform plasmids.

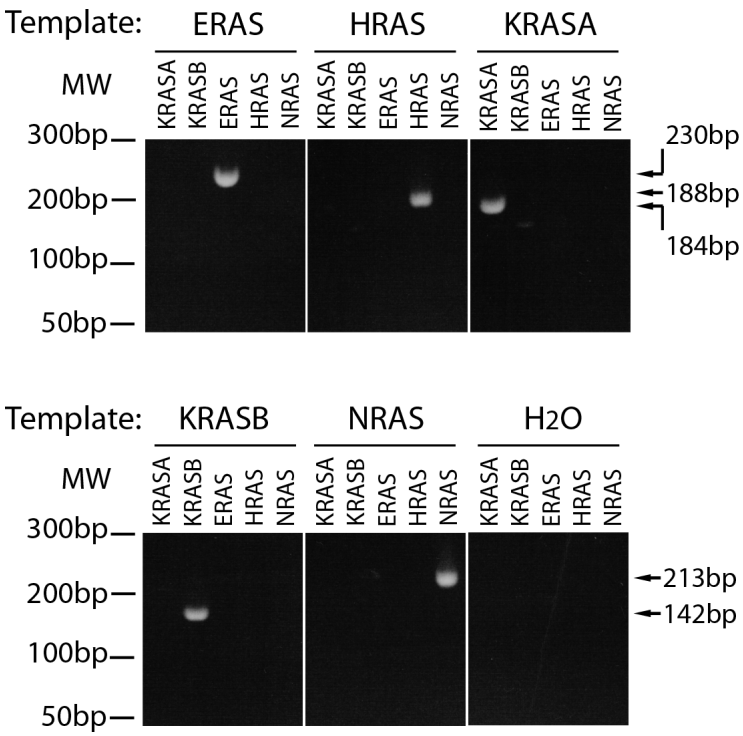

Fig. 3.7 Ras isoform primer specificity. Ras isoform-specific primers were used in end-point PCR reactions with 10 pg of each Ras isoform plasmid as DNA template. Nuclease-free water instead of cDNA was used as a negative control for each primer set. The PCR products were run on 2% agarose gels; PCR conditions: 95˚C for 5 mins, 94˚C for 30 sec, 62˚C for 30 sec, 72˚C for 30 sec, 40 cycles. PCR specific products had the following lengths: ERAS – 230bp, HRAS – 188, KRASA – 184bp, KRASB – 142bp, NRAS – 213bp.

3.2.2.4 Primer efficiency

Relative quantification in qRT-PCR relies on the assumption that the amount of DNA product doubles during each PCR cycle, which means the reactions are 100% efficient. To test this assumption, cDNA from undifferentiated mouse R1 ESCs was used to generate a 2-fold dilution series (Fig. 3.8) to measure reaction efficiency, as described in section 3.1.2.3. Fig. 3.8 summarises the linear graph equations, as well as the calculated percent efficiency of qRT-PCR reactions for each Ras isoform primer set. Overall, Ras isoform-specific primers demonstrated good reaction efficiency. Only the HRAS primer pair had >105% efficiency, although no non-specific amplification products were detected by melt curve analysis that might account for this over amplification. Moreover, all experimental data fit well with the regression line, which was represented by a

high coefficient of determination R^2 (above 0.980, Fig. 3.8). In summary, qRT-PCR optimisation for each Ras isoform primer pair gave good results both *in silico* and by empirical testing, which included optimisation of the T_a, primer specificity and reaction efficiency. The next sections will describe the quantitation methods used for qRT-PCR.

A.

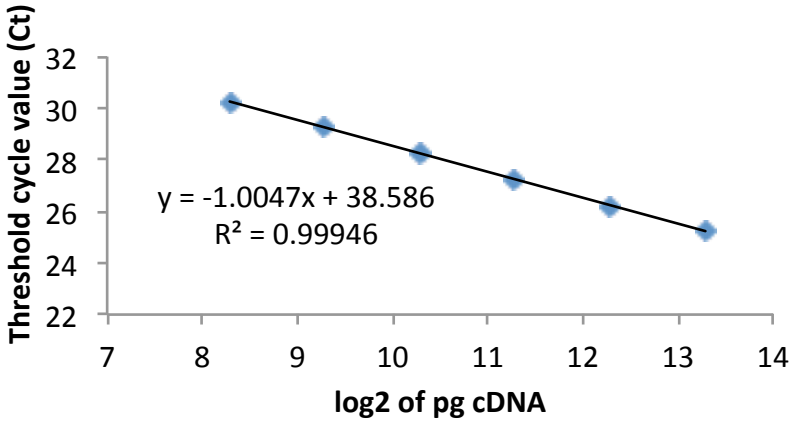

B.

Primers	Ct value range	Equation	R^2	%E
ERas	24-30	y = -1.0047x + 38.586	0.99946	99
HRas	28-34	y = -0.8907x + 40.798	0.99659	118
KRasA	28-34	y = -0.9934x + 41.582	0.98435	101
KRasB	24-30	y = -1.0389x + 37.734	0.99494	95
NRas	24-30	y = -1.0236x + 38.134	0.99921	97

Fig. 3.8 Mouse Ras isoform primer amplification efficiencies. Standard curves were generated on the basis of a 2-fold dilution series of a cDNA template from undifferentiated R1 ESCs p.26 with each Ras isoform primer set. The initial (neat) cDNA amount was 10 ng. After qRT-PCR, the average Ct values of two technical replicates were calculated for each dilution. **A.** An example standard curve graph for ERas primer set. **B.** A summary table for all Ras isoform primers that includes the C_T value range for all dilution points, the linear regression line equations, the coefficients of determination R^2 and the calculated percentage efficiencies %E of amplification. PCR conditions: 95˚C for 5 mins, 94˚C for 30 sec, 62˚C for 30 sec, 72˚C for 30 sec, 40 cycles.

3.2.2.5 Quantification of qRT-PCR results

To absolutely quantify Ras transcript expression, mouse Ras isoform plasmids (section 3.2.2.1) were used in 5-fold serial dilutions to generate standard curves specific for each Ras primer set (Table 3.3). Assuming that one base pair is about 675 Da (the average of the calculated unified atomic mass unit for A-T and C-G base pairs), and knowing that 1 Da = $1.660538921(73) \cdot 10^{-27}$ kg, the mass of a given plasmid molecule and, hence, the plasmid copy number can be calculated. To generate a standard curve, qRT-PCR is performed for template at each dilution and the obtained C_T values are plotted against the logarithm (base = dilution factor) of the starting plasmid quantity as illustrated for a 2-fold dilution series in Fig. 3.8. The best fit line through the data points gives a linear graph equation (Ong and Irvine, 2002, Higuchi et al., 1993). In the case of a 5-fold dilution series, as applied for the mouse Ras plasmids in this study, the expected C_T interval between each dilution point is 2.32 cycles, i.e. the slope of the linear equation would be -2.32, indicating 100% reaction efficiency.

In this study, the efficiency of each standard curve was assessed separately and is discussed in subsequent chapters. To absolutely quantify Ras isoforms in the test samples, the Ras isoform standards were run on each qRT-PCR plate along with the tested samples. The C_T values obtained from the test samples were then compared to C_T values of the standards and the absolute copy numbers were calculated based on the standard curve equation (the best fit line) (Ong and Irvine, 2002).

Table 3.3 5-fold dilution series of mouse Ras isoform plasmid standards. 0.2 ng/µl of each mouse Ras isoform-specific plasmid was used in 5-fold dilution series containing 12 dilution points (standard number). The standards were used in qRT-PCR assays to generate Ras isoform-specific standard curves, which were used to absolutely quantify Ras isoform expression in test samples. The following plasmids were used: pCR4-TOPO-ERas, pCR4-TOPO-HRas, pCR-Blunt II-TOPO-KRas-4A, pCMV-SPORT6-KRas4B, pCR4-TOPO-NRas. Plasmid copy numbers were calculated based on plasmid size in daltons (Da).

Standard number	Plasmid concentration (fg/µl)	Plasmid amount per assay/4 µl (fg)	Plasmid copy number				
			ERas	HRas	KRasA	KRasB	NRas
1	200000	800000	$1.48 \cdot 10^8$	$1.57 \cdot 10^8$	$1.54 \cdot 10^8$	$1.20 \cdot 10^8$	$1.71 \cdot 10^8$
2	40000	160000	$2.96 \cdot 10^7$	$3.15 \cdot 10^7$	$3.08 \cdot 10^7$	$2.39 \cdot 10^7$	$3.42 \cdot 10^7$
3	8000	32000	$5.92 \cdot 10^6$	$6.29 \cdot 10^6$	$6.16 \cdot 10^6$	$4.79 \cdot 10^6$	$6.85 \cdot 10^6$
4	1600	6400	$1.18 \cdot 10^6$	$1.26 \cdot 10^6$	$1.23 \cdot 10^6$	$9.58 \cdot 10^5$	$1.37 \cdot 10^6$
5	320	1280	$2.37 \cdot 10^5$	$2.52 \cdot 10^5$	$2.47 \cdot 10^5$	$1.92 \cdot 10^5$	$2.74 \cdot 10^5$
6	64	256	$4.74 \cdot 10^4$	$5.03 \cdot 10^4$	$4.93 \cdot 10^4$	$3.83 \cdot 10^4$	$5.48 \cdot 10^4$
7	12.8	51.2	$9.48 \cdot 10^3$	$1.01 \cdot 10^4$	$9.86 \cdot 10^3$	$7.66 \cdot 10^3$	$1.10 \cdot 10^4$
8	2.56	10.24	$1.90 \cdot 10^3$	$2.01 \cdot 10^3$	$1.97 \cdot 10^3$	$1.53 \cdot 10^3$	$2.19 \cdot 10^3$
9	0.512	2.048	$3.79 \cdot 10^2$	$4.03 \cdot 10^2$	$3.94 \cdot 10^2$	$3.06 \cdot 10^2$	$4.38 \cdot 10^2$
10	0.1024	0.4096	75.8	80.5	78.9	61.3	87.7
11	0.02048	0.08192	15.2	16.1	15.8	12.3	17.5
12	0.004096	0.016384	3.03	3.22	3.16	2.45	3.51

3.2.2.6 Reference genes for relative quantitation in qRT-PCR

Based on the available literature (discussed in section 3.1.2.5), amongst the various reference genes available, RNA polymerase II (POL2RE) was considered most likely to reflect stable mRNA levels across the murine samples examined in this study.

To test whether POL2RE would be a good reference gene, mouse POL2RE primers were kindly provided by Dr Aleksandra Rak-Raszewska (University of Liverpool) and tested both *in silico* and experimentally, as in previous sections for Ras primer pairs. Primer-BLAST and end-point PCR revealed no non-specific amplification products or primer-dimers for POL2RE primers (Fig. 3.9). T_a optimisation using temperature gradient showed specific amplification at all tested temperatures, with very good amplification at T_a around 62˚C, which was previously chosen to be used for qRT-PCR with Ras primer pairs. Furthermore, reaction efficiency was acceptable and the expression level (C_T value range) of POL2RE was similar to that for the more abundant Ras isoforms in cDNA from undifferentiated ESCs (Fig. 3.10).

A POL2RE-specific plasmid was generated to use as a standard for absolute quantification of POL2RE levels in test samples. As before, the proofreading Pfu polymerase together with POL2RE qRT-PCR primers that amplify a 278 bp fragment was used in end-point PCR with cDNA from undifferentiated mouse R1 ESCs (Fig. 3.11). The correct size product was excised, purified and subcloned into pCR4-TOPO vector, which was then sequence-verified. Finally, the POL2RE-specific plasmid was used in 5-fold dilution series to generate an absolute standard curve for copy number quantification (Table 3.4).

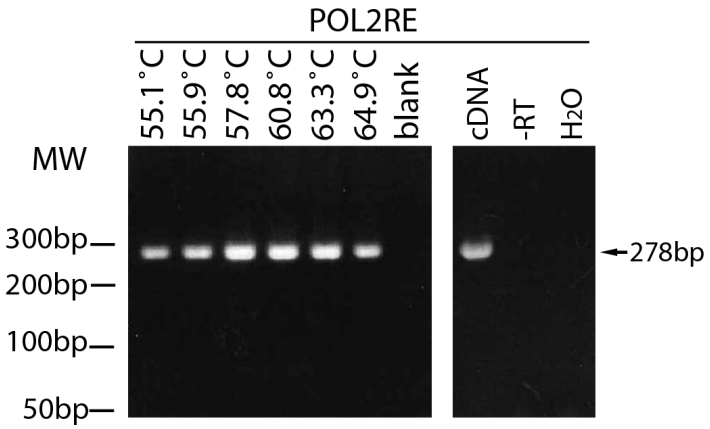

Fig. 3.9 T_a optimisation and primer specificity for mouse POL2RE primers. 20 ng of template cDNA from mouse undifferentiated R1 ESCs, together with POL2RE primers were used in end-point PCR with a T_a gradient of 55-65˚C (left panel). Nuclease-free water instead of cDNA was used as a blank (T_a = 59.0˚C). To further confirm primer specificity, end-point PCR was run at T_a = 62˚C with additional negative control "-RT" (right panel). PCR products were run on a 2% agarose gel and visualised with ethidium bromide. PCR conditions: 95˚C for 5 mins, 94˚C for 30sec, T_a for 30 sec, 72˚C for 30 sec, 40 cycles. Arrow denotes PCR product size. MW – molecular weight markers, POL2RE – RNA polymerase II, bp – base pair.

A.

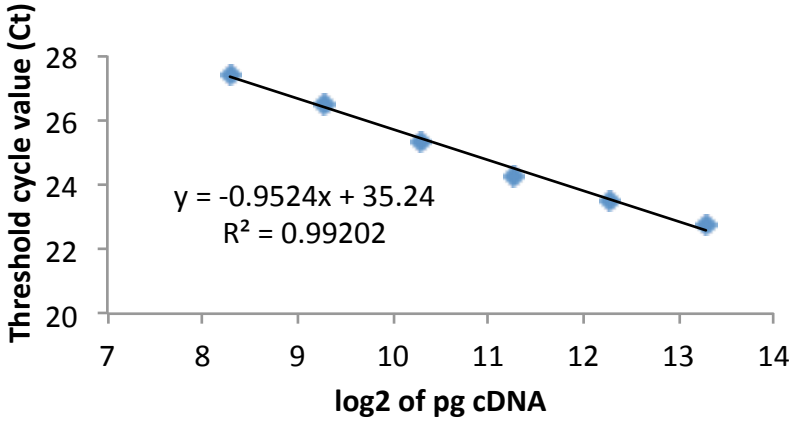

B.

Primers	Ct value range	Equation	R^2	%E
POL2RE	22-28	y = -0.9524x + 35.24	0.99202	107

Fig. 3.10 POL2RE primer amplification efficiency. A standard curve was generated on the basis of 2-fold dilution series of a cDNA template from undifferentiated R1 ESCs p.26 with POL2RE primer set (neat cDNA amount was 10 ng). The average Ct value of two technical replicates was calculated at each dilution. **A.** A standard curve graph for POL2RE primer set. **B.** A summary table for POL2RE reference gene that includes the linear regression line equation, the coefficient of determination R^2 and the calculated percentage efficiency %E of amplification. qRT-PCR conditions: 95˚C for 5 mins, 94˚C for 30 sec, 62˚C for 30 sec, 72˚C for 30 sec, 40 cycles.

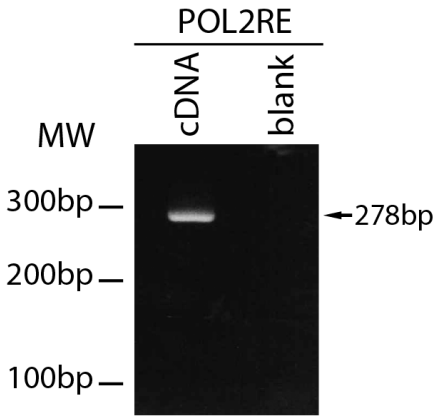

Fig. 3.11 Generation of mouse POL2RE reference gene fragment for subsequent subcloning into pCR4-TOPO plasmid. 40 ng of cDNA from undifferentiated R1 ESCs was used in end-point PCR with POL2RE primers and proofreading Pfu polymerase. Annealing temperature gradient of 55-65˚C was used. PCR products were run on 2% agarose gel and excised, purified and subcloned into pCR4-TOPO. PCR conditions: 95˚C for 5 mins, 94˚C for 30sec, 54.3˚C for 30 sec, 72˚C for 30 sec, 40 cycles. POL2RE – RNA polymerase II, MW – molecular weight marker, bp – base pair.

Table 3.4 5-fold dilution series of mouse POL2RE plasmid standards. 0.2 ng/µl of pCR4-TOPO-POL2RE plasmid was used in 5-fold dilution series containing 12 dilution points (standard number). The standards were used in qRT-PCR assays to generate RNA polymerase II (POL2RE) standard curve, which was used to absolutely quantify POL2RE expression in test samples. Plasmid copy numbers were calculated based on plasmid size in daltons (Da).

Standard number	Plasmid concentration (fg/µl)	Plasmid amount per assay/4 µl (fg)	Plasmid copy number
1	200000	800000	$1.69 \cdot 10^8$
2	40000	160000	$3.37 \cdot 10^7$
3	8000	32000	$6.74 \cdot 10^6$
4	1600	6400	$1.35 \cdot 10^6$
5	320	1280	$2.70 \cdot 10^5$
6	64	256	$5.39 \cdot 10^4$
7	12.8	51.2	$1.08 \cdot 10^4$
8	2.56	10.24	$2.16 \cdot 10^3$
9	0.512	2.048	$4.32 \cdot 10^2$
10	0.1024	0.4096	86.3
11	0.02048	0.08192	17.3
12	0.004096	0.016384	3.45

3.3 Summary and conclusions

In this chapter I have highlighted the careful design and the empirical optimisation of qRT-PCR primer pairs required to enable quantitative evaluation of Ras isoform expression at the transcript level.

The design of primer pairs that span or flank exon boundaries allowed cDNA to be selectively amplified without amplification of any genomic DNA that may contaminate sample preparations. The primer design has also enabled transcripts for each of the Ras isoforms to be clearly discriminated, including the closely related KRasA and KRasB transcripts. This was demonstrated in reactions that tested for cross-amplification by primers from the alternative cloned Ras templates. The expected C_T values for each Ras isoform from ESC mRNA were also determined.

The efficiency of amplification with each of the Ras primer pairs was within an acceptable range to allow quantitative analysis. For absolute quantitation, linearised plasmid dilution series were validated for use as standard curves. For relative quantification, POL2RE was evaluated as a potentially suitable reference gene.

The primers and protocols that were optimised in this chapter will now be used to evaluate Ras isoform expression during mouse ESC differentiation (Chapter 4) and between organ systems during mouse development (Chapter 5).

Chapter 4

Ras isoform expression in mouse embryonic stem cells

4.1 Introduction

4.1.1 Embryonic stem cells (ESCs) and embryoid body (EB) model of early embryogenesis

Embryonic stem cells (ESCs) are pluripotent stem cells derived from the undifferentiated inner cell mass (ICM) of a blastocyst, at day 4 to 5 of a pre-implantation embryo. ESCs that could be cultured *in vitro* were first isolated from the mouse embryo (mESC) in 1981 (Evans and Kaufman, 1981, Martin, 1981). The isolation of human ESCs (hESC) followed almost two decades later in 1998 (Thomson et al., 1998). Both mouse and human ESC are able to self-renew and show no signs of senescence after long-term culture; hence, ESCs are considered to be "immortal" (Evans and Kaufman, 1981, Suda et al., 1987, Brimble et al., 2004, Zalzman et al., 2010).

There is evidence that hESC might be at a higher developmental stage than mESC, as their expression profile more closely resembles mouse epiblast stem cells (mEpiSC), which are derived from the post-implantation embryo (Nichols et al., 2009, Tesar et al., 2007). Developmental stage differences are reinforced by distinct culturing conditions for mESC and hESC. The former are maintained in the undifferentiated state by co-culture on a feeder layer of mouse embryonic fibroblasts (mEFs) and/or by using mouse cytokine leukaemia inhibitory factor (LIF) in the medium (Koestenbauer et al., 2006, Williams et al., 1988). On the other hand, hESC require basic fibroblast growth factor (bFGF) (Xu et al., 2005) and maintenance on mEFs (Humphrey et al., 2004) or on either human-serum matrix or Matrigel with or without a conditioned medium (Koestenbauer et al., 2006, Schatten et al., 2005, Stojkovic et al., 2005). By contrast, bFGF causes differentiation of mESC (Stavridis and Smith, 2003).

Both mESC and hESC are pluripotent cells that are able to differentiate into any cell type of the three germ layers: ectoderm, endoderm and mesoderm. *In vivo*, following transplantation into blastocysts, mESC can support foetal development and produce viable, completely cell culture-derived mice (Nagy et al., 1990, Nagy et al., 1993). *In vitro*, mESC and hESC differentiate into embryoid bodies (EBs), which are cell aggregates that resemble the developing early embryo (Arnold and Robertson, 2009, Doetschman et al., 1985, Itskovitz-Eldor et al., 2000). EBs have been extensively used as a model to study normal embryonic development and early stages of cell lineage specifications (O'Shea, 2004, Robertson, 1987).

To induce spontaneous EB formation, mESC are cultured in suspension in non-adherent dishes in the absence of LIF (Doetschman et al., 1985, Leahy et al., 1999, Murray and Edgar, 2004). Following cell aggregation after 2 days of culture (Murray and Edgar, 2001), the peripheral cells of the EB differentiate into extraembryonic primitive endoderm cells, which recapitulate primitive endoderm (hypoblast) formation *in vivo* from the ICM of a blastocyst (Nadijcka and Hillman, 1974). Fig. 4.1 illustrates the morphology of the EB during the initial steps of spontaneous differentiation (endoderm protocol), employed in this study. Around day 4 of suspension culture, the primitive endoderm cells of the EB start to deposit extracellular matrix (ECM) in the form of a basement membrane (BM) that separates them from the underlying undifferentiated cells (Leahy et al., 1999). This parallels the Reichert's membrane, a thick BM that develops *in vivo* in the peri-implantation embryo from the trophoblast cells (that give rise to the placenta) and primitive endoderm cells (Salamat et al., 1995).

In the EB, the cells underlying the BM become polarised and differentiate into primitive ectoderm epithelium (Li et al., 2001, Murray and Edgar, 2000). The unpolarised cells that do not make contact with the BM undergo programmed cell death, which is coordinated by the BM itself. This process leads to the formation of central cavity, which resembles the proamniotic cavity as seen in the developing embryo (Coucouvanis and Martin, 1995). By day 8 of *in vitro* culture the EBs enlarge and the majority of them transition to cystic EBs

(Doetschman et al., 1985). Continued culture of EBs leads to the differentiation of primitive ectoderm cells into mesoderm that delaminate the BM and grow outside the EB (Fujiwara et al., 2007), which mimics gastrulation *in vivo* (Smyth et al., 1999, Tam and Behringer, 1997). Finally, derivatives of all three germ layers appear in differentiating EBs (Leahy et al., 1999), but any further development ceases after around 20 days of culture (Doetschman et al., 1985).

As opposed to spontaneous differentiation of EBs, in which primitive endoderm differentiation occurs as a first step, other protocols have been developed to specifically induce mesoderm differentiation, in order to study this particular germ line (Fehling et al., 2003, Notarianni and Evans, 2006, Rak-Raszewska et al., 2012). The highest number of mesodermal cells was obtained in a protocol using high concentrations of FCS in IMDM medium (Rak-Raszewska et al., 2012), which was also employed in this study (section 2.4) (Fig. 1, mesoderm protocol). Mesodermal differentiation starts after 2 days in suspension culture and after 4-5 days of differentiation mesodermal cells grow outside of the EB, in which the BM is not visible. The absence of the BM has been shown to accelerate mesoderm differentiation in suspension culture (Fujiwara et al., 2007). From day 7 of mesoderm differentiation, primitive endoderm and the BM start to form, which further leads to differentiation of EBs into all three germ layers (Rak-Raszewska et al., 2012).

Taken together, this study examines self-renewing R1 mESCs using the undifferentiation protocol with LIF supplementation and mEF feeder layer, as well as the above-described differentiation protocols. Both endoderm differentiation (spontaneous EB differentiation) and mesoderm differentiation protocols eventually give rise to all 3 germ layers and are summarised in Fig. 4.1.

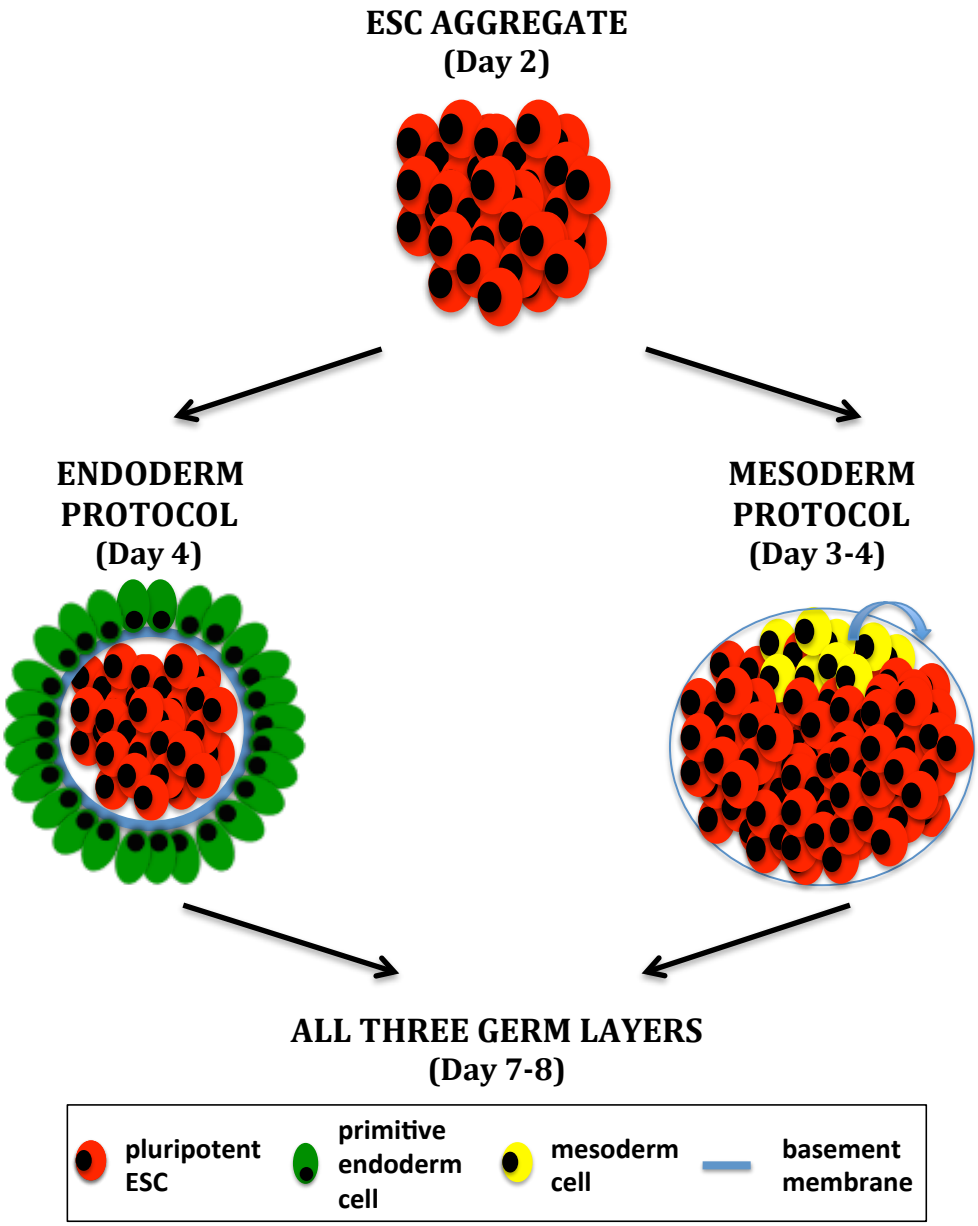

Fig. 4.1 Morphological changes of embryoid bodies (EBs) during differentiation of mouse embryonic stem cells (ESCs). After 2 days of suspension culture using endoderm or mesoderm differentiation protocols, ESCs form aggregates of undifferentiated, pluripotent cells. Around day 4 of endoderm differentiation protocol (spontaneous EB differentiation after withdrawal of LIF from the medium), primitive endoderm differentiates in the periphery of the EB and deposits a thick basement membrane (BM). After 3-4 days of culture using the mesoderm differentiation protocol, mesodermal cell differentiate and migrate outside the EB (blue arrow) and no visible BM is present. Both protocols lead to differentiation of EB into three germ layers, including ectoderm, and cavity formation.

4.1.2 Functions of Ras isoforms in ESCs

Based on a limited number of studies, distinct Ras isoforms play different roles during cellular differentiation. Dominant negative HRas mutant was shown to inhibit nerve-growth factor (NGF)-induced neuronal differentiation of PC12 cells (Szeberenyi et al., 1990). Subsequently, active HRas was shown to be crucial for induction of extraembryonic endoderm differentiation in mouse ESCs, through signalling via the Raf-MEK-ERK pathway (Yoshida-Koide et al., 2004), whereas constitutively active K-Ras was found to enhance self-renewal and proliferation of mouse ESCs in an undifferentiated state (Luo et al., 2007). Also, signalling of activated KRas was shown to be associated with cancer in endodermal stem cells, whereas activated HRas was shown to contribute to endoderm differentiation and growth arrest (Quinlan et al., 2008, Quinlan and Settleman, 2008). However, these studies generally involved overexpression of Ras isoforms rather than studying endogenous protein function. Besides, little is known about isoform-specific Ras effector pathways involved in regulation of stemness/differentiation.

It has been recently discovered that a new Ras isoform, ERas, is solely expressed in mESCs and is responsible for their transforming potential (Takahashi et al., 2003). ERas is constitutively active without mutation and it binds preferentially to downstream PI3K, but not to Raf. *ERas*-null mESCs maintain pluripotency, but display reduced tumourigenicity and growth. These findings may substantiate the importance of Ras isoform-specific signalling, especially in early development. The human *ERAS* homologue, however, contains a premature polyadenylation signal and is not expressed at protein level in hESCs (Kameda and Thomson, 2005).

The Ras isoform-specific differences in affecting self-renewal and differentiation of SCs might be attributed to either distinct functions of individual isoforms or to disparity of timing and/or level of their gene expression in particular cell types (Castellano and Santos, 2011). To investigate the possibility of the latter, this study aimed to determine endogenous expression levels of Ras isoforms in undifferentiated and differentiating R1 mESCs using qRT-PCR to calculate mRNA copy number per cell.

4.2 Results

4.2.1 Establishing ESC culture protocols

Undifferentiated R1 ESCs were cultured on an STO cell feeder layer from which they need to be separated before harvesting for subsequent RNA and protein extraction, as described in section 2.3.6 and illustrated in Fig. 4.2 A. To assess whether the separated ESCs were contaminated with STOs, media with suspended ESCs was plated on a separate gelatin-coated dish and examined under the microscope the following day. Most fields of view showed no or only occasional contaminating STOs (Fig. 4.2 B), which indicated that the cell separation method was successful.

In order to investigate the expression profiles of Ras isoforms during ESC differentiation, R1 mESCs were cultured in suspension using endoderm and mesoderm differentiation protocols (section 2.4). Embryoid bodies (EBs) formed aggregates at day 2 of differentiation (Fig. 4.3). Depending on the protocol, the morphology of EBs had distinct features. By day 4 of the endoderm differentiation protocol, primitive endodermal cells differentiated outside of visible basement membrane (BM) (Reichert's membrane). After this time, cell polarisation and differentiation of primitive ectoderm under the BM occurs (Murray and Edgar, 2000), but this was not visible in the bright field micrographs (Fig. 4.3, day 6 onwards). On day 8, the size of the EBs increased and the cells inside the EB underwent programmed cell death leading to cavity formation (Doetschman et al., 1985), which could be represented by darker areas in the centre of the EB (Fig. 4.3, day 8 onwards). At day 12, visible cell outgrowth appeared in the EB (Fig.4.3, day 12, MESO), indicating differentiation of primitive ectoderm cells into mesoderm (Fujiwara et al., 2007).

During the mesoderm differentiation protocol, extraembryonic endoderm and BM structures did not appear. Instead, mesoderm differentiating EBs were larger than those undergoing endoderm differentiation for the first 6 days of suspension culture (Fig. 4.3). From day 6, EBs became less round and regular in

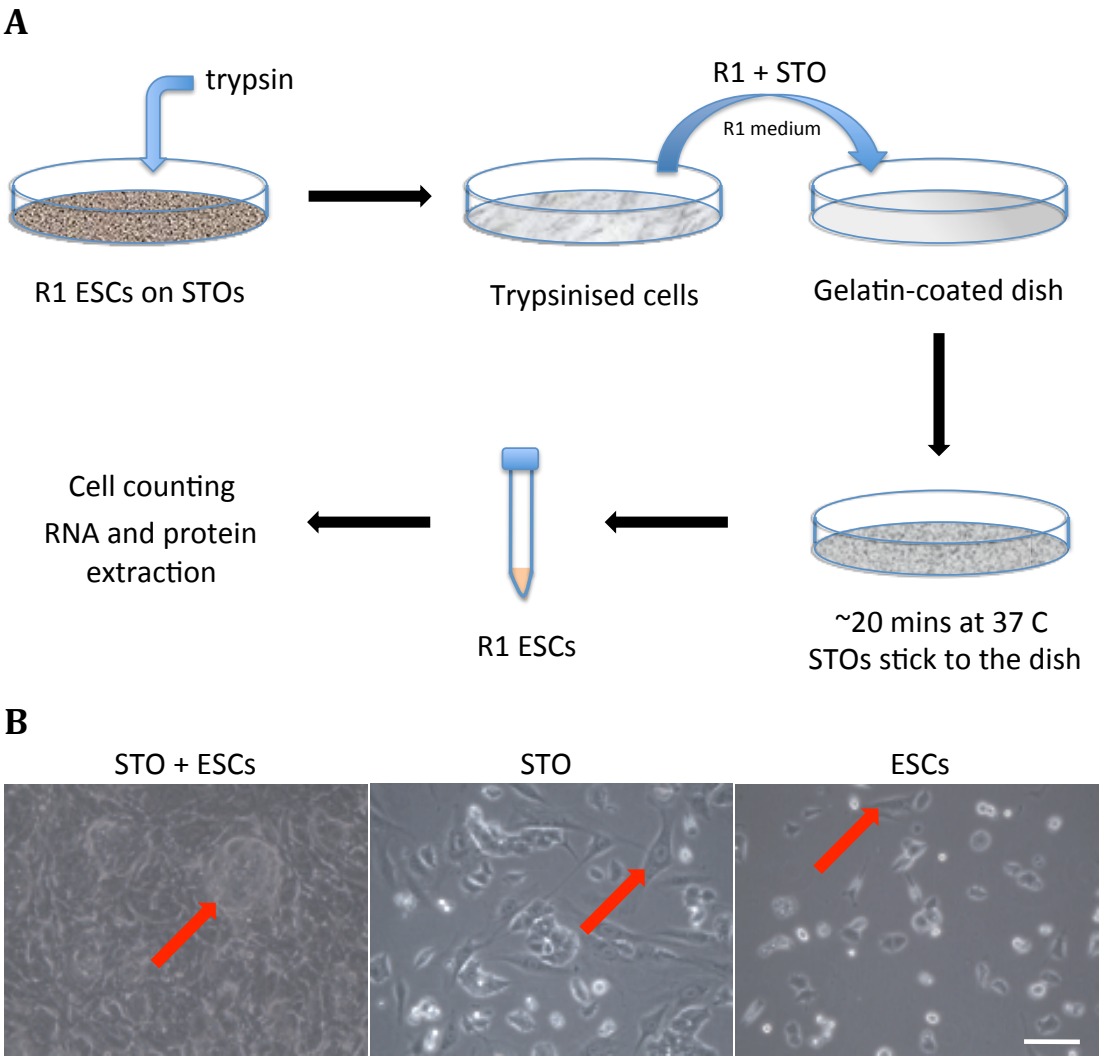

Fig. 4.2 Separation of undifferentiated R1 embryonic stem cells (ESCs) from STO feeder layer cells for cell harvesting. A A schematic representation of a protocol for R1 ESCs separation from STO feeder layer. Trypsinised R1 ESCs grown on STO feeder layer were transferred in R1 medium onto a gelatin-coated dish and incubated at 37°C. After about 20 mins the majority of STO fibroblasts adhered to the dish and the R1 medium with ESCs in solution was transferred to a Falcon tube for subsequent cell counting and RNA and protein extraction. **B** Micrographs showing the efficiency of separation of ESCs from STO feeder layer. **STO + ESCs** represents STO feeder layer with undifferentiated R1 ESCs. Red arrow indicates an ESC colony. **STO** indicates STO on gelatinised plate after R1 ESCs were removed. Red arrow indicates a large STO cell. **ESCs** micrograph depicts R1 cells after separation from STO feeder layer, plated on gelatinised dish. Red arrow indicates a contaminating STO cell. Scale bar = 100 µm

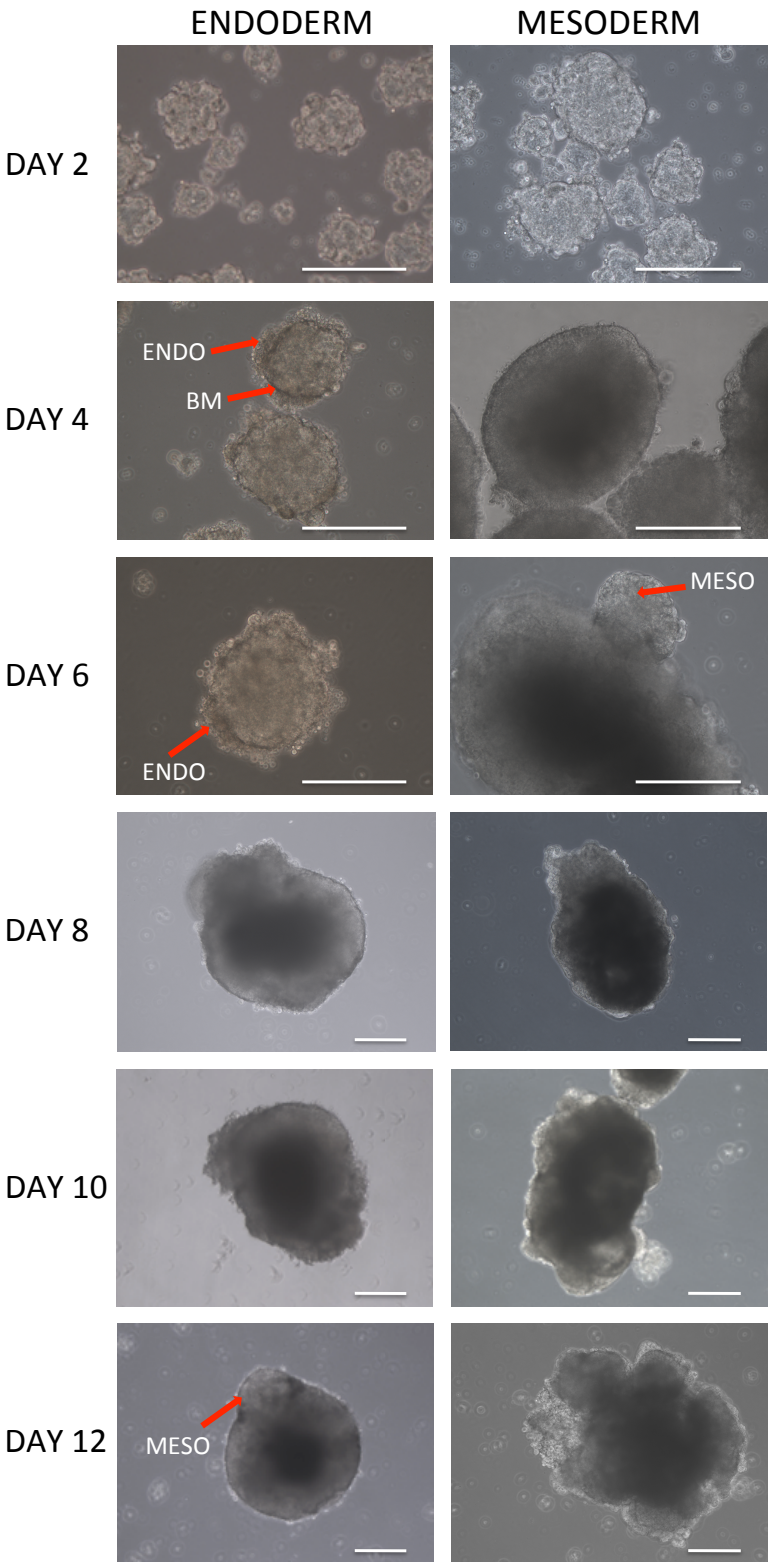

Fig. 4.3 Morphology of mouse embryoid bodies (EB) during differentiation. Representative bright field micrographs for endoderm and mesoderm differentiation protocols of R1 mouse embryonic stem cells (ESCs). During endoderm differentiation, basement membrane (BM) and endodermal cells (ENDO) outside the EB were visible (red arrows). Mesodermal cells (MESO) appeared outside the EB during mesoderm differentiation and later during endoderm differentiation (red arrows). Scale bar = 200 μm.

shape, as mesodermal cells started to differentiate and migrate outside the EB (Fig. 4.3, day 6, MESO). EBs became also more complex, as during this time primitive endoderm and the central cavity start to form, leading to differentiation of all three germ layers (Rak-Raszewska et al., 2012).

Overall, the micrographs of differentiating EBs depicted the formation of distinct morphological features specific for each differentiation protocol. These methods were used for studying early endoderm and mesoderm differentiation to measure Ras isoform transcript levels.

4.2.2 Quality control of RNA from ESCs

To accurately determine the abundance of Ras isoforms at the transcript level in undifferentiated and differentiating R1 ESCs, extracted RNA was quality checked by Nanodrop and agarose gel electrophoresis. Only samples with good yields and absorbance ratio A260/280 nm between 1.8 and 2.0, as well as showing distinct 18S and 28S rRNA bands on agarose gels (Becker et al., 2010) were subsequently used in qRT-PCR experiments. Fig. 4.4 presents the RNA agarose gels for all ESCs samples discussed in this chapter, which fulfilled these quality control criteria. For all samples the 28S rRNA band was approximately twice as abundant as the 18S band, which indicated high integrity of the extracted RNA (Becker et al., 2010). Moreover, there was no evidence of genomic DNA or of degraded RNA.

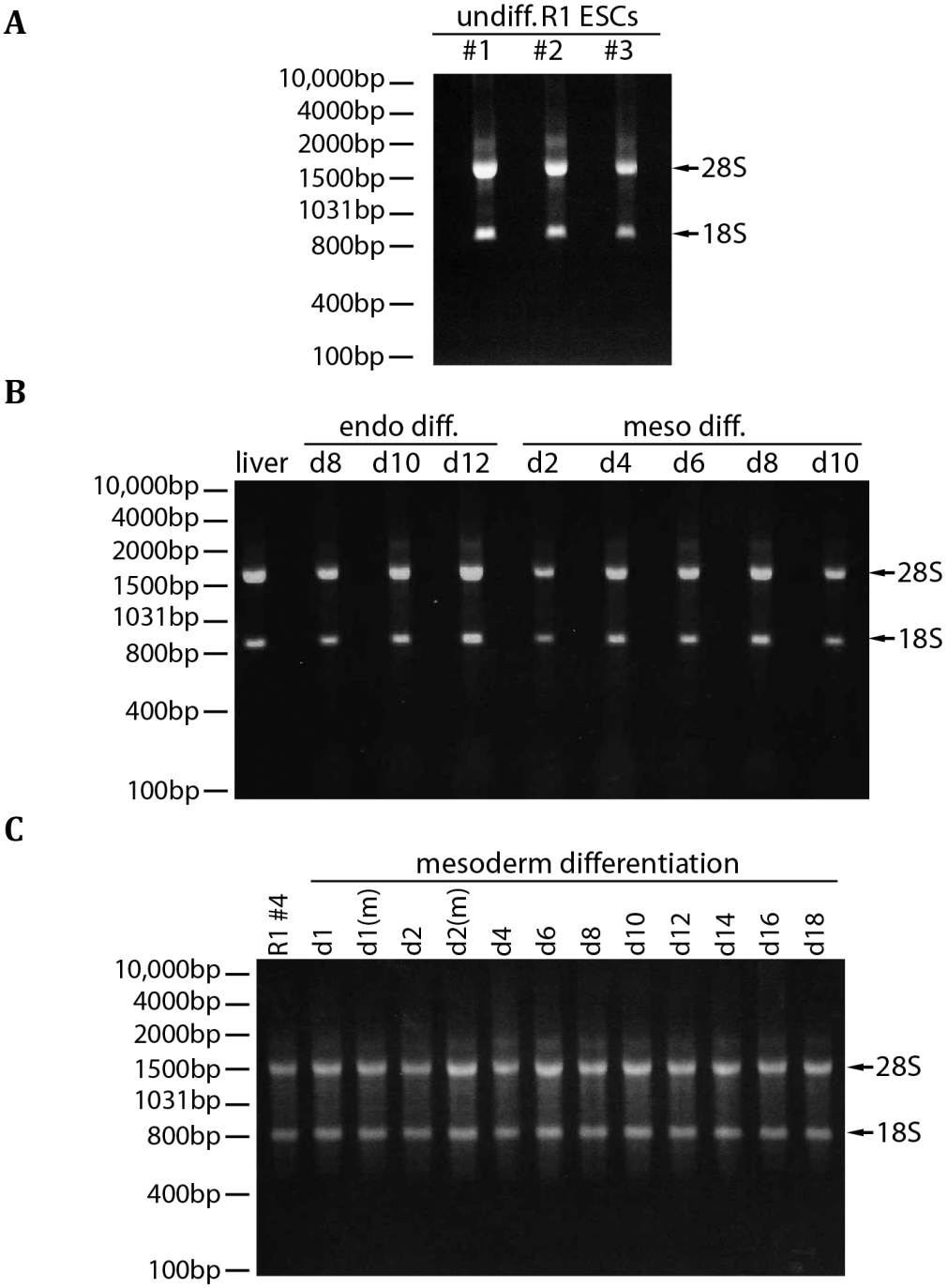

Fig. 4.4 Assessment of RNA quality by agarose gel electrophoresis of mouse R1 ESCs samples. RNA was extracted using Norgen RNA/protein extraction kit and 1µg of RNA was run per lane on 1.2% agarose gel. Two distinct 28S and 18S rRNA bands were visible in each sample, indicated by arrows. **A** RNA from undifferentiated ESCs. #1-3 indicate biological replicates (see text). **B** RNA from ESCs undergoing endoderm and mesoderm differentiation, as well as from mouse liver (E11.5). **C** RNA from undifferentiated and mesoderm differentiating ESCs. bp – base pairs of DNA ladder, undiff. – undifferentiated sample R1 #4 (see text), diff. – differentiation, d – day of differentiation, (m) – pre-differentiation medium, 28S and 18S – rRNA subunits.

4.2.3 Ras isoform transcript expression in undifferentiated R1 mESC

RNA extracted from 4 biological replicates (#1-4) of undifferentiated ESCs (Section 4.2.2) was analysed by qRT-PCR to quantify Ras isoform transcripts. The expression levels of POL2RE reference transcript, determined from the plasmid standard curve, averaged around 6 copies per pg of RNA. However, in one of the biological replicates (#4, used along with differentiation experiment in Fig. 4.7) less than 1 copy per pg of RNA was detected, which was significantly lower than in the remaining samples (7-8 copies/pg) (Table 4.1, Fig. 4.5 B). As the quality of RNA was good in all samples (Fig. 4.4 A and C) and the expression levels and percentage contribution of Ras isoforms across the four biological replicates did not vary significantly (Fig. 4.5 A), the downregulation of POL2RE expression in only one sample was unexpected and may be due to either sample handling error or to fluctuating expression of POL2RE in ESCs colonies. Moreover, percentage amplification efficiency as determined by POL2RE standard curves remained consistent for all replicates at around 77-78% with R^2 values >0.99 (Appendix, Fig. A4.1 and A4.2). Due to this uncertainty, the Ras isoform transcript levels were not normalised to POL2RE reference gene using the ΔC_T method, as this could introduce a bias into the final results.

Instead, the abundance of Ras isoform transcripts was calculated using Ras isoform-specific plasmid standard curves. Table 4.1 and Fig. 4.5 summarise the expression levels of the tested genes in 4 biological replicates of R1 ESCs (#1-4). Transcripts for all Ras isoforms were expressed and are represented as copy number per pg of RNA and copy number per cell. To estimate Ras transcript abundance per undifferentiated ESC, the average total RNA content per cell was calculated based on the number of cells used for RNA extraction and the RNA yields, and was approximately 20 pg. This value corresponds to previous findings in mouse ESCs (Calabrese et al., 2007).

The most abundant Ras isoform was KRasB with about 3 transcripts per pg of RNA (57 copies per cell), followed by NRas with almost 1.5 copies/pg (29 copies

per cell) and ERas with about 1 copy/pg (20 copies per cell). The least abundant Ras isoforms were HRas and KRasA, with 0.1 and 0.04 copies per pg of RNA, respectively, equivalent to just over 2 copies per cell and less than 1 copy/cell. Total Ras transcripts (pan Ras) levels added up to around 5.5 transcript copies per pg of RNA, which was equal to 109 copies per cell.

Table 4.1 Ras isoform and reference gene RNA polymerase II (POL2RE) transcript levels in undifferentiated mouse R1 ESCs. qRT-PCR was performed on 4 biological replicates of cDNA from undifferentiated R1 ESCs (R1 #1 – 4). Absolute expression levels were obtained by interpolation of plasmid standard curves, which were specific for each tested transcript and the average and standard deviation (SD) were calculated. The estimated copy number per cell (shown in parentheses) was based on the total RNA content per cell. Pan Ras – the sum of all Ras isoforms.

	Copy number per pg RNA (Estimated copy number per cell)						
Sample number	**ERas**	**HRas**	**KRasA**	**KRasB**	**NRas**	**Pan Ras**	**POL2RE**
R1 #1	1.152 (23.0)	0.091 (1.8)	0.024 (0.5)	2.284 (45.7)	1.496 (29.9)	5.047 (100.9)	7.880 (157.6)
R1 #2	1.249 (25.0)	0.111 (2.2)	0.026 (0.5)	3.900 (78.0)	1.579 (31.6)	6.865 (137.3)	8.168 (163.4)
R1 #3	0.975 (19.5)	0.089 (1.8)	0.019 (0.4)	2.863 (57.3)	1.763 (35.3)	5.709 (114.2)	7.821 (156.4)
R1 #4	0.604 (12.1)	0.185 (3.7)	0.073 (1.5)	2.436 (48.7)	0.956 (19.1)	4.254 (85.1)	0.712 (14.2)
average	0.995 (19.9)	0.119 (2.4)	0.036 (0.7)	2.871 (57.4)	1.448 (29.0)	5.469 (109.4)	6.145 (122.9)
SD	0.284 (5.7)	0.045 (0.9)	0.025 (0.5)	0.729 (14.6)	0.347 (6.9)	1.104 (22.1)	3.625 (72.5)

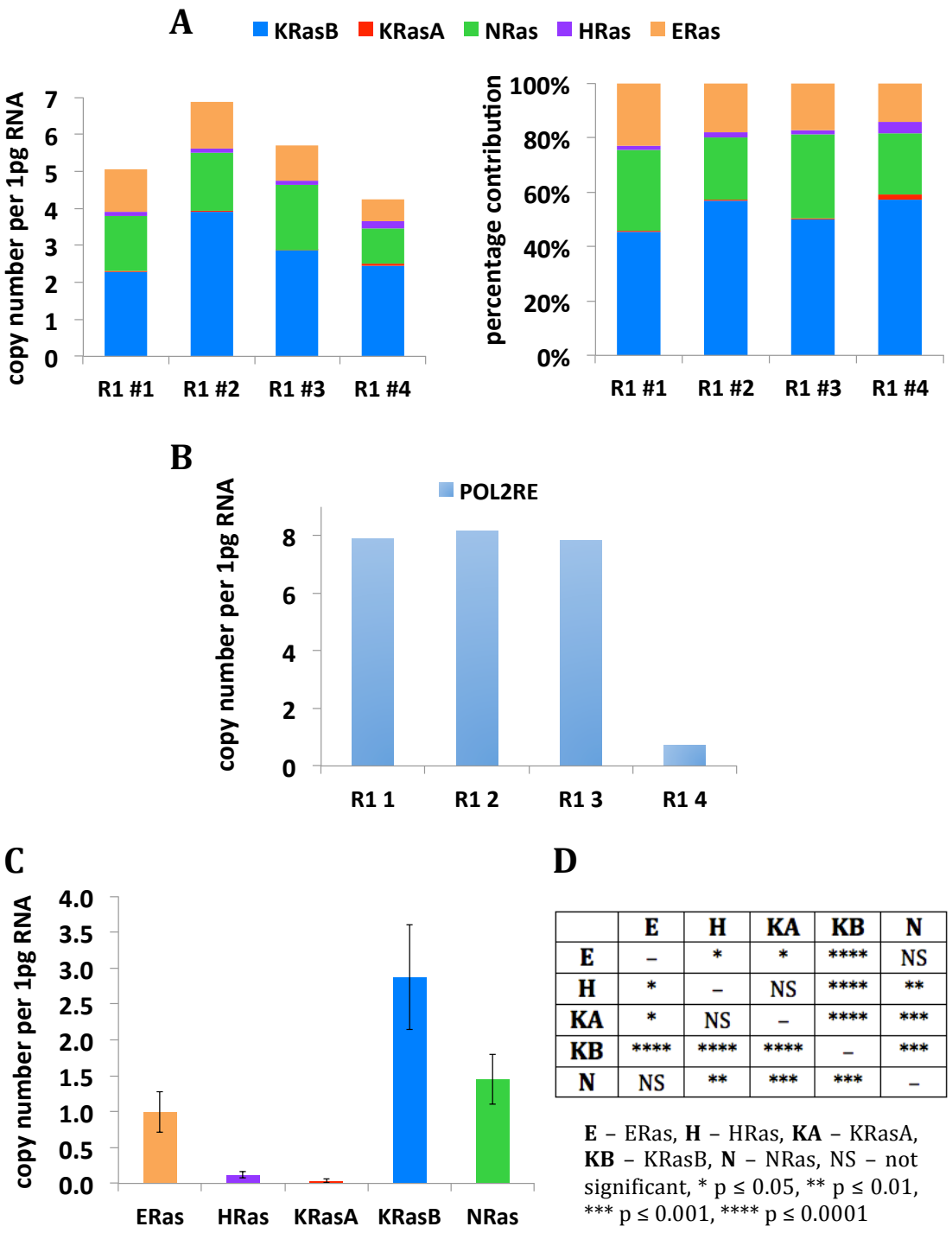

	E	H	KA	KB	N
E	–	*	*	****	NS
H	*	–	NS	****	**
KA	*	NS	–	****	***
KB	****	****	****	–	***
N	NS	**	***	***	–

Fig. 4.5 Ras isoform transcript abundance in undifferentiated R1 ESCs. qRT-PCR using Ras isoform-specific primers or reference gene POL2RE primers was performed on cDNA obtained from undifferentiated mouse R1 ESCs. Absolute copy numbers were calculated by interpolation of transcript-specific plasmid standard curves. **A** Ras isoform and **B** reference gene RNA polymerase II (POL2RE) transcript levels in each of 4 biological replicates of R1 ESCs (#1-4). **C** Average expression levels ± SD (n = 4) of Ras isoforms in undifferentiated R1 ESCs. Data in **C** was analysed by one-way ANOVA with Tukey's post hoc test and summarised in **D.**

4.2.4 Ras isoform transcript expression in differentiating R1 mESCs

In an initial experiment, embryoid bodies were harvested every two days until day 12 of differentiation. RNA from samples harvested at day 12 and before day 8 for mesoderm and endoderm differentiation, respectively, had ethanol contamination and gave poor RNA yields, hence, was not used for qRT-PCR analysis. The remaining samples from differentiating ESCs were quality checked using agarose gel electrophoresis (Fig. 4.4 B). RNA from mouse liver at embryonic day E11.5 was used as a reference of a tissue of endodermal origin (Friedman and Kaestner, 2011) to compare Ras isoform expression during endoderm differentiation.

Overall, during mesoderm differentiation this representation of the data suggests a decline in expression of all Ras isoforms, except for NRas, the levels of which were fluctuating (Fig. 4.6). As ERas isoform is only expressed in undifferentiated ESCs (Takahashi et al., 2003), its diminishing expression levels over time during mesoderm differentiation indicated a decrease in the number of such cells within the EB. This could further confirm that EBs were becoming more differentiated and the differentiation protocol was working successfully.

Ras isoform copies per pg of RNA were similar to Ras isoform expression levels in undifferentiated ESCs (biological replicates #1-3) (Fig. 4.5, 4.6). However, the least abundant Ras isoforms HRas and KRasA appeared to increase (2- and 10-fold, respectively) their expression levels early in mesoderm differentiation (Fig. 4.6, day 2) as compared to the levels in undifferentiated cells (day 0). Over time, however, expression levels returned to those of undifferentiated ESCs (day 10).

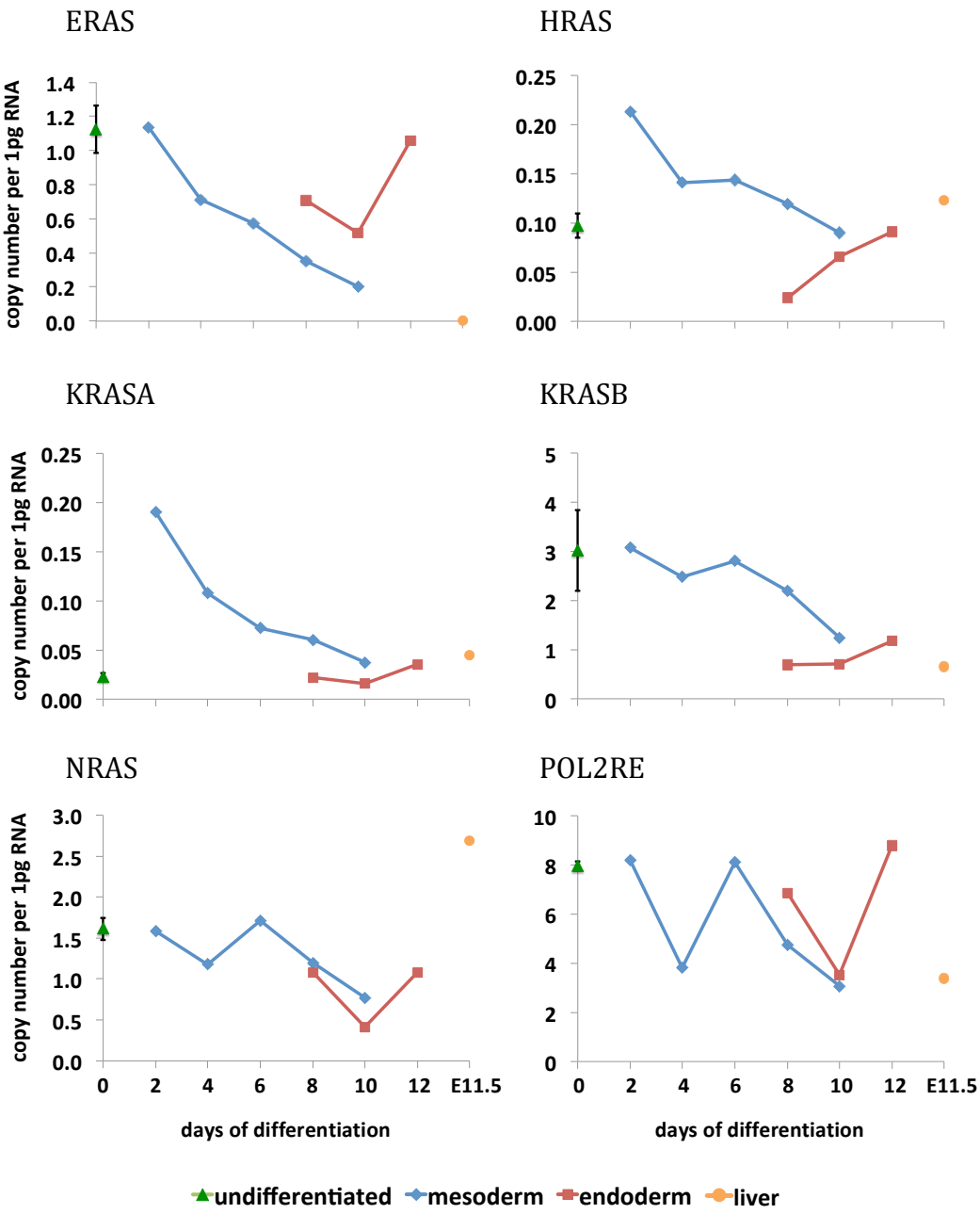

Fig. 4.6 Ras isoform transcript expression during endoderm and mesoderm differentiation of mouse ESCs. Copy number of Ras isoforms ERas, HRas, KRasA, KRasB, NRas, as well as reference gene RNA polymerase II (POL2RE) were calculated based on qRT-PCR using standard curves. cDNA was derived from undifferentiated (day 0 of differentiation, in triplicate) and differentiating (days 2-12, single experiment) R1 mouse ESCs and from mouse embryonic liver (E11.5). Differentiating cells were obtained from embryoid bodies following either mesoderm or endoderm differentiation protocols. Error bars for day 0 represent SD.

In contrast, due to the fact that the endoderm differentiation experiment had only three time points, it was difficult to identify any robust trends (Fig. 4.6). Interestingly, however, in embryonic liver, there was no detectable expression of ERas, which further confirmed that its expression is restricted to mESCs (Takahashi et al., 2003).

To replicate this initial experiment and investigate the expression profiles of Ras isoforms later in mesoderm differentiation, EBs were harvested from day 1 until day 18 of differentiation. Absolute quantification by qRT-PCR suggested that the expression of all Ras isoforms increased on day 1 of mesoderm differentiation as compared to undifferentiated cells (biological replicate #4) and showed large fluctuations in transcript levels throughout the course of the experiment (Fig. 4.7). Reference gene expression was fluctuating over time during differentiation (Fig. 4.6 and 4.7) and, hence, it was impossible to normalise the data using the ΔC_T method (section 3.1.2.4). Thus, fluctuations in expression levels may imply varying amounts of input RNA.

To control for this possibility, the results were "internally normalised" to show the percentage contribution of Ras isoform transcripts to the total Ras expression (Fig. 4.8). This way of representing the data now revealed a consistent pattern of Ras isoform contribution throughout mesoderm differentiation in both experiments. During endoderm differentiation relative isoform contribution was markedly different compared to mesoderm differentiation protocol, as the abundance of ERas was proportionally higher at the expense of KRasB levels.

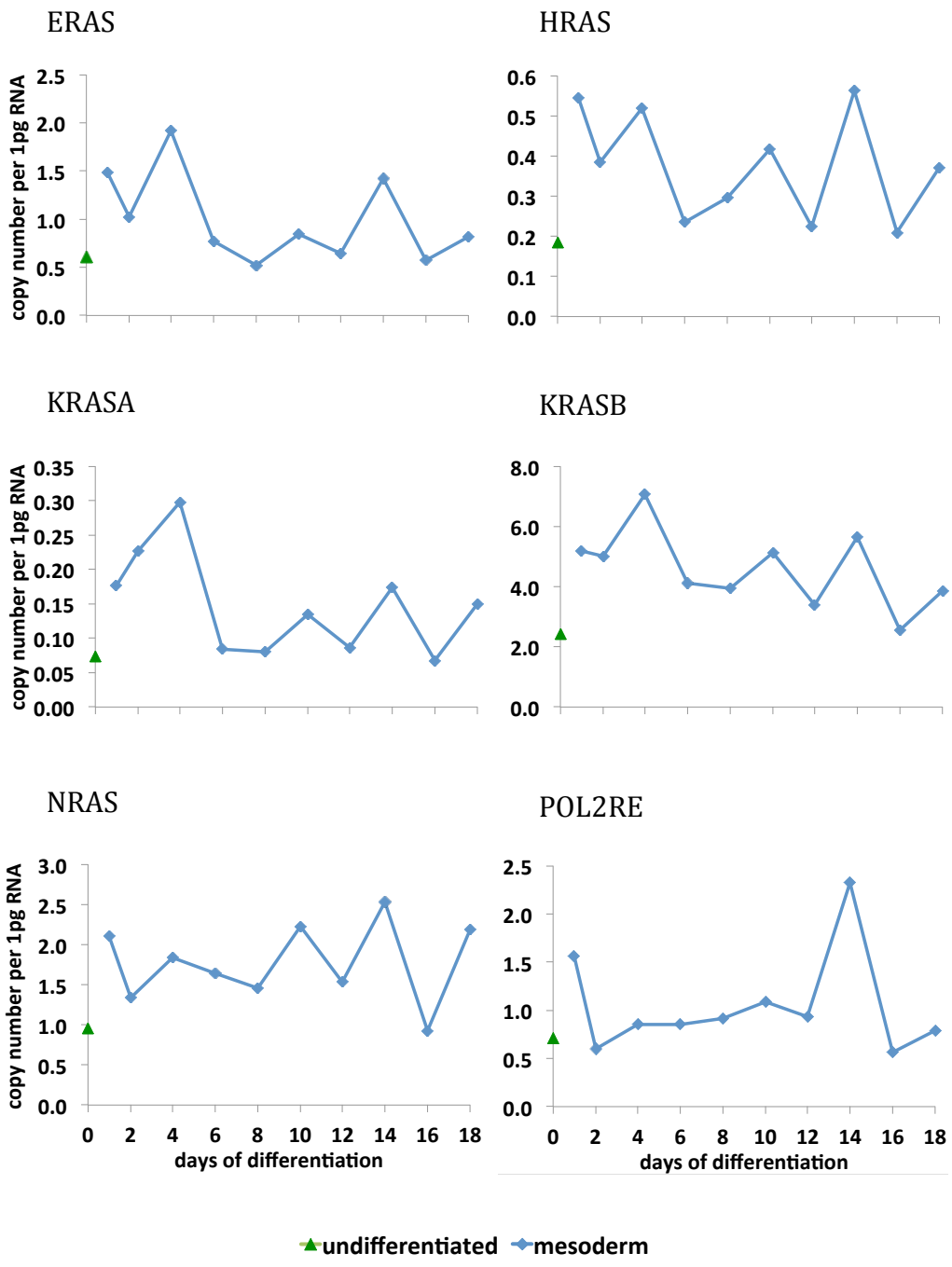

Fig. 4.7 Ras isoform expression during mesoderm differentiation of mouse ESCs. Copy numbers of Ras isoforms ERas, HRas, KRasA, KRasB, NRas, as well as a reference gene RNA polymerase II (POL2RE) were calculated based on qRT-PCR using plasmid standard curves. cDNA was derived from undifferentiated (day 0, R1 #4) and differentiating (days 1-18) R1 mouse ESCs. Differentiating cells were obtained from embryoid bodies following mesoderm differentiation protocol.

During mesoderm differentiation, the percentage contribution of ERas was steadily decreasing over time until day 10 (Fig. 4.8). This again confirms that ERas is expressed exclusively in undifferentiated mESC (Takahashi et al., 2003), which diminish in number as the EB matures. Interestingly, during mesoderm differentiation there was a peak in contribution of KRasA abundance at days 2 and 4 in both experiments.

To sum up, the expression pattern of Ras isoform transcripts during endoderm differentiation was different than that during mesoderm differentiation and in undifferentiated R1 mESCs. During endoderm differentiation, KRasB, NRas and ERas contribution to total Ras was similar at around 30% of total Ras expression. In contrast, during mesoderm differentiation and in undifferentiated mESC, the most abundant isoform was KRasB, with over 50% contribution to total Ras expression levels, followed by NRas (about 30%) and ERas (up to 18%). KRasA and HRas were the least abundant isoforms in both protocols, comprising only up to 4% of all Ras isoform levels.

4.3 Discussion

In this chapter the ESC and EB mouse models of self-renewal and differentiation (Evans and Kaufman, 1981, Leahy et al., 1999, Martin, 1981, Rak-Raszewska et al., 2012) were used to study abundance of Ras isoforms during early stages of mouse development. Methods for extracting RNA from undifferentiated and differentiating R1 ESCs and performing qRT-PCR were successfully optimised. Four biological replicates were analysed from undifferentiated ESCs, however, due to time constraints, only one or two biological replicates of endoderm or mesoderm differentiation protocols were examined. Bearing this in mind, the results of these experiments remain inconclusive, and require further repeats and validation.

The EB model of differentiation is a complex system that resembles early embryonic differentiation (Doetschman et al., 1985, Robertson, 1987) and

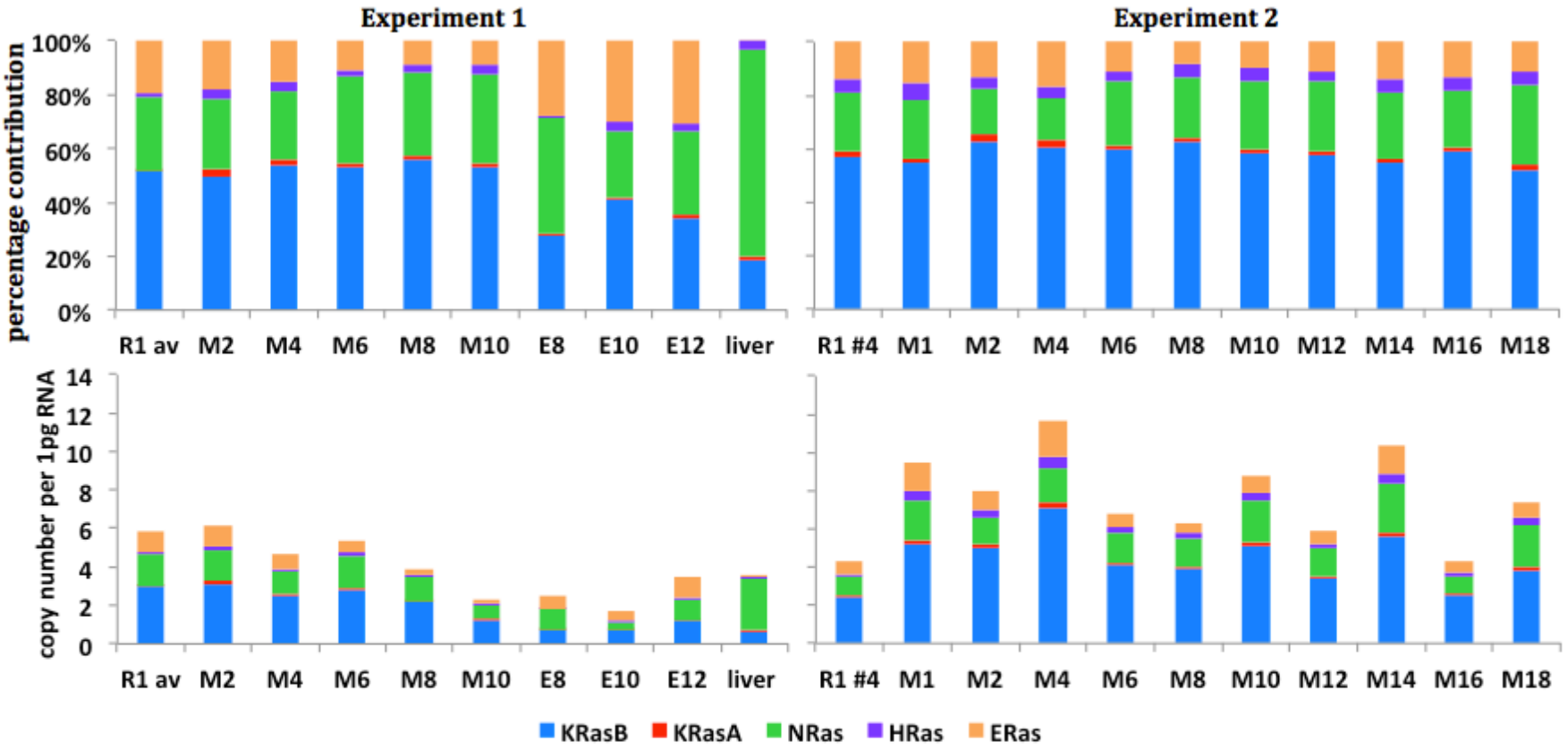

Fig. 4.8 Percentage contribution and total Ras isoform transcript expression in undifferentiated and differentiating mouse ESCs. qRT-PCR was performed on cDNA obtained from undifferentiated (R1 av – mean of R1 samples #1-3; R1#4) and differentiating R1 mESCs undergoing either mesoderm (M; days 1-18) or endoderm (E; days 8-12) differentiation, as well as from E11.5 mouse liver. Absolute copy number was calculated on the basis of Ras isoform-specific plasmid standard curves. Data re-plotted from Fig. 4.6 and 4.7 to "internally normalise" total Ras expression.

comprises cells of all three germ layers (Leahy et al., 1999). Thus, the extracted RNA from the differentiating EBs is not specific for a given germ layer, but it is only enriched in one of them and is generally heterogeneous. Therefore, future work on this model should include separation of germ layers before the RNA extraction step. One of the techniques to employ would be fluorescence activated cell sorting (FACS) that would enable separation of cells expressing a certain lineage marker, as previously done for mesodermal, *Brachyury*-expressing cells (Fehling et al., 2003, Rak-Raszewska et al., 2012). For this purpose, however, a specifically labelled cell line should be used, e.g. Bra-GFP, in which the *Brachyury* locus also expresses the green fluorescent protein (GFP). Similarly, to select neural cells and primitive neurons that derive from ectoderm germ layer, GFP may be expressed from the Tau and nestin enhancer loci (Lenka et al., 2002, Tucker et al., 2001). Definite endoderm (DE) cells, however, can be separated from differentiating mESC using DE-specific surface marker Cxcr4 by FACS (Li et al., 2011, Mfopou et al., 2014).

Another aspect of EB heterogeneity is that a population of undifferentiated cells is usually present, possibly because differentiated cells produce LIF (Rathjen et al., 1990), which supports self-renewal of ESC (Koestenbauer et al., 2006, Williams et al., 1988). On the other hand, ESC maintained in undifferentiated state may spontaneously differentiate in culture (Smith, 2001), again leading to heterogeneous cell populations. Such effect could be controlled by separating undifferentiated cells using FACS sorting based on GFP expressed from Oct4 locus, a transcription factor that controls self-renewal (Ensenat-Waser et al., 2006). Moreover, the STO feeder layer that maintains self-renewing ESCs, could be efficiently removed by magnetic separation using MACS technology and a fibroblast-specific marker mEF-SK4, leaving behind less than 0.15% of contaminating mEFs (Knoebel et al., 2010). These methods could also be employed in obtaining pure cell populations in future studies on Ras abundance in ESC.

Despite these limitations, some preliminary conclusions may be drawn from this study. Undifferentiated mESC express all Ras isoforms, where KRasB is the most abundant transcript, with over 50% contribution to total Ras expression

levels, followed by NRas (about 30%) and ERas (up to 18%) (Fig. 4.5 C). A similar trend is also reflected throughout mesoderm differentiation. Interestingly, ERas expression decreases over time in differentiating EBs, suggesting a gradual loss of self-renewal and stemness potential (Takahashi et al., 2003). During endoderm differentiation, the distribution of KRasB, NRas and ERas is approximately equal and comprises around 30% of total Ras isoform transcripts. KRasA and HRas are the least abundant isoforms in all protocols, comprising only up to 4% of all Ras isoform levels.

The total Ras isoform transcript levels sum up to around 109 copies per ESC, which places Ras isoforms among ~6% of the most abundant transcripts, based on expression data from NIH3T3 mouse fibroblasts (Schwanhausser et al., 2011). According to the same study, which used metabolic pulse labelling, NRas transcripts comprise around 23 copies per cell, close to the median transcript level of 17 copies per cell. In the current study, NRas abundance in undifferentiated ESC was similar and around 29 copies per cell, which supports previous findings. However, the abundance of other Ras isoforms was not quantified in the afore-mentioned study and the data was only available for fully differentiated fibroblasts, which may not be directly comparable to pluripotent and differentiating ESC used in the current study.

More relevant data may arise from the analysis of the transcriptional profile in single mouse blastomeres derived from 2- and 4-cell stage embryos (Tang et al., 2011). In that study, TaqMan RT-PCR detected all Ras isoforms at both developmental stages, apart from ERas, which was only detected in 2-cell stage embryo. That data, however, does not provide any quantitative information about relative transcript abundance, as it was not normalised and presented as C_T values only.

Unfortunately, no previous findings present Ras isoform abundance in ESC in absolute transcript copy numbers. Therefore, to validate the data in this study, more biological replicates of undifferentiated and differentiating mESC should be analysed. As a further confirmation of the results, a panRas primer pair could be designed for qRT-PCR. However, one crucial finding of this work was that

KRasB was the most abundant isoform in almost all analysed mESC samples, apart from endoderm differentiating EBs, in which it was equally expressed with NRas and ERas. This is particularly interesting, as KRasB is the only Ras isoform essential for mouse development (Koera et al., 1997, Nakamura et al., 2008, Plowman et al., 2003). This could indicate that functional differences between Ras isoforms arise from differences in their expression levels and possibly different sites of expression. A previous study demonstrated that HRas can substitute essential functions of KRas, when expressed from its locus, i.e. HRas knock in (KI) mice are viable, but develop cardiovascular problems later in adulthood (Potenza et al., 2005). This gives further evidence that Ras isoform functional difference could be due to differences in the control of gene expression and, hence, also different transcript abundance.

However, current data on Ras expression pattern in mESC does not consider Ras isoform protein levels, which may not directly correlate with trends of transcript abundance. According to NIH3T3 data (Schwanhausser et al., 2011), NRas protein levels were 9 times higher than KRasB protein levels, showing that KRasB was not the most abundant Ras isoform in this cell type. Therefore, future experiments on Ras isoform abundance in mESCs should include proteomics data, for which the timescale of the current study did not allow.

Chapter 5

Ras isoform expression in mouse tissues during development

5.1 Introduction

5.1.1 Ras isoform-specific mutation frequency and role in development

HRAS, *KRAS* and *NRAS*, the genes of the Ras subfamily, represent some of the most frequently mutated proto-oncogenes. The incidence of Ras mutations in all human cancers ranges between 9 to 30%, depending on the database used: COSMIC (v72) (Forbes et al., 2015), cBioPortal (Cerami et al., 2012, Gao et al., 2013), TumorPortal (Lawrence et al., 2014), ICGCDataPortal (v3.8.2.1 - API v1 - d21bce2) (International Cancer Genome et al., 2010), which were sumarised in two recent reviews (Prior et al., 2012, Cox et al., 2014). Although KRas is the most commonly mutated Ras isoform across all tested human tumour samples (86%), the mutation frequency of each Ras isoform is not uniform across different cancer types. KRas mutations constitute almost all Ras mutations in pancreatic and lung cancers and are predominant in multiple myeloma as well as in endometrial, stomach and colorectal cancers (Cox et al., 2014, Forbes et al., 2015). NRas mutations are prevalent in cutaneous melanoma, acute myelogenous leukaemia (AML) and thyroid cancer. HRas mutations are infrequent overall (3%), but they are the most common Ras mutations in head and neck squamous cell carcinoma (HNSCC) as well as in bladder cancer.

The reason why KRas mutations are prevalent in tissues of endodermal origin (pancreas, colon and lung) might be due to the fact that mutated KRas promotes proliferation and maintenance of stem-like properties of endodermal progenitors, therefore leading to expansion of cell populations that carry the mutation (Quinlan et al., 2008, Quinlan and Settleman, 2008). On the other hand, mutated HRas or NRas causes either differentiation of or no effect on endodermal progenitor cells, respectively. An alternative explanation for the

abundance of KRas mutations was suggested recently based on the high frequency of rare codons in KRas (Lampson et al., 2013). This was suggested to result in impaired expression of KRas. Since high expression of Ras protein leads to senescence rather than proliferation, the authors suggested that the lower expression of KRas versus the other isoforms might be advantageous in avoiding this non-productive phenotype when KRas is oncogenically mutated. Hence, more work is necessary to better understand Ras isoform coupling to different human cancers.

The importance of KRas is also highlighted during development, as its KRasB splice variant is the only Ras isoform essential for normal development in the mouse (Koera et al., 1997, Johnson et al., 1997, Plowman et al., 2003). KRas knock out (KO) mice die prenatally between E12.5 and birth due to thin ventricular walls of the heart, motoneuron death in the medulla and the spinal cord and liver defects. However, KO of KRasA-specific exon in inbred and crossbred mice has no effect on growth and development. Interestingly, HRas- or NRas-deficient mice separately exhibit a normal phenotype (Ise et al., 2000, Umanoff et al., 1995). A double knockout of both HRas and NRas loci also yields normal viable mice, further suggesting that both of these Ras isoforms are dispensable for normal mouse growth, development and fertility (Esteban et al., 2001, Nakamura et al., 2008). However, double knockout mice are born at lower than expected Mendelian frequency. This finding may suggest a partial functional overlap of Ras isoforms. Furthermore, although $KRas^{+/-}$ mice (heterozygous for KRas deletion) are viable, $KRas^{+/-}$; $NRas^{-/-}$ mice die during embryonic development or perinatally due to severe anaemia (Johnson et al., 1997). Also, double homozygous mutant $KRas^{-/-}$; $NRas^{-/-}$ or $KRas^{-/-}$; $HRas^{-/-}$ mice die before E9.5 or between E9.5 and E11.5, respectively, suggesting that these phenotypes are more severe than single KRas deletion (Johnson et al., 1997, Nakamura et al., 2008). Altogether, current studies imply that KRas alone is both crucial and sufficient for normal growth and development in mice, but partial functional overlap of other Ras isoforms also exists. HRas knock in (KI) mice, which express HRas from KRas locus and have no detectable KRas, are viable and born at predicted Mendelian ratios, hence showing that HRas can functionally replace KRas during mouse development (Potenza et al., 2005).

However, KRas$^{-/-}$ phenotype is only rescued until adulthood, as HRasKI mice develop later cardiovascular problems, suggesting a KRas-specific role in cardiovascular homeostasis. Similarly, KRas$^{-/-}$ phenotype can be rescued by a HRas human transgene, which encodes human HRas protein identical to that of mouse protein (Nakamura et al., 2008). The transgene is also able to functionally substitute all three *Ras* genes in *Ras* triple mutant mice (KRas$^{-/-}$; NRas$^{-/-}$; HRas$^{-/-}$).

5.1.2 Ras isoform-specific abundance in normal tissues

Whether Ras isoform functional redundancy seen in the above-described mouse models is due to the pattern and timing of Ras isoform expression, could be better understood by measuring Ras transcript and protein levels in a range of normal mouse tissues and at different developmental stages. Such work could also aid in delineating why KRasB is the key Ras isoform for mouse development (Koera et al., 1997, Plowman et al., 2003) and may explain why certain Ras isoforms couple to specific cancer types (Castellano and Santos, 2011).

Current data from a limited number of studies from both human and mouse suggests that distinct Ras isoforms are not equally abundant across different tissues and cell lines (Fig. 5.13). To compare Ras isoform expression at transcript level, a range of semi-quantitative techniques has been used in previous studies. For example, Northern blotting of mouse mRNA (Leon et al., 1987) allowed for relative comparison of isoform expression across a panel of tissues, derived from both adult and postnatal animals. However, comparison of mRNA levels between the different Ras isoforms was not possible and the study did not account for the two KRas splice variants. On the other hand, studies that aimed at comparing transcript expression levels of KRas splicing isoforms (using Northern blotting and semi-quantitative RT-PCR), did not include the remaining Ras isoforms in their work (Pells et al., 1997, Plowman et al., 2006, Plowman et al., 2003, Wang et al., 2001).

Current data on Ras isoform abundance at protein level in different tissue/cell types is also derived mainly from semi-quantitative methods, such as Western

blotting. Most studies are not comprehensive and only focus on some Ras isoforms or only certain tissues (Nunez Rodriguez et al., 2006, Sithanandam et al., 1998). Our laboratory previously found that Ras isoform-specific antibodies are not very accurate and difficult to work with, and instead, used a panRas antibody and siRNA approach to estimate Ras isoform abundance in Ras isoform knock down (KD) human cancer cell lines (Omerovic et al., 2008). In that study, KRas was observed to be the most abundant isoform across a panel of cancer cell lines.

A more quantitative method to measure Ras protein levels is quantitative mass spectrometry, which was used in previous studies utilising peptide standards. Up-to-date results mostly show conflicting data, in which total Ras abundance ranges over 5 orders of magnitude (<100 to >5,000,000 copies/cell) (Halvey et al., 2012, Nagaraj et al., 2011, Ruppen-Canas et al., 2012, Schwanhausser et al., 2011, Wang et al., 2011). However, these methods did not account for the inefficiencies linked to antibody-based enrichment, sample handling or proteolysis. Together, these studies do not give a fully comprehensive comparison of all Ras isoforms and use mainly semi-quantitative methods, often leading to contradicting results (Fig. 5.13). Moreover, most of the data comes from adult tissues or cell lines, missing the developmental outlook on Ras isoform expression during embryogenesis and postnatal development. Therefore, the aim of the current study is to provide a complete comparative map of all four major Ras isoform expression profiles across different tissue types as well as between the isoforms. The expression profiles are to be measured at different developmental time points using a mouse model. Also, as transcript expression levels do not necessarily reflect protein abundance (Schwanhausser et al., 2011), it is important to measure both mRNA and peptide levels. The quantitative methods used in this study comprise qRT-PCR (Chapter 3 describes method development), for measuring absolute transcript copy number, and mass spectrometry (MS) with protein standard absolute quantification (Mageean et al., 2015) to estimate protein copy number in SW48 colorectal cancer cell lines isogenic for Ras. In combination, they will allow the

first comparative analysis of absolute transcript and protein abundance between Ras isoforms.

5.2 Results

5.2.1 Expression studies using a mouse model

A model of normal mouse development (Fig. 5.1) was used to obtain three biological replicates of a range of tissues: brain, liver, lungs, heart, stomach, intestine, kidneys, skin and skeletal muscle. A widely used outbred strain of CD1 mice was chosen due to a good breeding performance and to reflect the heterogeneity found in the wild mice (Aldinger et al., 2009, Chia et al., 2005). Hence, CD1 strain was likely to reflect a generic mouse Ras expression profile.

During mouse embryonic development and at birth, tissues were harvested from separate litters at embryonic days (E) 11.5, 13.5, 16.5 and at postnatal day (P) 0 (birth). During postnatal development, pups were sacrificed from the same litters at P5, P10, P15, P20, P25 and P30, as well as their corresponding mothers. Therefore, biological replicates for the embryonic tissues represent pools of individuals from a single litter. Whereas the biological replicates for the postnatal samples represent separate litters where littermates represent each time-point. The adult sample is the mother from the cognate post-natal litter. Three biological replicates representing litters and mothers for each tissue type were analysed in this study to measure Ras isoform transcript abundance. In total, there were 27 individual mouse adult tissue samples and 240 pooled or individual tissue samples collected throughout mouse development. Pooled samples always represented distinct litters and were only collected when individual tissue samples were lighter than 10 mg (section 2.6). Mouse protein samples were first collected alongside RNA using the Norgen kit for simultaneous extraction of RNA and protein (section 2.7.8 and 2.8.2).

The rationale behind choosing 11 developmental stages in the mouse in this study, was to represent the best possible range of developmental changes, starting from the earliest time point, from which accurate manual collection of

distinct tissues/organs was possible. The first developmental stage of mouse development chosen for this study was E11.5, at which the mouse embryo has 43-48 pairs of somites and the buds of most major organs have already developed (brain, heart, liver, lungs, stomach) and are distinguishable (Kaufman, 1992). The developmental changes during mouse embryogenesis and postnatal period are described in detail in the introduction (section 1.1.4.2.1).

Most importantly, it has been known that KRas-deficient mice die prenatally between E12.5 and birth (Koera et al., 1997). Hence, in this study, tissues were collected from developmental time points before, during and after this lethal stage (time points: E11.5, E13.5, E16.5, P0 and P5, Fig. 5.1). Also, abnormally thin ventricular walls of the heart were observed in $KRas^{-/-}$ mouse embryos at E15.5, but not at E13.5 (Koera et al., 1997). Therefore, it was of interest to measure Ras isoform expression in the embryonic heart. Skeletal muscle tissue was used to compare Ras levels to those in cardiac muscle. The remaining tissues were chosen in order of Ras isoform mutation frequency: lungs, stomach, intestine and kidneys are the sites of cancers with frequent KRas mutations, while brain and skin are the equivalent sites for NRas and NRas/HRas mutations, respectively.

5.2.2 Extraction and quality control of RNA from mouse tissues

Mouse tissues were collected at 11 developmental time points (section 5.2.1) and RNA was extracted using Norgen extraction kit (section 2.7.8). RNA was then quality checked by Nanodrop and agarose gel electrophoresis (Fig. 5.2 and Fig. 5.3). Almost all samples fulfilled quality control criteria by showing distinct 18S rRNA bands on agarose gels (Palmer and Prediger, 2014) and no genomic DNA or other contaminants (adult intestine and P5 liver in Fig. 5.2 and adult skeletal muscle in Fig. 5.3 have very faint 18S rRNA band). RNA from each tissue from three biological replicates representing distinct litters and mothers were subsequently used in cDNA synthesis and qRT-PCR to determine Ras isoform transcript copy number.

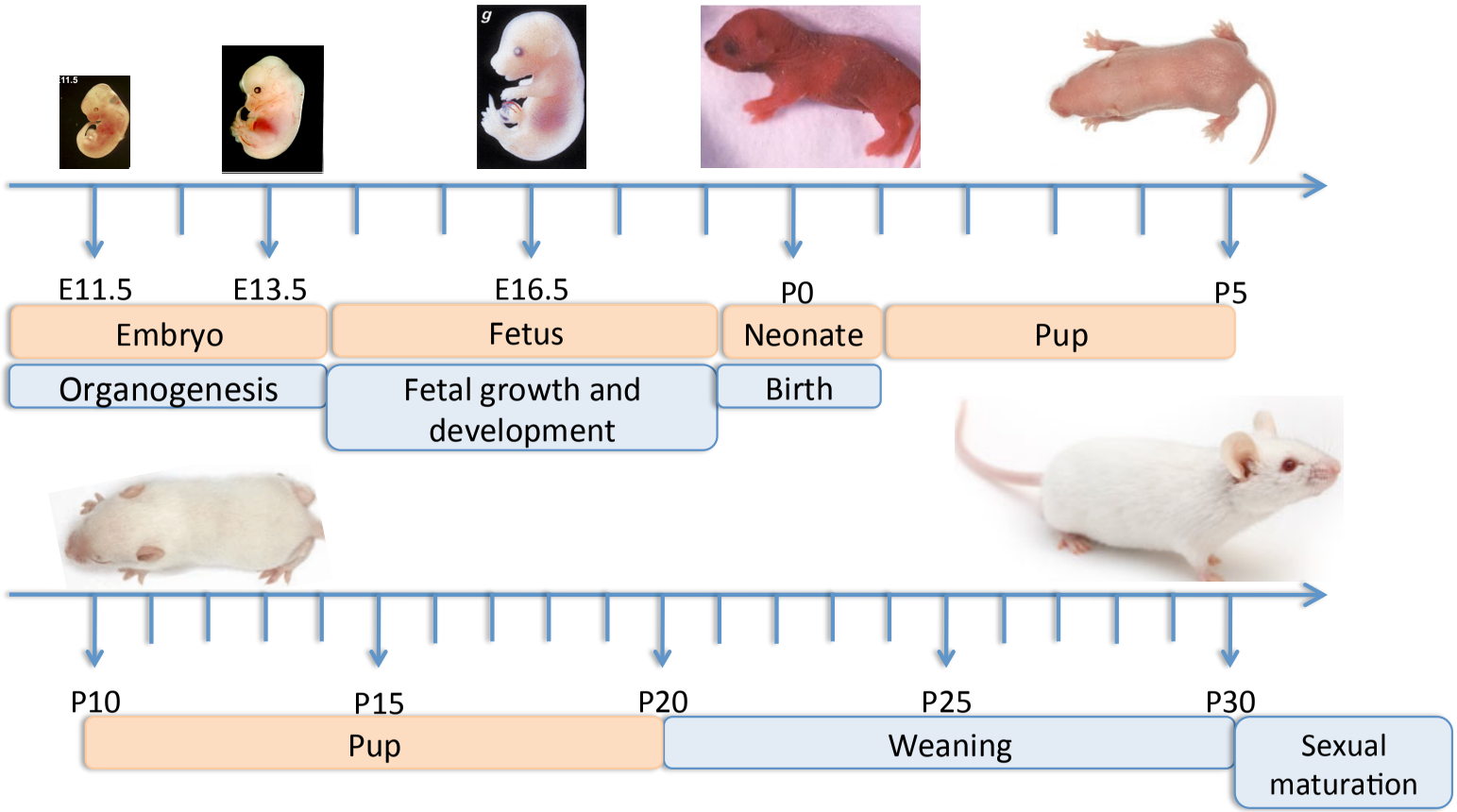

Fig. 5.1 Developmental time points at which mouse tissues were harvested for analysis of Ras abundance. Separate litters were sacrificed at embryonic days (E) E11.5, E13.5, E16.5 and postnatal day (P) P0, whereas pups from days P5 to P30 were obtained from the same litter together with the mother. Three biological replicates representing distinct litters and mothers were obtained and organs were harvested from each individual animal for analysis of Ras isoform abundance.

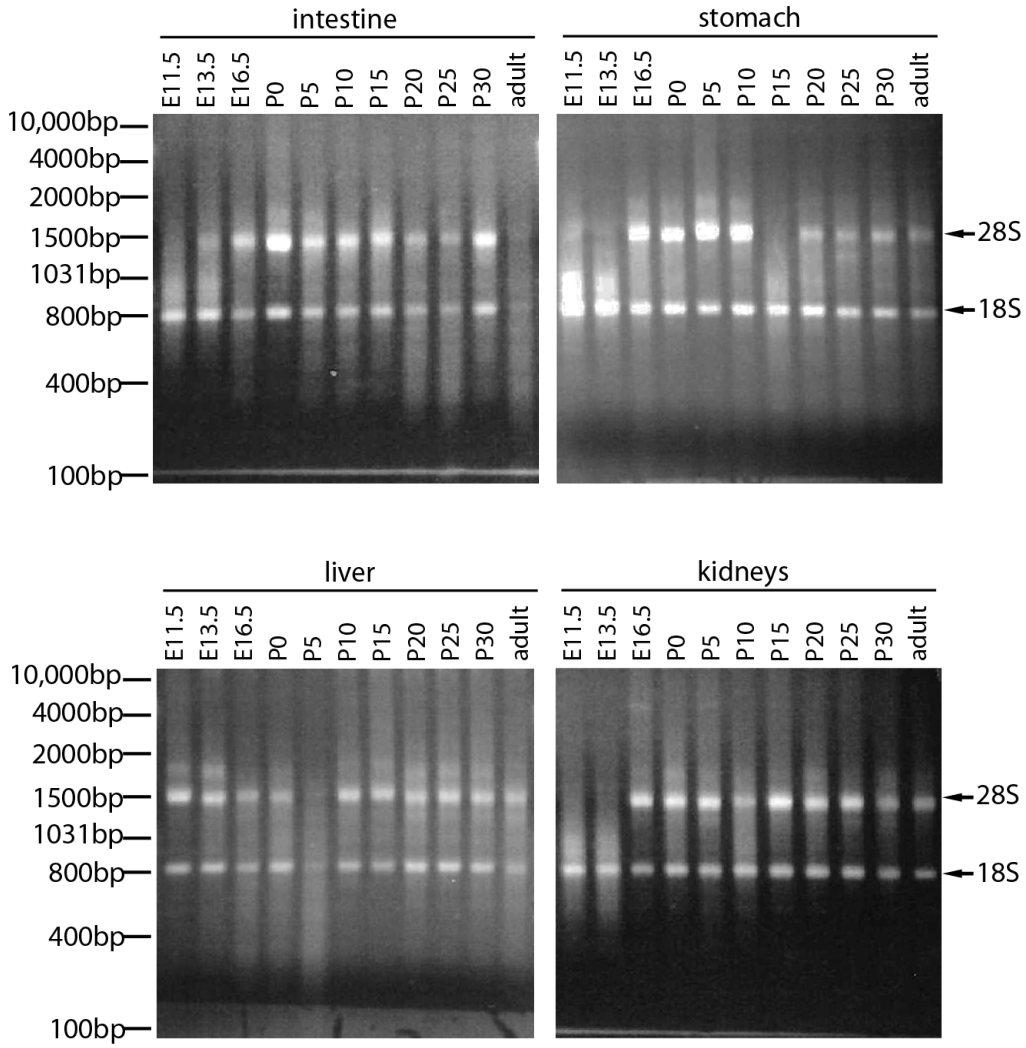

Fig. 5.2 Assessment of RNA quality by agarose gel electrophoresis of mouse tissues: intestine, stomach, liver and kidneys, throughout development. RNA was extracted using Norgen RNA/protein extraction kit and 1µg of RNA was run per lane on 1.2% agarose gel. Two distinct 28S and 18S rRNA bands are indicated by arrows. The figure is a representative example of three biological replicates of tissues harvested from the same litter and the corresponding adult mothers. E – embryonic day, P – postnatal day, bp – base pairs, 28S and 18S – rRNA subunits.

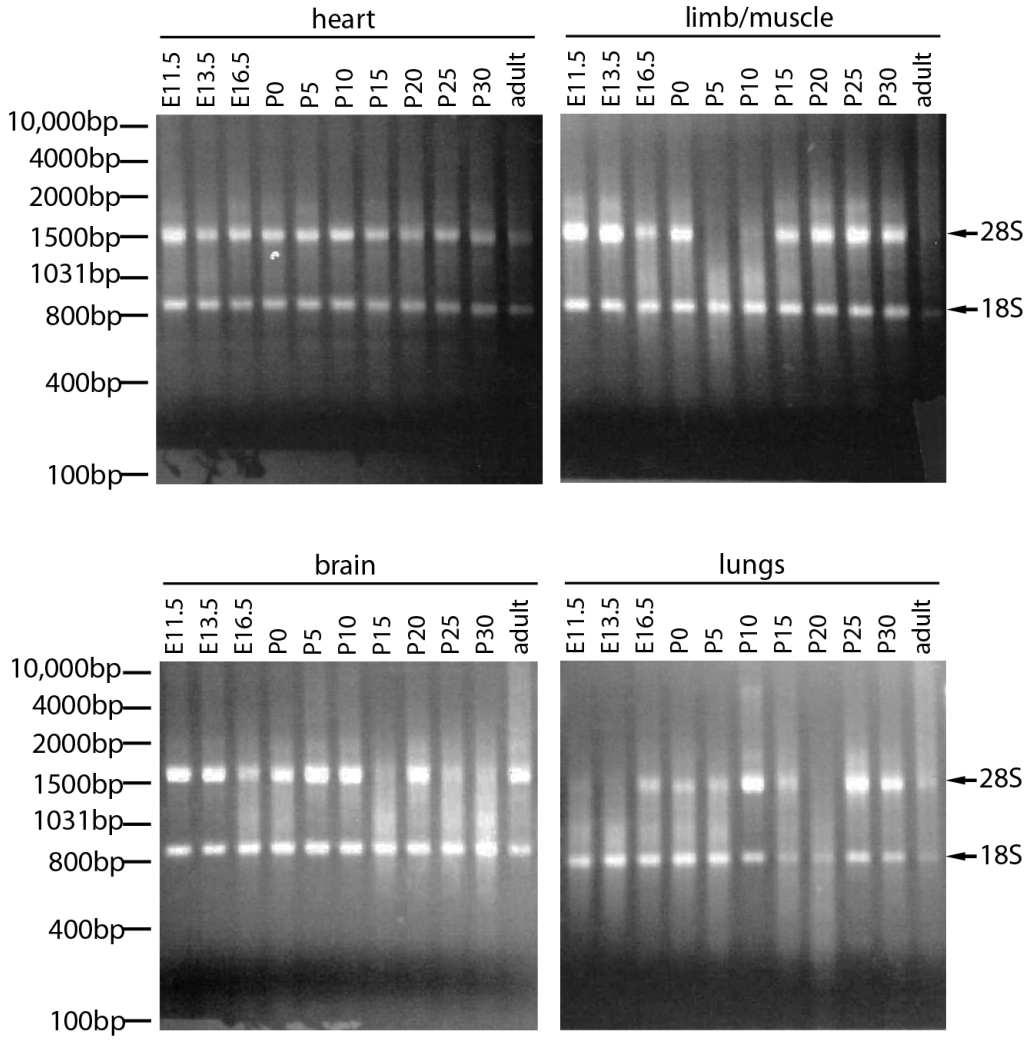

Fig. 5.3 Assessment of RNA quality by agarose gel electrophoresis of mouse tissues: heart, limb/muscle, brain and lungs, throughout development. RNA was extracted using Norgen RNA/protein extraction kit and 1µg of RNA was run per lane on 1.2% agarose gel. Two distinct 28S and 18S rRNA bands are indicated by arrows. The figure is a representative example of three biological replicates of tissues harvested from the same litter and the corresponding adult mothers. Limb/muscle denotes either limb harvested on E11.3 and E13.5 or skeletal muscle harvested on the remaining developmental time points. E – embryonic day, P – postnatal day, bp – base pairs, 28S and 18S – rRNA subunits.

5.2.3 Absolute transcript copy number of Ras isoforms in mouse adult tissues and during development

Ras isoform transcript levels were quantified by qRT-PCR in three biological replicates (representing distinct litters and mothers) of RNA from a panel of mouse adult tissues: brain, thymus, oesophagus, lung, heart, skeletal muscle, skin, intestine, stomach, liver, spleen, kidney, adrenal gland, bladder, uterus and ovary. The copy number of individual Ras isoforms was calculated across all biological replicates using a single standard curve with the best amplification efficiency (Appendix Fig. A5.1). This was done to normalise for on-plate differences where some plate-based standard curves exhibited poor PCR efficiency. The total Ras abundance (panRas) was calculated from the sum of all Ras isoform transcripts and was represented as copy number per pg of extracted RNA (Fig. 5.4 A). Overall, panRas transcript abundance across all tested tissue types ranged between 5-110 copies per pg RNA (average 26 copies/pg). Since a typical mammalian cell contains around 20 pg of RNA (Alberts et al., 1994, Copois et al., 2003, Ramskold et al., 2012), panRas transcript levels can be estimated to average approximately 520 copies per cell. The highest Ras transcript levels were found in the murine thymus (around 2200 copies per cell), whereas in the muscle Ras transcript abundance was the lowest (around 110 copies per cell).

The individual Ras isoform contribution to total Ras transcript levels varies across adult tissues (Fig. 5.4 B). Together, both KRasA and KRasB transcripts are the most abundant typically comprising >80% of total Ras, where KRasB is by far the major isoform. Interestingly, the contribution of KRasA transcript levels to total Ras exhibits the highest variation across different tissue types, from <1% in 8 of the 16 adult tissues to 9-20% in the kidney, liver, intestine and stomach. NRas represents on average 15% of total Ras transcript levels (range 6–30%), whilst HRas is in general the least abundant isoform in all tested tissues with an average 1.9% contribution to total Ras transcript levels. In summary, KRas dominates transcript abundance across all adult tissues with KRasB being typically 5-40-fold more abundant than NRas or HRas.

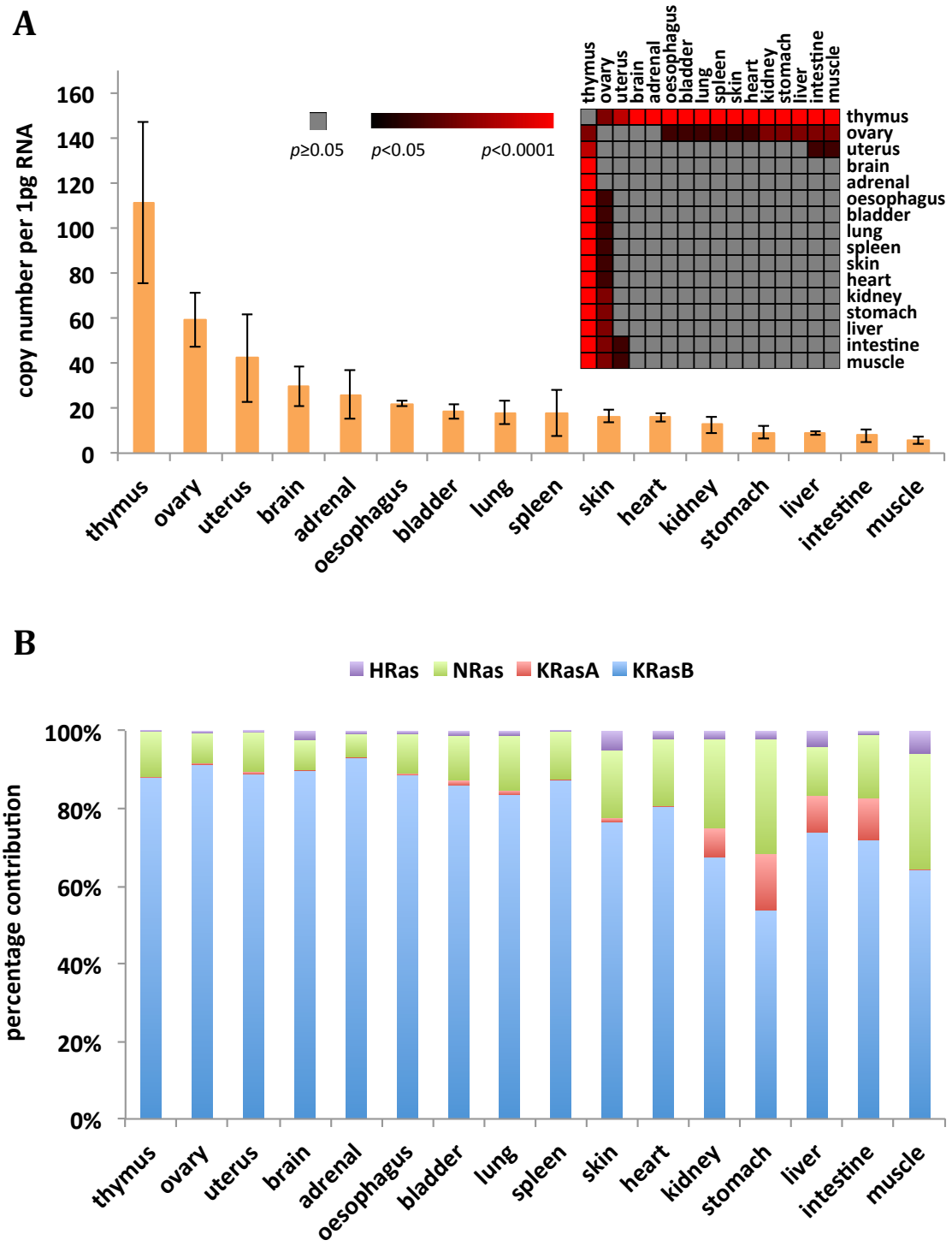

Fig. 5.4 Ras isoform transcript expression in adult mouse tissues. A Total Ras transcript copy number per pg of RNA based on summation of qRT-PCR data for Ras isoforms in adult mouse tissues, representing means ± SEM (n = 3). Data was analysed by one-way ANOVA with Fisher's LSD post hoc test (inset). **B** Percentage contribution of Ras isoforms to total Ras transcript copy number per pg of RNA in adult mouse tissues (n =3).

To measure Ras isoform abundance during mouse development, a restricted panel of tissues used for the adult investigation was chosen. The analysis consisted of 10 developmental time points using three biological replicates representing distinct litters. Data was collated with that for adult tissue from the corresponding mothers (Fig. 5.5 and Fig. 5.6). Overall, as observed for the adult tissues, KRasB was the most abundant transcript in all tested tissues. Generally, expression levels of each Ras isoform remained constant throughout mouse development; the two notable exceptions were for NRas and KRasA, for which statistical analysis was performed and summarised in Fig. 5.7.

NRas transcript levels showed a progressive decrease during embryonic development across many tissues. This can be most clearly seen in the brain and liver, where NRas exhibits a 10-fold decrease between day E11.5 and post-natal day 30 (Fig. 5.5 and Fig. 5.6). Intriguingly, the slope of these decreases differs; in liver the reduction in NRas transcript abundance ceases by post-natal day 5. In contrast, the brain exhibits a constant decrease over the entire time course; although the values for post-natal day 30 are equivalent to the adult brain levels, suggesting that further decreases are unlikely.

On the other hand, KRasA was the most dynamically regulated isoform. It showed a marked ≥10-fold increase in transcript levels in the intestine, stomach and kidney (Fig. 5.5) during embryonic development, which stabilised at adult levels just after birth (P0). Also, to a lesser extent, KRasA expression was increasing until around P25 in the liver (Fig. 5.5). Remarkably, given that KRasA has not previously been detected in the heart (Plowman et al., 2003), a transient peak reaching 10-fold baseline levels was observed just before and at birth (Fig. 5.6, E16.5 and P0). In contrast, KRasA transcript expression was continually low during development in skeletal muscle, lung and brain (Fig. 5.6).

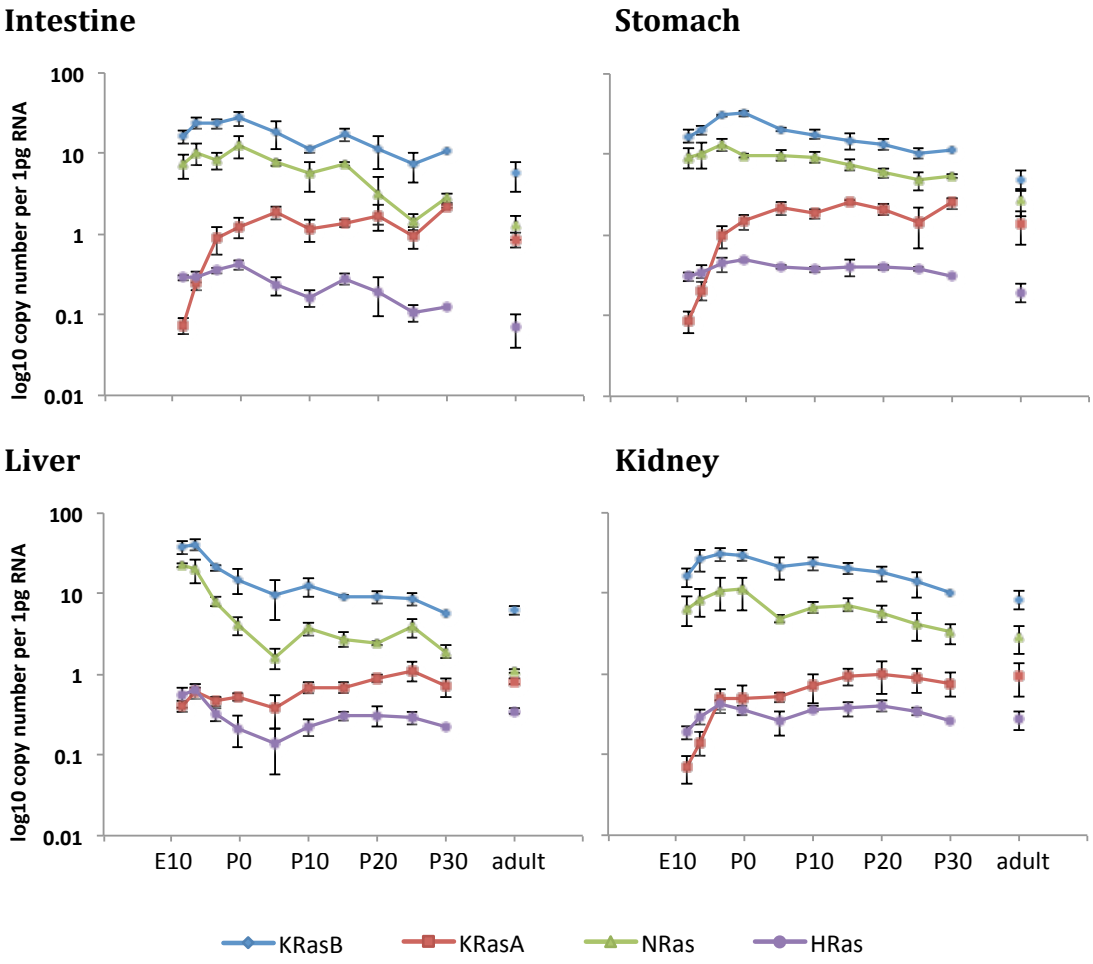

Fig. 5.5 Ras isoform transcript expression throughout mouse development in intestine, stomach, liver and kidney. Transcript levels were measured at 11 developmental time points by qRT-PCR and converted to copy number values using Ras isoform-specific standard curves (n = 3). The data represents means ± SEM (n=3), which was plotted on a logarithmic scale. E – embryonic day, P – postnatal day. Statistical analysis of trends depicted in text is summarised in Fig. 5.7.

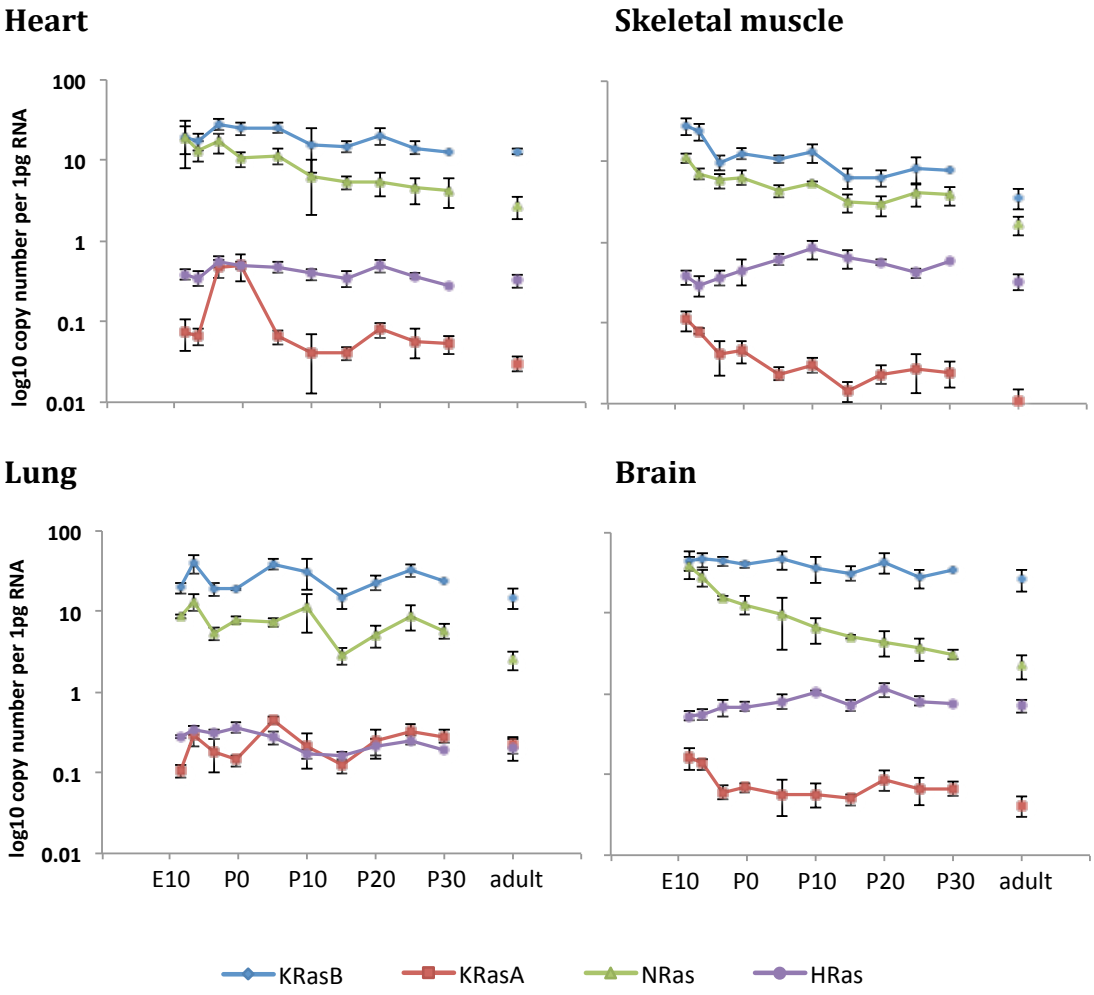

Fig. 5.6 Ras isoform transcript expression throughout mouse development in heart, muscle, brain and lung. Transcript levels were measured at 11 developmental time points by qRT-PCR and converted to copy number values using Ras isoform-specific standard curves (n = 3). The data represents means ± SEM (n=3), which was plotted on a logarithmic scale. E – embryonic day, P – postnatal day. Statistical analysis of trends depicted in text is summarised in Fig. 5.7.

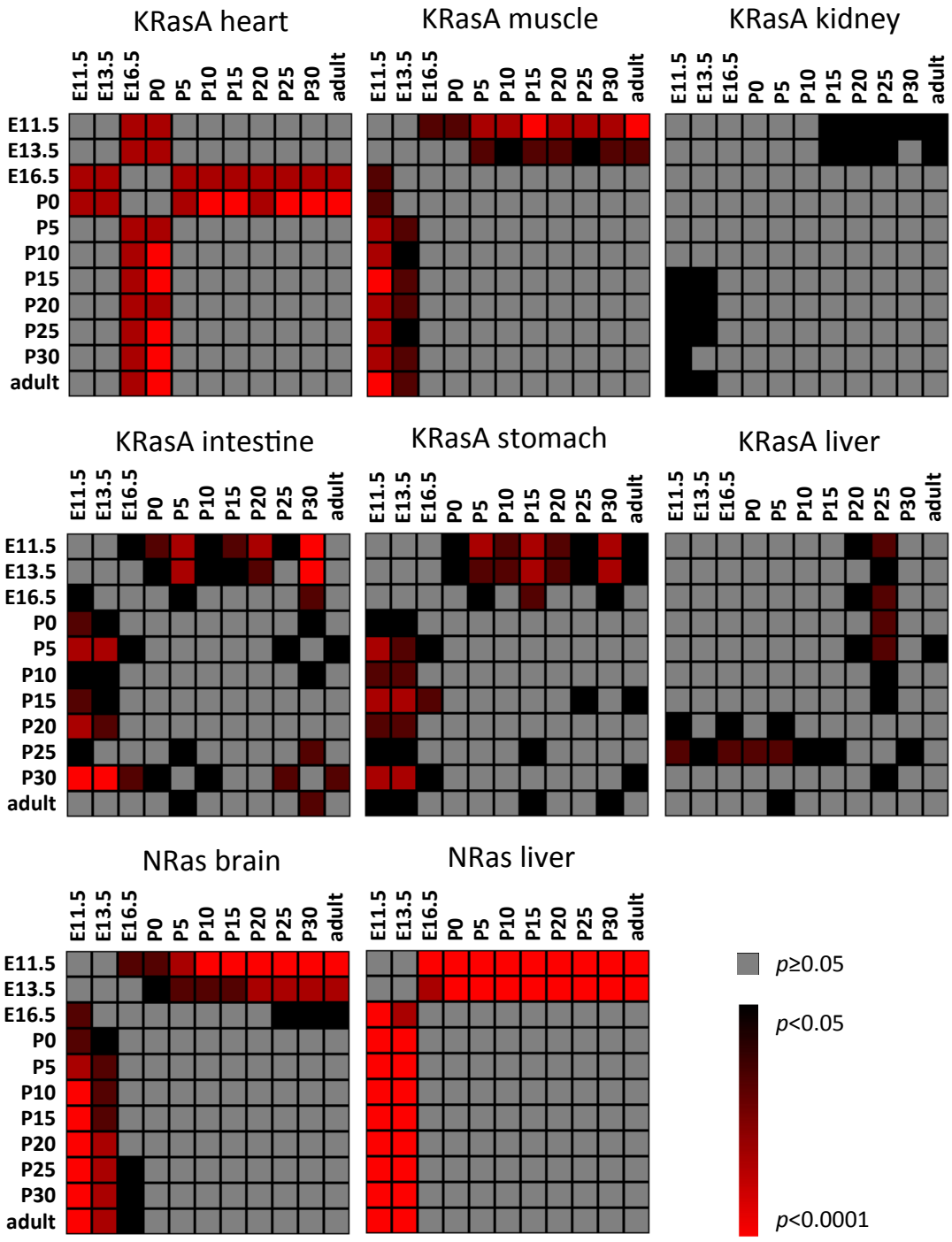

Fig. 5.7 Statistical significance of Ras isoform transcript expression data obtained by qRT-PCR throughout normal mouse development. Statistical significance of data from Fig. 5.5 and Fig. 5.6 was analysed by one-way ANOVA with Fisher's LSD post hoc test and represented as heat maps using MultiExperiment Viewer (MeV v4.8.1).

To better illustrate a full mouse developmental profile for each Ras isoform across all tested tissues, hierarchical clustering was performed on the qRT-PCR data from this study (Fig. 5.8, Fig. 5.9). This representation of the data revealed that panRas expression levels decrease during development in all tissues examined (Fig. 5.8). The same trend was also seen in the majority of tissues for most Ras isoforms, except for KRasA (Fig. 5.9). The tissues co-clustered based on trends in transcript levels, highlighting similar upregulation of KRasA in the kidney, stomach, intestine and liver. Strikingly, intestine, kidney and stomach cluster was also evident in the KRasB and NRas expression profiles. In contrast to KRasA, however, KRasB and NRas transcript levels decreased during postnatal development in these tissues. HRas, on the other hand, showed a distinct expression pattern from other isoforms, with a less clear clustering of the kidney, stomach and intestine.

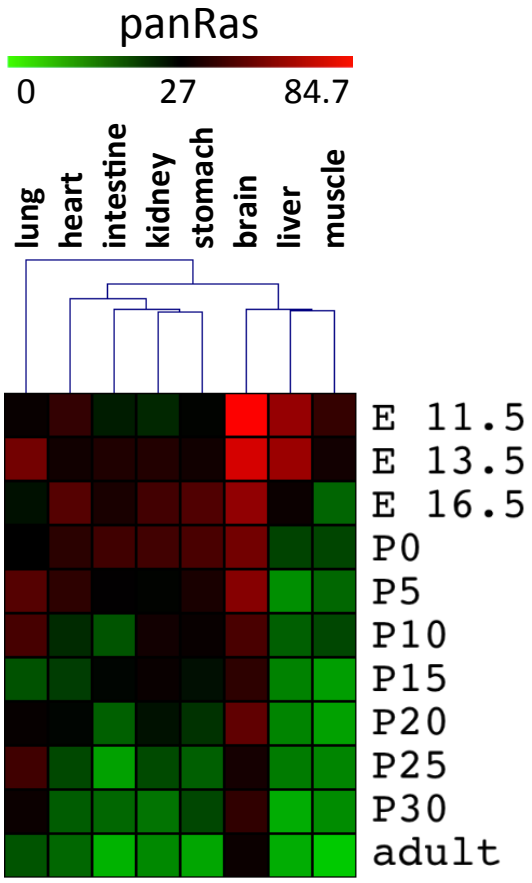

Fig. 5.8 Heat map representing relative total Ras (panRas) transcript expression throughout mouse development across different tissue types. Total Ras (panRas) transcript levels were calculated as a sum of Ras isoform transcript levels (KRasA, KRasB, NRas, HRas) obtained by qRT-PCR and represented as copies per pg of RNA by (n = 3). Heat map was generated by MultiExperiment Viewer (MeV v4.8.1) and hierarchically clustered using Pearson correlation. E – embryonic day, P – postnatal day.

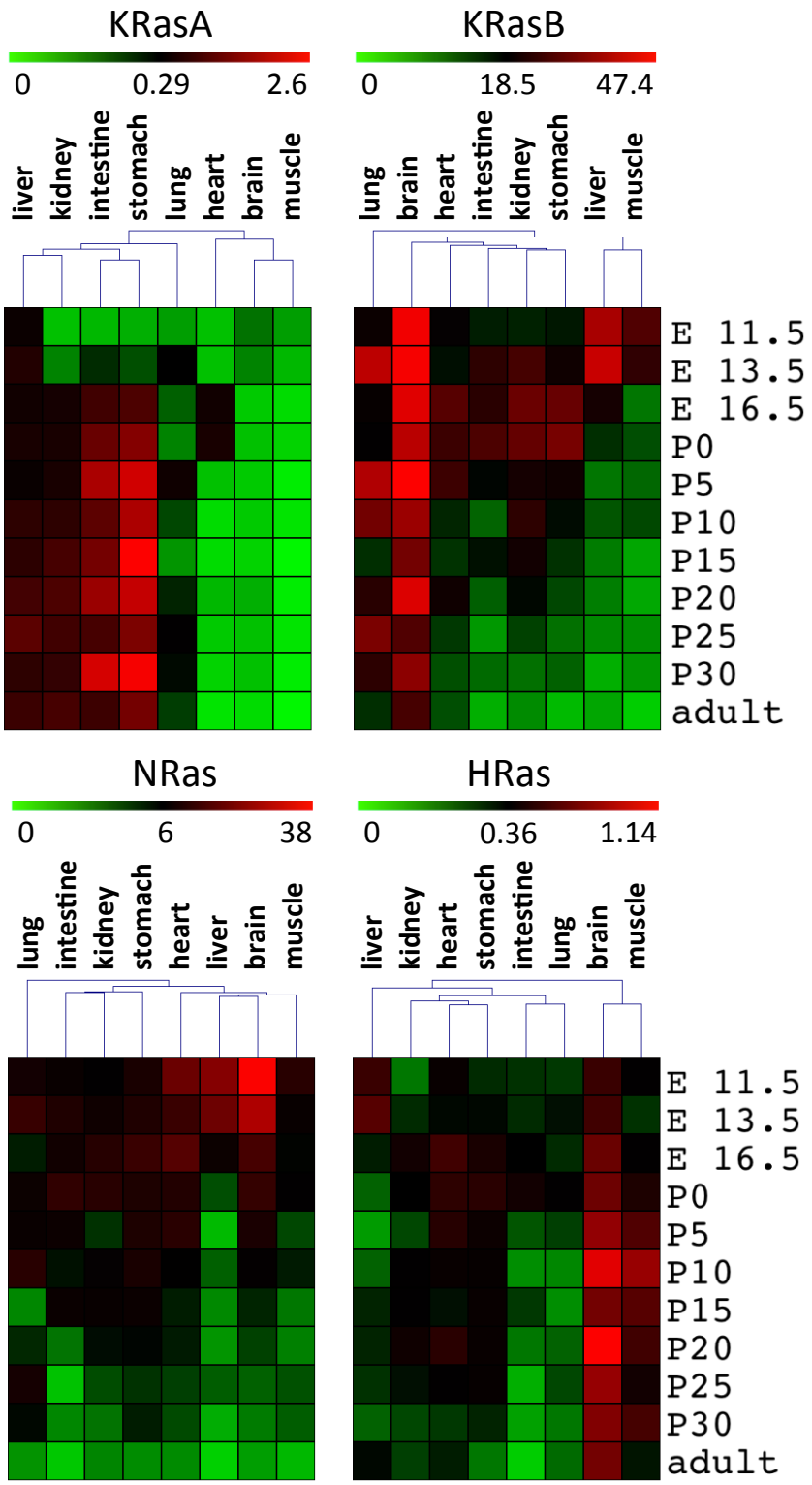

Fig. 5.9 Heat maps representing relative Ras isoform transcript expression throughout mouse development across different tissue types. Heat maps show absolute Ras transcript levels per pg of RNA calculated by qRT-PCR (n = 3) and were generated by hierarchical clustering using Pearson correlation (MultiExperiment Viewer MeV v4.8.1). E – embryonic day, P – postnatal day.

5.2.4 Absolute abundance of Ras isoform proteins in mouse adult tissues

To investigate whether the Ras transcript expression profiles were indicative of expression at the protein level, absolute quantification of Ras isoforms using mass spectrometry was employed. First, isotopically labelled Ras protein standards were quality checked by gel electrophoresis and Colloidal Blue staining (Fig. 5.10). The gel revealed distinct ~30 kDa bands of equal densities representing purified Ras standards of equal abundance. The NRas standard showed a high-density bovine serum albumin (BSA) band, which was used as a quenching solution to stop protein standards from attaching to the surface of a tube. The standards, apart from KRasA, were subsequently spiked at known concentrations into protein samples extracted from mouse tissues for Ras isoform quantification.

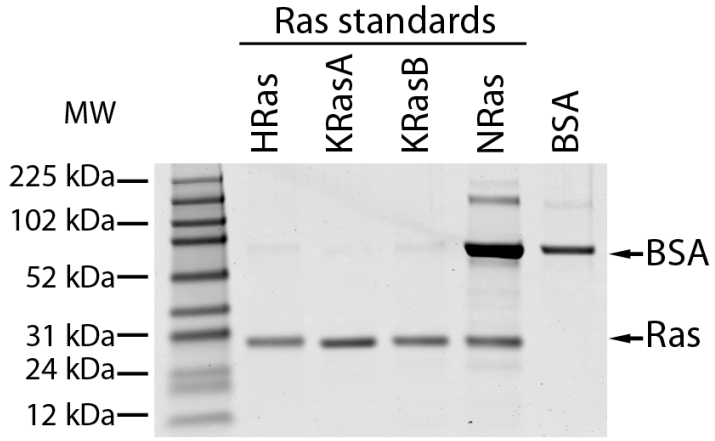

Fig. 5.10 Assessment of protein quality of Ras standards labelled with heavy arginine (Arg10) and lysine (Lys8) for proteomics by gel electrophoresis. 50 ng of each His-tagged Ras standard (supplied by Dr Craig Mageean, University of Liverpool, UK) and a BSA control were run on 4-12% Bis-Tris NuPAGE gel and stained with the Colloidal Blue Staining Kit. All Ras standards showed a distinct band of around 30 kDa (denoted by arrow "Ras") of similar abundance. 50 ng of bovine serum albumin (BSA) was run alongside as a quantity control (denoted by arrow "BSA"). The BSA in the NRas standard is from the BSA-coated tube that was used to reduce adsorption of the standard.

Due to a limited amount of time for this part of the study, only 5 adult mouse tissues were analysed by mass spectrometry in a pilot experiment: brain, intestine, liver, lung and pancreas. The latter tissue was not previously analysed by qRT-PCR due to poor RNA recovery. The choice of tissues was based on the transcript level results (brain and liver were initially representing tissues with high and low total Ras abundance, respectively) and previously known data on Ras contribution to human cancers (KRas is often mutated in colon, lung and pancreatic cancers (Cox et al., 2014)). The mass spectrometry data revealed that there was a significant variation between the three biological replicates and, hence, one set of samples was randomly chosen to generate three technical replicates, which are summarised in Fig. 5.11.

Total Ras protein levels were estimated by measuring a panRas peptide (amino acids 6-16) common to all Ras isoforms and revealed the highest panRas abundance in the brain, followed by lung, intestine, liver and pancreas, ranging from 45 to 770 ng panRas protein per mg total protein (Fig. 5.11 A, Appendix Table A5.1). Using the proteomics approach described in this chapter, Dr Craig Mageean (Prior Laboratory, University of Liverpool, UK) has observed 90-220 ng of endogenous panRas per mg of total protein in SW48 colon cancer cells, which was estimated to be around ~250,000-540,000 copies of Ras per cell (Mageean et al., 2015).

The use of Ras protein standards allows each isoform to be precisely quantified. Unfortunately, KRasA analysis has not been optimised whilst NRas peptides were not detected due to an error with the settings used on the mass spectrometer. Nonetheless, NRas and KRasA protein abundance was estimated by subtracting the other isoforms abundance from panRas expression levels. Intriguingly, whilst KRas4B transcripts were 18-80-fold more abundant than HRas transcripts in these tissues, the protein abundance of these two isoforms is far more similar (Fig. 5.6 and Fig. 5.11). However, KRasB was not detected in the liver and had a low abundance in pancreas, where KRasA and/or NRas were estimated to be the dominant isoforms.

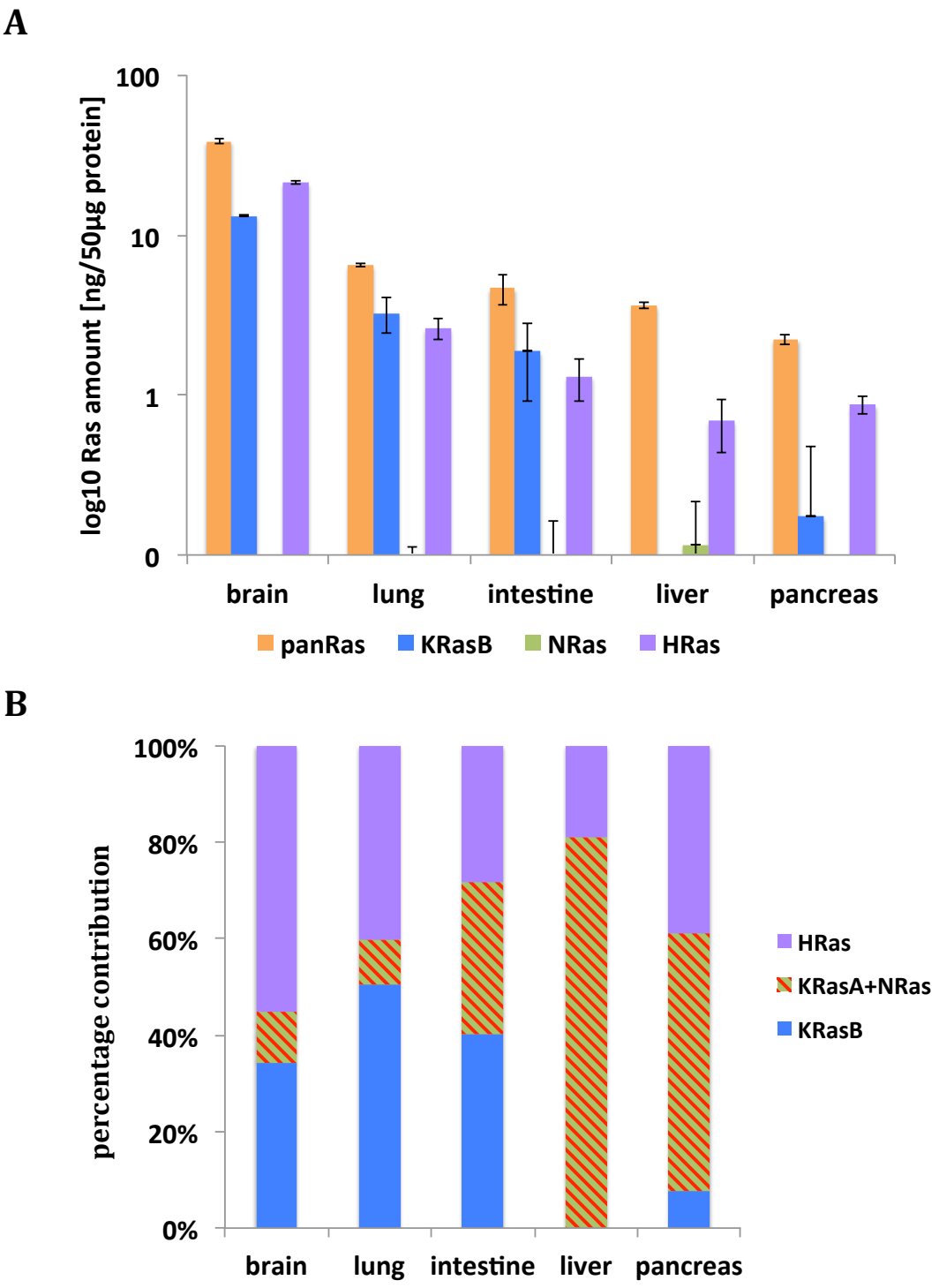

Fig. 5.11 Ras isoform protein levels in adult mouse tissues. A Total Ras (panRas) as well as individual Ras isoform protein levels per 50µg of protein based on absolute quantification by mass spectrometry (MS) of adult mouse tissues are represented as means ± SD (n = 3 technical replicates) on a log scale. **B** Percentage contribution of Ras isoform protein levels to total measured Ras in mouse adult tissues (n = 3 technical replicates). KRasA and NRas percentage contribution (KRasA+NRas) was estimated by subtracting KRasB and HRas contributions from total Ras. MS analysis was performed by Dr Rosalind Jenkins (University of Liverpool, UK).

In summary, proteomics data from this study shows a similar order of decreasing expression level of total Ras as compared to mRNA levels in the following tissues: brain, lung, intestine and liver (Fig. 5.4 A and Fig. 5.11 A). However, the relative isoform contributions to total Ras abundance are not equivalent at the transcript versus protein level. For example, HRas represented only 2.4% of total Ras transcripts in the brain versus the KRasB contribution of ~90%, yet >50% of total Ras protein abundance measured by quantitative mass spectrometry was HRas. Fig. 5.12 summarises the correlation between panRas abundance at transcript and protein level in the four mouse organs for which both transcript and protein data was obtained. Yet, it is important to emphasise that this proteomics study should be interpreted with some caution as it is only preliminary and represents technical, not biological repeats.

5.3 Discussion

This study aimed to quantitatively measure Ras isoform transcript and protein expression levels in various normal mouse tissues. Previous investigations on Ras expression pattern often show contradictory results (Fig. 5.13) due to differences in methods and the examined samples as well as non-comprehensive and semi-quantitative approach. The experimental strategy for the study of this thesis was designed to provide a more comprehensive analysis of Ras isoform expression compared to previous studies (Leon et al., 1987, Plowman et al., 2006, Plowman et al., 2003, Shyamsundar et al., 2005). Transcript levels were analysed in sixteen major adult mouse tissues, as well as at 10 time points during embryonic and postnatal development in eight tissues. This study used more quantitative methods that also allowed cross comparison between isoforms in contrast to previous analyses. Transcript copy number per pg of RNA and per cell were calculated based on qRT-PCR, giving the first quantitative data across all four main Ras isoforms (Fig. 5.13). Proteomics data, although preliminary, gave the first insight into Ras isoform protein copy number in normal mouse tissues.

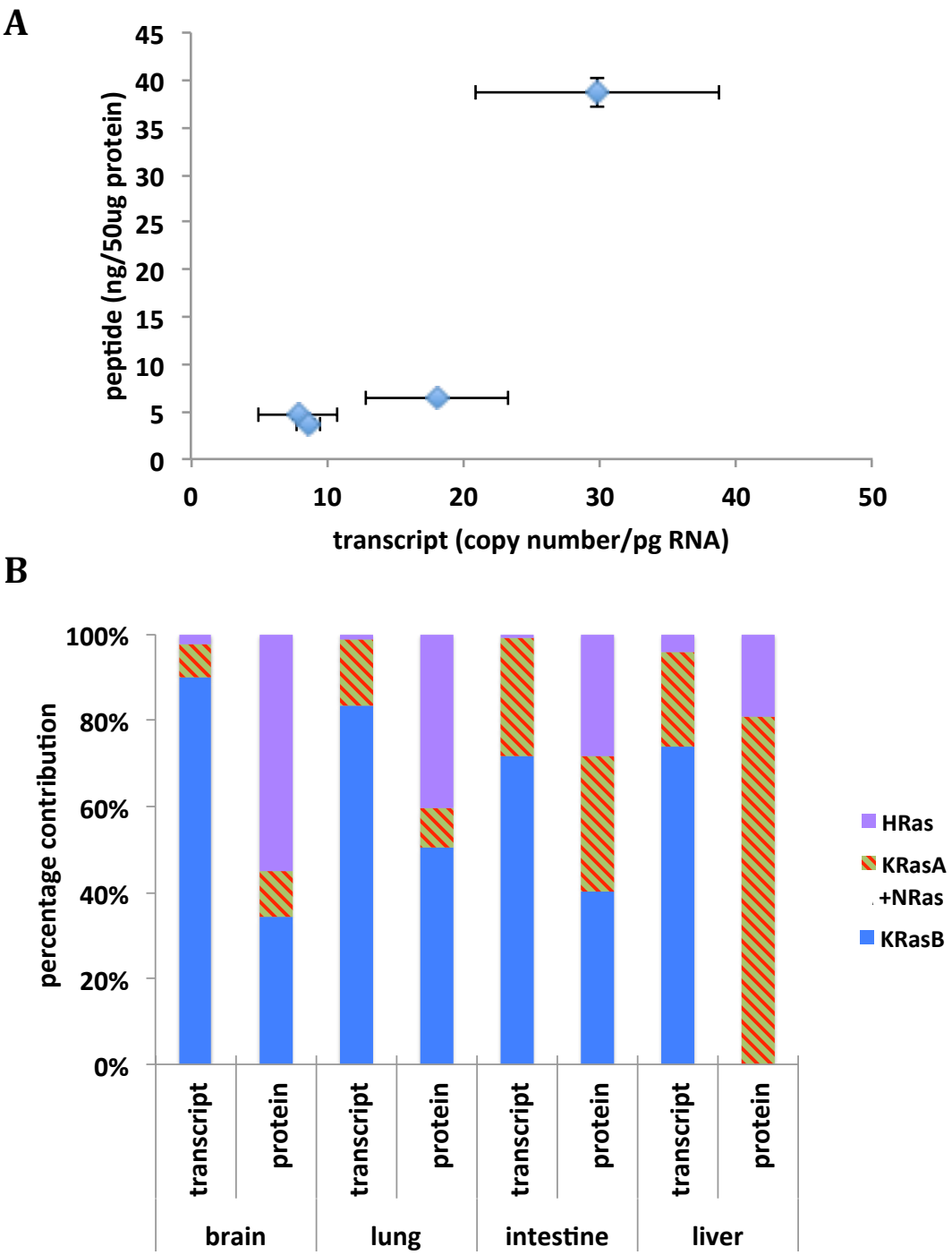

Fig. 5.12 Protein and transcript levels of Ras isoforms in normal adult mouse tissues. A Protein/RNA correspondence plot for panRas expression. panRas peptide abundance was obtained from quantitative mass spectrometry (section 2.9) and panRas transcript abundance from qRT-PCR (section 2.7.12), both from normal mouse adult tissues (brain, lung, intestine and liver). Mean panRas peptide abundance ± SEM (n = 3 technical replicates) was plotted against mean panRas transcript copy number ± SEM (n = 3 biological replicates). **B** Percentage contribution of Ras isoforms to total Ras at transcript and protein level (a summary of Fig. 5.4 B and Fig. 5.11B). KRasA and NRas percentage contribution at protein level were estimated on the basis of panRas abundance.

5.3.1 Comparison with previous studies

In general, transcript abundance results of the current study on adult mouse tissues showed little similarity with previous Northern blotting data, when compared across tissues per Ras isoform (Fig. 5.13) (Leon et al., 1987). HRas transcript abundance was found to be high in the adult mouse skin, brain and skeletal muscle and lowly abundant in the spleen. However, the earlier data identified the liver and ovary as sites with the least HRas expression, whereas in this chapter they were close to median values for HRas expression across the tissue studied. In the current study, NRas transcripts were most abundant in the thymus, ovary and uterus. The thymus was also identified as a site of high NRas expression in the Leon study and similarly to this earlier work, this study showed that NRas abundance is lowest in the liver. Finally, there is some similarity with previous data that found high expression of KRas in the thymus and low in the skeletal muscle and liver.

A further improvement compared to previous published work is that the qRT-PCR data has scored Ras isoform transcript abundance in absolute terms, which allowed for direct comparison between the isoforms. In contrast, the Northern blotting data only measured relative expression levels per isoform. Thus, according to Northern blotting data, Ras isoform transcript expression may appear to be relatively low or high in certain tissues, but this does not account for total Ras expression. For example, although HRas transcript abundance appears to be high in the brain (Fig. 5.13, study 2), in reality it is low when compared to other Ras isoforms (Fig. 5.4). The same is true for the relative expression of KRas and NRas, which cannot be directly compared in the Northern blotting results. On the other hand, this study showed that during gestation both KRas isoforms and NRas generally decrease in transcript expression levels over time (Fig. 5.7), which also agrees with the Northern blotting data (Leon et al., 1987).

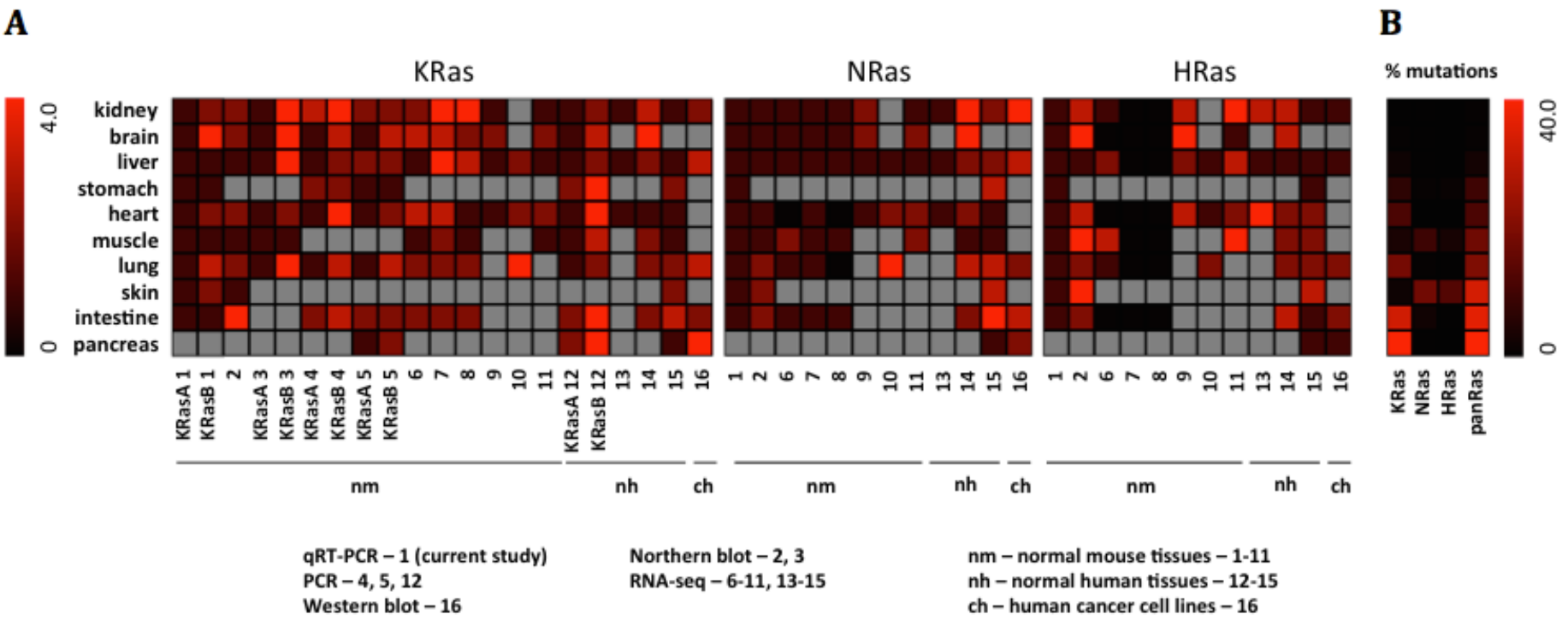

Fig. 5.13 Ras isoform abundance in 10 different tissue types across a range of studies compared to Ras isoform-specific mutation frequency in human cancers derived from the corresponding tissue of origin. A Relative Ras isoform abundance was assigned according to the method in section 2.10 for each study (1-16). The data was obtained/curated from the following: 1 – current study, 2 – (Leon et al., 1987), 3 – (Wang et al., 2001), 4 – (Pells et al., 1997), 5 – (Plowman et al., 2003), 6 – CD1 mouse, 7 – DBA/2J mouse, 8 – C57BL/6 mouse (6-8: ArrayExpress E-GEOD-41637), 9 – (Brawand et al., 2011), 10 – (Keane et al., 2011), 11 – (Barbosa-Morais et al., 2012), 12 – (Plowman et al., 2006), 13 – (Brawand et al., 2011), 14 – (Barbosa-Morais et al., 2012), 15 – (Uhlen et al., 2015), 16 – (Omerovic et al., 2008). **B** "% mutation" represents mutation frequency of Ras isoforms in cancers derived from the corresponding tissues (COSMIC v71)(Forbes et al., 2015). Heat maps were generated by MultiExperiment Viewer (MeV v4.8.1).

Transcript expression of KRasA and KRasB splice isoforms in adult mouse tissues in the current study (Fig. 5.4) is similar to the results of a more recent work that investigated transcript levels of both these splice variants by semi-quantitative RT-PCR in adult mice (Plowman et al., 2003). It showed that KRasA was highly abundant in the intestine, kidneys and liver and was also expressed in the stomach and lungs, but not present in the adult heart and brain and that KRasB was the dominant splice variant expressed at high levels in all tissues. A similar transcript expression pattern of KRasA and KRasB isoforms was also previously shown in normal adult human tissues (Plowman et al., 2006, Plowman et al., 2003).

According to the current work, transcript expression levels of all Ras isoforms (panRas) averaged around 26 copies per pg RNA across all the normal tissues examined in adult mice. Based on the estimated RNA amount per cell (Alberts et al., 1994, Copois et al., 2003, Ramskold et al., 2012), this value is equivalent to around 520 Ras transcripts per cell.

After internal normalisation to total Ras transcript levels, both KRas splice variants constituted the most abundant Ras isoforms across all tested mouse adult tissues. One way to compare the tissues is to divide them into groups based on their germ layer origin. The liver, lungs and the epithelium of the gastrointestinal tract (including intestine and stomach) are of endodermal origin (Gilbert, 2010). Whilst the pattern of Ras isoform transcript expression across all these tissues is varying, it is notable that these are all of the tissues where KRasA is expressed at high levels, apart from the lungs (Fig. 5.4 B). Another exception to this is the kidney, which harbours high KRasA levels, but is of mesodermal origin (Gilbert, 2010). Other mesoderm-derived tissues, cardiac and skeletal muscles, have very low KRasA levels (Fig. 5.4 B). Finally, the skin, which is both of mesodermal and ectodermal origin (Gilbert, 2010), shows low levels of KRasA, whereas the brain, which is derived from the ectoderm (Gilbert, 2010), is the site where Ras expression almost exclusively consists of KRasB. Therefore, whilst it is difficult to identify clear correlations between tissue origin and Ras expression, the link between endoderm-derived tissues and KRasA expression may be of interest.

5.3.2 Dynamic KRasA expression

Very low KRasA abundance detected by qRT-PCR in mouse adult heart, skeletal muscle and brain, among the others, may actually indicate no KRasA expression (Fig. 5.4 B and Fig. 5.6). The obtained C_T values for these tissues were around 31, which was within the range of the C_T values for plasmid standard curves and, hence, KRasA transcript abundance was calculated by interpolation. However, the analysed tissues might have had some contaminants of neighbouring tissues, e.g. connective tissues and blood, which could contain higher amounts of KRasA, giving a positive signal for the tested tissue. This could be further investigated by measuring KRasA abundance in mouse tissue samples obtained by microdissection.

KRasA was the most dynamically regulated Ras isoform over time during mouse development. Its transcript levels increased by 10-fold in the intestine, stomach and kidneys during gestation (Fig. 5.5). Also, in this study, KRasA transcripts were detected for the first time in the mouse heart, appearing transiently between E16.5 and P0 (Fig. 5.6). During this phase of development, the murine heart grows in size and its axis becomes more oblique (Savolainen et al., 2009). The only major changes occur in the atrioventricular valve leaflets and coronary arteries. Whether KRasA plays a role at this stage of heart development is unknown; however, previous work using KRas and KRasA KO mice has shown that KRasB has an essential function in cardiovascular homeostasis, but KRasA is dispensable (Potenza et al., 2005, Koera et al., 1997). KRas-deficient mice die between E12.5 and term due to, among the others, thin ventricular walls of the heart. To further examine the role of KRasA in heart development, it would be useful to check whether its expression is restricted only to specific sites in the developing heart. For instance, this could be done by microdissecting the atrioventricular valve leaflets and ventricular walls and performing qRT-PCR.

5.3.3 Correlation between Ras isoform expression and cancer

Based on the current results, it was of interest whether Ras isoform tissue-specific expression pattern related to the incidence of Ras isoform-specific mutations in tumours derived from particular tissues type. For example, it has been previously shown that higher transcript levels of KRasA in mouse lung tissue correlate with increased risk of developing lung tumour (Wang et al., 2001). Among murine tissues examined in the current study, stomach, intestine, lungs and kidneys are the sites of predominantly KRas-driven tumours, namely gastric, colorectal and lung adenocarcinomas and renal papillary cell carcinoma (Cox et al., 2014). All these tissues have high transcript expression of KRasA and KRasB isoforms, which contribute to over 68% of total Ras (Fig. 5.4 B).

More generally, it is difficult to identify any link between expression and Ras mutation incidence in cancer due to the high abundance of KRas transcripts across all tissues (Fig. 5.4 B and Fig. 5.13). For example, in the liver, which is the origin of hepatocellular carcinoma, the majority of Ras mutations are due to activation of NRas (60% of total Ras), followed by KRas (40% of total Ras) (Forbes et al., 2015). In this tissue, NRas transcript expression contributes to 12% of total Ras, whereas both KRas splice variants constitute 83%.

Several studies suggested that there is a positive correlation between gene expression level and mutation frequency (Comeron, 2004, Majewski, 2003), especially for ubiquitously expressed genes (Cui et al., 2012a, Ramskold et al., 2009), both in somatic cells (Cui et al., 2012a) and in the germline (Cui et al., 2012b, Park et al., 2012). The underlying reason for such observation is thought to be the imbalance between transcription-associated mutagenesis (TAM) (Hendriks et al., 2010, Herman and Dworkin, 1971, Savic and Kanazir, 1972) and transcription-coupled-repair (TCR) (Green et al., 2003, Hanawalt, 1994, Svejstrup, 2002), resulting in the increased density of single nucleotide polymorphisms (SNP) (Cui et al., 2012a, Cui et al., 2012b, Park et al., 2012). This thesis shows, however, that Ras transcript expression pattern in different mouse adult tissues does not appear to correlate with the incidence of Ras

isoform mutations in human cancers. There might be a few reasons why this correlation is not as expected, based on the TAM-TCR hypothesis.

First, the tested tissues were derived from mouse, not human samples, and the genetics and tumour incidence in both species varies and may not be directly comparable (Anisimov et al., 2005). Hence, to better understand the association between gene expression and mutation frequency, normal human tissues should be studied instead. Second, each cancer type derives only from a particular cell type or a cancer stem cell (Lobo et al., 2007) and it would be more appropriate to examine Ras expression patterns only in these particular cell types. The whole organs, as examined in this study, comprise a mixture of tissues, which may each have a distinct Ras isoform expression profile. Finally, the incidence of Ras isoform-specific mutations in different tissues may rather arise from the predisposition of Ras isoform loci to particular carcinogens, which usually affects particular tissue types. For instance, tobacco smoke carcinogens affect the lungs and the mutational hotspot caused by these carcinogens is codon 12 of KRas, but not of NRas or HRas (Feng et al., 2002). This preferential mutation in one of the three Ras loci might be explained by preferential DNA-carcinogen adduct formation and poor repair mechanism at this particular site. Further research suggested that such preferential mechanisms at codon 12 of KRas might be due to an unknown epigenetic modification (Hu et al., 2003).

Curiously, another study depicted that differential susceptibility for certain mutations in different Ras genes might be due to distinct sequences surrounding each Ras gene. It showed that *HrasKI* mice, which express HRas under the regulation of KRas promoter and completely lack KRas expression, still develop lung tumours due to mutation in *HrasKI* allele when treated with urethane, which normally causes only KRas mutations in wild type mice (To et al., 2008). On the other hand, induced skin tumours develop as a result of mutation of endogenous *Hras* allele, not the "knock-in" *HrasKI*. Hence, the predisposition of KRas mutations to induce lung tumour and HRas mutations to induce skin tumour, may likely be due to both Ras genes having unique cis-acting regulatory elements (CRE). CREs are non-coding DNA sites found near

the gene, which are usually binding sites for transcription factors. Taken together, the reason why specific cancers and mutations couple to certain Ras isoforms appears to be complex and it is possible that a mixture of factors could affect it, including gene regulatory elements, expression levels and epigenetic regulation.

5.3.4 Transcript versus protein abundance

To examine whether Ras isoform expression profiles at transcript level hold true also at protein level, the study of this thesis used proteomics analysis on samples derived from the same mouse tissues previously used for qRT-PCR analysis (section 5.2.2 and 5.2.3). An earlier study in NIH3T3 mouse fibroblasts showed that 41% genes correlated in relative abundance at the protein and transcript level and that the protein abundance per cell is about 900 times higher than that of the corresponding mRNA (Schwanhausser et al., 2011). The study of this thesis generated preliminary data on absolute quantification of Ras isoform protein expression in adult mouse tissues (Fig. 5.11).

However, the contribution of individual Ras isoforms to total Ras abundance at protein level did not parallel the Ras transcript profiles in this study (Fig. 5.4, Fig. 5.12 B). Specifically, KRas protein contributed far less to total Ras abundance than predicted from the transcript data. The findings in this thesis contrast with mass spectrometry analysis in NIH3T3 cells (Schwanhausser et al., 2011), which found that NRas is a dominant Ras isoform contributing to around 85% of total Ras, while KRas and HRas are lowly abundant with 10% and 5% contribution, respectively. However, the proteome data was generally consistent with previous findings across different human cancer cell lines, in which Western blotting revealed that typically KRas is the dominant isoform, whereas HRas contributes to less than 10% of total Ras (Omerovic et al., 2008).

The method used in this thesis to quantitatively determine Ras protein abundance at endogenous levels utilised full-length Ras standards that were spiked into the lysate prior to any further sample processing, which allowed

avoiding inefficiencies associated with gel extraction and Ras proteolysis (Mageean et al., 2015). This was in contrast to previous studies, which spiked in the standards just prior to the analysis by the mass spectrometer and resulted in a wide spread of the data (Halvey et al., 2012, Ruppen-Canas et al., 2012, Wang et al., 2011).

The preliminary results presented in this thesis showed that panRas protein levels ranged between 44-770 ng of panRas per mg of total protein, depending on tissue type (Appendix Table A5.1). This value is similar to 90-220 ng of endogenous panRas per mg of total protein found in SW48 colorectal cancer cell line using the same method (Mageean et al., 2015) and it is especially striking that intestinal tissue examined in this thesis had 93 ng of panRas per mg of total protein. It is difficult to estimate the absolute number of Ras protein molecules per cell, as total protein content per cell is approximate and may vary depending on cell type (Lodish et al., 2000). Unfortunately, the measurement of cell number in heterogeneous tissues was beyond the scope of this study. Nevertheless, it might be accurate to estimate the total Ras abundance in the intestine to around 250,000 molecules per cell, as this was the calculated value based on 90 ng of panRas per mg protein in SW48 cell line (Mageean et al., 2015).

The discrepancy between relative transcript versus protein abundance of each Ras isoform (Fig. 5.12 B) might be explained by a recent finding, which showed that *KRAS* is poorly translated as compared to *HRAS* due to the presence of rare codons in the genomic sequence of *KRAS* (Lampson et al., 2013). Rare codons appear infrequently in the genomic sequence as compared to other degenerate codons that encode for the same amino acid. As a result, rare codons impede translation and cause ribosome stalling, thus leading to lower than expected protein levels. Interestingly, rare codon bias in the *KRAS* gene in conserved across mammalian species and, hence, is relevant to the to mouse KRas protein levels investigated in this thesis.

Rare codons found in *KRAS* not only affect KRas protein levels, but are also suggested to influence its tumourigenic potential, making it a weaker oncogene than HRas (Lampson et al., 2013). This result seems in contrary to the prevalence of KRas mutation in human cancer (Cox et al., 2014, Prior et al., 2012). However, rare codon bias and low expression are suggested to predispose KRas to initiate tumourigenesis in untransformed cells, which would otherwise undergo senescence due to oncogenic stress caused by high expression of the mutated protein. Yet, the data in this thesis argues against this model since KRas protein abundance was generally similar to the other isoforms. Therefore, the high transcript abundance of KRas isoforms appears to be a compensatory mechanism for inefficient protein translation to ensure similar protein abundance to the other Ras isoforms.

Overall, the data from this study suggests that KRas, and especially KRasB, is the most abundant Ras isoform in all mouse tissues and developmental stages, at least at transcript level. This result may partially explain why KRas is the most frequently mutated Ras isoform in human cancers (Cox et al., 2014, Prior et al., 2012) and why KRasB is the only developmentally essential Ras isoform in the mouse (Koera et al., 1997, Plowman et al., 2003). Future studies should focus on Ras expression pattern in particular cell types and ideally should include samples from human biopsies. There still remain tissues, such as the pancreas, which should be examined, but for which the scope of this study and technical problems did not allow. Moreover, proteomics data from this study represented technical repeats and, hence, further confirmation of expression patterns is required using biological replicates. Nonetheless, this work generated the first comprehensive developmental map of Ras isoform transcript abundance in normal mouse tissues and gave the insight into the differential regulation of Ras isoform expression. Establishing baseline expression levels in normal tissues could be key to better understanding of isoform-specific Ras coupling to different cancers, as well as better interpretation of current and future data on Ras levels and signalling in malignant tissues.

Chapter 6

Isoform-specific Ras signalling

6.1 Introduction

All cells express three almost identical Ras proteins (HRas, KRasB and NRas). Mouse knockout data demonstrates that KRasB is uniquely required for normal development, whereas HRas and NRas are dispensable, suggesting isoform-specific functions of the Ras proteins (Koera et al., 1997, Johnson et al., 1997, Plowman et al., 2003, Umanoff et al., 1995, Esteban et al., 2001). Similarly, KRas is far more frequently mutated in cancer implying a particular oncogenic potency that is not yet fully understood (Cox et al., 2014, Quinlan and Settleman, 2008).

Current research suggests that stimulation of downstream signalling is Ras isoform-specific, due to differential coupling of isoforms to effector proteins (Voice et al., 1999, Yan et al., 1998) and feedback loops (Eser et al., 2014, Fivaz et al., 2008, Thevathasan et al., 2013). Early studies based on ectopic overexpression of Ras isoforms revealed that HRas and NRas are better activators of PI3K whilst KRasA and KRasB were better activators of Raf and Rac than the other Ras isoforms (Voice et al., 1999, Yan et al., 1998). A key drawback with this approach is that overexpression of Ras can lead to signalling perturbation and profound phenotypic outputs such as senescence that are not seen with oncogenic Ras signalling from the endogenous locus (Serrano et al., 1997, Tuveson et al., 2004). More recent work utilised *in vivo* approaches, such as knock-in (KI) mice (Di Nicolantonio and Bardelli, 2013, Haigis et al., 2008, Tuveson et al., 2006), as well as methods to examine endogenous Ras signalling in various cell lines, using siRNA (Fleming et al., 2005, Omerovic et al., 2008) and gene KI (isogenic cell lines – (Arena et al., 2007, Vartanian et al., 2013)).

Unfortunately, most of these techniques analysed only one or two Ras isoforms in an endogenous context or likely showed compensation effects of other isoforms, as in case of siRNA (Omerovic et al., 2008). Therefore, the aim of this

chapter is to present a method, in which the signalling of all three Ras isoforms is compared in a normal physiological environment. The use of mouse models bearing specific KI of a mutation for each Ras isoform would be costly and time-consuming. Thus, a panel of cell lines isogenic with an endogenous heterozygous codon mutation for each Ras isoform represents a plausible higher-throughput alternative allowing endogenous isoform-specific Ras signalling to be compared against the same genetic background.

Isogenic cells harbouring oncogenic KRas variants have already been generated and extensively characterised. These comprise colorectal HCT-116 (G13D) and DLD-1 (G13D) and HEC1A (G12D) endometrial cells where the indicated mutant KRas allele was deleted (Kim et al., 2004, Shirasawa et al., 1993) and MCF10a breast cancer cells where a G12V mutation was introduced into a KRas wild type allele (Konishi et al., 2007). There are two specific problems with these models. The first is that for HCT-116, DLD-1 and HEC1A the parental cell line has only one wild type KRas allele, potentially reducing endogenous KRas protein expression compared to the mutant isogenic cell line. The second is that for all of the isogenic models there has been a focus on KRas effectors and there are no corresponding mutations in the other Ras isoforms that have been generated.

More recently a panel of isogenic colorectal SW48 cells harbouring different KRas point mutations has been generated using adeno-associated virus (AAV) gene editing technology (De Roock et al., 2010). These have been supplemented by Horizon Discovery, so that now there is a panel of 14 Ras mutant variant isogenic SW48 cells. These include cells harbouring G12V mutations in HRas or KRas that have now been complemented by NRas G12V SW48 cells produced by the Prior laboratory.

Colorectal cancer (CRC) is the third most common human cancer (Hamilton et al., 2010) and colorectal adenocarcinoma is its most prevalent type, which is derived from epithelial cells of the colorectal mucosa (Fleming et al., 2012). Ras mutations occur in over 50% of colorectal adenocarcinoma cases, making it the second cancer type with most prevalent Ras mutations (Forbes et al., 2015,

Prior et al., 2012). 85% of these mutations are in the KRAS gene, with the remaining ones occurring in the NRAS gene and no mutations in HRAS.

Although the most common KRas mutation in colorectal cancers is G12D (Forbes et al., 2015), substitution of the same codon with valine residue (G12V) leads to more aggressive cancer phenotypes and is associated with lower survival rates in patients, compared to other KRas mutations, as well as the wild type protein (Winder et al., 2009). Indeed, G12V mutation of Ras is generally associated with greater transforming efficiency than G12D and other mutations (Fasano et al., 1984, Seeburg et al., 1984). In a mouse colorectal cancer model, KRasG12V also shows higher metastatic efficiency and lower apoptosis than another common mutant KRasG13D (Alamo et al., 2015). Consistent with this, different activating oncogenic mutations of KRas exhibit distinct proteome and phosphoproteome signatures (Hammond et al., 2015, Miller and Miller, 2011). This also has therapeutic implications since colorectal cancer tumours with codon 12 mutations of KRas are resistant to the EGFR inhibitor cetuximab as opposed to tumours with wild type KRas or bearing other KRas mutations (Amado et al., 2008, Karapetis et al., 2008). Therefore, when investigating the differences in isoform-specific oncogenic Ras signalling, it is important that each isoform harbours the same oncogenic mutation.

In this chapter, SW48 cell lines that are isogenic except for the potent G12V mutation in each of the three Ras isoforms (cell lines harbouring $HRas^{G12V}$, $KRas^{G12V}$ or $NRas^{G12V}$), as well as wild type parental cell line, were used to further delineate the subtleties of isoform-specific signal transduction in an endogenous context. The differences in downstream signalling between the cell lines were examined by comparing the two canonical signalling cascades that stem from activated Ras – MAPK and PI3K pathways (Karnoub and Weinberg, 2008, Moodie et al., 1993, Rodriguez-Viciana et al., 1994) (Fig. 6.1). The levels of activation of downstream effectors by phosphorylation were measured by Western blotting using phospho-specific antibodies: pMEK, pERK, pAkt and pp70S6K. Finally, this chapter describes preliminary optimisation of reagents for a network biology study, where differences in Ras isoform-dependent signalling networks will be determined by utilising effector-specific inhibitors, as well as distinct GFs that activate the various RTKs upstream of Ras.

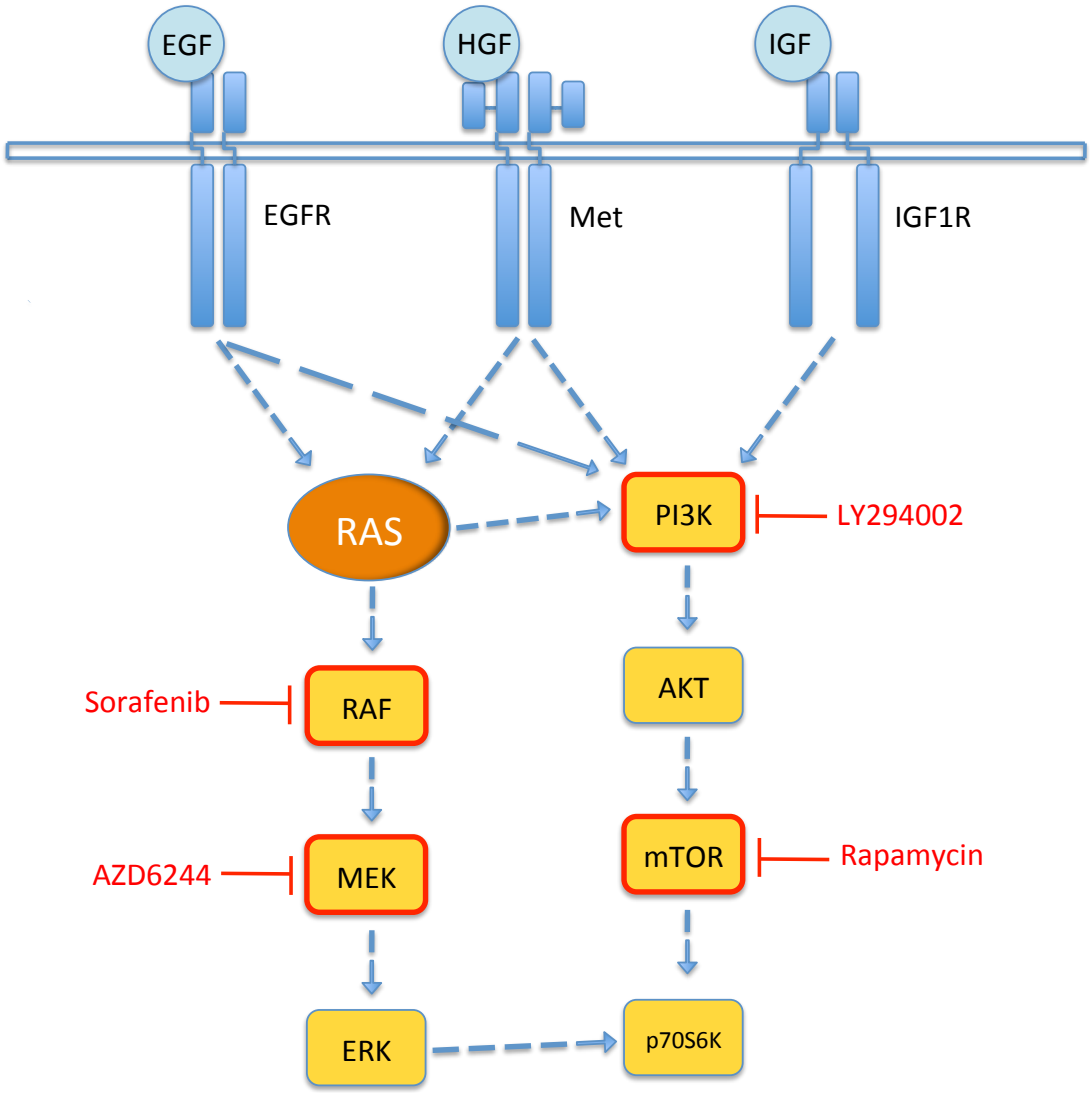

Fig. 6.1 A schematic representation of Ras-dependent signalling network measured by effector-specific inhibitors and receptor agonists. The two canonical signalling cascades downstream of Ras comprise the mitogen-activated protein kinase (MAPK) Raf-Mek-ERK and the phosphoinositide 3-kinase (PI3K) pathways. Effector-specific inhibitors used in this study are depicted in red and their targets are shown in red boxes. The growth factors (GFs) used to stimulate receptor tyrosine kinases (RTK) upstream of Ras are shown in blue circles adjacent to the receptors.

6.2 Results

6.2.1 Cell growth kinetics of SW48 isogenic cell lines

To compare cell growth kinetics between SW48 cell lines isogenic for Ras isoform mutations, CellTiter-Glo® Luminescent Cell Viability Assay was used to measure the number of viable cells during cell culture. The assay measures cellular ATP and therefore is a read-out of cellular metabolism, which at least in part will correlate with the growth kinetics of the cells. Parental SW48 cell line was empirically observed to be the fastest growing of all SW48 isogenics and, hence, was chosen to optimise the seeding density (Fig. 6.1). The cell line was seeded on a 96-well plate at the following densities, each in 5 technical replicates: 0, 250, 500, 750, 1000, 1250, 1500, 2000, 2500, 3000, 4000 and 5000 cells per well. The luminescence was measured after 5 days of continuous cell culture and background luminescence from wells with medium only was subtracted.

Based on the results (Fig. 6.2), SW48 parental cell line showed a linear growth at cell densities up to around 1000 cells per well, from which the growth curve started to plateau. To make sure that the cell growth is within the linear range after 5 days of culture, 750 cells per well were chosen as a starting density for the next experiment, in which the growth kinetics of all SW48 isogenic cell lines was measured (Fig. 6.3).

The growth kinetics of all Ras isogenic cell lines was measured every day for 5 days inclusive. The luminescence data was then normalised to day 1 to account for the possible seeding differences at day 0. According to the results (Fig. 6.3), the slowest growth rate was seen in the SW48 cell line bearing $NRas^{G12V}$ mutation whereas the remaining Ras mutant cell lines were equivalent to the parental SW48 cells. The growth rate is slower at the beginning, then accelerates from day 3, and here again the acceleration is more rapid for parental, $KRas^{G12V}$ and $HRas^{G12V}$ cell lines, as compared to $NRas^{G12V}$. On day 5 the basal difference between normalised luminescence is around 40% higher for parental compared to $NRas^{G12V}$ isogenic cell line. In conclusion, G12V

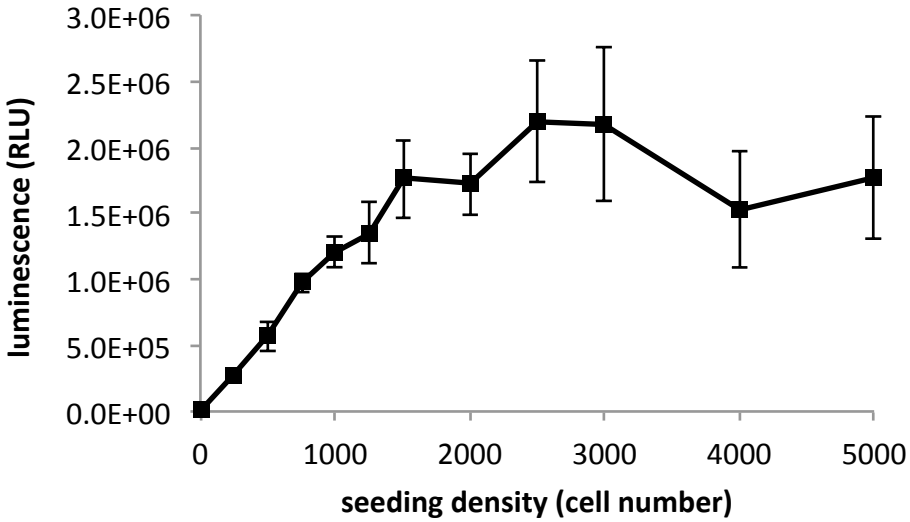

Fig. 6.2 Optimisation of seeding density of SW48 parental cell line for cell viability assay. Parental cells seeded at the indicated densities were measured after 5 days of cell culture using the CellTiter-Glo viability assay. Data represents means ± SD (n = 5 technical repeats). RLU – relative light units.

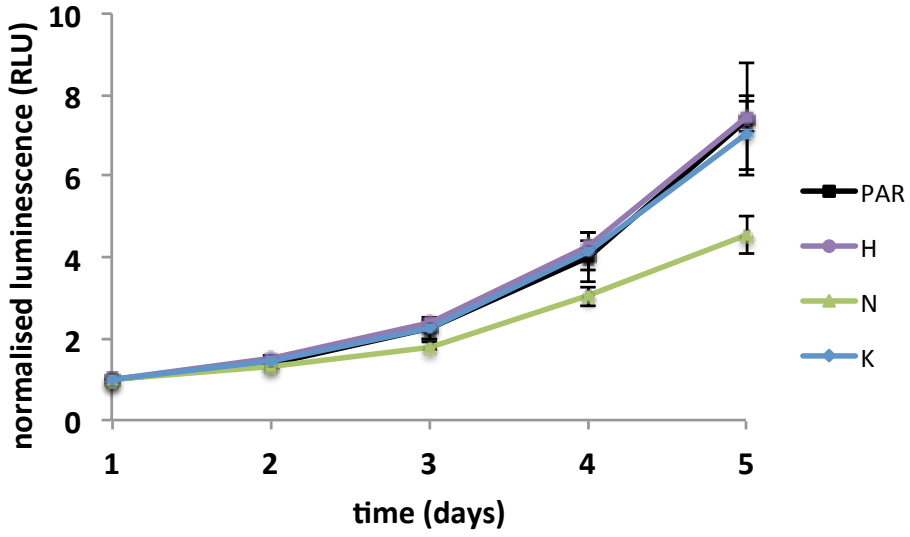

Fig. 6.3 Cell growth differences between Ras isogenic cell lines measured by cell viability assay. 750 SW48 cells per well were seeded and grown for the indicated number of days before cell viability was measured using CellTiter-Glo. Luminescence was normalised to day 1. Data represents means ± SD (n = 3 independent biological repeats). RLU – relative light units, PAR – parental, H – $HRas^{G12V}$, N – $NRas^{G12V}$, K – $KRas^{G12V}$ SW48 cell lines.

mutation seems to negatively affect the growth of SW48 colorectal cancer cell line when present in NRas, but not in other Ras isoforms. However, such effect might be clone-specific and, hence more clones bearing Ras mutations should be tested.

To investigate whether the G12V mutation affects Ras isoform abundance, Western blotting was performed on lysates from all isogenic SW48 cell lines using isoform-specific antibodies (Fig. 6.4). When compared to actin loading control, the expression of Ras isoforms and total Ras was slightly variable across the different isogenic cell lines, both when cultured in normal medium (10% FBS) or starved. This experiment, however, represents only one biological repeat.

6.2.2 Differential activation of PI3K and MAPK pathways

To compare the effect of EGF stimulation on SW48 Ras isogenic cell lines, the activation of two canonical pathways – MAPK and PI3K pathways – was measured by Western blotting (Fig. 6.5A and Fig. 6.6A). To check the potency of activation at different EGF concentrations and to calculate the EC_{50} (effective concentration needed to result in 50% of activation), a range of EGF concentrations was chosen: 0.1, 0.25, 0.5, 1, 1.5, 2, 5, 10, 20, 30 and 50 ng/ml. Cell were starved for 16 hours and then stimulated for 5 minutes, apart from a control. To measure the activation of PI3K pathway, pAkt levels were quantified using pAkt-specific antibody and densitometry software. Similarly, to measure activation of MAPK pathway, pMEK levels were quantified. The data was normalised to actin loading control, total Akt or MEK protein, and to 3 maximum EGF stimulations (Fig, 6.5B and Fig. 6.6B).

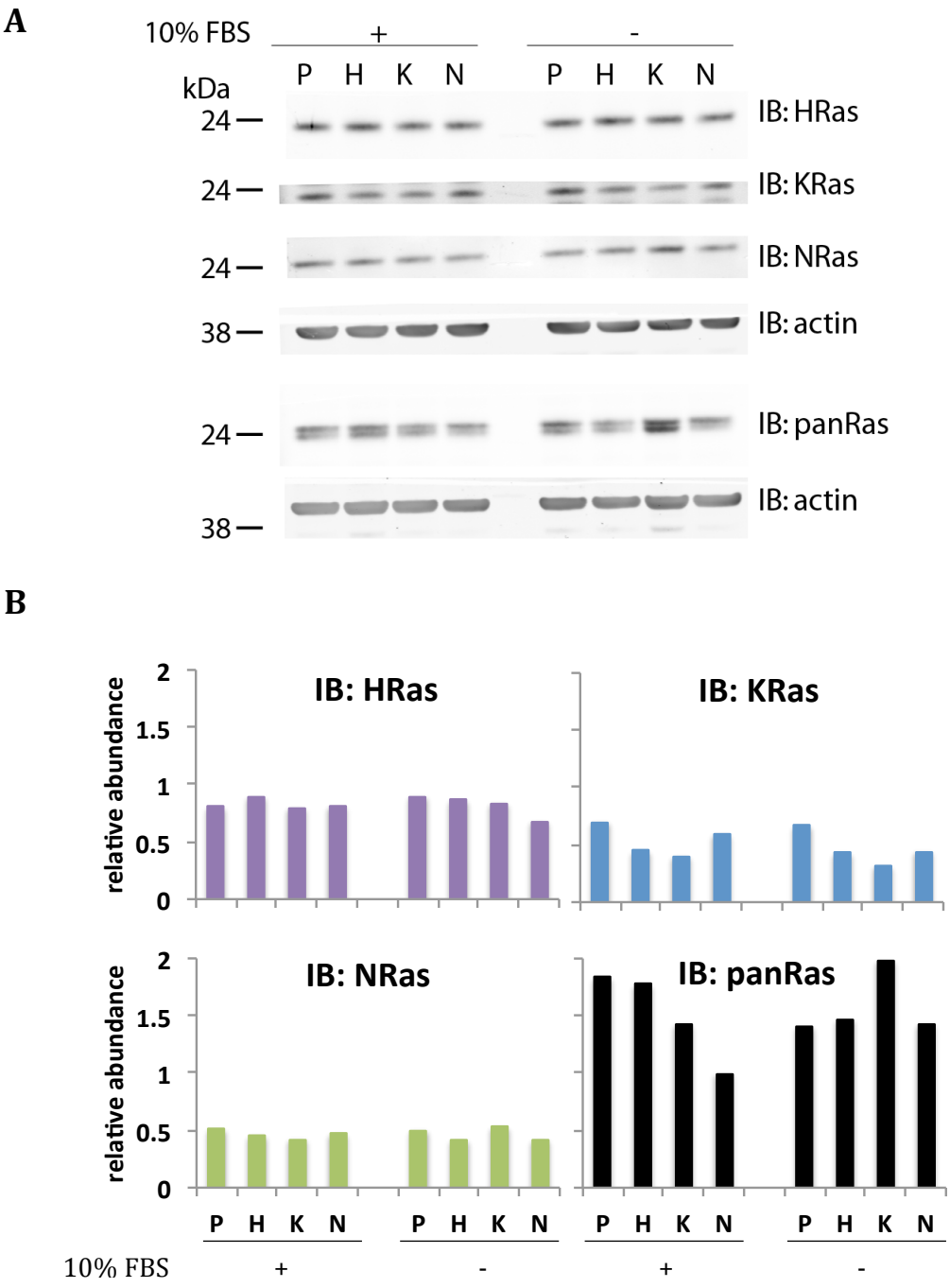

Fig. 6.4 Ras isoform protein levels in SW48 isogenic cell lines. SW48 isogenic cell lines were grown in either normal medium (10% FBS) or were starved for 24 hours. After cell lysis, samples were run on SDS-PAGE, followed by Western blotting. **A** Each sample was immunoblotted with panRas antibody and with Ras isoform specific antibodies. Representative actin is showed for Ras isoforms and panRas. **B** The immunoblots were quantified and normalised to actin (n=1). P – parental, H – $HRas^{G12V}$, N – $NRas^{G12V}$, K – $KRas^{G12V}$ SW48 cell lines.

For both pAkt and pMEK, $HRas^{G12V}$ displayed the most sensitive response with an EC_{50} of 0.44 and 1.07 ng/ml respectively. In comparison, the EC_{50} of Parental and $NRas^{G12V}$ were in the 1.30 – 2.36 ng/ml range whilst $KRas^{G12V}$ was the most resistant to EGF stimulation with EC_{50} of 2.71 and 3.40 ng/ml for pAkt and pMEK respectively (Fig. 6.5B and Fig. 6.6B). Therefore, $HRas^{G12V}$ isogenic cell line responds at least two times more potently to EGF stimulation in activating PI3K and MAPK signalling as compared to parental and the other mutated Ras isoform cell lines. Whilst EC_{50} values have been determined based on the maximal signal observed, it looks like some of the stimulations may not have plateaued. This is most evident for Parental and $KRas^{G12V}$ cells. Therefore, further work could be done to extend the upper range of EGF concentrations to confirm the saturating doses.

One potential confounding factor with directly comparing the cells lines is that the Western blot membrane of each cell line was developed at different times. Therefore, whilst the dose response can be fairly compared, it is not possible to know whether the absolute intensities observed were equivalent between cell lines, i.e. are there quantitative differences in the relative output of the Ras isoforms in response to a given stimulation? To address this, the samples from all isogenic cell lines stimulated with 1.5 and 30ng/ml EGF concentrations, representing sub-saturating and approximately saturating doses, were re-run altogether on one blot (Fig. 6.7). The results recapitulated the data seen in Figures 6.4 and 6.5 in showing that HRasG12V cells were more sensitive to stimulation by the sub-saturating dose of EGF compared to the other Ras isoforms. Importantly, at the higher concentration of EGF, HRasG12V cells exhibit significantly higher pAKT and pMEK responses than the other cell lines. The attenuated response of KRasG12V cells in particular may mean that KRasG12V is uncoupled from the signalling cascades or that there has been an upregulation of negative feedback.

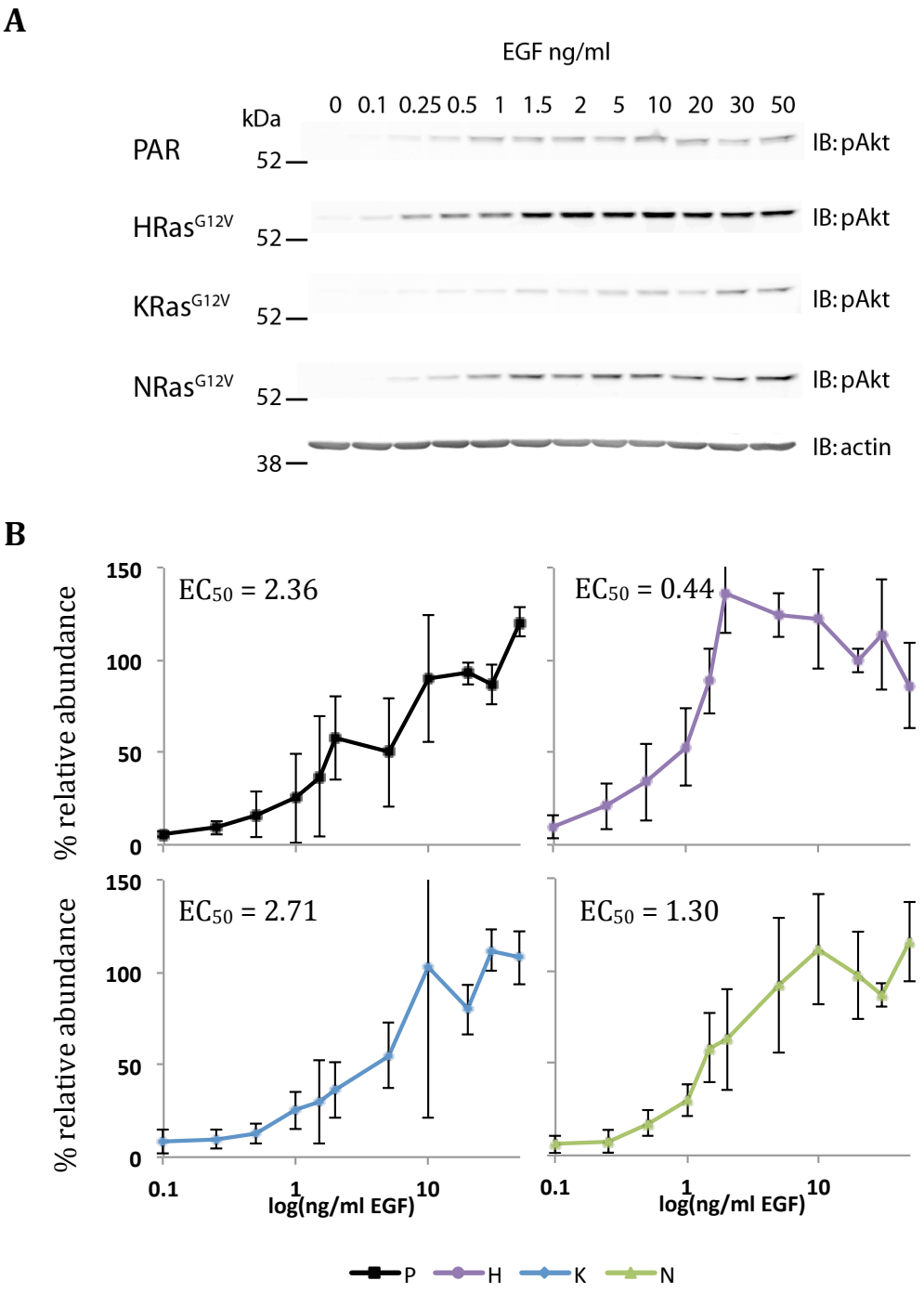

Fig. 6.5 Activation of downstream PI3K signalling pathway in Ras isogenic SW48 cell lines depending on stimulation with different concentrations of EGF. A A representative immunoblotting of Akt-pS457 (pAkt) and one actin blot. **B** Relative quantitation of Akt-pS457 activation normalised to actin, total Akt and maximum GF responses, where 100% = the mean of the 3 highest concentrations of GF stimulations. Data represents means ± SD (n = 3 independent biological repeats). P – parental, H – HRas^{G12V}, N – NRas^{G12V}, K – KRas^{G12V} SW48 cell lines.

A

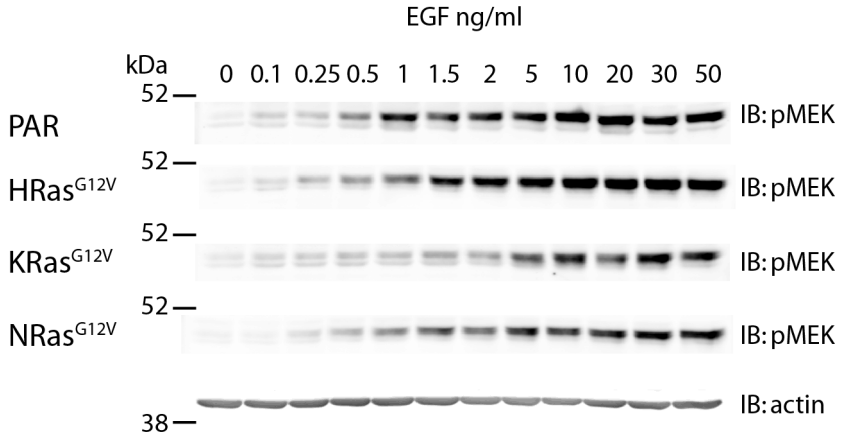

B

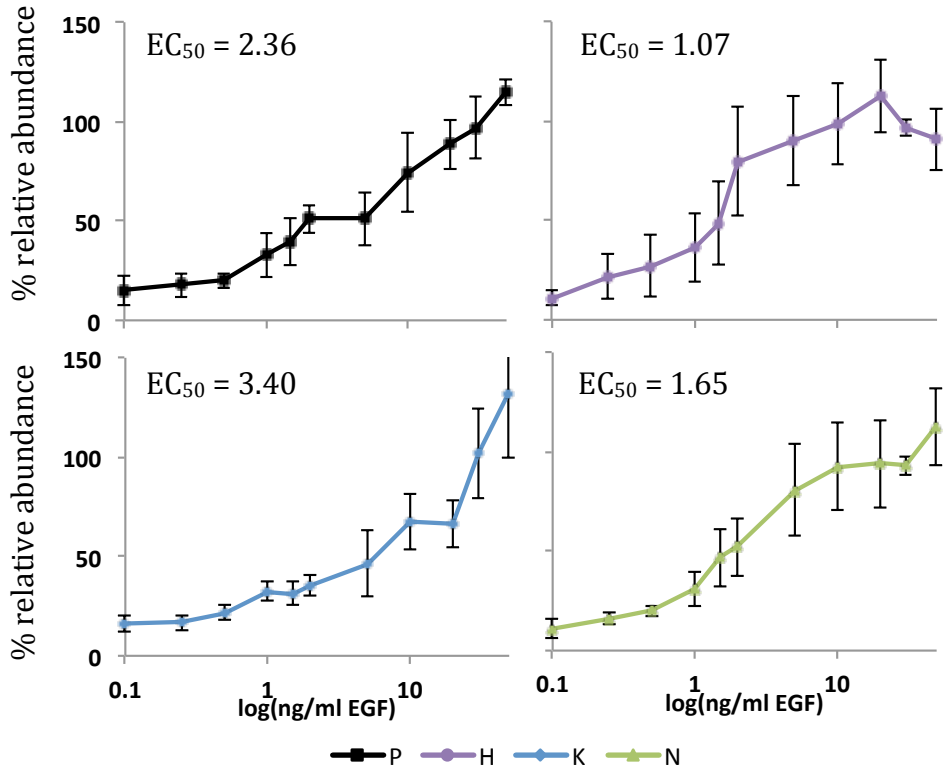

Fig. 6.6 Activation of downstream MAPK signalling pathway in Ras isogenic SW48 cell lines depending on stimulation with different concentrations of EGF. A A representative immunoblotting of MEK-pS217/pS221 (pMEK) and one actin blot. **B** Relative quantitation of MEK-pS217/pS221 activation normalised to actin, total MEK and maximal GF responses where 100% = the mean of the 3 highest concentrations of GF stimulations. Data represents means ± SD (n = 3 independent biological repeats). P – parental, H – HRas^{G12V}, N – NRas^{G12V}, K – KRas^{G12V} SW48 cell lines.

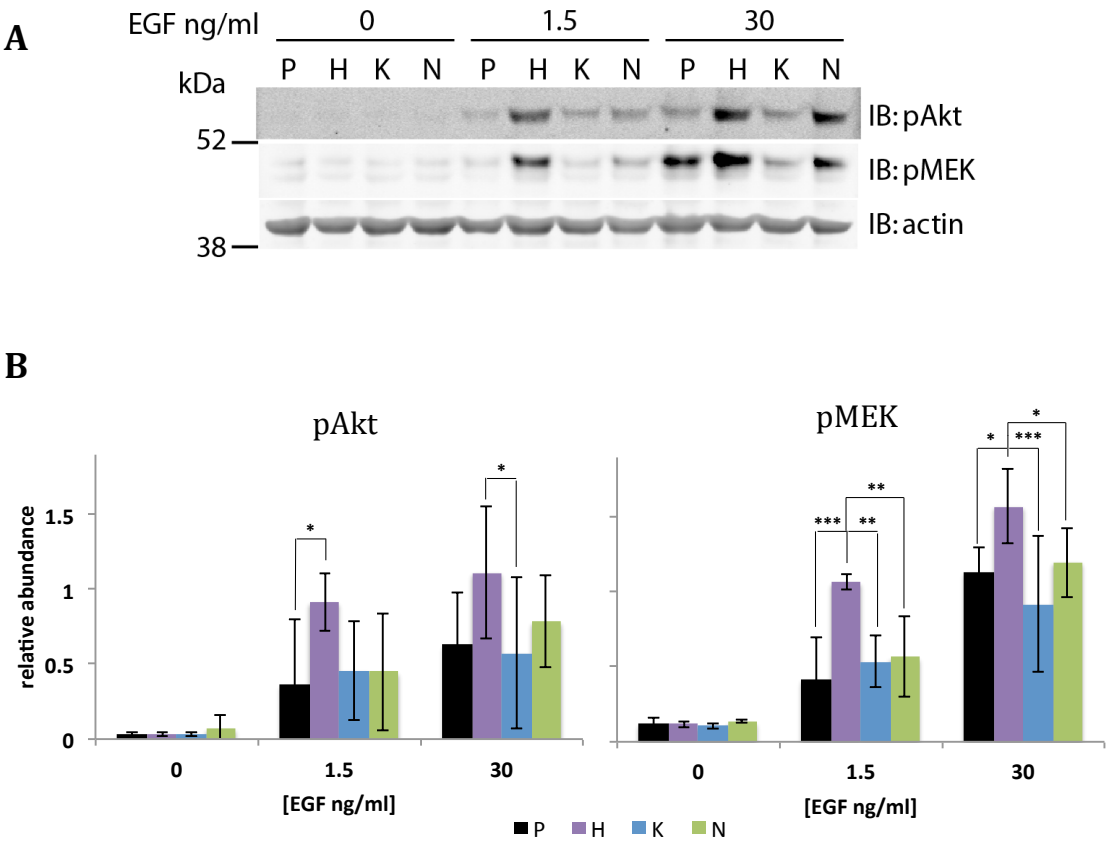

Fig. 6.7 Activation of MAPK and PI3K pathways in Ras isoform SW48 isogenic cell lines by EGF stimulation. A A representative blot (n = 3 biological replicates) – a re-run of samples from EGF gradient in Fig. 6.5 and Fig. 6.6 now in one blot. **B** Relative quantification of Akt-pS473 (pAkt) and MEK-pS217/pS221 (pMEK) from **A** normalised to actin and total Akt or MEK protein. SW48 cell lines: P – parental, H – $HRas^{G12V}$, K – $KRas^{G12V}$, N – $NRas^{G12V}$. Data was analysed by one-way ANOVA with Fisher's LSD post-hoc test. * $p \leq 0.05$, ** $p \leq 0.01$

To complement these data, a separate experiment was carried out, where Ras isogenic cell lines were cultured in normal (10% FBS) medium or were starved for 16 hours and stimulated for 5 minutes with either 0.5 or 30ng/ml EGF (Fig. 6.8). When normalised to actin loading control and total Akt or MEK, the results also indicated that pAkt and pMEK are activated more potently by $HRas^{G12V}$. Moreover, ERK activation downstream of MEK was measured and revealed that at a higher EGF concentration $HRas^{G12V}$ is slightly less potent than wild type Ras. For $KRas^{G12V}$ the pattern of activating Akt and MEK was similar as in previous

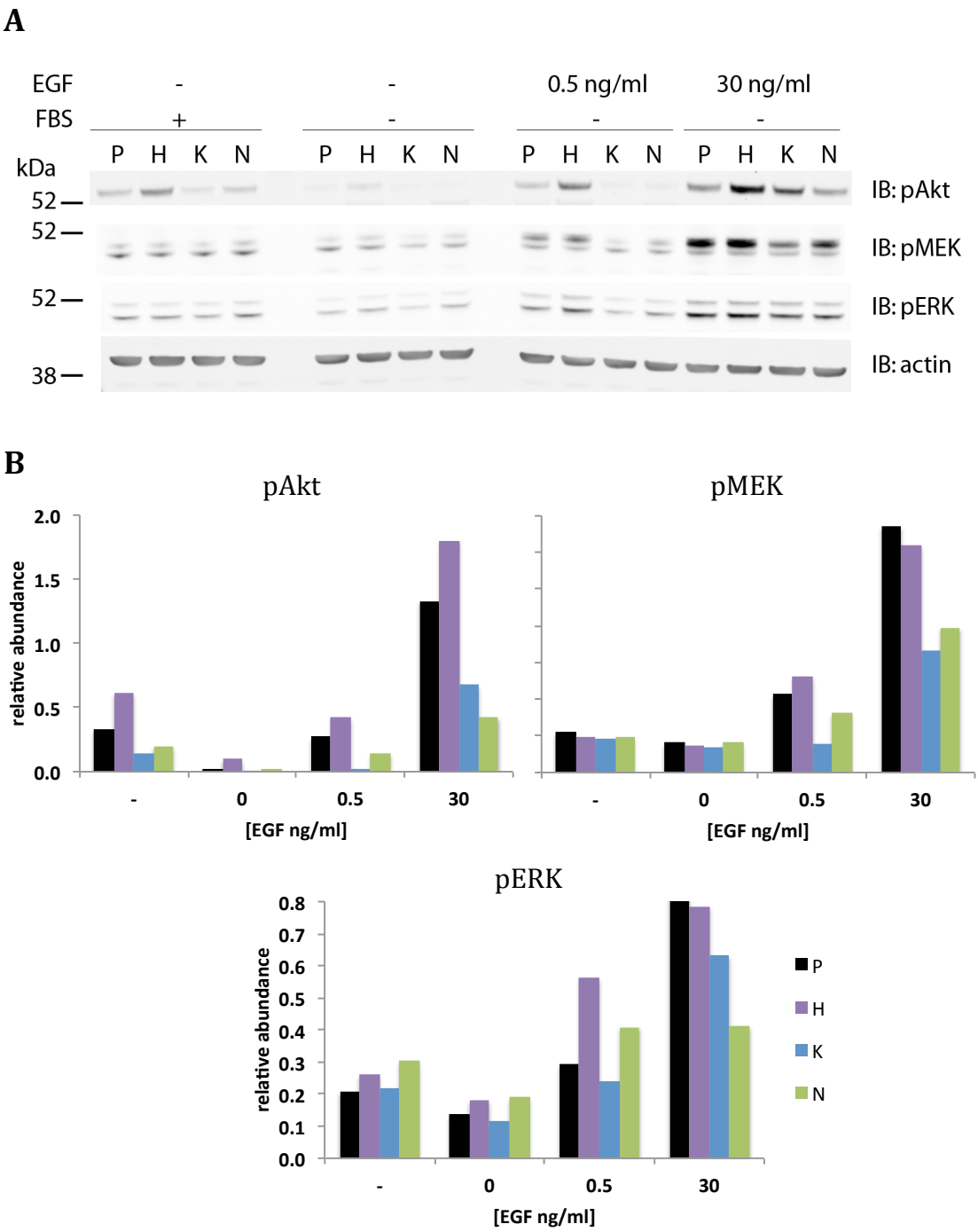

Fig. 6.8 Differential response to EGF in Ras isoform SW48 isogenic cell lines. Cells were cultured either in normal medium (10% FBS) or were starved and stimulated with different EGF concentrations. **A** Immunoblotting of Akt-pS473 (pAkt), MEK-pS217/pS221 (pMEK), ERK-pT202/pY204 (pERK) and representative actin (n = 1). **B** Relative quantification of **A** normalised to actin and total Akt, MEK or ERK protein. SW48 cell lines: P – parental, H – $HRas^{G12V}$, K – $KRas^{G12V}$, N – $NRas^{G12V}$.

experiments and it was also present for downstream ERK. However, these results were only based on one biological repeat and, hence, more experiments are needed to determine phosphorylation status of ERK.

All in all, Western blotting of Ras isogenic cell lines suggests that there are different signalling strengths downstream of Ras depending on the isoform mutated and they all respond differently to EGF stimulation in activating canonical pathways PI3K and MAPK. These differences may arise from varying sensitivity of Ras isoforms to stimulation and negative feedback loops within pathways, which will be further discussed in the next sections.

6.2.3 Isoform-specific Ras networks

The following sections describe outcomes of stimulation and inhibition of Ras-dependent pathways. For each experiment, a concentration gradient of either a GF or an inhibitor was used to measure the differences in signalling and phosphorylation status of proteins either upstream or downstream of Ras by Western blotting.

6.2.3.1 Stimulation of Ras upstream signalling

To check the phosphorylation status of receptors upstream of Ras, SW48 isogenic cell lines were starved for 24 hours and stimulated for 20 minutes with gradients of the following GFs: EGF, HGF and IGF – to stimulate EGFR, Met and IGFR1β receptors, respectively (Fig. 6.9-6.11). Both phosphorylated and total protein were measured and normalised to actin loading control. For EGFR, the Y1068 site was monitored for phosphorylation, as it is one of the three major autophosphorylation sites of EGFR, the other being Y1148 and Y1173 (Abe et al., 2006, Downward et al., 1984). The phosphorylation status of EGFR may be altered in cell lines bearing the oncogenic G12V mutation in Ras, due to feedback loops from downstream ERK back to the receptor (Klinger et al., 2013). The most EGFR stimulation was achieved in $KRas^{G12V}$ isogenic cell line, implying that mutated KRas positively regulates upstream EGFR activation

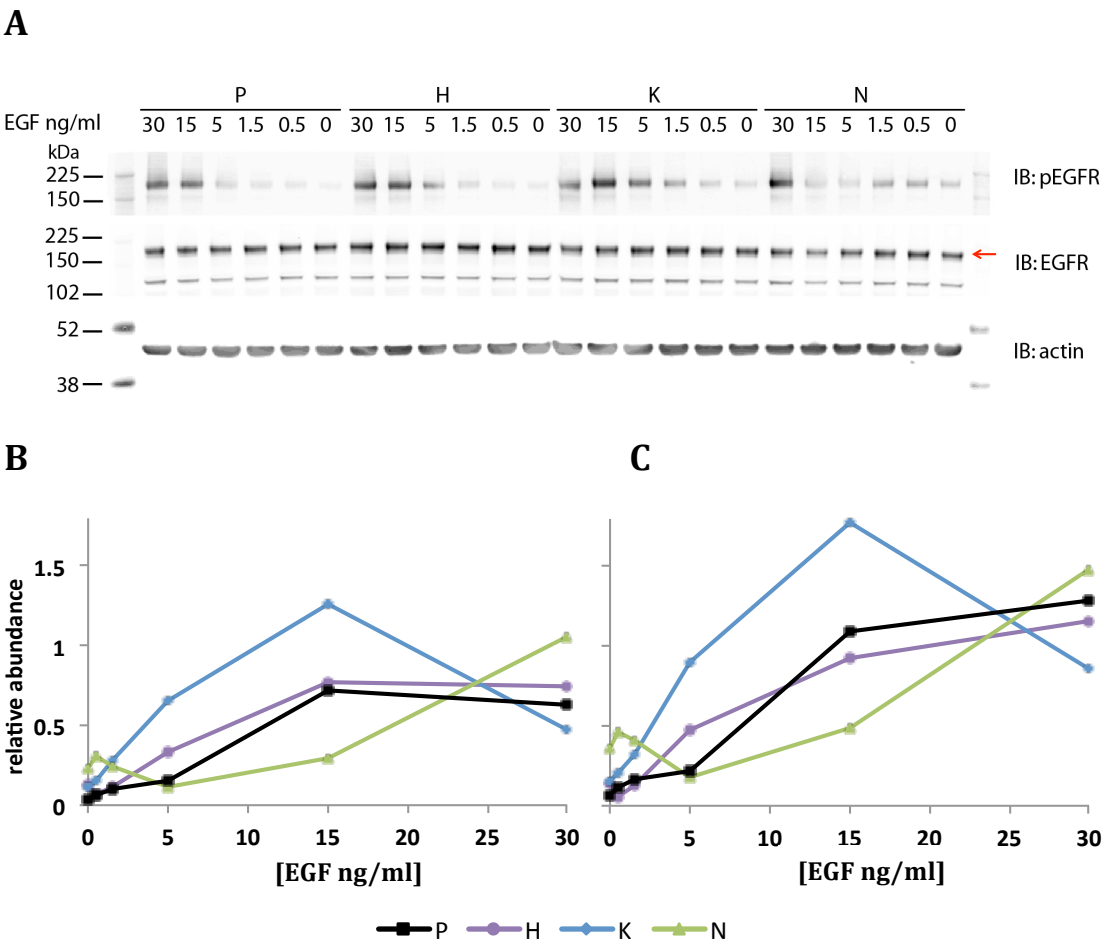

Fig. 6.9 Phosphorylation status of EGFR in SW48 Ras isogenic cell lines. Cells were starved and stimulated with different EGF concentrations. **A** Immunoblot of EGFR, EGFR-pY1068 (pEGFR) and representative actin. **B** Relative quantification of EGFR-pY1068 normalised to actin and **C** to actin and total EGFR protein. Arrow indicates the size of the blotted protein.

(Fig. 6.9). On the other hand, NRasG12V trends towards the lowest activation of EGFR, whilst HRasG12V is similar to that of wild type Ras. There may also be subtle differences in receptor abundance that are investigated further later (Fig. 6.12).

For Met receptor, the highest phosphorylation status is present in KRasG12V cell line, whereas the remaining cell lines show similar amounts of pMet (Fig. 6.10). Phosphorylation of Met has still not plateaued in the KRasG12V cell line, whereas for all of the other cell lines ≤25 ng/ml HGF is saturating. The higher pMet seen in the KRasG12V cell line may be due to the fact that these cells express significantly more Met receptor than the others (Fig. 6.12).

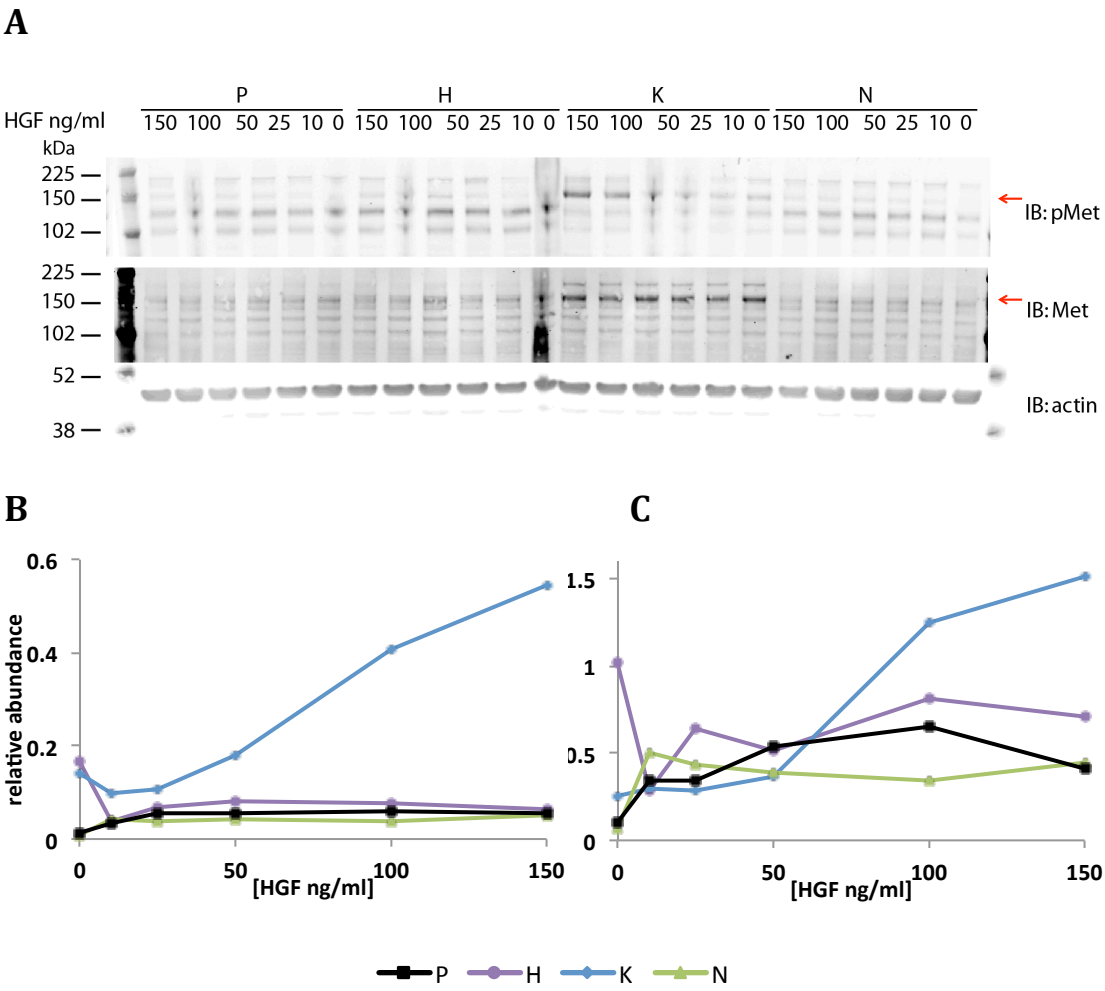

Fig. 6.10 Phosphorylation status of Met receptor in SW48 Ras isogenic cell lines. Cells were starved and stimulated with different HGF concentrations.. **A** Immunoblot of Met, Met-pS217/S221 (pMet) and representative actin. **B** Relative quantification of Met-pS217/S221 normalised to actin and **C** normalised to actin and total Met protein. Arrows indicate the size of the blotted protein.

The amount of pIGFR1β in IGF-stimulated Ras isogenic cell lines is also variable between cell lines when normalised to actin loading control only with HRasG12V cells showing the highest responses (Fig. 6.11B). However, when the IGFR1β data are also normalised to total IGFR1β protein, the relative amount of IGFR1β phosphorylation is the highest in KRasG12V and lowest in HRasG12V cell line (Fig. 6.11C).

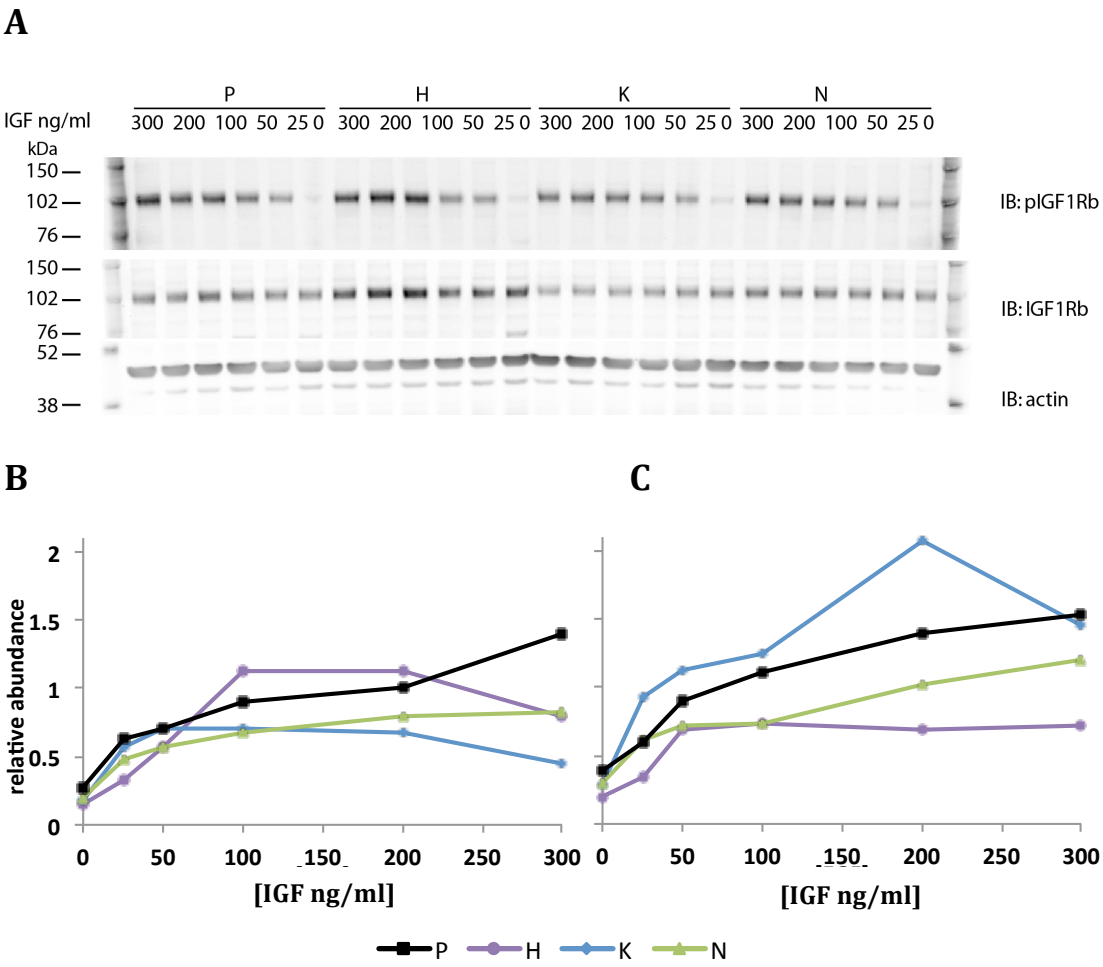

Fig. 6.11 Phosphorylation status of IGFR1β in SW48 Ras isogenic cell lines. Cells were starved and stimulated with different IGF concentrations. **A** Immunoblot of IGFR1β, pIGFR1β (IGFR1β-pY1135/Y1136 and Insulin Receptor β-pY1150/Y1151) and representative actin. **B** Relative quantification of pIGFR1β normalised to actin and **C** normalised to actin and total IGFR1β protein.

The abundance of receptors measured in previous figures (Fig. 6.9-6.11) without GF stimulation (0ng/ml) and normalised to actin was collated in Fig. 6.12 across all Ras isogenic cell lines. Based on the results, there was a trend for higher EGFR expression in the SW48 cell lines with mutant Ras isoforms compared to wild type (parental). The highest EGFR abundance is for HRasG12V cell line (40% more than parental). In contrast, Met receptor is the most highly expressed in KRasG12V cell line, whereas its expression is similar in the remaining cell lines. This is consistent with previous work that found increased Met receptor expression in isogenic cell lines expressing oncogenic KRas with

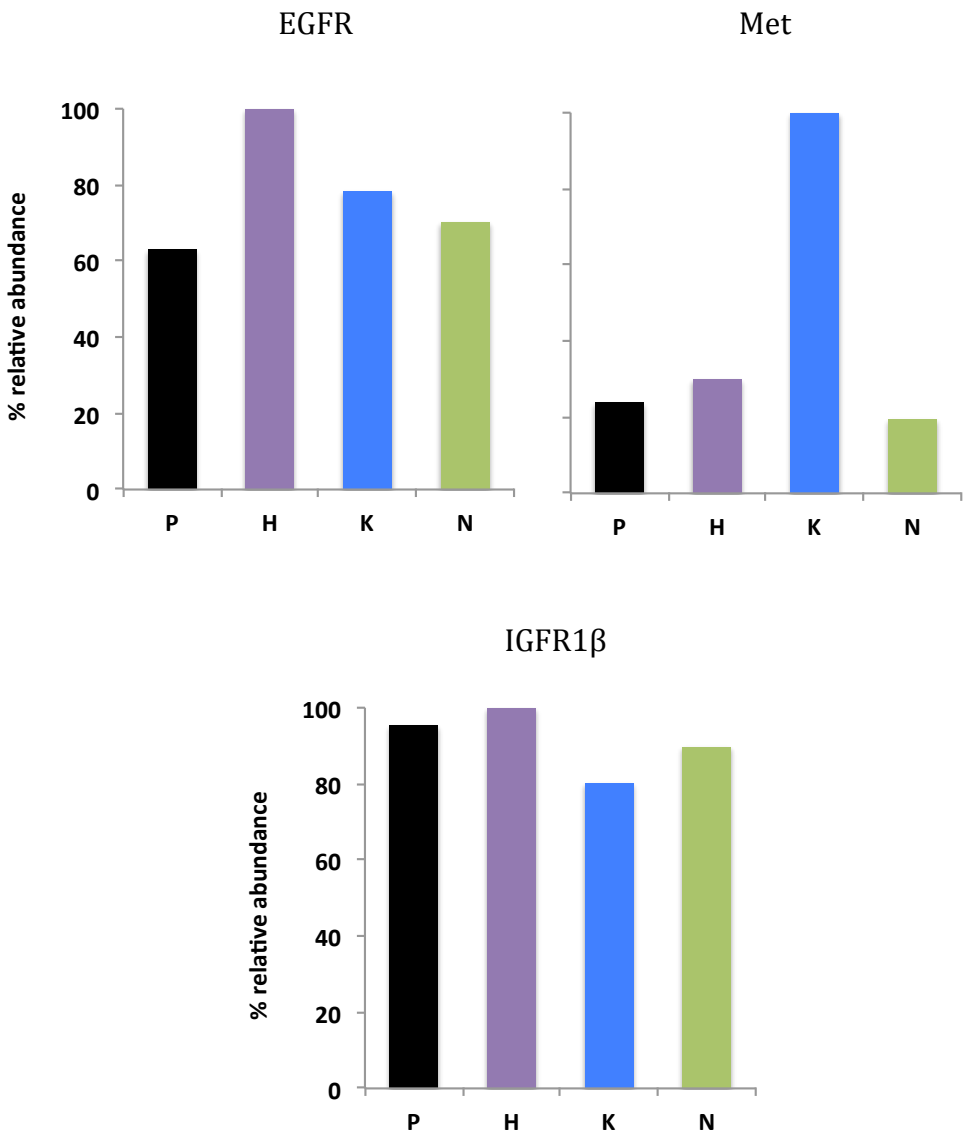

Fig. 6.12 Differential expression of cell membrane receptors in SW48 isogenic cell lines. The data was collated from Fig. 6.9-6.11 for no stimulation with GF (starved state) normalised to actin and represented as percentage of maximum expression. P – parental, H – $HRas^{G12V}$, N – $NRas^{G12V}$, K – $KRas^{G12V}$ SW48 cell lines.

G12 mutations (Hammond et al., 2015). Whilst IGFR1β levels are equivalent across most of the cell lines, there is a trend for reduced expression in the KRasG12V cell line.

In summary, both upstream and downstream components of the Ras signalling pathway exhibit clear differences in abundance or phosphorylation in each Ras isoform mutant cell line. Further work is required to reproduce some of these data and to determine the extent to which these changes are dependent on the presence of the mutant Ras protein.

6.2.3.2 Inhibition of Ras downstream signalling

Network biology analysis requires measurement of both the activation of nodes within a network and the network responses to inhibition of nodes. The use of inhibitors helps to reveal the extent to which negative feedback loops are engaged within the network. To optimise the conditions for future network biology analysis, concentration gradients of a range of inhibitors were used to measure attenuation of signalling downstream of the target. Inhibition was performed for 1 hour, followed by stimulation for 20 minutes with 20% FBS containing the inhibitor. LY294002 was used to reversibly inhibit PI3K (Mena et al., 2014, Wu et al., 2014) and the level of inhibition of downstream Akt was measured by Western blotting for pAkt (Fig. 6.13). An almost complete attenuation of phosphorylation of Akt was seen at around 20μM drug concentration and the IC_{50} across all Ras isoforms were similar (0.01-0.02). Total Akt protein levels were equivalent across all cell lines.

The next inhibitor used was AZD6244 (Selumetinib), which reversibly inhibits MEK1/2 (Garon et al., 2010, Huynh et al., 2007). Complete attenuation of downstream pERK signal was seen at 10μM concentration in all Ras isogenic cell lines. Again, the IC_{50} values were similar across the cell lines (0.004-0.005) (Fig. 6.14). Total protein levels of ERK were similar across all isogenic cell lines.

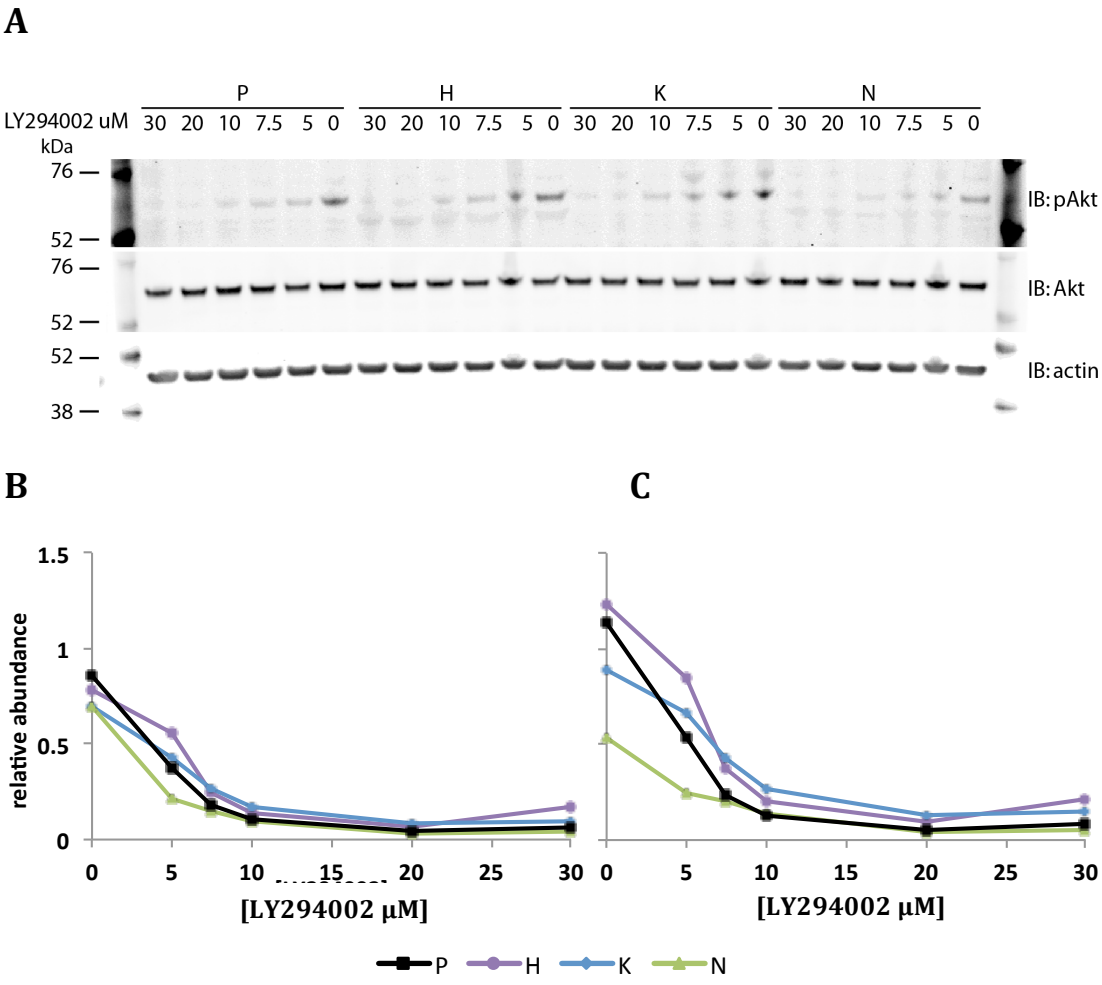

Fig. 6.13 Inhibition of PI3K in SW48 Ras isogenic cell lines with different LY294002 concentrations. A Immunoblotting of Akt, Akt-pS473 (pAkt) and representative actin. **B** Relative quantification of Akt-pS473 (pAkt) to actin and **C** to actin and total Akt protein. Isogenic cells were serum starved for 24 hours before addition of LY294002 for 1 hour and then addition of 20% FBS for 20 minutes. n=1. P – parental, H – $HRas^{G12V}$, N – $NRas^{G12V}$, K – $KRas^{G12V}$ SW48 cell lines.

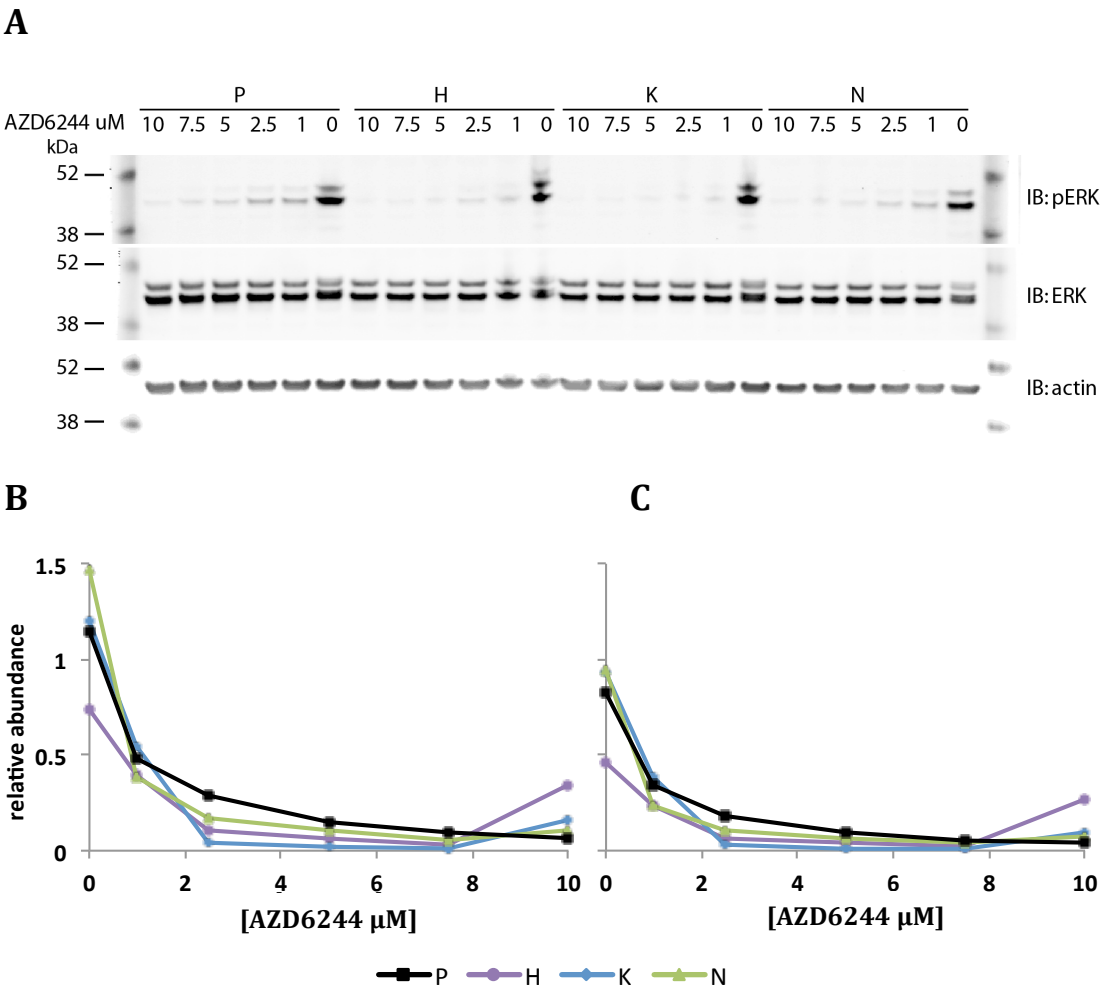

Fig. 6.14 Inhibition of MEK1/2 in SW48 Ras isogenic cell lines with different AZD6244 concentrations. **A** Immunoblotting of ERK, ERK-pT202/pY204 (pERK) and representative actin. **B** Relative quantification of ERK-pT202/pY204 (pERK) to actin and **C** to actin and total ERK protein. Isogenic cells were serum starved for 24 hours before addition of AZD6244 for 1 hour and then addition of 20% FBS for 20 minutes. n=1. P – parental, H – $HRas^{G12V}$, N – $NRas^{G12V}$, K – $KRas^{G12V}$ SW48 cell lines.

To specifically inhibit mTOR signalling, a gradient of concentrations of a reversible inhibitor Rapamycin (Edwards and Wandless, 2007) was used in Ras isogenic cell lines. The level of phosphorylation of the downstream mTOR target p70S6K was measured by Western blotting (Fig. 6.15) and showed

varying levels of inhibition depending on the Ras isoform that was mutated. First of all, Parental and NRasG12V cells display only low pp70S6K levels compared to the other Ras mutant cell lines. This means that it is difficult to distinguish responses to treatment with different concentrations of Rapamycin (Fig. 6.15B). The most striking observation is that the HRasG12V and KRasG12V cell lines display reciprocal responses to Rapamycin treatment with pp70S6K almost completely reduced at around 0.2 μM in HRasG12V cells. In contrast, the KRasG12V cell line showed an initial reduction of pp70S6K before it went up again and exceeded basal level straight at doses greater than 0.2 μM of Rapamycin. This may suggest relief of a negative feedback loop.

The final inhibitor used was Sorafenib, which inhibits Raf kinase (Wilhelm et al., 2004). However, it also inhibits tyrosine kinase receptors involved in angiogenesis at higher doses. To measure its inhibition effectiveness at inhibiting Ras in Ras isogenic cell lines, phosphorylation of the Raf effector MEK was measured (Fig. 6.16). Unfortunately, pMEK levels did not seem to decrease with higher Sorafenib concentrations in neither of the cell lines. This observation could not be explained by the sensitivity of pMEK antibody, as it was working in previous experiments (Fig. 6.5, Fig. 6.6, Fig. 6.7). It seemed plausible at first to check Sorafenib inhibition potency at higher concentrations and/or longer inhibition times. Hence, optimisation of Raf inhibition by Sorafenib is shown in the next section.

Importantly, the above data represents only single biological replicates and more repeats are needed to ascertain the true differences between Ras isoform-dependent signalling.

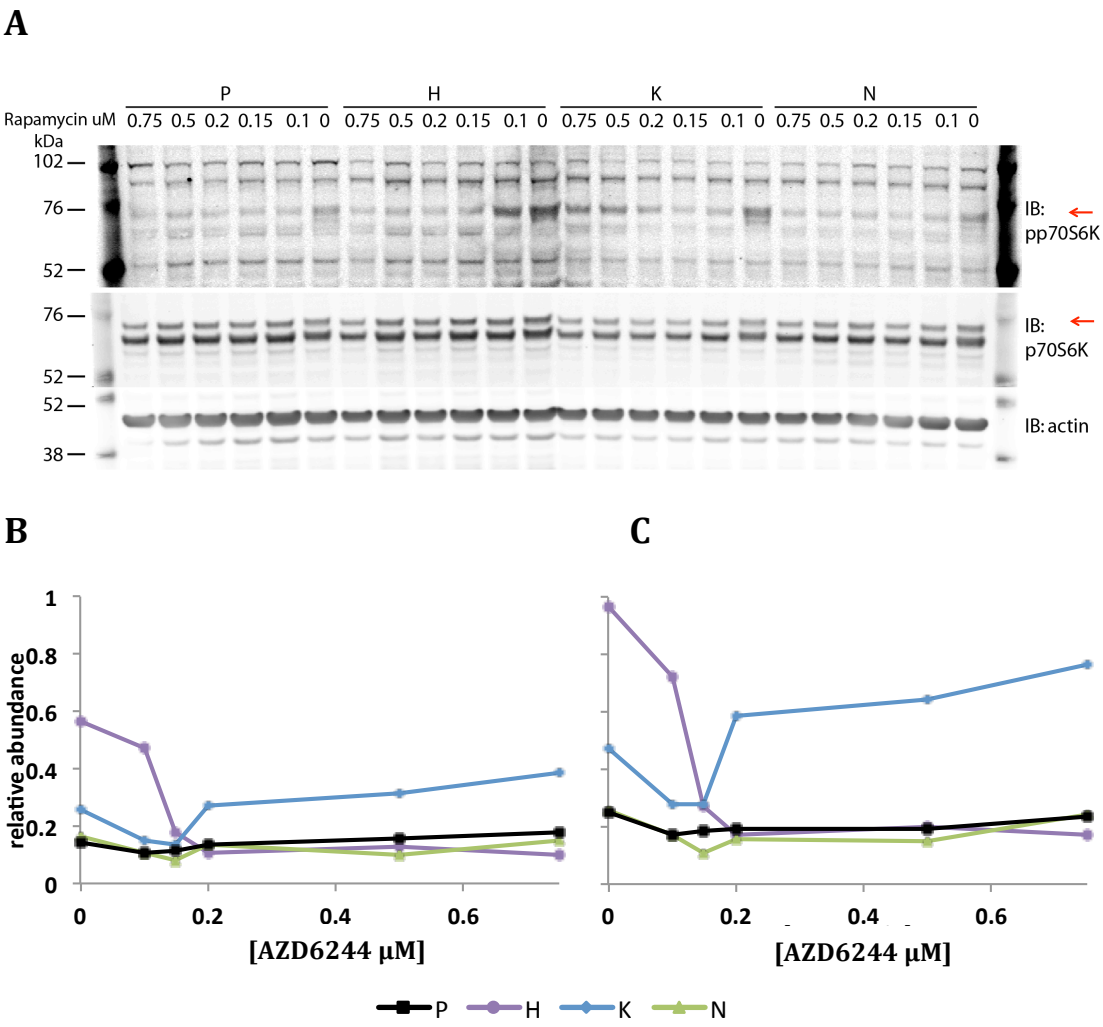

Fig. 6.15 Inhibition of mTOR in SW48 Ras isogenic cell lines with different Rapamycin concentrations. **A** Immunoblotting of p70S6K, p70S6K-pT389 (pp70S6K) and representative actin. **B** Relative quantification of p70S6K-pT389 (pp70S6K) to actin and **C** to actin and total p70S6K protein. Isogenic cells were serum starved for 24 hours before addition of Rapamycin for 1 hour and then addition of 20% FBS for 20 minutes. n=1. Arrows indicate the size of the blotted protein. P – parental, H – $HRas^{G12V}$, N – $NRas^{G12V}$, K – $KRas^{G12V}$ SW48 cell lines.

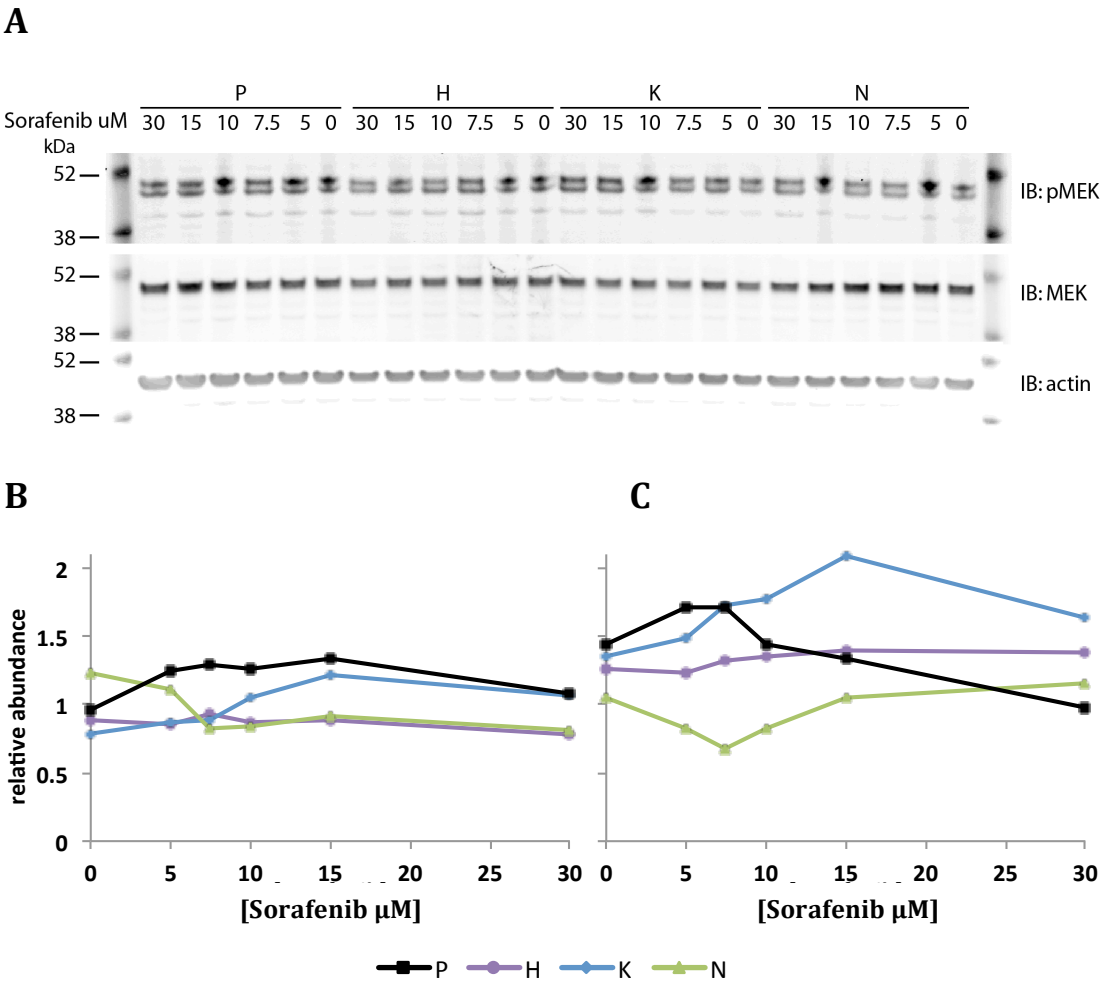

Fig. 6.16 Inhibition of Raf in SW48 Ras isogenic cell lines with different Sorafenib concentrations. A Immunoblot of MEK, MEK-pS217/pS221 (pMEK), and representative actin. **B** Relative quantification of MEK-pS217/pS221 (pMEK), to actin and **C** to actin and total MEK protein. Isogenic cells were serum starved for 24 hours before addition of Sorafenib for 1 hour and then addition of 20% FBS for 20 minutes. n=1. P – parental, H – $HRas^{G12V}$, N – $NRas^{G12V}$, K – $KRas^{G12V}$ SW48 cell lines.

6.2.3.3 Optimisation of Raf inhibition in Ras isogenic cell lines

To optimise Raf inhibition in Ras isogenic cell lines, Sorafenib concentration was increased to 100 μM and incubation time to either 2 or 16 hours. Parental SW48 cell line was treated as a representative. To check whether Sorafenib was working properly, a control sample treated with the same inhibitor, but from a different supplier (Santa Cruz), was used alongside the old one on a Western blot (Fig. 6.17). Moreover, pERK levels were measured together with pMEK and the corresponding non-phosphorylated protein.

According to the results, the inhibitor seemed to have a bigger effect on cell lines which were starved and then stimulated with 20% FBS, rather than grown in normal 10% FBS medium. Surprisingly, in non-starved samples the longer the inhibition and the higher the dose, the more activation of MEK and ERK was achieved, which was also true for the control sample with the drug from another supplier. For serum-starved and stimulated cell lines, the inhibitor seemed to inhibit downstream Raf signalling, when compared to non-treated control. After 2 hours of inhibition, the levels of both pMEK and pERK decreased, with the higher response seen with 100μM Sorafenib. After 16 hours, however, the levels of phosphorylation decreased dramatically, especially for pERK and the upper band of pMEK, which may represent different phosphorylation status of MEK or one of the MEK isoforms. At the same time, the levels of total protein of MEK and ERK also seemed to decrease. Nevertheless, 30μM or 100μM Sorafenib appeared to potently inhibit Raf kinase when pre-incubated for 16 hours (Figure 6.17).

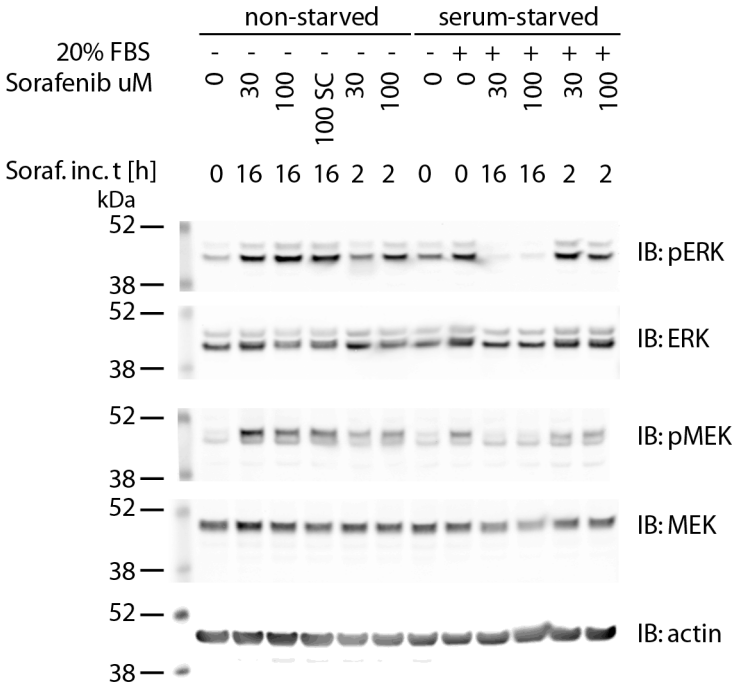

Fig. 6.17 Inhibition of Raf in SW48 parental cell line with Sorafenib for 16 hours. Cells were grown either in normal (10% FBS) medium (non-starved) or were serum-starved and stimulated with 20% FBS for 20 min. Sorafenib was added for the indicated amounts of time before stimulation and cell harvesting. The figure represents immunoblotting of MEK, MEK-pS217/pS221 (pMEK), ERK, ERK-pT202/pY204 (pERK) and representative actin. Soraf. inc. t [h] – Sorafenib incubation time in hours.

Complete response to inhibition by Sorafenib was achieved already at 30μM after 16 hours of incubation for the parental cell line. Hence, this concentration was used as a maximum in the concentration gradient to measure the response to inhibition in the remaining isogenic cell lines (Fig. 6.18). Unfortunately, the previously observed response in the parental cell line was not reproduced. After 16 hours of inhibition, pMEK levels seemed to increase with higher concentrations of Sorafenib. Such increase in phosphorylation was also seen for KRasG12V cell line. However, for NRasG12V and HRasG12V cell lines, the increase in pMEK levels was followed by a rapid decrease in phosphorylation at 30μM and 20μM of Sorafenib, respectively. For HRasG12V very few cells were recovered from the treatment with Sorafenib at 30μM and therefore the corresponding lane on the Western blot was left blank (Fig. 6.18). It seemed that

both HRasG12V and NRasG12V cell lines were more responsive to Sorafenib treatment than the parental and KRasG12V cell lines. Nonetheless, the inhibitory effect seemed also to contribute to cellular toxicity, at least in HRasG12V cell line.

To investigate whether inhibition with Sorafenib leads to apoptosis in Ras isogenic cell lines, Western blotting was used to detect cleaved PARP, which signals undergoing programed cell death due to DNA damage and/or cellular stress. Interestingly, higher amounts of cleaved PARP (Fig. 6.18, lower band of PARP) were present in samples treated with more inhibitor (10-30μM), concluding that Sorafenib exerted a toxic effect on the cells.

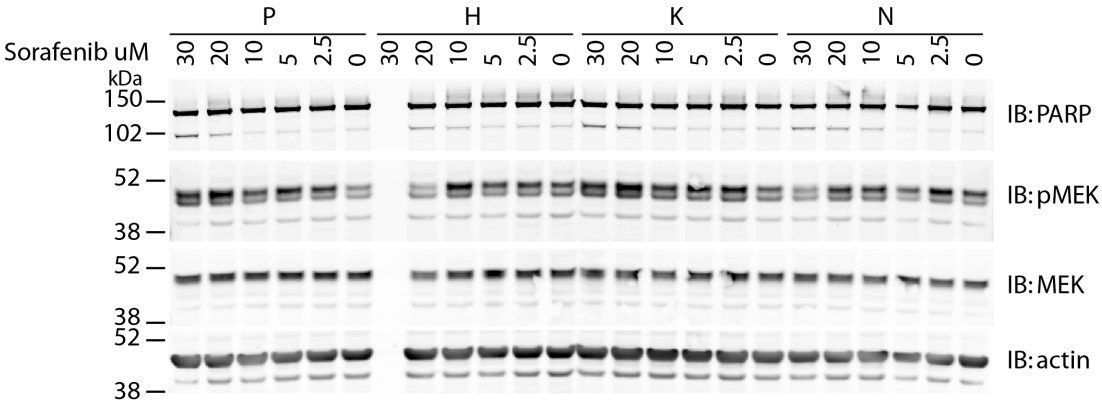

Fig. 6.18 Inhibition of Raf with Sorafenib for 16 hours in SW48 Ras isogenic cell lines and apoptotic effect. Cells were grown in serum-free medium for 24 hours and then incubated with different concentrations of Sorafenib (30μM, 20μM, 10μM, 5μM, 2.5μM) for 16 hours and stimulated with 20% FBS for 20 minutes. Protein lysates were immunoblotted for cleaved PARP, MEK, MEK-pS217/pS221 (pMEK) and actin (representative blot shown). P – parental, H – HRasG12V, K – KRasG12V, N- NRasG12V SW48 isogenic cell lines.

To further examine the response of cells to the treatment with Sorafenib, visible changes to cell appearance were observed using phase contrast microscopy (Fig. 6.19). The experiment was a blind study, as the pictures were taken randomly without knowing which cell line they represent.

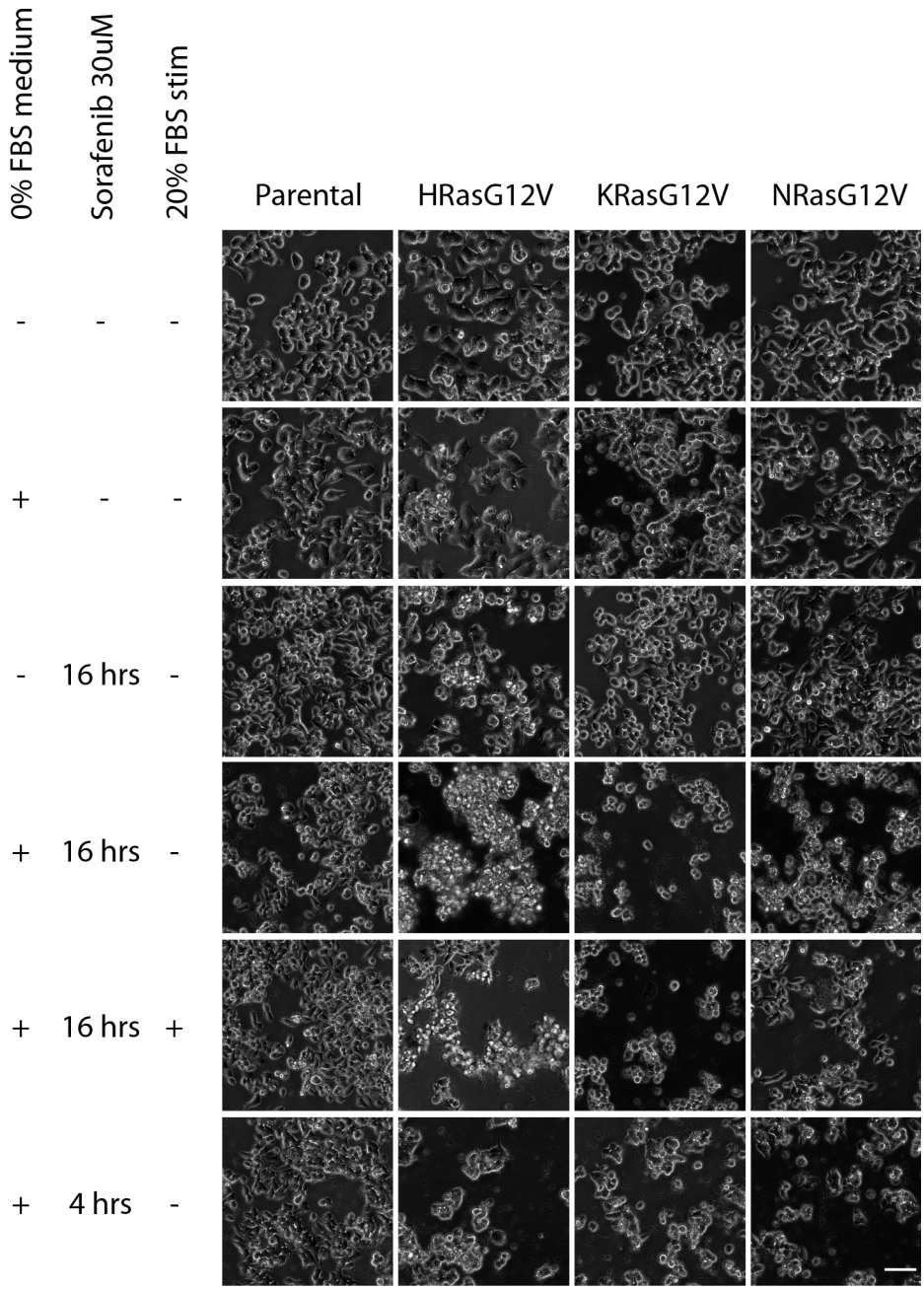

Fig. 6.19 Micrographs of SW48 Ras isogenic cell lines treated with Raf inhibitor Sorafenib. Cells were grown in full medium (10% FBS) or were serum starved (0% FBS) for 24 hours, followed by incubation with 30μM Sorafenib for 16 or 4 hours. Cells were then stimulated with 20% FBS for 20 minutes and visualised by contrast microscopy. Scale bar = 100 μm.

When grown in full medium (10% FBS), the cell size for SW48 HRasG12V was bigger than for the remaining SW48 cell lines (Fig. 6.19). The cell size difference was even more striking for serum-starved cell lines. When treated with 30μM Sorafenib for 16 hours, in non-starved cell lines, cell size decreased substantially as compared to non-treated cells, as if the cells were shrinking, perhaps due to apoptosis or the loss of adhesion. Remarkably, cell density seemed to be constant, regardless of Sorafenib treatment.

In starved cells incubated with Sorafenib, the cells also looked apoptotic, but the density dramatically decreased, especially in KRasG12V cell line, as compared to non-starved cells. In SW48 $HRas^{G12V}$ cell line, clumps of cells detached from the plate surface were floating in the medium, suggesting that the reduction in density may be due to dysfunctional adhesion.

The shrinking/apoptotic effect of Sorafenib treatment was also apparent in cells which were starved and stimulated with 20% FBS for 20 minutes. SW48 parental cell line seemed to maintain higher density than its Ras isogenic derivative cell lines. This might be due to a lower number of apoptotic cells in SW48 parental cell line and may indicate better resistance to Sorafenib treatment. For HRasG12V cell line, a cluster of floating cells was present again, which could explain why a low number of cells were recovered in the previous experiment (Fig. 6.18). Finally, when treated with Sorafenib for only 4 hours, the shrinking effect was still preserved in parental cell line, but not in the remaining cell line. Cell densities also appeared to be higher, as compared to treatment for 16 hours.

To conclude, Sorafenib is toxic for SW48 cell lines isogenic for G12V mutation in Ras isoforms, as it negatively affects cell density, suggesting a loss in viable cells. For parental cell line, the changes in density are not clearly visible, implying that these cells are more resistant to treatment with Sorafenib. Inhibition of pMEK or pERK responses could not be reproducibly achieved in any of the cell lines.

6.3 Discussion

This chapter focused on endogenous Ras isoform-dependent signalling in a context of a human colorectal cancer cell line. Fully diploid SW48 cell lines isogenic for a heterozygous G12V mutation in each of the three RAS genes allowed to directly compare Ras isoform signalling outcomes by providing identical genetic background for each cell line and endogenous protein levels.

The limitations of this study included the use of only single cell clones, i.e. only one of each NRas, KRas and HRas cell line clone with G12V mutation was compared. The lack of comparison of cell lines derived from other clones of the parental SW48 cell line raises the possibility of unnoticed clonal artefacts, which may have been taken as true isoform-specific responses. Cells derived from the parental cell line by clonal selection (limited dilution method – (Dexter et al., 1978)) can show different phenotypical properties, such as doubling time, colony formation in soft agar and metastatic potential (Li et al., 2001, Ware et al., 2007). Hence, it is important to compare at least 2-3 different clones to assure the accuracy of the results.

Nevertheless, these preliminary results suggested marked differences between the signalling of distinct Ras isoforms and the phenotypic changes of the isogenic cell lines. G12V mutation seemed to decrease the cell growth when present in NRas, but not in other Ras isoforms (Fig. 6.3). A previous study in a colon cancer mouse model expressing the G12D mutation in either KRas or NRas has shown that only oncogenic KRas can contribute to hyperplasia in the colon (Haigis et al., 2008), hence, higher growth rate could also be expected for the SW48 cell line with oncogenic KRas. However, this does not explain why the NRasG12V cell line is actually growing slower than all remaining isogenic cell lines, including the parental. Another reason could be that cells with mutant NRas undergo differentiation at higher densities (Fig. 6.3, day 3) (Roberts et al., 2006b, Zweibaum et al., 1983). SW48 cells are actually poorly to moderately differentiated (Huschtscha et al., 1991, MacKay et al., 1995), so there is a possibility that under certain environmental or endogenous stimuli they could differentiate further and, hence, cease proliferating (Jogi et al., 2012). Yet

another explanation for slower growth rate of NRasG12V cell line would be induction of apoptosis. Previous research demonstrated that oncogenic Ras is capable of stimulating pro-apoptotic signals via RASSF1-mediated or even MAPK-mediated cascades (Vos et al., 2000, Cox and Der, 2003). These findings pose a chance that in case of SW48 cell line such apoptotic event would be plausible. Either way, to confirm whether differentiation or programmed cell death actually occurred, further experiments would have to validate the presence of specific markers – e.g. CDX1 as a marker of intestinal differentiation (Bonner et al., 1995, Chan et al., 2009, Mallo et al., 1997) or Bax as a pro-apoptotic marker (Paradiso et al., 2001). What is also interesting to note, G12V mutation did not accelerate proliferation of SW48 cell line when present in KRas or HRas, implying that these isoforms may not further contribute to the transforming potential of these cells.

Another striking difference between Ras isogenic cell lines were the distinct levels of activation of downstream signalling, as measured by phosphorylation of Akt, MEK and ERK (Fig. 6.5-6.8). Based on Western blotting, after stimulation with EGF, human HRas protein seemed to provide better pAkt and pMEK signals than other Ras isoforms. Interestingly, pERK appeared to be less affected by activate HRas, at least when compared with wild type protein (Fig. 6.8). It is important to take into account the mutations already existing in wt SW48 cell line, which are G719S in EGFR, S33Y in CTNNB1 and S668fs*39 (frame shift) in FBXW7 (Forbes et al., 2015, Ahmed et al., 2013). The mutation present in EGFR is hyperactivating and resutls in around 10-fold more active protein than wt (Yun et al., 2007). Mutations in EGFR are generally not frequent in colorectal cancer (Barber et al., 2004, Lynch et al., 2004, Moroni et al., 2005, Nagahara et al., 2005, Yunxia et al., 2010, Oh et al., 2011) and their significance in disease prognosis and treatment has not been established. On the other hand, mutations of the S33 codon of beta-catenin (CTNNB1 gene) are common in various human cancers, including hereditary non-polyposis colorectal cancer (Akiyama et al., 2000, Johnson et al., 2005, Kim et al., 2003, Saegusa and Okayasu, 2001). Mutations in beta-catenin may confer resistance to PI3K and Akt inhibitors (Tenbaum et al., 2012). Finally, F-box and WD repeat domain-containing 7

(FBXW7) is a part of an E3 ubiquitin ligase complex and a tumour suppressor often mutated in colorectal cancer (Markowitz and Bertagnolli, 2009, Wang et al., 2012). Mutations in FBXW7 may also sensitise cells to treatment with mTOR inhibitors (Jardim et al., 2014, Mao et al., 2008, Wang et al., 2013).

Notably, these endogenous mutations in SW48 cell line could affect Ras-dependent signalling, especially the changes in upstream RTK receptor EGFR. Although these mutations uniformly affect all Ras isogenic cell lines, they could have a greater impact on a particular isoform which participates in a feedback loop. Earlier studies demonstrated that Ras is involved in a negative feedback loop from MEK to upstream ERBB, EGFR or IGFR receptors, which is relieved by MEK or BRAF inhibition that leads to activation of ERK or PI3K and Akt (Ebi et al., 2011, Klinger et al., 2013, Lamba et al., 2014, Misale et al., 2014, Molina-Arcas et al., 2013, Prahallad et al., 2012, Sun et al., 2014, Turke et al., 2012, Van Schaeybroeck et al., 2014). This negative regulation was seen in studies focused on KRas signalling and whether this is a generic or an isoform-specific signalling mechanism remains to be revealed. In this context, the increased stimulation in PI3K and MAPK pathways seen in the HRasG12V mutant cell line could be explained by the fact that HRas may not take part in negative feedback regulation, as opposed to the other Ras isoforms. Rather, KRas and NRas mutant cell lines may show decreased levels of pAkt and pMEK due to feedback inhibition of upstream signalling receptors. Interestingly, pERK levels do not seem to be affected by these feedback loops, as ERK might be the final node in these negative regulation loops and its high levels of activation may aid in their propagation.

To further investigate the differences in network biology in a Ras isoform-dependent background, each isogenic cell line was treated with specific GFs and pathway component inhibitors (Fig. 6.9 – 6.16). The data of this study provided some preliminary results, which can be used for studying relative coupling of isoforms to downstream effectors and involvement in feedback loops. Previous work utilised a combined empirical and theoretical means of modelling signalling networks in an EGFR-dependent context (Klinger et al., 2013). In that

study, the phosphorylation status of cell lines prior and after treatment was measured using multiplex proteomics and the data was examined using a modular response analysis (MDA), which allows to quantitatively measure negative and positive feedback loops, as well as cross talks between pathways. This is important as such signal transduction subtleties may exert significant effects on the pharmacologic action of drugs (Cirit et al., 2010, Friday et al., 2008, Fritsche-Guenther et al., 2011, Sturm et al., 2010). This chapter aimed to optimise the necessary reagents, both receptor agonists (GFs) and inhibitors, for the experimental part of such network biology approach. The data obtained for saturating and sub-saturating levels of these reagents will be used in future work, which combines inhibition and stimulation to delineate differences in phosphorylation status and, hence variations in the regulation of signalling networks.

The results of this chapter suggest that stimulation with EGF exerts a differential effect on Ras isoform signal propagation (Fig. 6.9). Highest levels of phosphorylated EGFR were present in KRasG12V cell line, followed by HRasG12V, however, total receptor levels were higher in the latter (Fig. 6.12). Activation of EGFR requires dimerisation, which can be driven by either ligand-binding or increased receptor expression (Yarden and Schlessinger, 1987a, Yarden and Schlessinger, 1987b). A crucial step in EGFR activation is the release of the intrinsic autoinhibition of its kinase domain by the formation of an asymmetric dimer between the kinase domains of the receptor (Kovacs et al., 2015, Zhang et al., 2006). The C lobe of one kinase domain (activator) allosterically binds to the N lobe of the other kinase domain (receiver) and switches it on. Such asymmetry of EGFR dimer may lead to different phosphorylation of the activator and receiver tyrosine residues in the intracellular tail (Kovacs et al., 2015).

The observed increase in RTK abundance in the study of this thesis might be linked with a positive feedback loop in HRasG12V mutant cell line, e.g. due to increased transcription of EGFR downstream of Ras. *Egfr* gene expression is regulated by Sp1, ETF and c-jun transcription factors (Kageyama et al., 1988a, Kageyama et al., 1988b, Mialon et al., 2005), whereas Ras signalling affects a

myriad of downstream TFs, including c-jun (Chang et al., 2003, Chen et al., 2001). Hence, it is possible that Ras also regulates *Egfr* transcription via c-jun. On the other hand, receptor abundance on the cell membrane depends on the subtle equilibrium between receptor degradation and recycling (Chi et al., 2011, Doherty and McMahon, 2009, Jones et al., 2006, Maxfield and McGraw, 2004). Thus, such increase in EGFR levels may be a result of either a decrease in protein degradation due to reduction in receptor phosphorylation and subsequent ubiquitination (Roepstorff et al., 2009), or an elevated recycling of the receptor back to the cell membrane, which could be especially affecting HRasG12V cell line. To examine whether EGFR protein levels increased as a result of one of these mechanisms, transcript levels could be measured by qPCR and ubiquitination status checked by pull down assay. Also, EGFR levels could be quantified after shorter stimulation times with EGF, e.g. after 5 min instead of 20 min, which would allow for looking at the receptor before internalisation (Henriksen et al., 2013).

On the other hand, Met receptor abundance was observed to be highest in KRasG12V cell line, whereas the remaining cell lines did not seem to have any of the receptor expressed (Fig. 6.10 and 6.12). This is particularly interesting, as increased Met abundance was observed before in SW48 cell line bearing G12 codon mutations (including G12V) in KRas, but not G13D mutation or parental cell line (Hammond et al., 2015). This increased receptor abundance was correlated with increased levels of doublecortin-like kinase-1 (DCLK1), A-kinase anchor protein 12 (AKAP12) and Caveolin-1. In contrary, tight junction protein ZO-2 and the aldehyde dehydrogenase ALDH3A1 showed concerted decrease in protein abundance in KRasG12V cell line, compared to parental. Remarkably, caveolin-1 has been shown to be regulated by KRas in colon tumourigenesis (Basu Roy et al., 2013), whereas DCLK1 has been shown to be an intestinal tumour stem cell-specific marker (Nakanishi et al., 2013). DCLK1 protein expression pattern correlates well with Met expression in KRas mutant SW48 cell lines, suggesting regulatory mechanism for gene expression (Hammond et al., 2015). It would be useful to examine whether DCLK1 levels

also correspond to Met abundance in the remaining Ras isogenic cell lines using Western blotting or proteomics.

Finally, IGF1Rβ stimulation with IGF revealed that KRasG12V cell line had relatively highest phosphorylation status of this RTK, although total receptor levels were lowest, as compared to other isogenic cell lines (Fig. 6.11 and 6.12). This preliminary data suggests that oncogenic KRas may mediate a positive feedback loop back to IGF1Rβ, which finally may lead to downregulation of receptor abundance. This, however, will require further confirmation. In conclusion, the RTKs examined in this study in context of Ras signalling imply tangible differences between Ras isoforms and should be studied further using more biological replicates.

Similarly to stimulation data shown in this chapter, experiments involving inhibition of Ras pathway components were briefly examined using single biological replicates and, hence, provide initial optimisations for the drugs chosen (Fig. 6.13-6.16). While PI3K inhibitor LY94002 and MEK1/2 inhibitor AZD6244 seem to potently inhibit their targets in all isogenic cell lines (Fig. 6.13-6.14), mTOR inhibitor rapamycin appears to only suppress signalling in the HRasG12V cell line (Fig. 6.15). Both NRasG12V and parental cell lines may not have any basal phosphorylated p70S6K, which may mean that their mTOR signalling to downstream effectors is somehow suppressed. This may be further reflected by the fact that SW48 cells with HRasG12V mutation appear to be the largest when grown in normal or starved culture media (Fig. 6.19), as mTOR signalling, which is potently active in this cell line, is associated with protein synthesis and cell growth via its downstream substrate p70S6K (Fingar et al., 2004, Laplante and Sabatini, 2009). Moreover, rapamycin inhibits signalling in KRasG12V cell line only at lower drug concentrations and further titration reverses this inhibitory effect. It seems that there might be a negative feedback loop in KRasG12V cell line, which might be relieved upon mTOR inhibition. This assumption could be tested using the network biology approach described above (Klinger et al., 2013).

Lastly, inhibition of Raf with sorafenib requires further optimisation, as its inhibitory effect on parental SW48 cell line (Fig. 6.17) could not be replicated in later experiments and in KRasG12V isogenic cell line (Fig. 6.18). Sorafenib appears to be toxic, especially in HRasG12V cell line, and it may induce apoptosis in the tested cell lines (Fig. 6.18-6.19). Previous studies demonstrated that Raf inhibitors, including sorafenib, paradoxically activate MAPK signalling in cell lines with wt BRAF and oncogenic Ras (Hall-Jackson et al., 1999, Holderfield et al., 2014, Poulikakos et al., 2010). This is due to Raf kinases taking part in negative feedback regulation via MEK-dependent mechanism, e.g. active ERK phosphorylates and inhibits both BRAF and CRAF, which impedes their heterodimerisation and, hence, coupling with Ras (Dougherty et al., 2005, Ritt et al., 2010). Use of Raf inhibitors relieves this negative regulation and contributes to activation of downstream MEK. Furthermore, Raf itself suppresses its own activation: BRAF has been shown to inhibit the activity of CRAF (Garnett et al., 2005) and Raf dimers inhibit each other via trans-autophosphorylation. Interestingly, oncogenic KRas has been demonstrated to reinforce the activation of CRAF in cells treated with Raf inhibitors (Hatzivassiliou et al., 2010, Heidorn et al., 2010). Taken together, these means of Raf self-regulation and feedback loops suggest that also SW48 cell line, especially with mutant KRasG12V, could support the paradox of Raf activation after treatment with sorafenib inhibitor.

In summary, this chapter demonstrated that Ras isoform signalling presents subtle, but potentially significant differences in coupling MAPK and PI3K pathways. The more extensive signalling networks examined provided the first insights into distinct isoform-specific features of Ras in an endogenous context, However, only single biological repeats were examined and the study provides only preliminary data. Future work with more biological replicates should confirm the outcomes of this work and further investigation into network biology using MDA approach should provide details of Ras isoform-specific feedback loops, which may prove useful for the development of cancer therapeutics.

Chapter 7

Conclusions and Perspectives

The three founding members of Ras superfamily, HRas, KRas (KRasA and KRasB splice variants) and NRas, are the key signalling molecules involved in a multitude of cellular processes and are some of the most common human proto-oncogenes. These highly homologous GTPases, however, exhibit isoform-specific coupling to different human cancers (Cox et al., 2014, Forbes et al., 2015, Prior et al., 2012) and the KRasB isoform alone is sufficient for normal mouse development (Koera et al., 1997, Johnson et al., 1997, Plowman et al., 2003, Umanoff et al., 1995, Esteban et al., 2001). These discrepancies may be the result of Ras isoform-specific expression across tissues and during development and the differences in coupling and activation of Ras downstream effectors.

The first part of this thesis provided the first measurement of the absolute copy number of Ras isoform transcript levels, as well as the first comprehensive map of spatiotemporal expression of Ras across all four isoforms in mouse ESC line and in a panel of mouse tissues throughout development. This study optimised a quantitative method based on real time RT-PCR, which allowed estimating Ras isoform transcript in copy number. The average amount of total Ras (panRas) was around 5 copies/pg RNA in ESCs and around 26 copies/pg RNA in mouse tissues. Mass spectrometry analysis provided the preliminary results on Ras isoform expression at protein level, with an estimated 44-770 ng of panRas/mg of total protein.

At the transcript level, KRasB was the most abundant isoform, whereas HRas was always lowly expressed. The expression of the ESC-specific Ras isoform ERas was high in undifferentiated cells, but was steadily decreasing over time during cellular differentiation. In mouse tissues, KRasA was the most dynamically regulated isoform, with increasing expression in the stomach, intestine, kidney and liver over time during embryonic development. Interestingly, KRasA was shown for the first time to be expressed in the

embryonic heart. At the protein level, the expression of KRasB and HRas in murine tissues was by and large similar and it did not parallel transcript levels. However, these proteomic data were only preliminary and represented single biological repeats. Moreover, the protein levels of NRas could not be measured due to a technical error. Therefore, future work is necessary to provide more biological replicates and to include the expression of the remaining Ras isoforms.

Together, the expression studies reported in this thesis provide the most comprehensive and quantitative approach for studying Ras isoform expression to date, at least at the transcript level. Knowing the basal expression of Ras in a normal endogenous context provides the first insights into understanding the extent of Ras isoform functional overlap in comparative models. The differences in transcript versus protein levels obtained in this study may be explained by a recent work, which showed that *KRAS*, as compared to *HRAS*, is poorly translated due to the presence of rare codons in its genomic sequence (Lampson et al., 2013). The study also argues that rare codons make KRas a weaker oncogene than HRas. However, low protein levels of KRas may prompt tumourigenesis, as high expression of the mutated protein may lead to oncogenic stress and cellular senescence. The study of this thesis contradicts this model, as KRasB protein expression, although proportionally lower than at the transcript level, is similar to the other Ras isoforms.

Finally, the first hypothesis of this thesis (section 1.3) can be rejected:

Hypothesis 1: The expression levels can explain Ras isoform functional non-redundancy during development.

Expression levels do not justify the developmental requirement of KRasB (Koera et al., 1997, Johnson et al., 1997, Plowman et al., 2003, Umanoff et al., 1995, Esteban et al., 2001). Although KRasB is the major Ras isoform at transcript level, its protein expression is similar to the levels of HRas, which is dispensable for normal mouse development. Table 7.1 summarises the

milestones of this thesis that help us better understand the functional differences between the four main Ras isoforms.

The second part of this study examined Ras isoform-specific signalling in an endogenous context. The use of fully diploid SW48 colorectal cancer cell lines isogenic for a heterozygous oncogenic G12V mutation in each of the *RAS* genes provided a comprehensive approach for studying all Ras isoforms in the same genetic background. HRas, as compared to other Ras isoforms, has been found to couple better to both downstream MAPK and PI3K pathways, by providing more activating phosphorylation to MEK, ERK and Akt (Table 7.1).

Moreover, the study of this thesis gave the first preliminary results on broader Ras isoform signalling networks, enabling the investigation of negative or positive feedback loops. The results provided the initial optimisation of GFs and inhibitors for a future modelling signalling network study, based on multiplex proteomics and modular response analysis used previously (Klinger et al., 2013). However, this preliminary data gave evidence that oncogenic KRas may relieve the negative feedback loop back to the RTKs (Table 7.1). Nevertheless, the data presented in this thesis are from a single experiment and will require further work for validation. Also, single clones for each isogenic cell line were used in this study, hence, future experiments should utilise 2-3 different clones for each cell line to exclude any potential clonal artefacts that may bias the results. However, the data proves the second hypothesis of this thesis (section 1.3):

Hypothesis 2: Endogenous Ras isoforms signal differently from each other.

Previously, Ras isoform signalling was studied in overexpression systems (Voice et al., 1999, Yan et al., 1998), where the signalling outcomes could be the result of signal perturbation or senescence, which are not observed at endogenous levels of Ras (Serrano et al., 1997, Tuveson et al., 2004). These studies observed that KRas is a better activator of Raf, while HRas and NRas are more readily

Table 7.1 The main changes in the understanding of Ras isoform cellular and functional differences after the study of this thesis. For references please refer to text. PM – plasma membrane.

<table>
<tr><th rowspan="2">Property</th><th colspan="4">Ras isoform</th></tr>
<tr><th>HRas</th><th>KRasB</th><th>KRasA</th><th>NRas</th></tr>
<tr><td>Upstream activators</td><td></td><td colspan="2">Strongest positive feedback/relief of negative feedback to EGFR, Met and IGFR1β</td><td></td></tr>
<tr><td rowspan="2">MAPK/PI3K association</td><td>Strongest activator of pMEK and pAkt</td><td colspan="2">Weakest activator of pMEK and pAkt</td><td>Moderate/weak activator of pMEK and pAkt</td></tr>
<tr><td colspan="4">Endogenous signalling distinct from exogenous signalling</td></tr>
<tr><td rowspan="2">mRNA expression</td><td rowspan="2">Ubiquitous, no dynamic expression</td><td>Highly abundant, ubiquitous;</td><td>Ubiquitously expressed, major KRas isoform in some tissues, expressed in mouse embryonic heart</td><td>Moderately abundant, ubiquitous,</td></tr>
<tr><td colspan="3">Dynamic expression</td></tr>
<tr><td rowspan="2">Protein expression</td><td>Highly abundant;</td><td>Similar levels to HRas</td><td rowspan="2"></td><td rowspan="2"></td></tr>
<tr><td colspan="2">Transcript vs proteins levels do not correlate</td></tr>
</table>

activating PI3K. This is in contrary to the results of this thesis, which showed that endogenous HRas is a better activator of both MAPK and PI3K pathways, while endogenous KRas is the weakest activator of MAPK.

In summary, quantification of Ras isoform expression levels and signalling outcomes may lead to better understanding of normal physiological functions of endogenous Ras. The methods used in this study provide the best quantitative approaches for studying Ras isoforms to date. The results obtained are imperative for future studies involving models of Ras isoform signalling and may be key to delineating Ras isoform-specific coupling to different cancer types, contribution to normal development and potential future therapeutics.

Bibliography

ABANKWA, D., GORFE, A. A., INDER, K. & HANCOCK, J. F. 2010. Ras membrane orientation and nanodomain localization generate isoform diversity. *Proc Natl Acad Sci U S A,* 107**,** 1130-5.

ABANKWA, D., HANZAL-BAYER, M., ARIOTTI, N., PLOWMAN, S. J., GORFE, A. A., PARTON, R. G., MCCAMMON, J. A. & HANCOCK, J. F. 2008. A novel switch region regulates H-ras membrane orientation and signal output. *EMBO J,* 27**,** 727-35.

ABE, M., KURODA, Y., HIROSE, M., WATANABE, Y., NAKANO, M. & HANDA, T. 2006. Inhibition of autophosphorylation of epidermal growth factor receptor by small peptides in vitro. *Br J Pharmacol,* 147**,** 402-11.

AGUDO-IBANEZ, L., NUNEZ, F., CALVO, F., BERENJENO, I. M., BUSTELO, X. R. & CRESPO, P. 2007. Transcriptomal profiling of site-specific Ras signals. *Cell Signal,* 19**,** 2264-76.

AHMED, D., EIDE, P. W., EILERTSEN, I. A., DANIELSEN, S. A., EKNAES, M., HEKTOEN, M., LIND, G. E. & LOTHE, R. A. 2013. Epigenetic and genetic features of 24 colon cancer cell lines. *Oncogenesis,* 2**,** e71.

AKIYAMA, Y., NAGASAKI, H., YAGI, K. O., NOMIZU, T. & YUASA, Y. 2000. Beta-catenin and adenomatous polyposis coli (APC) mutations in adenomas from hereditary non-polyposis colorectal cancer patients. *Cancer Lett,* 157**,** 185-91.

AL-MULLA, F., MILNER-WHITE, E. J., GOING, J. J. & BIRNIE, G. D. 1999. Structural differences between valine-12 and aspartate-12 Ras proteins may modify carcinoma aggression. *J Pathol,* 187**,** 433-8.

ALAMO, P., GALLARDO, A., DI NICOLANTONIO, F., PAVON, M. A., CASANOVA, I., TRIAS, M., MANGUES, M. A., LOPEZ-POUSA, A., VILLAVERDE, A., VAZQUEZ, E., BARDELLI, A., CESPEDES, M. V. & MANGUES, R. 2015. Higher metastatic efficiency of KRas G12V than KRas G13D in a colorectal cancer model. *FASEB J,* 29**,** 464-76.

ALBERTS, B., BRAY, D., LEWIS, J., RAFF, M., ROBERTS, K. & WATSON, J. D. 1994. *Molecular Biology of the Cell,* New York, Garland Publishing.

ALDINGER, K. A., SOKOLOFF, G., ROSENBERG, D. M., PALMER, A. A. & MILLEN, K. J. 2009. Genetic variation and population substructure in outbred CD-1 mice: implications for genome-wide association studies. *PLoS One,* 4**,** e4729.

ALLEN, N. P., DONNINGER, H., VOS, M. D., ECKFELD, K., HESSON, L., GORDON, L., BIRRER, M. J., LATIF, F. & CLARK, G. J. 2007. RASSF6 is a novel member of the RASSF family of tumor suppressors. *Oncogene,* 26**,** 6203-11.

ALTSCHUL, S. F., GISH, W., MILLER, W., MYERS, E. W. & LIPMAN, D. J. 1990. Basic local alignment search tool. *J Mol Biol,* 215**,** 403-10.

AMADO, R. G., WOLF, M., PEETERS, M., VAN CUTSEM, E., SIENA, S., FREEMAN, D. J., JUAN, T., SIKORSKI, R., SUGGS, S., RADINSKY, R., PATTERSON, S. D. & CHANG, D. D. 2008. Wild-type KRAS is required for panitumumab efficacy in patients with metastatic colorectal cancer. *J Clin Oncol,* 26**,** 1626-34.

ANDEOL, Y., GUSSE, M. & MECHALI, M. 1990. Characterization and expression of a Xenopus ras during oogenesis and development. *Dev Biol,* 139**,** 24-34.

ANISIMOV, V. N., UKRAINTSEVA, S. V. & YASHIN, A. I. 2005. Cancer in rodents: does it tell us about cancer in humans? *Nat Rev Cancer,* 5**,** 807-19.

AOKI, Y., NIIHORI, T., NARUMI, Y., KURE, S. & MATSUBARA, Y. 2008. The RAS/MAPK syndromes: novel roles of the RAS pathway in human genetic disorders. *Hum Mutat,* 29**,** 992-1006.

APOLLONI, A., PRIOR, I. A., LINDSAY, M., PARTON, R. G. & HANCOCK, J. F. 2000. H-ras but not K-ras traffics to the plasma membrane through the exocytic pathway. *Mol Cell Biol,* 20**,** 2475-87.

ARENA, S., ISELLA, C., MARTINI, M., DE MARCO, A., MEDICO, E. & BARDELLI, A. 2007. Knock-in of oncogenic Kras does not transform mouse somatic cells but triggers a transcriptional response that classifies human cancers. *Cancer Res,* 67**,** 8468-76.

ARNOLD, S. J. & ROBERTSON, E. J. 2009. Making a commitment: cell lineage allocation and axis patterning in the early mouse embryo. *Nat Rev Mol Cell Biol,* 10**,** 91-103.

AUGSTEN, M., PUSCH, R., BISKUP, C., RENNERT, K., WITTIG, U., BEYER, K., BLUME, A., WETZKER, R., FRIEDRICH, K. & RUBIO, I. 2006. Live-cell imaging of endogenous Ras-GTP illustrates predominant Ras activation at the plasma membrane. *EMBO Rep,* 7**,** 46-51.

BARBER, T. D., VOGELSTEIN, B., KINZLER, K. W. & VELCULESCU, V. E. 2004. Somatic mutations of EGFR in colorectal cancers and glioblastomas. *N Engl J Med,* 351**,** 2883.

BASU ROY, U. K., HENKHAUS, R. S., LOUPAKIS, F., CREMOLINI, C., GERNER, E. W. & IGNATENKO, N. A. 2013. Caveolin-1 is a novel regulator of K-RAS-dependent migration in colon carcinogenesis. *Int J Cancer,* 133**,** 43-57.

BAUM, E. Z. & BEBERNITZ, G. A. 1990. K-ras oncogene expression in Xenopus laevis. *Oncogene,* 5**,** 763-7.

BECKER, C., HAMMERLE-FICKINGER, A., RIEDMAIER, I. & PFAFFL, M. W. 2010. mRNA and microRNA quality control for RT-qPCR analysis. *Methods,* 50**,** 237-43.

BEITEL, G. J., CLARK, S. G. & HORVITZ, H. R. 1990. Caenorhabditis elegans ras gene let-60 acts as a switch in the pathway of vulval induction. *Nature,* 348**,** 503-9.

BENGTSSON, M., KARLSSON, H. J., WESTMAN, G. & KUBISTA, M. 2003. A new minor groove binding asymmetric cyanine reporter dye for real-time PCR. *Nucleic Acids Res,* 31**,** e45.

BIO-RAD LABORATORIES, I. 2006. *Real-Time PCR Applications Guide*, Bio-Rad Laboratories, Inc.

BIVONA, T. G., QUATELA, S. E., BODEMANN, B. O., AHEARN, I. M., SOSKIS, M. J., MOR, A., MIURA, J., WIENER, H. H., WRIGHT, L., SABA, S. G., YIM, D., FEIN, A., PEREZ DE CASTRO, I., LI, C., THOMPSON, C. B., COX, A. D. & PHILIPS, M. R. 2006. PKC regulates a farnesyl-electrostatic switch on K-Ras that promotes its association with Bcl-XL on mitochondria and induces apoptosis. *Mol Cell,* 21**,** 481-93.

BLAUKAT, A., BARAC, A., CROSS, M. J., OFFERMANNS, S. & DIKIC, I. 2000. G protein-coupled receptor-mediated mitogen-activated protein kinase activation through cooperation of Galpha(q) and Galpha(i) signals. *Mol Cell Biol,* 20**,** 6837-48.

BOGUSKI, M. S. & MCCORMICK, F. 1993. Proteins regulating Ras and its relatives. *Nature,* 366**,** 643-54.

BONNER, C. A., LOFTUS, S. K. & WASMUTH, J. J. 1995. Isolation, characterization, and precise physical localization of human CDX1, a caudal-type homeobox gene. *Genomics,* 28**,** 206-11.

BOS, J. L., REHMANN, H. & WITTINGHOFER, A. 2007. GEFs and GAPs: critical elements in the control of small G proteins. *Cell,* 129**,** 865-77.

BRIMBLE, S. N., ZENG, X., WEILER, D. A., LUO, Y., LIU, Y., LYONS, I. G., FREED, W. J., ROBINS, A. J., RAO, M. S. & SCHULZ, T. C. 2004. Karyotypic stability, genotyping, differentiation, feeder-free maintenance, and gene expression sampling in three human embryonic stem cell lines derived prior to August 9, 2001. *Stem Cells Dev,* 13**,** 585-97.

BRUNGER, A. T., MILBURN, M. V., TONG, L., DEVOS, A. M., JANCARIK, J., YAMAIZUMI, Z., NISHIMURA, S., OHTSUKA, E. & KIM, S. H. 1990. Crystal

structure of an active form of RAS protein, a complex of a GTP analog and the HRAS p21 catalytic domain. *Proc Natl Acad Sci U S A,* 87**,** 4849-53.

BUDAY, L. & DOWNWARD, J. 1993. Epidermal growth factor regulates p21ras through the formation of a complex of receptor, Grb2 adapter protein, and Sos nucleotide exchange factor. *Cell,* 73**,** 611-20.

BURNETTE, W. N. 1981. "Western blotting": electrophoretic transfer of proteins from sodium dodecyl sulfate--polyacrylamide gels to unmodified nitrocellulose and radiographic detection with antibody and radioiodinated protein A. *Anal Biochem,* 112**,** 195-203.

BUSTIN, S. A. 2000. Absolute quantification of mRNA using real-time reverse transcription polymerase chain reaction assays. *J Mol Endocrinol,* 25**,** 169-93.

CALABRESE, J. M., SEILA, A. C., YEO, G. W. & SHARP, P. A. 2007. RNA sequence analysis defines Dicer's role in mouse embryonic stem cells. *Proc Natl Acad Sci U S A,* 104**,** 18097-102.

CALOCA, M. J., ZUGAZA, J. L. & BUSTELO, X. R. 2003. Exchange factors of the RasGRP family mediate Ras activation in the Golgi. *J Biol Chem,* 278**,** 33465-73.

CAMPISI, J., GRAY, H. E., PARDEE, A. B., DEAN, M. & SONENSHEIN, G. E. 1984. Cell-cycle control of c-myc but not c-ras expression is lost following chemical transformation. *Cell,* 36**,** 241-7.

CANTOR, S. B., URANO, T. & FEIG, L. A. 1995. Identification and characterization of Ral-binding protein 1, a potential downstream target of Ral GTPases. *Mol Cell Biol,* 15**,** 4578-84.

CAPON, D. J., SEEBURG, P. H., MCGRATH, J. P., HAYFLICK, J. S., EDMAN, U., LEVINSON, A. D. & GOEDDEL, D. V. 1983. Activation of Ki-ras2 gene in human colon and lung carcinomas by two different point mutations. *Nature,* 304**,** 507-13.

CARNAHAN, M. N., VEAZEY, K. J., MULLER, D., TINGLING, J. D., MIRANDA, R. C. & GOLDING, M. C. 2013. Identification of cell-specific patterns of reference gene stability in quantitative reverse-transcriptase polymerase chain reaction studies of embryonic, placental and neural stem models of prenatal ethanol exposure. *Alcohol,* 47**,** 109-20.

CASEY, P. J., SOLSKI, P. A., DER, C. J. & BUSS, J. E. 1989. p21ras is modified by a farnesyl isoprenoid. *Proc Natl Acad Sci U S A,* 86**,** 8323-7.

CASTELLANO, E. & SANTOS, E. 2011. Functional specificity of ras isoforms: so similar but so different. *Genes Cancer,* 2**,** 216-31.

CERAMI, E., GAO, J., DOGRUSOZ, U., GROSS, B. E., SUMER, S. O., AKSOY, B. A., JACOBSEN, A., BYRNE, C. J., HEUER, M. L., LARSSON, E., ANTIPIN, Y., REVA, B., GOLDBERG, A. P., SANDER, C. & SCHULTZ, N. 2012. The cBio cancer genomics portal: an open platform for exploring multidimensional cancer genomics data. *Cancer Discov,* 2**,** 401-4.

CHAN, C. W., WONG, N. A., LIU, Y., BICKNELL, D., TURLEY, H., HOLLINS, L., MILLER, C. J., WILDING, J. L. & BODMER, W. F. 2009. Gastrointestinal differentiation marker Cytokeratin 20 is regulated by homeobox gene CDX1. *Proc Natl Acad Sci U S A,* 106**,** 1936-41.

CHANG, E. H., FURTH, M. E., SCOLNICK, E. M. & LOWY, D. R. 1982a. Tumorigenic transformation of mammalian cells induced by a normal human gene homologous to the oncogene of Harvey murine sarcoma virus. *Nature,* 297**,** 479-83.

CHANG, E. H., GONDA, M. A., ELLIS, R. W., SCOLNICK, E. M. & LOWY, D. R. 1982b. Human genome contains four genes homologous to transforming genes of Harvey and Kirsten murine sarcoma viruses. *Proc Natl Acad Sci U S A,* 79**,** 4848-52.

CHANG, F., STEELMAN, L. S., LEE, J. T., SHELTON, J. G., NAVOLANIC, P. M., BLALOCK, W. L., FRANKLIN, R. A. & MCCUBREY, J. A. 2003. Signal transduction mediated by the Ras/Raf/MEK/ERK pathway from cytokine receptors to transcription factors: potential targeting for therapeutic intervention. *Leukemia,* 17**,** 1263-93.

CHANG, L. & KARIN, M. 2001. Mammalian MAP kinase signalling cascades. *Nature,* 410**,** 37-40.

CHARDIN, P., CAMONIS, J. H., GALE, N. W., VAN AELST, L., SCHLESSINGER, J., WIGLER, M. H. & BAR-SAGI, D. 1993. Human Sos1: a guanine nucleotide exchange factor for Ras that binds to GRB2. *Science,* 260**,** 1338-43.

CHEN, J., FUJII, K., ZHANG, L., ROBERTS, T. & FU, H. 2001. Raf-1 promotes cell survival by antagonizing apoptosis signal-regulating kinase 1 through a MEK-ERK independent mechanism. *Proc Natl Acad Sci U S A,* 98**,** 7783-8.

CHENG, R., BRADFORD, S., BARNES, D., WILLIAMS, D., HENDRICKS, J. & BAILEY, G. 1997. Cloning, sequencing, and embryonic expression of an N-ras proto-oncogene isolated from an enriched zebrafish (Danio rerio) cDNA library. *Mol Mar Biol Biotechnol,* 6**,** 40-7.

CHI, S., CAO, H., WANG, Y. & MCNIVEN, M. A. 2011. Recycling of the epidermal growth factor receptor is mediated by a novel form of the clathrin adaptor protein Eps15. *J Biol Chem,* 286**,** 35196-208.

CHIA, R., ACHILLI, F., FESTING, M. F. & FISHER, E. M. 2005. The origins and uses of mouse outbred stocks. *Nat Genet,* 37**,** 1181-6.

CHIEN, A., EDGAR, D. B. & TRELA, J. M. 1976. Deoxyribonucleic acid polymerase from the extreme thermophile Thermus aquaticus. *J Bacteriol,* 127**,** 1550-7.

CHIU, V. K., BIVONA, T., HACH, A., SAJOUS, J. B., SILLETTI, J., WIENER, H., JOHNSON, R. L., 2ND, COX, A. D. & PHILIPS, M. R. 2002. Ras signalling on the endoplasmic reticulum and the Golgi. *Nat Cell Biol,* 4**,** 343-50.

CHO, K. J., KASAI, R. S., PARK, J. H., CHIGURUPATI, S., HEIDORN, S. J., VAN DER HOEVEN, D., PLOWMAN, S. J., KUSUMI, A., MARAIS, R. & HANCOCK, J. F. 2012. Raf inhibitors target ras spatiotemporal dynamics. *Curr Biol,* 22**,** 945-55.

CHOU, Q., RUSSELL, M., BIRCH, D. E., RAYMOND, J. & BLOCH, W. 1992. Prevention of pre-PCR mis-priming and primer dimerization improves low-copy-number amplifications. *Nucleic Acids Res,* 20**,** 1717-23.

CHOY, E., CHIU, V. K., SILLETTI, J., FEOKTISTOV, M., MORIMOTO, T., MICHAELSON, D., IVANOV, I. E. & PHILIPS, M. R. 1999. Endomembrane trafficking of ras: the CAAX motif targets proteins to the ER and Golgi. *Cell,* 98**,** 69-80.

CIRIT, M., WANG, C. C. & HAUGH, J. M. 2010. Systematic quantification of negative feedback mechanisms in the extracellular signal-regulated kinase (ERK) signaling network. *J Biol Chem,* 285**,** 36736-44.

CIRSTEA, I. C., KUTSCHE, K., DVORSKY, R., GREMER, L., CARTA, C., HORN, D., ROBERTS, A. E., LEPRI, F., MERBITZ-ZAHRADNIK, T., KONIG, R., KRATZ, C. P., PANTALEONI, F., DENTICI, M. L., JOSHI, V. A., KUCHERLAPATI, R. S., MAZZANTI, L., MUNDLOS, S., PATTON, M. A., SILENGO, M. C., ROSSI, C., ZAMPINO, G., DIGILIO, C., STUPPIA, L., SEEMANOVA, E., PENNACCHIO, L. A., GELB, B. D., DALLAPICCOLA, B., WITTINGHOFER, A., AHMADIAN, M. R., TARTAGLIA, M. & ZENKER, M. 2010. A restricted spectrum of NRAS mutations causes Noonan syndrome. *Nat Genet,* 42**,** 27-9.

CLYDE-SMITH, J., SILINS, G., GARTSIDE, M., GRIMMOND, S., ETHERIDGE, M., APOLLONI, A., HAYWARD, N. & HANCOCK, J. F. 2000. Characterization of RasGRP2, a plasma membrane-targeted, dual specificity Ras/Rap exchange factor. *J Biol Chem,* 275**,** 32260-7.

COLICELLI, J. 2004. Human RAS superfamily proteins and related GTPases. *Sci STKE,* 2004**,** RE13.

COLLADO, M. & SERRANO, M. 2010. Senescence in tumours: evidence from mice and humans. *Nat Rev Cancer,* 10**,** 51-7.

COMERON, J. M. 2004. Selective and mutational patterns associated with gene expression in humans: influences on synonymous composition and intron presence. *Genetics,* 167**,** 1293-304.

COPOIS, V., BRET, C., BIBEAU, F., BROUILLET, J. P., DEL RIO, M., BERTHE, M. L., MAUDELONDE, T. & BOULLE, N. 2003. Assessment of RNA quality extracted from laser-captured tissues using miniaturized capillary electrophoresis. *Lab Invest,* 83**,** 599-602.

COUCOUVANIS, E. & MARTIN, G. R. 1995. Signals for death and survival: a two-step mechanism for cavitation in the vertebrate embryo. *Cell,* 83**,** 279-87.

COX, A. D. & DER, C. J. 2003. The dark side of Ras: regulation of apoptosis. *Oncogene,* 22**,** 8999-9006.

COX, A. D. & DER, C. J. 2010. Ras history: The saga continues. *Small GTPases,* 1**,** 2-27.

COX, A. D., FESIK, S. W., KIMMELMAN, A. C., LUO, J. & DER, C. J. 2014. Drugging the undruggable RAS: Mission possible? *Nat Rev Drug Discov,* 13**,** 828-51.

CRAWFORD, L. W., FOLEY, J. F. & ELMORE, S. A. 2010. Histology atlas of the developing mouse hepatobiliary system with emphasis on embryonic days 9.5-18.5. *Toxicol Pathol,* 38**,** 872-906.

CRESPO, P. & LEON, J. 2000. Ras proteins in the control of the cell cycle and cell differentiation. *Cell Mol Life Sci,* 57**,** 1613-36.

CROSS, D. A., ALESSI, D. R., COHEN, P., ANDJELKOVICH, M. & HEMMINGS, B. A. 1995. Inhibition of glycogen synthase kinase-3 by insulin mediated by protein kinase B. *Nature,* 378**,** 785-9.

CUI, P., DING, F., LIN, Q., ZHANG, L., LI, A., ZHANG, Z., HU, S. & YU, J. 2012a. Distinct contributions of replication and transcription to mutation rate variation of human genomes. *Genomics Proteomics Bioinformatics,* 10**,** 4-10.

CUI, P., LIN, Q., DING, F., HU, S. & YU, J. 2012b. The transcript-centric mutations in human genomes. *Genomics Proteomics Bioinformatics,* 10**,** 11-22.

CURLEY, J. P., JORDAN, E. R., SWANEY, W. T., IZRAELIT, A., KAMMEL, S. & CHAMPAGNE, F. A. 2009. The meaning of weaning: influence of the weaning period on behavioral development in mice. *Dev Neurosci,* 31**,** 318-31.

DAVIDSON, A. J. 2008. Mouse kidney development. *StemBook.* Cambridge (MA).

DE LA VEGA, M., BURROWS, J. F., MCFARLANE, C., GOVENDER, U., SCOTT, C. J. & JOHNSTON, J. A. 2010. The deubiquitinating enzyme USP17 blocks N-Ras membrane trafficking and activation but leaves K-Ras unaffected. *J Biol Chem,* 285**,** 12028-36.

DE ROOCK, W., JONKER, D. J., DI NICOLANTONIO, F., SARTORE-BIANCHI, A., TU, D., SIENA, S., LAMBA, S., ARENA, S., FRATTINI, M., PIESSEVAUX, H., VAN CUTSEM, E., O'CALLAGHAN, C. J., KHAMBATA-FORD, S., ZALCBERG, J. R., SIMES, J., KARAPETIS, C. S., BARDELLI, A. & TEJPAR, S. 2010. Association of KRAS p.G13D mutation with outcome in patients with chemotherapy-refractory metastatic colorectal cancer treated with cetuximab. *JAMA,* 304**,** 1812-20.

DEFEO, D., GONDA, M. A., YOUNG, H. A., CHANG, E. H., LOWY, D. R., SCOLNICK, E. M. & ELLIS, R. W. 1981. Analysis of two divergent rat genomic clones homologous to the transforming gene of Harvey murine sarcoma virus. *Proc Natl Acad Sci U S A,* 78**,** 3328-32.

DEGEN, H.-J., DEUFEL, A., EISEL, D., GRÜNEWALD-JANHO, S. & KEESEY, J. 2006. *PCR Applications Manual*, Roche Diagnostics GmbH.

DELLA ROCCA, G. J., VAN BIESEN, T., DAAKA, Y., LUTTRELL, D. K., LUTTRELL, L. M. & LEFKOWITZ, R. J. 1997. Ras-dependent mitogen-activated protein kinase activation by G protein-coupled receptors. Convergence of Gi- and Gq-mediated pathways on calcium/calmodulin, Pyk2, and Src kinase. *J Biol Chem,* 272**,** 19125-32.

DENAYER, E., DE RAVEL, T. & LEGIUS, E. 2008. Clinical and molecular aspects of RAS related disorders. *J Med Genet,* 45**,** 695-703.

DENT, P., HASER, W., HAYSTEAD, T. A., VINCENT, L. A., ROBERTS, T. M. & STURGILL, T. W. 1992. Activation of mitogen-activated protein kinase kinase by v-Raf in NIH 3T3 cells and in vitro. *Science,* 257**,** 1404-7.

DER, C. J., KRONTIRIS, T. G. & COOPER, G. M. 1982. Transforming genes of human bladder and lung carcinoma cell lines are homologous to the ras genes of Harvey and Kirsten sarcoma viruses. *Proc Natl Acad Sci U S A,* 79**,** 3637-40.

DERVEAUX, S., VANDESOMPELE, J. & HELLEMANS, J. 2010. How to do successful gene expression analysis using real-time PCR. *Methods,* 50**,** 227-30.

DEXTER, D. L., KOWALSKI, H. M., BLAZAR, B. A., FLIGIEL, Z., VOGEL, R. & HEPPNER, G. H. 1978. Heterogeneity of tumor cells from a single mouse mammary tumor. *Cancer Res,* 38**,** 3174-81.

DHAR, R., NIETO, A., KOLLER, R., DEFEO-JONES, D. & SCOLNICK, E. M. 1984. Nucleotide sequence of two rasH related-genes isolated from the yeast Saccharomyces cerevisiae. *Nucleic Acids Res,* 12**,** 3611-8.

DI NICOLANTONIO, F. & BARDELLI, A. 2013. Mouse models of Kras-mutant colorectal cancer: valuable GEMMs for drug testing? *Clin Cancer Res,* 19**,** 2794-6.

DICKSON, B., SPRENGER, F., MORRISON, D. & HAFEN, E. 1992. Raf functions downstream of Ras1 in the Sevenless signal transduction pathway. *Nature,* 360**,** 600-3.

DIKIC, I., TOKIWA, G., LEV, S., COURTNEIDGE, S. A. & SCHLESSINGER, J. 1996. A role for Pyk2 and Src in linking G-protein-coupled receptors with MAP kinase activation. *Nature,* 383**,** 547-50.

DOETSCHMAN, T. C., EISTETTER, H., KATZ, M., SCHMIDT, W. & KEMLER, R. 1985. The in vitro development of blastocyst-derived embryonic stem cell lines: formation of visceral yolk sac, blood islands and myocardium. *J Embryol Exp Morphol,* 87**,** 27-45.

DOHERTY, G. J. & MCMAHON, H. T. 2009. Mechanisms of endocytosis. *Annu Rev Biochem,* 78**,** 857-902.

DON, R. H., COX, P. T., WAINWRIGHT, B. J., BAKER, K. & MATTICK, J. S. 1991. 'Touchdown' PCR to circumvent spurious priming during gene amplification. *Nucleic Acids Res,* 19**,** 4008.

DORSAM, R. T. & GUTKIND, J. S. 2007. G-protein-coupled receptors and cancer. *Nat Rev Cancer,* 7**,** 79-94.

DOUGHERTY, M. K., MULLER, J., RITT, D. A., ZHOU, M., ZHOU, X. Z., COPELAND, T. D., CONRADS, T. P., VEENSTRA, T. D., LU, K. P. & MORRISON, D. K. 2005. Regulation of Raf-1 by direct feedback phosphorylation. *Mol Cell,* 17**,** 215-24.

DOWNWARD, J., PARKER, P. & WATERFIELD, M. D. 1984. Autophosphorylation sites on the epidermal growth factor receptor. *Nature,* 311**,** 483-5.

DRAGAN, A. I., PAVLOVIC, R., MCGIVNEY, J. B., CASAS-FINET, J. R., BISHOP, E. S., STROUSE, R. J., SCHENERMAN, M. A. & GEDDES, C. D. 2012. SYBR Green I: fluorescence properties and interaction with DNA. *J Fluoresc,* 22**,** 1189-99.

DURBIN, R. & THIERRY-MIEG, J. 1994. *THE ACEDB GENOME DATABASE,* New York, Plenum Press.

EBI, H., CORCORAN, R. B., SINGH, A., CHEN, Z., SONG, Y., LIFSHITS, E., RYAN, D. P., MEYERHARDT, J. A., BENES, C., SETTLEMAN, J., WONG, K. K., CANTLEY, L. C. & ENGELMAN, J. A. 2011. Receptor tyrosine kinases exert dominant control over PI3K signaling in human KRAS mutant colorectal cancers. *J Clin Invest,* 121**,** 4311-21.

ECKERT, K. A. & KUNKEL, T. A. 1990. High fidelity DNA synthesis by the Thermus aquaticus DNA polymerase. *Nucleic Acids Res,* 18**,** 3739-44.

ECKFELD, K., HESSON, L., VOS, M. D., BIECHE, I., LATIF, F. & CLARK, G. J. 2004. RASSF4/AD037 is a potential ras effector/tumor suppressor of the RASSF family. *Cancer Res,* 64**,** 8688-93.

EDWARDS, S. R. & WANDLESS, T. J. 2007. The rapamycin-binding domain of the protein kinase mammalian target of rapamycin is a destabilizing domain. *J Biol Chem,* 282**,** 13395-401.

EGAN, S. E., GIDDINGS, B. W., BROOKS, M. W., BUDAY, L., SIZELAND, A. M. & WEINBERG, R. A. 1993. Association of Sos Ras exchange protein with Grb2 is implicated in tyrosine kinase signal transduction and transformation. *Nature,* 363**,** 45-51.

EHRHARDT, A., DAVID, M. D., EHRHARDT, G. R. & SCHRADER, J. W. 2004. Distinct mechanisms determine the patterns of differential activation of H-Ras, N-Ras, K-Ras 4B, and M-Ras by receptors for growth factors or antigen. *Mol Cell Biol,* 24**,** 6311-23.

ELLIS, R. W., DEFEO, D., FURTH, M. E. & SCOLNICK, E. M. 1982. Mouse cells contain two distinct ras gene mRNA species that can be translated into a p21 onc protein. *Mol Cell Biol,* 2**,** 1339-45.

ELLIS, R. W., DEFEO, D., SHIH, T. Y., GONDA, M. A., YOUNG, H. A., TSUCHIDA, N., LOWY, D. R. & SCOLNICK, E. M. 1981. The p21 src genes of Harvey and Kirsten sarcoma viruses originate from divergent members of a family of normal vertebrate genes. *Nature,* 292**,** 506-11.

EMANOIL-RAVIER, R., POCHART, F., CANIVET, M., GARCETTE, M., TOBALY-TAPIERO, J. & PERIES, J. 1985. Interferon-mediated regulation of myc and Ki-ras oncogene expression in long-term-treated murine viral transformed cells. *J Interferon Res,* 5**,** 613-9.

ENSENAT-WASER, R., SANTANA, A., VICENTE-SALAR, N., CIGUDOSA, J. C., ROCHE, E., SORIA, B. & REIG, J. A. 2006. Isolation and characterization of residual undifferentiated mouse embryonic stem cells from embryoid body cultures by fluorescence tracking. *In Vitro Cell Dev Biol Anim,* 42**,** 115-23.

ESER, S., SCHNIEKE, A., SCHNEIDER, G. & SAUR, D. 2014. Oncogenic KRAS signalling in pancreatic cancer. *Br J Cancer,* 111**,** 817-22.

ESTEBAN, L. M., VICARIO-ABEJON, C., FERNANDEZ-SALGUERO, P., FERNANDEZ-MEDARDE, A., SWAMINATHAN, N., YIENGER, K., LOPEZ, E., MALUMBRES, M., MCKAY, R., WARD, J. M., PELLICER, A. & SANTOS, E. 2001. Targeted genomic disruption of H-ras and N-ras, individually or in combination, reveals the dispensability of both loci for mouse growth and development. *Mol Cell Biol,* 21**,** 1444-52.

EVANS, M. J. & KAUFMAN, M. H. 1981. Establishment in culture of pluripotential cells from mouse embryos. *Nature,* 292**,** 154-6.

FASANO, O., ALDRICH, T., TAMANOI, F., TAPAROWSKY, E., FURTH, M. & WIGLER, M. 1984. Analysis of the transforming potential of the human H-ras gene by random mutagenesis. *Proc Natl Acad Sci U S A,* 81**,** 4008-12.

FEHLING, H. J., LACAUD, G., KUBO, A., KENNEDY, M., ROBERTSON, S., KELLER, G. & KOUSKOFF, V. 2003. Tracking mesoderm induction and its specification to the hemangioblast during embryonic stem cell differentiation. *Development,* 130**,** 4217-27.

FEIG, L. A. 2003. Ral-GTPases: approaching their 15 minutes of fame. *Trends Cell Biol,* 13**,** 419-25.

FEIG, L. A., BAST, R. C., JR., KNAPP, R. C. & COOPER, G. M. 1984. Somatic activation of rasK gene in a human ovarian carcinoma. *Science,* 223**,** 698-701.

FENG, Z., HU, W., CHEN, J. X., PAO, A., LI, H., ROM, W., HUNG, M. C. & TANG, M. S. 2002. Preferential DNA damage and poor repair determine ras gene mutational hotspot in human cancer. *J Natl Cancer Inst,* 94**,** 1527-36.

FERNANDEZ-MEDARDE, A. & SANTOS, E. 2011. Ras in cancer and developmental diseases. *Genes Cancer,* 2**,** 344-58.

FIALA, O., PESEK, M., FINEK, J., BENESOVA, L., BELSANOVA, B. & MINARIK, M. 2013. The dominant role of G12C over other KRAS mutation types in the negative prediction of efficacy of epidermal growth factor receptor tyrosine kinase inhibitors in non-small cell lung cancer. *Cancer Genet,* 206**,** 26-31.

FINGAR, D. C., RICHARDSON, C. J., TEE, A. R., CHEATHAM, L., TSOU, C. & BLENIS, J. 2004. mTOR controls cell cycle progression through its cell growth effectors S6K1 and 4E-BP1/eukaryotic translation initiation factor 4E. *Mol Cell Biol,* 24**,** 200-16.

FINLAY, H. M., MCCULLOUGH, L. & CANHAM, P. B. 1995. Three-dimensional collagen organization of human brain arteries at different transmural pressures. *J Vasc Res,* 32**,** 301-12.

FIVAZ, M., BANDARA, S., INOUE, T. & MEYER, T. 2008. Robust neuronal symmetry breaking by Ras-triggered local positive feedback. *Curr Biol,* 18**,** 44-50.

FLEMING, J. B., SHEN, G. L., HOLLOWAY, S. E., DAVIS, M. & BREKKEN, R. A. 2005. Molecular consequences of silencing mutant K-ras in pancreatic cancer cells: justification for K-ras-directed therapy. *Mol Cancer Res,* 3**,** 413-23.

FLEMING, M., RAVULA, S., TATISHCHEV, S. F. & WANG, H. L. 2012. Colorectal carcinoma: Pathologic aspects. *J Gastrointest Oncol,* 3**,** 153-73.

FORBES, S. A., BEARE, D., GUNASEKARAN, P., LEUNG, K., BINDAL, N., BOUTSELAKIS, H., DING, M., BAMFORD, S., COLE, C., WARD, S., KOK, C. Y., JIA, M., DE, T., TEAGUE, J. W., STRATTON, M. R., MCDERMOTT, U. & CAMPBELL, P. J. 2015. COSMIC: exploring the world's knowledge of somatic mutations in human cancer. *Nucleic Acids Res,* 43**,** D805-11.

FRANKEN, S. M., SCHEIDIG, A. J., KRENGEL, U., RENSLAND, H., LAUTWEIN, A., GEYER, M., SCHEFFZEK, K., GOODY, R. S., KALBITZER, H. R., PAI, E. F. & ET AL. 1993. Three-dimensional structures and properties of a transforming and a nontransforming glycine-12 mutant of p21H-ras. *Biochemistry,* 32**,** 8411-20.

FRIDAY, B. B., YU, C., DY, G. K., SMITH, P. D., WANG, L., THIBODEAU, S. N. & ADJEI, A. A. 2008. BRAF V600E disrupts AZD6244-induced abrogation of negative feedback pathways between extracellular signal-regulated kinase and Raf proteins. *Cancer Res,* 68**,** 6145-53.

FRIEDMAN, J. R. & KAESTNER, K. H. 2011. On the origin of the liver. *J Clin Invest,* 121**,** 4630-3.

FRITSCHE-GUENTHER, R., WITZEL, F., SIEBER, A., HERR, R., SCHMIDT, N., BRAUN, S., BRUMMER, T., SERS, C. & BLUTHGEN, N. 2011. Strong negative feedback from Erk to Raf confers robustness to MAPK signalling. *Mol Syst Biol,* 7**,** 489.

FUJIWARA, H., HAYASHI, Y., SANZEN, N., KOBAYASHI, R., WEBER, C. N., EMOTO, T., FUTAKI, S., NIWA, H., MURRAY, P., EDGAR, D. & SEKIGUCHI, K. 2007. Regulation of mesodermal differentiation of mouse embryonic stem cells by basement membranes. *J Biol Chem,* 282**,** 29701-11.

GALE, N. W., KAPLAN, S., LOWENSTEIN, E. J., SCHLESSINGER, J. & BAR-SAGI, D. 1993. Grb2 mediates the EGF-dependent activation of guanine nucleotide exchange on Ras. *Nature,* 363**,** 88-92.

GAO, J., AKSOY, B. A., DOGRUSOZ, U., DRESDNER, G., GROSS, B., SUMER, S. O., SUN, Y., JACOBSEN, A., SINHA, R., LARSSON, E., CERAMI, E., SANDER, C. & SCHULTZ, N. 2013. Integrative analysis of complex cancer genomics and clinical profiles using the cBioPortal. *Sci Signal,* 6**,** pl1.

GARNETT, M. J., RANA, S., PATERSON, H., BARFORD, D. & MARAIS, R. 2005. Wild-type and mutant B-RAF activate C-RAF through distinct mechanisms involving heterodimerization. *Mol Cell,* 20**,** 963-9.

GARON, E. B., FINN, R. S., HOSMER, W., DERING, J., GINTHER, C., ADHAMI, S., KAMRANPOUR, N., PITTS, S., DESAI, A., ELASHOFF, D., FRENCH, T., SMITH, P. & SLAMON, D. J. 2010. Identification of common predictive

markers of in vitro response to the Mek inhibitor selumetinib (AZD6244; ARRY-142886) in human breast cancer and non-small cell lung cancer cell lines. *Mol Cancer Ther,* 9**,** 1985-94.

GIBBS, J. B., MARSHALL, M. S., SCOLNICK, E. M., DIXON, R. A. & VOGEL, U. S. 1990. Modulation of guanine nucleotides bound to Ras in NIH3T3 cells by oncogenes, growth factors, and the GTPase activating protein (GAP). *J Biol Chem,* 265**,** 20437-42.

GIBBS, J. B., SIGAL, I. S., POE, M. & SCOLNICK, E. M. 1984. Intrinsic GTPase activity distinguishes normal and oncogenic ras p21 molecules. *Proc Natl Acad Sci U S A,* 81**,** 5704-8.

GILBERT, S. F. 2010. *Developmental Biology*, Sinauer Associates, Inc.

GIUBELLINO, A., BURKE, T. R., JR. & BOTTARO, D. P. 2008. Grb2 signaling in cell motility and cancer. *Expert Opin Ther Targets,* 12**,** 1021-33.

GIULIETTI, A., OVERBERGH, L., VALCKX, D., DECALLONNE, B., BOUILLON, R. & MATHIEU, C. 2001. An overview of real-time quantitative PCR: applications to quantify cytokine gene expression. *Methods,* 25**,** 386-401.

GOMEZ, G. A. & DANIOTTI, J. L. 2005. H-Ras dynamically interacts with recycling endosomes in CHO-K1 cells: involvement of Rab5 and Rab11 in the trafficking of H-Ras to this pericentriolar endocytic compartment. *J Biol Chem,* 280**,** 34997-5010.

GREEN, P., EWING, B., MILLER, W., THOMAS, P. J., PROGRAM, N. C. S. & GREEN, E. D. 2003. Transcription-associated mutational asymmetry in mammalian evolution. *Nat Genet,* 33**,** 514-7.

GREMER, L., GILSBACH, B., AHMADIAN, M. R. & WITTINGHOFER, A. 2008. Fluoride complexes of oncogenic Ras mutants to study the Ras-RasGap interaction. *Biol Chem,* 389**,** 1163-71.

HAIGIS, K. M., KENDALL, K. R., WANG, Y., CHEUNG, A., HAIGIS, M. C., GLICKMAN, J. N., NIWA-KAWAKITA, M., SWEET-CORDERO, A., SEBOLT-LEOPOLD, J., SHANNON, K. M., SETTLEMAN, J., GIOVANNINI, M. & JACKS, T. 2008. Differential effects of oncogenic K-Ras and N-Ras on proliferation, differentiation and tumor progression in the colon. *Nat Genet,* 40**,** 600-8.

HALL, A., MARSHALL, C. J., SPURR, N. K. & WEISS, R. A. 1983. Identification of transforming gene in two human sarcoma cell lines as a new member of the ras gene family located on chromosome 1. *Nature,* 303**,** 396-400.

HALL, B. E., BAR-SAGI, D. & NASSAR, N. 2002. The structural basis for the transition from Ras-GTP to Ras-GDP. *Proc Natl Acad Sci U S A,* 99**,** 12138-42.

HALL-JACKSON, C. A., EYERS, P. A., COHEN, P., GOEDERT, M., BOYLE, F. T., HEWITT, N., PLANT, H. & HEDGE, P. 1999. Paradoxical activation of Raf by a novel Raf inhibitor. *Chem Biol,* 6**,** 559-68.

HALVEY, P. J., FERRONE, C. R. & LIEBLER, D. C. 2012. GeLC-MRM quantitation of mutant KRAS oncoprotein in complex biological samples. *J Proteome Res,* 11**,** 3908-13.

HAMILTON, S. R., BOSMAN, F. T. & BOFFETTA, P. 2010. Carcinoma of the colon and rectum. In: WHO Classification of Tumours of the Digestive System. . Lyon, France: IARC Press, International Agency for Research on Cancer.

HAMMOND, D. E., MAGEEAN, C. J., RUSILOWICZ, E. V., WICKENDEN, J. A., CLAGUE, M. J. & PRIOR, I. A. 2015. Differential reprogramming of isogenic colorectal cancer cells by distinct activating KRAS mutations. *J Proteome Res,* 14**,** 1535-46.

HAN, M., GOLDEN, A., HAN, Y. & STERNBERG, P. W. 1993. C. elegans lin-45 raf gene participates in let-60 ras-stimulated vulval differentiation. *Nature,* 363**,** 133-40.

HAN, M. & STERNBERG, P. W. 1990. let-60, a gene that specifies cell fates during C. elegans vulval induction, encodes a ras protein. *Cell,* 63**,** 921-31.

HANAWALT, P. C. 1994. Transcription-coupled repair and human disease. *Science,* 266**,** 1957-8.

HANCOCK, J. F., MAGEE, A. I., CHILDS, J. E. & MARSHALL, C. J. 1989. All ras proteins are polyisoprenylated but only some are palmitoylated. *Cell,* 57**,** 1167-77.

HANCOCK, J. F., PATERSON, H. & MARSHALL, C. J. 1990. A polybasic domain or palmitoylation is required in addition to the CAAX motif to localize p21ras to the plasma membrane. *Cell,* 63**,** 133-9.

HARVEY, J. J. 1964. An Unidentified Virus Which Causes the Rapid Production of Tumours in Mice. *Nature,* 204**,** 1104-5.

HATZIVASSILIOU, G., SONG, K., YEN, I., BRANDHUBER, B. J., ANDERSON, D. J., ALVARADO, R., LUDLAM, M. J., STOKOE, D., GLOOR, S. L., VIGERS, G., MORALES, T., ALIAGAS, I., LIU, B., SIDERIS, S., HOEFLICH, K. P., JAISWAL, B. S., SESHAGIRI, S., KOEPPEN, H., BELVIN, M., FRIEDMAN, L. S. & MALEK, S. 2010. RAF inhibitors prime wild-type RAF to activate the MAPK pathway and enhance growth. *Nature,* 464**,** 431-5.

HEID, C. A., STEVENS, J., LIVAK, K. J. & WILLIAMS, P. M. 1996. Real time quantitative PCR. *Genome Res,* 6**,** 986-94.

HEIDORN, S. J., MILAGRE, C., WHITTAKER, S., NOURRY, A., NICULESCU-DUVAS, I., DHOMEN, N., HUSSAIN, J., REIS-FILHO, J. S., SPRINGER, C. J., PRITCHARD, C. & MARAIS, R. 2010. Kinase-dead BRAF and oncogenic RAS cooperate to drive tumor progression through CRAF. *Cell,* 140**,** 209-21.

HELLEMANS, J., MORTIER, G., DE PAEPE, A., SPELEMAN, F. & VANDESOMPELE, J. 2007. qBase relative quantification framework and software for management and automated analysis of real-time quantitative PCR data. *Genome Biol,* 8**,** R19.

HENDRIKS, G., CALLEJA, F., BESARATINIA, A., VRIELING, H., PFEIFER, G. P., MULLENDERS, L. H., JANSEN, J. G. & DE WIND, N. 2010. Transcription-dependent cytosine deamination is a novel mechanism in ultraviolet light-induced mutagenesis. *Curr Biol,* 20**,** 170-5.

HENRIKSEN, L., GRANDAL, M. V., KNUDSEN, S. L., VAN DEURS, B. & GROVDAL, L. M. 2013. Internalization mechanisms of the epidermal growth factor receptor after activation with different ligands. *PLoS One,* 8**,** e58148.

HERMAN, R. K. & DWORKIN, N. B. 1971. Effect of gene induction on the rate of mutagenesis by ICR-191 in Escherichia coli. *J Bacteriol,* 106**,** 543-50.

HIGUCHI, R., DOLLINGER, G., WALSH, P. S. & GRIFFITH, R. 1992. Simultaneous amplification and detection of specific DNA sequences. *Biotechnology (N Y),* 10**,** 413-7.

HIGUCHI, R., FOCKLER, C., DOLLINGER, G. & WATSON, R. 1993. Kinetic PCR analysis: real-time monitoring of DNA amplification reactions. *Biotechnology (N Y),* 11**,** 1026-30.

HINOI, T., KISHIDA, S., KOYAMA, S., IKEDA, M., MATSUURA, Y. & KIKUCHI, A. 1996. Post-translational modifications of Ras and Ral are important for the action of Ral GDP dissociation stimulator. *J Biol Chem,* 271**,** 19710-6.

HOEBEECK, J., VAN DER LUIJT, R., POPPE, B., DE SMET, E., YIGIT, N., CLAES, K., ZEWALD, R., DE JONG, G. J., DE PAEPE, A., SPELEMAN, F. & VANDESOMPELE, J. 2005. Rapid detection of VHL exon deletions using real-time quantitative PCR. *Lab Invest,* 85**,** 24-33.

HOFER, F., FIELDS, S., SCHNEIDER, C. & MARTIN, G. S. 1994. Activated Ras interacts with the Ral guanine nucleotide dissociation stimulator. *Proc Natl Acad Sci U S A,* 91**,** 11089-93.

HOLDER, M. K. & BLAUSTEIN, J. D. 2014. Puberty and adolescence as a time of vulnerability to stressors that alter neurobehavioral processes. *Front Neuroendocrinol,* 35**,** 89-110.

HOLDERFIELD, M., NAGEL, T. E. & STUART, D. D. 2014. Mechanism and consequences of RAF kinase activation by small-molecule inhibitors. *Br J Cancer,* 111**,** 640-5.

HOWE, L. R., LEEVERS, S. J., GOMEZ, N., NAKIELNY, S., COHEN, P. & MARSHALL, C. J. 1992. Activation of the MAP kinase pathway by the protein kinase raf. *Cell,* 71**,** 335-42.

HU, W., FENG, Z. & TANG, M. S. 2003. Preferential carcinogen-DNA adduct formation at codons 12 and 14 in the human K-ras gene and their possible mechanisms. *Biochemistry,* 42**,** 10012-23.

HUANG, Z., FASCO, M. J. & KAMINSKY, L. S. 1996. Optimization of Dnase I removal of contaminating DNA from RNA for use in quantitative RNA-PCR. *Biotechniques,* 20**,** 1012-4, 1016, 1018-20.

HUMPHREY, R. K., BEATTIE, G. M., LOPEZ, A. D., BUCAY, N., KING, C. C., FIRPO, M. T., ROSE-JOHN, S. & HAYEK, A. 2004. Maintenance of pluripotency in human embryonic stem cells is STAT3 independent. *Stem Cells,* 22**,** 522-30.

HUSCHTSCHA, L., ROZENGURT, E. & BODMER, W. F. 1991. Growth factor requirements of human colorectal tumour cells: relations to cellular differentiation. *Eur J Cancer,* 27**,** 1680-4.

HUYNH, H., SOO, K. C., CHOW, P. K. & TRAN, E. 2007. Targeted inhibition of the extracellular signal-regulated kinase kinase pathway with AZD6244 (ARRY-142886) in the treatment of hepatocellular carcinoma. *Mol Cancer Ther,* 6**,** 138-46.

IBIZA, S., PEREZ-RODRIGUEZ, A., ORTEGA, A., MARTINEZ-RUIZ, A., BARREIRO, O., GARCIA-DOMINGUEZ, C. A., VICTOR, V. M., ESPLUGUES, J. V., ROJAS, J. M., SANCHEZ-MADRID, F. & SERRADOR, J. M. 2008. Endothelial nitric oxide synthase regulates N-Ras activation on the Golgi complex of antigen-stimulated T cells. *Proc Natl Acad Sci U S A,* 105**,** 10507-12.

IMAJO, M., TSUCHIYA, Y. & NISHIDA, E. 2006. Regulatory mechanisms and functions of MAP kinase signaling pathways. *IUBMB Life,* 58**,** 312-7.

INTERNATIONAL CANCER GENOME, C., HUDSON, T. J., ANDERSON, W., ARTEZ, A., BARKER, A. D., BELL, C., BERNABE, R. R., BHAN, M. K., CALVO, F., EEROLA, I., GERHARD, D. S., GUTTMACHER, A., GUYER, M., HEMSLEY, F. M., JENNINGS, J. L., KERR, D., KLATT, P., KOLAR, P., KUSADA, J., LANE, D. P., LAPLACE, F., YOUYONG, L., NETTEKOVEN, G., OZENBERGER, B., PETERSON, J., RAO, T. S., REMACLE, J., SCHAFER, A. J., SHIBATA, T., STRATTON, M. R., VOCKLEY, J. G., WATANABE, K., YANG, H., YUEN, M. M., KNOPPERS, B. M., BOBROW, M., CAMBON-THOMSEN, A., DRESSLER, L. G., DYKE, S. O., JOLY, Y., KATO, K., KENNEDY, K. L., NICOLAS, P., PARKER, M. J., RIAL-SEBBAG, E., ROMEO-CASABONA, C. M., SHAW, K. M., WALLACE,

S., WIESNER, G. L., ZEPS, N., LICHTER, P., BIANKIN, A. V., CHABANNON, C., CHIN, L., CLEMENT, B., DE ALAVA, E., DEGOS, F., FERGUSON, M. L., GEARY, P., HAYES, D. N., HUDSON, T. J., JOHNS, A. L., KASPRZYK, A., NAKAGAWA, H., PENNY, R., PIRIS, M. A., SARIN, R., SCARPA, A., SHIBATA, T., VAN DE VIJVER, M., FUTREAL, P. A., ABURATANI, H., BAYES, M., BOTWELL, D. D., CAMPBELL, P. J., ESTIVILL, X., GERHARD, D. S., GRIMMOND, S. M., GUT, I., HIRST, M., LOPEZ-OTIN, C., MAJUMDER, P., MARRA, M., MCPHERSON, J. D., NAKAGAWA, H., NING, Z., PUENTE, X. S., RUAN, Y., SHIBATA, T., STRATTON, M. R., STUNNENBERG, H. G., SWERDLOW, H., VELCULESCU, V. E., WILSON, R. K., XUE, H. H., YANG, L., SPELLMAN, P. T., BADER, G. D., BOUTROS, P. C., CAMPBELL, P. J., et al. 2010. International network of cancer genome projects. *Nature,* 464**,** 993-8.

ISE, K., NAKAMURA, K., NAKAO, K., SHIMIZU, S., HARADA, H., ICHISE, T., MIYOSHI, J., GONDO, Y., ISHIKAWA, T., AIBA, A. & KATSUKI, M. 2000. Targeted deletion of the H-ras gene decreases tumor formation in mouse skin carcinogenesis. *Oncogene,* 19**,** 2951-6.

ITSKOVITZ-ELDOR, J., SCHULDINER, M., KARSENTI, D., EDEN, A., YANUKA, O., AMIT, M., SOREQ, H. & BENVENISTY, N. 2000. Differentiation of human embryonic stem cells into embryoid bodies compromising the three embryonic germ layers. *Mol Med,* 6**,** 88-95.

JARDIM, D. L., WHELER, J. J., HESS, K., TSIMBERIDOU, A. M., ZINNER, R., JANKU, F., SUBBIAH, V., NAING, A., PIHA-PAUL, S. A., WESTIN, S. N., ROY-CHOWDHURI, S., MERIC-BERNSTAM, F. & HONG, D. S. 2014. FBXW7 mutations in patients with advanced cancers: clinical and molecular characteristics and outcomes with mTOR inhibitors. *PLoS One,* 9**,** e89388.

JAUMOT, M., YAN, J., CLYDE-SMITH, J., SLUIMER, J. & HANCOCK, J. F. 2002. The linker domain of the Ha-Ras hypervariable region regulates interactions with exchange factors, Raf-1 and phosphoinositide 3-kinase. *J Biol Chem,* 277**,** 272-8.

JOGI, A., VAAPIL, M., JOHANSSON, M. & PAHLMAN, S. 2012. Cancer cell differentiation heterogeneity and aggressive behavior in solid tumors. *Ups J Med Sci,* 117**,** 217-24.

JOHN, J., FRECH, M. & WITTINGHOFER, A. 1988. Biochemical properties of Ha-ras encoded p21 mutants and mechanism of the autophosphorylation reaction. *J Biol Chem,* 263**,** 11792-9.

JOHNSON, L., GREENBAUM, D., CICHOWSKI, K., MERCER, K., MURPHY, E., SCHMITT, E., BRONSON, R. T., UMANOFF, H., EDELMANN, W., KUCHERLAPATI, R. & JACKS, T. 1997. K-ras is an essential gene in the mouse with partial functional overlap with N-ras. *Genes Dev,* 11**,** 2468-81.

JOHNSON, V., VOLIKOS, E., HALFORD, S. E., EFTEKHAR SADAT, E. T., POPAT, S., TALBOT, I., TRUNINGER, K., MARTIN, J., JASS, J., HOULSTON, R., ATKIN, W., TOMLINSON, I. P. & SILVER, A. R. 2005. Exon 3 beta-catenin mutations are specifically associated with colorectal carcinomas in hereditary non-polyposis colorectal cancer syndrome. *Gut,* 54**,** 264-7.

JONES, M. C., CASWELL, P. T. & NORMAN, J. C. 2006. Endocytic recycling pathways: emerging regulators of cell migration. *Curr Opin Cell Biol,* 18**,** 549-57.

JONES, M. K. & JACKSON, J. H. 1998. Ras-GRF activates Ha-Ras, but not N-Ras or K-Ras 4B, protein in vivo. *J Biol Chem,* 273**,** 1782-7.

JULLIEN-FLORES, V., DORSEUIL, O., ROMERO, F., LETOURNEUR, F., SARAGOSTI, S., BERGER, R., TAVITIAN, A., GACON, G. & CAMONIS, J. H. 1995. Bridging Ral GTPase to Rho pathways. RLIP76, a Ral effector with CDC42/Rac GTPase-activating protein activity. *J Biol Chem,* 270**,** 22473-7.

KAGEYAMA, R., MERLINO, G. T. & PASTAN, I. 1988a. Epidermal growth factor (EGF) receptor gene transcription. Requirement for Sp1 and an EGF receptor-specific factor. *J Biol Chem,* 263**,** 6329-36.

KAGEYAMA, R., MERLINO, G. T. & PASTAN, I. 1988b. A transcription factor active on the epidermal growth factor receptor gene. *Proc Natl Acad Sci U S A,* 85**,** 5016-20.

KAMATA, T. & FERAMISCO, J. R. 1984. Epidermal growth factor stimulates guanine nucleotide binding activity and phosphorylation of ras oncogene proteins. *Nature,* 310**,** 147-50.

KAMEDA, T. & THOMSON, J. A. 2005. Human ERas gene has an upstream premature polyadenylation signal that results in a truncated, noncoding transcript. *Stem Cells,* 23**,** 1535-40.

KARAPETIS, C. S., KHAMBATA-FORD, S., JONKER, D. J., O'CALLAGHAN, C. J., TU, D., TEBBUTT, N. C., SIMES, R. J., CHALCHAL, H., SHAPIRO, J. D., ROBITAILLE, S., PRICE, T. J., SHEPHERD, L., AU, H. J., LANGER, C., MOORE, M. J. & ZALCBERG, J. R. 2008. K-ras mutations and benefit from cetuximab in advanced colorectal cancer. *N Engl J Med,* 359**,** 1757-65.

KARARLI, T. T. 1995. Comparison of the gastrointestinal anatomy, physiology, and biochemistry of humans and commonly used laboratory animals. *Biopharm Drug Dispos,* 16**,** 351-80.

KARGE, W. H., 3RD, SCHAEFER, E. J. & ORDOVAS, J. M. 1998. Quantification of mRNA by polymerase chain reaction (PCR) using an internal standard and a nonradioactive detection method. *Methods Mol Biol,* 110**,** 43-61.

KARNOUB, A. E. & WEINBERG, R. A. 2008. Ras oncogenes: split personalities. *Nat Rev Mol Cell Biol,* 9**,** 517-31.

KAUFMAN, M. H. 1992. *The Atlas of Mouse Development*, Academic Press.

KE, L. D., CHEN, Z. & YUNG, W. K. 2000. A reliability test of standard-based quantitative PCR: exogenous vs endogenous standards. *Mol Cell Probes,* 14**,** 127-35.

KELLEY, G. G., REKS, S. E., ONDRAKO, J. M. & SMRCKA, A. V. 2001. Phospholipase C(epsilon): a novel Ras effector. *EMBO J,* 20**,** 743-54.

KHOKHLATCHEV, A., RABIZADEH, S., XAVIER, R., NEDWIDEK, M., CHEN, T., ZHANG, X. F., SEED, B. & AVRUCH, J. 2002. Identification of a novel Ras-regulated proapoptotic pathway. *Curr Biol,* 12**,** 253-65.

KIJIMA, H., YAMAZAKI, H., NAKAMURA, M., SCANLON, K. J., OSAMURA, R. Y. & UEYAMA, Y. 2004. Ribozyme against mutant K-ras mRNA suppresses tumor growth of pancreatic cancer. *Int J Oncol,* 24**,** 559-64.

KIKUCHI, A., DEMO, S. D., YE, Z. H., CHEN, Y. W. & WILLIAMS, L. T. 1994. ralGDS family members interact with the effector loop of ras p21. *Mol Cell Biol,* 14**,** 7483-91.

KIKUCHI, A. & WILLIAMS, L. T. 1996. Regulation of interaction of ras p21 with RalGDS and Raf-1 by cyclic AMP-dependent protein kinase. *J Biol Chem,* 271**,** 588-94.

KIM, A., DAVIS, R. & HIGUCHI, M. 2015. Intracellular oxygen determined by respiration regulates localization of Ras and prenylated proteins. *Cell Death Dis,* 6**,** e1825.

KIM, I. J., KANG, H. C., PARK, J. H., SHIN, Y., KU, J. L., LIM, S. B., PARK, S. Y., JUNG, S. Y., KIM, H. K. & PARK, J. G. 2003. Development and applications of a beta-catenin oligonucleotide microarray: beta-catenin mutations are dominantly found in the proximal colon cancers with microsatellite instability. *Clin Cancer Res,* 9**,** 2920-5.

KIM, J. S., LEE, C., FOXWORTH, A. & WALDMAN, T. 2004. B-Raf is dispensable for K-Ras-mediated oncogenesis in human cancer cells. *Cancer Res,* 64**,** 1932-7.

KIRSTEN, W. H. & MAYER, L. A. 1967. Morphologic responses to a murine erythroblastosis virus. *J Natl Cancer Inst,* 39**,** 311-35.

KLINGER, B., SIEBER, A., FRITSCHE-GUENTHER, R., WITZEL, F., BERRY, L., SCHUMACHER, D., YAN, Y., DUREK, P., MERCHANT, M., SCHAFER, R., SERS, C. & BLUTHGEN, N. 2013. Network quantification of EGFR

signaling unveils potential for targeted combination therapy. *Mol Syst Biol,* 9**,** 673.

KNOEBEL, S., KURTZ, A., SCHWARZ, C., ECKARDT, D., BARRAL, S. & BOSSIO, A. 2010. *Novel fibroblast-specific marker for rapid, efficient removal of mEFs from stem cell cultures by magnetic separation.,* San Francisco, CA.

KOERA, K., NAKAMURA, K., NAKAO, K., MIYOSHI, J., TOYOSHIMA, K., HATTA, T., OTANI, H., AIBA, A. & KATSUKI, M. 1997. K-ras is essential for the development of the mouse embryo. *Oncogene,* 15**,** 1151-9.

KOESTENBAUER, S., ZECH, N. H., JUCH, H., VANDERZWALMEN, P., SCHOONJANS, L. & DOHR, G. 2006. Embryonic stem cells: similarities and differences between human and murine embryonic stem cells. *Am J Reprod Immunol,* 55**,** 169-80.

KONISHI, H., KARAKAS, B., ABUKHDEIR, A. M., LAURING, J., GUSTIN, J. P., GARAY, J. P., KONISHI, Y., GALLMEIER, E., BACHMAN, K. E. & PARK, B. H. 2007. Knock-in of mutant K-ras in nontumorigenic human epithelial cells as a new model for studying K-ras mediated transformation. *Cancer Res,* 67**,** 8460-7.

KOVACS, E., ZORN, J. A., HUANG, Y., BARROS, T. & KURIYAN, J. 2015. A structural perspective on the regulation of the epidermal growth factor receptor. *Annu Rev Biochem,* 84**,** 739-64.

KOZERA, B. & RAPACZ, M. 2013. Reference genes in real-time PCR. *J Appl Genet,* 54**,** 391-406.

KRAEMER, N., NEUBERT, G., ISSA, L., NINNEMANN, O., SEILER, A. E. & KAINDL, A. M. 2012. Reference genes in the developing murine brain and in differentiating embryonic stem cells. *Neurol Res,* 34**,** 664-8.

KRAMER, M. F. & COEN, D. M. 2006. Enzymatic amplification of DNA by PCR: standard procedures and optimization. *Curr Protoc Cytom,* Appendix 3**,** Appendix 3K.

KRENGEL, U., SCHLICHTING, I., SCHERER, A., SCHUMANN, R., FRECH, M., JOHN, J., KABSCH, W., PAI, E. F. & WITTINGHOFER, A. 1990. Three-dimensional structures of H-ras p21 mutants: molecular basis for their inability to function as signal switch molecules. *Cell,* 62**,** 539-48.

KUBISTA, M., ANDRADE, J. M., BENGTSSON, M., FOROOTAN, A., JONAK, J., LIND, K., SINDELKA, R., SJOBACK, R., SJOGREEN, B., STROMBOM, L., STAHLBERG, A. & ZORIC, N. 2006. The real-time polymerase chain reaction. *Mol Aspects Med,* 27**,** 95-125.

KYRIAKIS, J. M., APP, H., ZHANG, X. F., BANERJEE, P., BRAUTIGAN, D. L., RAPP, U. R. & AVRUCH, J. 1992. Raf-1 activates MAP kinase-kinase. *Nature,* 358**,** 417-21.

LAMBA, S., RUSSO, M., SUN, C., LAZZARI, L., CANCELLIERE, C., GRERNRUM, W., LIEFTINK, C., BERNARDS, R., DI NICOLANTONIO, F. & BARDELLI, A. 2014. RAF suppression synergizes with MEK inhibition in KRAS mutant cancer cells. *Cell Rep,* 8**,** 1475-83.

LAMBERT, J. M., LAMBERT, Q. T., REUTHER, G. W., MALLIRI, A., SIDEROVSKI, D. P., SONDEK, J., COLLARD, J. G. & DER, C. J. 2002. Tiam1 mediates Ras activation of Rac by a PI(3)K-independent mechanism. *Nat Cell Biol,* 4**,** 621-5.

LAMPSON, B. L., PERSHING, N. L., PRINZ, J. A., LACSINA, J. R., MARZLUFF, W. F., NICCHITTA, C. V., MACALPINE, D. M. & COUNTER, C. M. 2013. Rare codons regulate KRas oncogenesis. *Curr Biol,* 23**,** 70-5.

LANGBEHEIM, H., SHIH, T. Y. & SCOLNICK, E. M. 1980. Identification of a normal vertebrate cell protein related to the p21 src of Harvey murine sarcoma virus. *Virology,* 106**,** 292-300.

LAPLANTE, M. & SABATINI, D. M. 2009. mTOR signaling at a glance. *J Cell Sci,* 122**,** 3589-94.

LAUDE, A. J. & PRIOR, I. A. 2008. Palmitoylation and localisation of RAS isoforms are modulated by the hypervariable linker domain. *J Cell Sci,* 121**,** 421-7.

LAWRENCE, M. S., STOJANOV, P., MERMEL, C. H., ROBINSON, J. T., GARRAWAY, L. A., GOLUB, T. R., MEYERSON, M., GABRIEL, S. B., LANDER, E. S. & GETZ, G. 2014. Discovery and saturation analysis of cancer genes across 21 tumour types. *Nature,* 505**,** 495-501.

LEAHY, A., XIONG, J. W., KUHNERT, F. & STUHLMANN, H. 1999. Use of developmental marker genes to define temporal and spatial patterns of differentiation during embryoid body formation. *J Exp Zool,* 284**,** 67-81.

LEIBOVITZ, A., STINSON, J. C., MCCOMBS, W. B., 3RD, MCCOY, C. E., MAZUR, K. C. & MABRY, N. D. 1976. Classification of human colorectal adenocarcinoma cell lines. *Cancer Res,* 36**,** 4562-9.

LENKA, N., LU, Z. J., SASSE, P., HESCHELER, J. & FLEISCHMANN, B. K. 2002. Quantitation and functional characterization of neural cells derived from ES cells using nestin enhancer-mediated targeting in vitro. *J Cell Sci,* 115**,** 1471-85.

LEON, J., GUERRERO, I. & PELLICER, A. 1987. Differential expression of the ras gene family in mice. *Mol Cell Biol,* 7**,** 1535-40.

LI, F., HE, Z., LI, Y., LIU, P., CHEN, F., WANG, M., ZHU, H., DING, X., WANGENSTEEN, K. J., HU, Y. & WANG, X. 2011. Combined activin A/LiCl/Noggin treatment improves production of mouse embryonic stem cell-derived definitive endoderm cells. *J Cell Biochem,* 112**,** 1022-34.

LI, N., BATZER, A., DALY, R., YAJNIK, V., SKOLNIK, E., CHARDIN, P., BAR-SAGI, D., MARGOLIS, B. & SCHLESSINGER, J. 1993. Guanine-nucleotide-releasing factor hSos1 binds to Grb2 and links receptor tyrosine kinases to Ras signalling. *Nature,* 363**,** 85-8.

LI, X., CHEN, Y., SCHEELE, S., ARMAN, E., HAFFNER-KRAUSZ, R., EKBLOM, P. & LONAI, P. 2001. Fibroblast growth factor signaling and basement membrane assembly are connected during epithelial morphogenesis of the embryoid body. *J Cell Biol,* 153**,** 811-22.

LIU, L., ZHU, S., GONG, Z. & LOW, B. C. 2008. K-ras/PI3K-Akt signaling is essential for zebrafish hematopoiesis and angiogenesis. *PLoS One,* 3**,** e2850.

LOBO, N. A., SHIMONO, Y., QIAN, D. & CLARKE, M. F. 2007. The biology of cancer stem cells. *Annu Rev Cell Dev Biol,* 23**,** 675-99.

LODISH, H., BERK, A., ZIPURSKY, S. L., MATSUDAIRA, P., BALTIMORE, D. & DARNELL, J. 2000. *Molecular Cell Biology,* New York, W. H. Freeman.

LOPEZ, I., MAK, E. C., DING, J., HAMM, H. E. & LOMASNEY, J. W. 2001. A novel bifunctional phospholipase c that is regulated by Galpha 12 and stimulates the Ras/mitogen-activated protein kinase pathway. *J Biol Chem,* 276**,** 2758-65.

LORENTZEN, A., KINKHABWALA, A., ROCKS, O., VARTAK, N. & BASTIAENS, P. I. 2010. Regulation of Ras localization by acylation enables a mode of intracellular signal propagation. *Sci Signal,* 3**,** ra68.

LOWENSTEIN, E. J., DALY, R. J., BATZER, A. G., LI, W., MARGOLIS, B., LAMMERS, R., ULLRICH, A., SKOLNIK, E. Y., BAR-SAGI, D. & SCHLESSINGER, J. 1992. The SH2 and SH3 domain-containing protein GRB2 links receptor tyrosine kinases to ras signaling. *Cell,* 70**,** 431-42.

LOWY, D. R. & WILLUMSEN, B. M. 1989. Protein modification: new clue to Ras lipid glue. *Nature,* 341**,** 384-5.

LUNDBERG, K. S., SHOEMAKER, D. D., ADAMS, M. W., SHORT, J. M., SORGE, J. A. & MATHUR, E. J. 1991. High-fidelity amplification using a thermostable DNA polymerase isolated from Pyrococcus furiosus. *Gene,* 108**,** 1-6.

LUO, F., HAMOUDI, R., BROOKS, D. G., PATEK, C. E. & ARENDS, M. J. 2007. Stem cell gene expression changes induced specifically by mutated K-ras. *Gene Expr,* 14**,** 101-15.

LUO, J. Q., LIU, X., FRANKEL, P., ROTUNDA, T., RAMOS, M., FLOM, J., JIANG, H., FEIG, L. A., MORRIS, A. J., KAHN, R. A. & FOSTER, D. A. 1998. Functional association between Arf and RalA in active phospholipase D complex. *Proc Natl Acad Sci U S A,* 95**,** 3632-7.

LUTFALLA, G. & UZE, G. 2006. Performing quantitative reverse-transcribed polymerase chain reaction experiments. *Methods Enzymol,* 410**,** 386-400.

LYNCH, S. J., SNITKIN, H., GUMPER, I., PHILIPS, M. R., SABATINI, D. & PELLICER, A. 2015. The differential palmitoylation states of N-Ras and H-Ras determine their distinct Golgi subcompartment localizations. *J Cell Physiol,* 230**,** 610-9.

LYNCH, T. J., BELL, D. W., SORDELLA, R., GURUBHAGAVATULA, S., OKIMOTO, R. A., BRANNIGAN, B. W., HARRIS, P. L., HASERLAT, S. M., SUPKO, J. G., HALUSKA, F. G., LOUIS, D. N., CHRISTIANI, D. C., SETTLEMAN, J. & HABER, D. A. 2004. Activating mutations in the epidermal growth factor receptor underlying responsiveness of non-small-cell lung cancer to gefitinib. *N Engl J Med,* 350**,** 2129-39.

MACKAY, S. L., YASWEN, L. R., TARNUZZER, R. W., MOLDAWER, L. L., BLAND, K. I., COPELAND, E. M., 3RD & SCHULTZ, G. S. 1995. Colon cancer cells that are not growth inhibited by TGF-beta lack functional type I and type II TGF-beta receptors. *Ann Surg,* 221**,** 767-76; discussion 776-7.

MAEDA, Y., DAVE, V. & WHITSETT, J. A. 2007. Transcriptional control of lung morphogenesis. *Physiol Rev,* 87**,** 219-44.

MAGEEAN, C. 2014. *Cellular responses to oncogenic Ras signalling.* PhD, University of Liverpool.

MAGEEAN, C. J., GRIFFITHS, J. R., SMITH, D. L., CLAGUE, M. J. & PRIOR, I. A. 2015. Absolute Quantification of Endogenous Ras Isoform Abundance. *PLoS One,* 10**,** e0142674.

MAJEWSKI, J. 2003. Dependence of mutational asymmetry on gene-expression levels in the human genome. *Am J Hum Genet,* 73**,** 688-92.

MALLO, G. V., RECHRECHE, H., FRIGERIO, J. M., ROCHA, D., ZWEIBAUM, A., LACASA, M., JORDAN, B. R., DUSETTI, N. J., DAGORN, J. C. & IOVANNA, J. L. 1997. Molecular cloning, sequencing and expression of the mRNA encoding human Cdx1 and Cdx2 homeobox. Down-regulation of Cdx1 and Cdx2 mRNA expression during colorectal carcinogenesis. *Int J Cancer,* 74**,** 35-44.

MALUMBRES, M. & BARBACID, M. 2003. RAS oncogenes: the first 30 years. *Nat Rev Cancer,* 3**,** 459-65.

MANNE, V., BEKESI, E. & KUNG, H. F. 1985. Ha-ras proteins exhibit GTPase activity: point mutations that activate Ha-ras gene products result in decreased GTPase activity. *Proc Natl Acad Sci U S A,* 82**,** 376-80.

MAO, J. H., KIM, I. J., WU, D., CLIMENT, J., KANG, H. C., DELROSARIO, R. & BALMAIN, A. 2008. FBXW7 targets mTOR for degradation and cooperates with PTEN in tumor suppression. *Science,* 321**,** 1499-502.

MARGOLIS, B. & SKOLNIK, E. Y. 1994. Activation of Ras by receptor tyrosine kinases. *J Am Soc Nephrol,* 5**,** 1288-99.

MARKOWITZ, S. D. & BERTAGNOLLI, M. M. 2009. Molecular origins of cancer: Molecular basis of colorectal cancer. *N Engl J Med,* 361**,** 2449-60.

MARTIN, G. R. 1981. Isolation of a pluripotent cell line from early mouse embryos cultured in medium conditioned by teratocarcinoma stem cells. *Proc Natl Acad Sci U S A,* 78**,** 7634-8.

MARTIN, G. R. & EVANS, M. J. 1975. Differentiation of clonal lines of teratocarcinoma cells: formation of embryoid bodies in vitro. *Proc Natl Acad Sci U S A,* 72**,** 1441-5.

MASUDA, T., KARIYA, K., SHINKAI, M., OKADA, T. & KATAOKA, T. 1995. Protein kinase Byr2 is a target of Ras1 in the fission yeast Schizosaccharomyces pombe. *J Biol Chem,* 270**,** 1979-82.

MATALLANAS, D., AROZARENA, I., BERCIANO, M. T., AARONSON, D. S., PELLICER, A., LAFARGA, M. & CRESPO, P. 2003. Differences on the inhibitory specificities of H-Ras, K-Ras, and N-Ras (N17) dominant negative mutants are related to their membrane microlocalization. *J Biol Chem,* 278**,** 4572-81.

MATALLANAS, D., SANZ-MORENO, V., AROZARENA, I., CALVO, F., AGUDO-IBANEZ, L., SANTOS, E., BERCIANO, M. T. & CRESPO, P. 2006. Distinct utilization of effectors and biological outcomes resulting from site-specific Ras activation: Ras functions in lipid rafts and Golgi complex are dispensable for proliferation and transformation. *Mol Cell Biol,* 26**,** 100-16.

MAXFIELD, F. R. & MCGRAW, T. E. 2004. Endocytic recycling. *Nat Rev Mol Cell Biol,* 5**,** 121-32.

MCGRATH, J. P., CAPON, D. J., GOEDDEL, D. V. & LEVINSON, A. D. 1984. Comparative biochemical properties of normal and activated human ras p21 protein. *Nature,* 310**,** 644-9.

MCGRATH, J. P., CAPON, D. J., SMITH, D. H., CHEN, E. Y., SEEBURG, P. H., GOEDDEL, D. V. & LEVINSON, A. D. 1983. Structure and organization of

the human Ki-ras proto-oncogene and a related processed pseudogene. *Nature,* 304**,** 501-6.

MCPHERSON, M. J. & MØLLER, S. G. 2006. *PCR*, Taylor & Francis Group.

MENA, H. A., LOKAJCZYK, A., DIZIER, B., STRIER, S. E., VOTO, L. S., BOISSON-VIDAL, C., SCHATTNER, M. & NEGROTTO, S. 2014. Acidic preconditioning improves the proangiogenic responses of endothelial colony forming cells. *Angiogenesis,* 17**,** 867-79.

MENDOZA, M. C., ER, E. E. & BLENIS, J. 2011. The Ras-ERK and PI3K-mTOR pathways: cross-talk and compensation. *Trends Biochem Sci,* 36**,** 320-8.

METZGER, R. J., KLEIN, O. D., MARTIN, G. R. & KRASNOW, M. A. 2008. The branching programme of mouse lung development. *Nature,* 453**,** 745-50.

MFOPOU, J. K., GEERAERTS, M., DEJENE, R., VAN LANGENHOVEN, S., ABERKANE, A., VAN GRUNSVEN, L. A. & BOUWENS, L. 2014. Efficient definitive endoderm induction from mouse embryonic stem cell adherent cultures: a rapid screening model for differentiation studies. *Stem Cell Res,* 12**,** 166-77.

MIALON, A., SANKINEN, M., SODERSTROM, H., JUNTTILA, T. T., HOLMSTROM, T., KOIVUSALO, R., PAPAGEORGIOU, A. C., JOHNSON, R. S., HIETANEN, S., ELENIUS, K. & WESTERMARCK, J. 2005. DNA topoisomerase I is a cofactor for c-Jun in the regulation of epidermal growth factor receptor expression and cancer cell proliferation. *Mol Cell Biol,* 25**,** 5040-51.

MILBURN, M. V., TONG, L., DEVOS, A. M., BRUNGER, A., YAMAIZUMI, Z., NISHIMURA, S. & KIM, S. H. 1990. Molecular switch for signal transduction: structural differences between active and inactive forms of protooncogenic ras proteins. *Science,* 247**,** 939-45.

MILLAN, O., BALLESTER, A., CASTRILLO, A., OLIVA, J. L., TRAVES, P. G., ROJAS, J. M. & BOSCA, L. 2003. H-Ras-specific activation of NF-kappaB protects NIH 3T3 cells against stimulus-dependent apoptosis. *Oncogene,* 22**,** 477-83.

MILLER, M. S. & MILLER, L. D. 2011. RAS Mutations and Oncogenesis: Not all RAS Mutations are Created Equally. *Front Genet,* 2**,** 100.

MISALE, S., ARENA, S., LAMBA, S., SIRAVEGNA, G., LALLO, A., HOBOR, S., RUSSO, M., BUSCARINO, M., LAZZARI, L., SARTORE-BIANCHI, A., BENCARDINO, K., AMATU, A., LAURICELLA, C., VALTORTA, E., SIENA, S., DI NICOLANTONIO, F. & BARDELLI, A. 2014. Blockade of EGFR and MEK intercepts heterogeneous mechanisms of acquired resistance to anti-EGFR therapies in colorectal cancer. *Sci Transl Med,* 6**,** 224ra26.

MITIKU, N. & BAKER, J. C. 2007. Genomic analysis of gastrulation and organogenesis in the mouse. *Dev Cell,* 13**,** 897-907.

MOLINA-ARCAS, M., HANCOCK, D. C., SHERIDAN, C., KUMAR, M. S. & DOWNWARD, J. 2013. Coordinate direct input of both KRAS and IGF1 receptor to activation of PI3 kinase in KRAS-mutant lung cancer. *Cancer Discov,* 3**,** 548-63.

MOODIE, S. A., WILLUMSEN, B. M., WEBER, M. J. & WOLFMAN, A. 1993. Complexes of Ras.GTP with Raf-1 and mitogen-activated protein kinase kinase. *Science,* 260**,** 1658-61.

MORONI, M., SARTORE-BIANCHI, A., BENVENUTI, S., ARTALE, S., BARDELLI, A. & SIENA, S. 2005. Somatic mutation of EGFR catalytic domain and treatment with gefitinib in colorectal cancer. *Ann Oncol,* 16**,** 1848-9.

MORRISON, T. B., WEIS, J. J. & WITTWER, C. T. 1998. Quantification of low-copy transcripts by continuous SYBR Green I monitoring during amplification. *Biotechniques,* 24**,** 954-962.

MULLIS, K., FALOONA, F., SCHARF, S., SAIKI, R., HORN, G. & ERLICH, H. 1986. Specific enzymatic amplification of DNA in vitro: the polymerase chain reaction. *Cold Spring Harb Symp Quant Biol,* 51 Pt 1**,** 263-73.

MURRAY, M. J., CUNNINGHAM, J. M., PARADA, L. F., DAUTRY, F., LEBOWITZ, P. & WEINBERG, R. A. 1983. The HL-60 transforming sequence: a ras oncogene coexisting with altered myc genes in hematopoietic tumors. *Cell,* 33**,** 749-57.

MURRAY, P. & EDGAR, D. 2000. Regulation of programmed cell death by basement membranes in embryonic development. *J Cell Biol,* 150**,** 1215-21.

MURRAY, P. & EDGAR, D. 2001. Regulation of laminin and COUP-TF expression in extraembryonic endodermal cells. *Mech Dev,* 101**,** 213-5.

MURRAY, P. & EDGAR, D. 2004. The topographical regulation of embryonic stem cell differentiation. *Philos Trans R Soc Lond B Biol Sci,* 359**,** 1009-20.

NADIJCKA, M. & HILLMAN, N. 1974. Ultrastructural studies of the mouse blastocyst substages. *J Embryol Exp Morphol,* 32**,** 675-95.

NAGAHARA, H., MIMORI, K., OHTA, M., UTSUNOMIYA, T., INOUE, H., BARNARD, G. F., OHIRA, M., HIRAKAWA, K. & MORI, M. 2005. Somatic mutations of epidermal growth factor receptor in colorectal carcinoma. *Clin Cancer Res,* 11**,** 1368-71.

NAGARAJ, N., WISNIEWSKI, J. R., GEIGER, T., COX, J., KIRCHER, M., KELSO, J., PAABO, S. & MANN, M. 2011. Deep proteome and transcriptome mapping of a human cancer cell line. *Mol Syst Biol,* 7**,** 548.

NAGY, A., GOCZA, E., DIAZ, E. M., PRIDEAUX, V. R., IVANYI, E., MARKKULA, M. & ROSSANT, J. 1990. Embryonic stem cells alone are able to support fetal development in the mouse. *Development,* 110**,** 815-21.

NAGY, A., ROSSANT, J., NAGY, R., ABRAMOW-NEWERLY, W. & RODER, J. C. 1993. Derivation of completely cell culture-derived mice from early-passage embryonic stem cells. *Proc Natl Acad Sci U S A,* 90**,** 8424-8.

NAKAMURA, K., ICHISE, H., NAKAO, K., HATTA, T., OTANI, H., SAKAGAMI, H., KONDO, H. & KATSUKI, M. 2008. Partial functional overlap of the three ras genes in mouse embryonic development. *Oncogene,* 27**,** 2961-8.

NAKANISHI, Y., SENO, H., FUKUOKA, A., UEO, T., YAMAGA, Y., MARUNO, T., NAKANISHI, N., KANDA, K., KOMEKADO, H., KAWADA, M., ISOMURA, A., KAWADA, K., SAKAI, Y., YANAGITA, M., KAGEYAMA, R., KAWAGUCHI, Y., TAKETO, M. M., YONEHARA, S. & CHIBA, T. 2013. Dclk1 distinguishes between tumor and normal stem cells in the intestine. *Nat Genet,* 45**,** 98-103.

NAVE, B. T., OUWENS, M., WITHERS, D. J., ALESSI, D. R. & SHEPHERD, P. R. 1999. Mammalian target of rapamycin is a direct target for protein kinase B: identification of a convergence point for opposing effects of insulin and amino-acid deficiency on protein translation. *Biochem J,* 344 Pt 2**,** 427-31.

NEUMAN-SILBERBERG, F. S., SCHEJTER, E., HOFFMANN, F. M. & SHILO, B. Z. 1984. The Drosophila ras oncogenes: structure and nucleotide sequence. *Cell,* 37**,** 1027-33.

NICHOLS, J., SILVA, J., ROODE, M. & SMITH, A. 2009. Suppression of Erk signalling promotes ground state pluripotency in the mouse embryo. *Development,* 136**,** 3215-22.

NICOT, N., HAUSMAN, J. F., HOFFMANN, L. & EVERS, D. 2005. Housekeeping gene selection for real-time RT-PCR normalization in potato during biotic and abiotic stress. *J Exp Bot,* 56**,** 2907-14.

NISHIDA, E. & GOTOH, Y. 1993. The MAP kinase cascade is essential for diverse signal transduction pathways. *Trends Biochem Sci,* 18**,** 128-31.

NOLAN, T., HANDS, R. E. & BUSTIN, S. A. 2006. Quantification of mRNA using real-time RT-PCR. *Nat Protoc,* 1**,** 1559-82.

NOTARIANNI, E. & EVANS, M. J. 2006. *Embryonic Stem Cells: A Practical Approach,* New York, Oxford University Press.

NUNEZ RODRIGUEZ, N., LEE, I. N., BANNO, A., QIAO, H. F., QIAO, R. F., YAO, Z., HOANG, T., KIMMELMAN, A. C. & CHAN, A. M. 2006. Characterization of R-ras3/m-ras null mice reveals a potential role in trophic factor signaling. *Mol Cell Biol,* 26**,** 7145-54.

NYGREN, J., SVANVIK, N. & KUBISTA, M. 1998. The interactions between the fluorescent dye thiazole orange and DNA. *Biopolymers,* 46**,** 39-51.

O'SHEA, K. S. 2004. Self-renewal vs. differentiation of mouse embryonic stem cells. *Biol Reprod,* 71**,** 1755-65.

OH, B. Y., LEE, R. A., CHUNG, S. S. & KIM, K. H. 2011. Epidermal growth factor receptor mutations in colorectal cancer patients. *J Korean Soc Coloproctol,* 27**,** 127-32.

OLIVA, J. L., PEREZ-SALA, D., CASTRILLO, A., MARTINEZ, N., CANADA, F. J., BOSCA, L. & ROJAS, J. M. 2003. The cyclopentenone 15-deoxy-delta 12,14-prostaglandin J2 binds to and activates H-Ras. *Proc Natl Acad Sci U S A,* 100**,** 4772-7.

OLIVEIRA, J. B., BIDERE, N., NIEMELA, J. E., ZHENG, L., SAKAI, K., NIX, C. P., DANNER, R. L., BARB, J., MUNSON, P. J., PUCK, J. M., DALE, J., STRAUS, S. E., FLEISHER, T. A. & LENARDO, M. J. 2007. NRAS mutation causes a human autoimmune lymphoproliferative syndrome. *Proc Natl Acad Sci U S A,* 104**,** 8953-8.

OLIVIER, J. P., RAABE, T., HENKEMEYER, M., DICKSON, B., MBAMALU, G., MARGOLIS, B., SCHLESSINGER, J., HAFEN, E. & PAWSON, T. 1993. A Drosophila SH2-SH3 adaptor protein implicated in coupling the sevenless tyrosine kinase to an activator of Ras guanine nucleotide exchange, Sos. *Cell,* 73**,** 179-91.

OMEROVIC, J., HAMMOND, D. E., CLAGUE, M. J. & PRIOR, I. A. 2008. Ras isoform abundance and signalling in human cancer cell lines. *Oncogene,* 27**,** 2754-62.

OMEROVIC, J. & PRIOR, I. A. 2009. Compartmentalized signalling: Ras proteins and signalling nanoclusters. *FEBS J,* 276**,** 1817-25.

ONG, Y. L. & IRVINE, A. 2002. Quantitative real-time PCR: a critique of method and practical considerations. *Hematology,* 7**,** 59-67.

OSAKI, M., OSHIMURA, M. & ITO, H. 2004. PI3K-Akt pathway: its functions and alterations in human cancer. *Apoptosis,* 9**,** 667-76.

OSTREM, J. M., PETERS, U., SOS, M. L., WELLS, J. A. & SHOKAT, K. M. 2013. K-Ras(G12C) inhibitors allosterically control GTP affinity and effector interactions. *Nature,* 503**,** 548-51.

PAI, E. F., KABSCH, W., KRENGEL, U., HOLMES, K. C., JOHN, J. & WITTINGHOFER, A. 1989. Structure of the guanine-nucleotide-binding domain of the Ha-ras oncogene product p21 in the triphosphate conformation. *Nature,* 341**,** 209-14.

PAI, E. F., KRENGEL, U., PETSKO, G. A., GOODY, R. S., KABSCH, W. & WITTINGHOFER, A. 1990. Refined crystal structure of the triphosphate conformation of H-ras p21 at 1.35 A resolution: implications for the mechanism of GTP hydrolysis. *EMBO J,* 9**,** 2351-9.

PALMER, M. & PREDIGER, E. 2014. RNA Quality and RNA Sample Assessment - TechNotes 11(1). Life Technologies.

PAMONSINLAPATHAM, P., HADJ-SLIMANE, R., LEPELLETIER, Y., ALLAIN, B., TOCCAFONDI, M., GARBAY, C. & RAYNAUD, F. 2009. p120-Ras GTPase activating protein (RasGAP): a multi-interacting protein in downstream signaling. *Biochimie,* 91**,** 320-8.

PAOLACCI, A. R., TANZARELLA, O. A., PORCEDDU, E. & CIAFFI, M. 2009. Identification and validation of reference genes for quantitative RT-PCR normalization in wheat. *BMC Mol Biol,* 10**,** 11.

PAPAGEORGE, A., LOWY, D. & SCOLNICK, E. M. 1982. Comparative biochemical properties of p21 ras molecules coded for by viral and cellular ras genes. *J Virol,* 44**,** 509-19.

PARADA, L. F., TABIN, C. J., SHIH, C. & WEINBERG, R. A. 1982. Human EJ bladder carcinoma oncogene is homologue of Harvey sarcoma virus ras gene. *Nature,* 297**,** 474-8.

PARADISO, A., SIMONE, G., LENA, M. D., LEONE, B., VALLEJO, C., LACAVA, J., DELLAPASQUA, S., DAIDONE, M. G. & COSTA, A. 2001. Expression of apoptosis-related markers and clinical outcome in patients with advanced colorectal cancer. *Br J Cancer,* 84**,** 651-8.

PARK, C., QIAN, W. & ZHANG, J. 2012. Genomic evidence for elevated mutation rates in highly expressed genes. *EMBO Rep,* 13**,** 1123-9.

PEARSON, G., ROBINSON, F., BEERS GIBSON, T., XU, B. E., KARANDIKAR, M., BERMAN, K. & COBB, M. H. 2001. Mitogen-activated protein (MAP) kinase pathways: regulation and physiological functions. *Endocr Rev,* 22**,** 153-83.

PELLS, S., DIVJAK, M., ROMANOWSKI, P., IMPEY, H., HAWKINS, N. J., CLARKE, A. R., HOOPER, M. L. & WILLIAMSON, D. J. 1997. Developmentally-regulated expression of murine K-ras isoforms. *Oncogene,* 15**,** 1781-6.

PEREZ DE CASTRO, I., BIVONA, T. G., PHILIPS, M. R. & PELLICER, A. 2004. Ras activation in Jurkat T cells following low-grade stimulation of the T-cell

receptor is specific to N-Ras and occurs only on the Golgi apparatus. *Mol Cell Biol,* 24**,** 3485-96.

PHILIPS, M. R. 2005. Compartmentalized signalling of Ras. *Biochem Soc Trans,* 33**,** 657-61.

PLOWMAN, S. J., BERRY, R. L., BADER, S. A., LUO, F., ARENDS, M. J., HARRISON, D. J., HOOPER, M. L. & PATEK, C. E. 2006. K-ras 4A and 4B are co-expressed widely in human tissues, and their ratio is altered in sporadic colorectal cancer. *J Exp Clin Cancer Res,* 25**,** 259-67.

PLOWMAN, S. J., WILLIAMSON, D. J., O'SULLIVAN, M. J., DOIG, J., RITCHIE, A. M., HARRISON, D. J., MELTON, D. W., ARENDS, M. J., HOOPER, M. L. & PATEK, C. E. 2003. While K-ras is essential for mouse development, expression of the K-ras 4A splice variant is dispensable. *Mol Cell Biol,* 23**,** 9245-50.

PONCHEL, F., TOOMES, C., BRANSFIELD, K., LEONG, F. T., DOUGLAS, S. H., FIELD, S. L., BELL, S. M., COMBARET, V., PUISIEUX, A., MIGHELL, A. J., ROBINSON, P. A., INGLEHEARN, C. F., ISAACS, J. D. & MARKHAM, A. F. 2003. Real-time PCR based on SYBR-Green I fluorescence: an alternative to the TaqMan assay for a relative quantification of gene rearrangements, gene amplifications and micro gene deletions. *BMC Biotechnol,* 3**,** 18.

POTENZA, N., VECCHIONE, C., NOTTE, A., DE RIENZO, A., ROSICA, A., BAUER, L., AFFUSO, A., DE FELICE, M., RUSSO, T., POULET, R., CIFELLI, G., DE VITA, G., LEMBO, G. & DI LAURO, R. 2005. Replacement of K-Ras with H-Ras supports normal embryonic development despite inducing cardiovascular pathology in adult mice. *EMBO Rep,* 6**,** 432-7.

POULIKAKOS, P. I., ZHANG, C., BOLLAG, G., SHOKAT, K. M. & ROSEN, N. 2010. RAF inhibitors transactivate RAF dimers and ERK signalling in cells with wild-type BRAF. *Nature,* 464**,** 427-30.

POWERS, S., KATAOKA, T., FASANO, O., GOLDFARB, M., STRATHERN, J., BROACH, J. & WIGLER, M. 1984. Genes in S. cerevisiae encoding proteins with domains homologous to the mammalian ras proteins. *Cell,* 36**,** 607-12.

PRAHALLAD, A., SUN, C., HUANG, S., DI NICOLANTONIO, F., SALAZAR, R., ZECCHIN, D., BEIJERSBERGEN, R. L., BARDELLI, A. & BERNARDS, R. 2012. Unresponsiveness of colon cancer to BRAF(V600E) inhibition through feedback activation of EGFR. *Nature,* 483**,** 100-3.

PRIOR, I. A. & HANCOCK, J. F. 2001. Compartmentalization of Ras proteins. *J Cell Sci,* 114**,** 1603-8.

PRIOR, I. A., LEWIS, P. D. & MATTOS, C. 2012. A comprehensive survey of Ras mutations in cancer. *Cancer Res,* 72**,** 2457-67.

PRIOR, I. A., MUNCKE, C., PARTON, R. G. & HANCOCK, J. F. 2003. Direct visualization of Ras proteins in spatially distinct cell surface microdomains. *J Cell Biol,* 160**,** 165-70.

QUILLIAM, L. A., HUFF, S. Y., RABUN, K. M., WEI, W., PARK, W., BROEK, D. & DER, C. J. 1994. Membrane-targeting potentiates guanine nucleotide exchange factor CDC25 and SOS1 activation of Ras transforming activity. *Proc Natl Acad Sci U S A,* 91**,** 8512-6.

QUILLIAM, L. A., KHOSRAVI-FAR, R., HUFF, S. Y. & DER, C. J. 1995. Guanine nucleotide exchange factors: activators of the Ras superfamily of proteins. *Bioessays,* 17**,** 395-404.

QUINLAN, M. P., QUATELA, S. E., PHILIPS, M. R. & SETTLEMAN, J. 2008. Activated Kras, but not Hras or Nras, may initiate tumors of endodermal origin via stem cell expansion. *Mol Cell Biol,* 28**,** 2659-74.

QUINLAN, M. P. & SETTLEMAN, J. 2008. Explaining the preponderance of Kras mutations in human cancer: An isoform-specific function in stem cell expansion. *Cell Cycle,* 7**,** 1332-5.

RAK-RASZEWSKA, A., WILM, B., EDGAR, D., KENNY, S., WOOLF, A. S. & MURRAY, P. 2012. Development of embryonic stem cells in recombinant kidneys. *Organogenesis,* 8**,** 125-36.

RAMSKOLD, D., LUO, S., WANG, Y. C., LI, R., DENG, Q., FARIDANI, O. R., DANIELS, G. A., KHREBTUKOVA, I., LORING, J. F., LAURENT, L. C., SCHROTH, G. P. & SANDBERG, R. 2012. Full-length mRNA-Seq from single-cell levels of RNA and individual circulating tumor cells. *Nat Biotechnol,* 30**,** 777-82.

RAMSKOLD, D., WANG, E. T., BURGE, C. B. & SANDBERG, R. 2009. An abundance of ubiquitously expressed genes revealed by tissue transcriptome sequence data. *PLoS Comput Biol,* 5**,** e1000598.

RATHJEN, P. D., TOTH, S., WILLIS, A., HEATH, J. K. & SMITH, A. G. 1990. Differentiation inhibiting activity is produced in matrix-associated and diffusible forms that are generated by alternate promoter usage. *Cell,* 62**,** 1105-14.

RAUEN, K. A. 2007. HRAS and the Costello syndrome. *Clin Genet,* 71**,** 101-8.

REDDY, E. P., REYNOLDS, R. K., SANTOS, E. & BARBACID, M. 1982. A point mutation is responsible for the acquisition of transforming properties by the T24 human bladder carcinoma oncogene. *Nature,* 300**,** 149-52.

REYMOND, C. D., GOMER, R. H., MEHDY, M. C. & FIRTEL, R. A. 1984. Developmental regulation of a Dictyostelium gene encoding a protein homologous to mammalian ras protein. *Cell,* 39**,** 141-8.

RIRIE, K. M., RASMUSSEN, R. P. & WITTWER, C. T. 1997. Product differentiation by analysis of DNA melting curves during the polymerase chain reaction. *Anal Biochem,* 245**,** 154-60.

RITT, D. A., MONSON, D. M., SPECHT, S. I. & MORRISON, D. K. 2010. Impact of feedback phosphorylation and Raf heterodimerization on normal and mutant B-Raf signaling. *Mol Cell Biol,* 30**,** 806-19.

ROBERTS, A., ALLANSON, J., JADICO, S. K., KAVAMURA, M. I., NOONAN, J., OPITZ, J. M., YOUNG, T. & NERI, G. 2006a. The cardiofaciocutaneous syndrome. *J Med Genet,* 43**,** 833-42.

ROBERTS, A. E., ARAKI, T., SWANSON, K. D., MONTGOMERY, K. T., SCHIRIPO, T. A., JOSHI, V. A., LI, L., YASSIN, Y., TAMBURINO, A. M., NEEL, B. G. & KUCHERLAPATI, R. S. 2007. Germline gain-of-function mutations in SOS1 cause Noonan syndrome. *Nat Genet,* 39**,** 70-4.

ROBERTS, M. L., DROSOPOULOS, K. G., VASILEIOU, I., STRICKER, M., TAOUFIK, E., MAERCKER, C., GUIALIS, A., ALEXIS, M. N. & PINTZAS, A. 2006b. Microarray analysis of the differential transformation mediated by Kirsten and Harvey Ras oncogenes in a human colorectal adenocarcinoma cell line. *Int J Cancer,* 118**,** 616-27.

ROBERTSON, E. J. 1987. Embryo-derived stem cell lines. *In:* ROBERTSON, E. J. (ed.) *Teratocarcinomas and Embryonic Stem Cells: A Practical Approach.* Oxford: IRL Press.

ROCKS, O., PEYKER, A., KAHMS, M., VERVEER, P. J., KOERNER, C., LUMBIERRES, M., KUHLMANN, J., WALDMANN, H., WITTINGHOFER, A. & BASTIAENS, P. I. 2005. An acylation cycle regulates localization and activity of palmitoylated Ras isoforms. *Science,* 307**,** 1746-52.

RODRIGUEZ-VICIANA, P., WARNE, P. H., DHAND, R., VANHAESEBROECK, B., GOUT, I., FRY, M. J., WATERFIELD, M. D. & DOWNWARD, J. 1994. Phosphatidylinositol-3-OH kinase as a direct target of Ras. *Nature,* 370**,** 527-32.

RODRIGUEZ-VICIANA, P., WARNE, P. H., VANHAESEBROECK, B., WATERFIELD, M. D. & DOWNWARD, J. 1996. Activation of phosphoinositide 3-kinase by interaction with Ras and by point mutation. *EMBO J,* 15**,** 2442-51.

ROEPSTORFF, K., GRANDAL, M. V., HENRIKSEN, L., KNUDSEN, S. L., LERDRUP, M., GROVDAL, L., WILLUMSEN, B. M. & VAN DEURS, B. 2009. Differential effects of EGFR ligands on endocytic sorting of the receptor. *Traffic,* 10**,** 1115-27.

ROJAS, A. M., FUENTES, G., RAUSELL, A. & VALENCIA, A. 2012. The Ras protein superfamily: evolutionary tree and role of conserved amino acids. *J Cell Biol,* 196**,** 189-201.

ROSSE, C., HATZOGLOU, A., PARRINI, M. C., WHITE, M. A., CHAVRIER, P. & CAMONIS, J. 2006. RalB mobilizes the exocyst to drive cell migration. *Mol Cell Biol,* 26**,** 727-34.

ROY, S., PLOWMAN, S., ROTBLAT, B., PRIOR, I. A., MUNCKE, C., GRAINGER, S., PARTON, R. G., HENIS, Y. I., KLOOG, Y. & HANCOCK, J. F. 2005. Individual palmitoyl residues serve distinct roles in H-ras trafficking, microlocalization, and signaling. *Mol Cell Biol,* 25**,** 6722-33.

ROY, S., WYSE, B. & HANCOCK, J. F. 2002. H-Ras signaling and K-Ras signaling are differentially dependent on endocytosis. *Mol Cell Biol,* 22**,** 5128-40.

ROZAKIS-ADCOCK, M., FERNLEY, R., WADE, J., PAWSON, T. & BOWTELL, D. 1993. The SH2 and SH3 domains of mammalian Grb2 couple the EGF receptor to the Ras activator mSos1. *Nature,* 363**,** 83-5.

RUPPEN-CANAS, I., LOPEZ-CASAS, P. P., GARCIA, F., XIMENEZ-EMBUN, P., MUNOZ, M., MORELLI, M. P., REAL, F. X., SERNA, A., HIDALGO, M. & ASHMAN, K. 2012. An improved quantitative mass spectrometry analysis of tumor specific mutant proteins at high sensitivity. *Proteomics,* 12**,** 1319-27.

RYCHLIK, W., SPENCER, W. J. & RHOADS, R. E. 1990. Optimization of the annealing temperature for DNA amplification in vitro. *Nucleic Acids Res,* 18**,** 6409-12.

SAEGUSA, M. & OKAYASU, I. 2001. Frequent nuclear beta-catenin accumulation and associated mutations in endometrioid-type endometrial and ovarian carcinomas with squamous differentiation. *J Pathol,* 194**,** 59-67.

SAIKI, R. K., GELFAND, D. H., STOFFEL, S., SCHARF, S. J., HIGUCHI, R., HORN, G. T., MULLIS, K. B. & ERLICH, H. A. 1988. Primer-directed enzymatic amplification of DNA with a thermostable DNA polymerase. *Science,* 239**,** 487-91.

SALAMAT, M., MIOSGE, N. & HERKEN, R. 1995. Development of Reichert's membrane in the early mouse embryo. *Anat Embryol (Berl),* 192**,** 275-81.

SAMID, D., SCHAFF, Z., CHANG, E. H. & FRIEDMAN, R. M. 1985. Interferon-induced modulation of human ras oncogene expression. *Prog Clin Biol Res,* 192**,** 265-8.

SANTOS, E., MARTIN-ZANCA, D., REDDY, E. P., PIEROTTI, M. A., DELLA PORTA, G. & BARBACID, M. 1984. Malignant activation of a K-ras oncogene in lung carcinoma but not in normal tissue of the same patient. *Science,* 223**,** 661-4.

SANTOS, E., TRONICK, S. R., AARONSON, S. A., PULCIANI, S. & BARBACID, M. 1982. T24 human bladder carcinoma oncogene is an activated form of

the normal human homologue of BALB- and Harvey-MSV transforming genes. *Nature,* 298**,** 343-7.

SARASTE, M., SIBBALD, P. R. & WITTINGHOFER, A. 1990. The P-loop--a common motif in ATP- and GTP-binding proteins. *Trends Biochem Sci,* 15**,** 430-4.

SARKISIAN, C. J., KEISTER, B. A., STAIRS, D. B., BOXER, R. B., MOODY, S. E. & CHODOSH, L. A. 2007. Dose-dependent oncogene-induced senescence in vivo and its evasion during mammary tumorigenesis. *Nat Cell Biol,* 9**,** 493-505.

SATOH, T., ENDO, M., NAKAFUKU, M., AKIYAMA, T., YAMAMOTO, T. & KAZIRO, Y. 1990a. Accumulation of p21ras.GTP in response to stimulation with epidermal growth factor and oncogene products with tyrosine kinase activity. *Proc Natl Acad Sci U S A,* 87**,** 7926-9.

SATOH, T., ENDO, M., NAKAFUKU, M., NAKAMURA, S. & KAZIRO, Y. 1990b. Platelet-derived growth factor stimulates formation of active p21ras.GTP complex in Swiss mouse 3T3 cells. *Proc Natl Acad Sci U S A,* 87**,** 5993-7.

SAVIC, D. J. & KANAZIR, D. T. 1972. The effect of a histidine operator-constitutive mutation on UV-induced mutability within the histidine operon of Salmonella typhimurium. *Mol Gen Genet,* 118**,** 45-50.

SAVOLAINEN, S. M., FOLEY, J. F. & ELMORE, S. A. 2009. Histology atlas of the developing mouse heart with emphasis on E11.5 to E18.5. *Toxicol Pathol,* 37**,** 395-414.

SCHATTEN, G., SMITH, J., NAVARA, C., PARK, J. H. & PEDERSEN, R. 2005. Culture of human embryonic stem cells. *Nat Methods,* 2**,** 455-63.

SCHEID, M. P. & WOODGETT, J. R. 2001. Phosphatidylinositol 3' kinase signaling in mammary tumorigenesis. *J Mammary Gland Biol Neoplasia,* 6**,** 83-99.

SCHLAEPFER, D. D., HANKS, S. K., HUNTER, T. & VAN DER GEER, P. 1994. Integrin-mediated signal transduction linked to Ras pathway by GRB2 binding to focal adhesion kinase. *Nature,* 372**,** 786-91.

SCHLICHTING, I., ALMO, S. C., RAPP, G., WILSON, K., PETRATOS, K., LENTFER, A., WITTINGHOFER, A., KABSCH, W., PAI, E. F., PETSKO, G. A. & ET AL. 1990. Time-resolved X-ray crystallographic study of the conformational change in Ha-Ras p21 protein on GTP hydrolysis. *Nature,* 345**,** 309-15.

SCHMITTGEN, T. D., ZAKRAJSEK, B. A., MILLS, A. G., GORN, V., SINGER, M. J. & REED, M. W. 2000. Quantitative reverse transcription-polymerase chain reaction to study mRNA decay: comparison of endpoint and real-time methods. *Anal Biochem,* 285**,** 194-204.

SCHUBBERT, S., ZENKER, M., ROWE, S. L., BOLL, S., KLEIN, C., BOLLAG, G., VAN DER BURGT, I., MUSANTE, L., KALSCHEUER, V., WEHNER, L. E., NGUYEN, H., WEST, B., ZHANG, K. Y., SISTERMANS, E., RAUCH, A., NIEMEYER, C. M., SHANNON, K. & KRATZ, C. P. 2006. Germline KRAS mutations cause Noonan syndrome. *Nat Genet,* 38**,** 331-6.

SCHWANHAUSSER, B., BUSSE, D., LI, N., DITTMAR, G., SCHUCHHARDT, J., WOLF, J., CHEN, W. & SELBACH, M. 2011. Global quantification of mammalian gene expression control. *Nature,* 473**,** 337-42.

SCOLNICK, E. M., PAPAGEORGE, A. G. & SHIH, T. Y. 1979. Guanine nucleotide-binding activity as an assay for src protein of rat-derived murine sarcoma viruses. *Proc Natl Acad Sci U S A,* 76**,** 5355-9.

SCOLNICK, E. M. & PARKS, W. P. 1974. Harvey sarcoma virus: a second murine type C sarcoma virus with rat genetic information. *J Virol,* 13**,** 1211-9.

SCOLNICK, E. M., RANDS, E., WILLIAMS, D. & PARKS, W. P. 1973. Studies on the nucleic acid sequences of Kirsten sarcoma virus: a model for formation of a mammalian RNA-containing sarcoma virus. *J Virol,* 12**,** 458-63.

SEEBURG, P. H., COLBY, W. W., CAPON, D. J., GOEDDEL, D. V. & LEVINSON, A. D. 1984. Biological properties of human c-Ha-ras1 genes mutated at codon 12. *Nature,* 312**,** 71-5.

SEKULIC, A., HUDSON, C. C., HOMME, J. L., YIN, P., OTTERNESS, D. M., KARNITZ, L. M. & ABRAHAM, R. T. 2000. A direct linkage between the phosphoinositide 3-kinase-AKT signaling pathway and the mammalian target of rapamycin in mitogen-stimulated and transformed cells. *Cancer Res,* 60**,** 3504-13.

SERRANO, M., LIN, A. W., MCCURRACH, M. E., BEACH, D. & LOWE, S. W. 1997. Oncogenic ras provokes premature cell senescence associated with accumulation of p53 and p16INK4a. *Cell,* 88**,** 593-602.

SHIH, T. Y., WEEKS, M. O., YOUNG, H. A. & SCHOLNICK, E. M. 1979. Identification of a sarcoma virus-coded phosphoprotein in nonproducer cells transformed by Kirsten or Harvey murine sarcoma virus. *Virology,* 96**,** 64-79.

SHIMA, F., IJIRI, Y., MURAOKA, S., LIAO, J., YE, M., ARAKI, M., MATSUMOTO, K., YAMAMOTO, N., SUGIMOTO, T., YOSHIKAWA, Y., KUMASAKA, T., YAMAMOTO, M., TAMURA, A. & KATAOKA, T. 2010. Structural basis for conformational dynamics of GTP-bound Ras protein. *J Biol Chem,* 285**,** 22696-705.

SHIMIZU, K., BIRNBAUM, D., RULEY, M. A., FASANO, O., SUARD, Y., EDLUND, L., TAPAROWSKY, E., GOLDFARB, M. & WIGLER, M. 1983. Structure of the

Ki-ras gene of the human lung carcinoma cell line Calu-1. *Nature,* 304**,** 497-500.

SHIRASAWA, S., FURUSE, M., YOKOYAMA, N. & SASAZUKI, T. 1993. Altered growth of human colon cancer cell lines disrupted at activated Ki-ras. *Science,* 260**,** 85-8.

SHYAMSUNDAR, R., KIM, Y. H., HIGGINS, J. P., MONTGOMERY, K., JORDEN, M., SETHURAMAN, A., VAN DE RIJN, M., BOTSTEIN, D., BROWN, P. O. & POLLACK, J. R. 2005. A DNA microarray survey of gene expression in normal human tissues. *Genome Biol,* 6**,** R22.

SIMON, M. A., DODSON, G. S. & RUBIN, G. M. 1993. An SH3-SH2-SH3 protein is required for p21Ras1 activation and binds to sevenless and Sos proteins in vitro. *Cell,* 73**,** 169-77.

SITHANANDAM, G., RAMAKRISHNA, G., DIWAN, B. A. & ANDERSON, L. M. 1998. Selective mutation of K-ras by N-ethylnitrosourea shifts from codon 12 to codon 61 during fetal mouse lung maturation. *Oncogene,* 17**,** 493-502.

SJOLANDER, A., YAMAMOTO, K., HUBER, B. E. & LAPETINA, E. G. 1991. Association of p21ras with phosphatidylinositol 3-kinase. *Proc Natl Acad Sci U S A,* 88**,** 7908-12.

SMITH, A. G. 2001. Embryo-derived stem cells: of mice and men. *Annu Rev Cell Dev Biol,* 17**,** 435-62.

SMYTH, N., VATANSEVER, H. S., MURRAY, P., MEYER, M., FRIE, C., PAULSSON, M. & EDGAR, D. 1999. Absence of basement membranes after targeting the LAMC1 gene results in embryonic lethality due to failure of endoderm differentiation. *J Cell Biol,* 144**,** 151-60.

SONG, C., SATOH, T., EDAMATSU, H., WU, D., TADANO, M., GAO, X. & KATAOKA, T. 2002. Differential roles of Ras and Rap1 in growth factor-dependent activation of phospholipase C epsilon. *Oncogene,* 21**,** 8105-13.

SPAARGAREN, M. & BISCHOFF, J. R. 1994. Identification of the guanine nucleotide dissociation stimulator for Ral as a putative effector molecule of R-ras, H-ras, K-ras, and Rap. *Proc Natl Acad Sci U S A,* 91**,** 12609-13.

STAVRIDIS, M. P. & SMITH, A. G. 2003. Neural differentiation of mouse embryonic stem cells. *Biochem Soc Trans,* 31**,** 45-9.

STOJKOVIC, P., LAKO, M., PRZYBORSKI, S., STEWART, R., ARMSTRONG, L., EVANS, J., ZHANG, X. & STOJKOVIC, M. 2005. Human-serum matrix supports undifferentiated growth of human embryonic stem cells. *Stem Cells,* 23**,** 895-902.

STURM, O. E., ORTON, R., GRINDLAY, J., BIRTWISTLE, M., VYSHEMIRSKY, V., GILBERT, D., CALDER, M., PITT, A., KHOLODENKO, B. & KOLCH, W. 2010. The mammalian MAPK/ERK pathway exhibits properties of a negative feedback amplifier. *Sci Signal,* 3**,** ra90.

SUDA, Y., SUZUKI, M., IKAWA, Y. & AIZAWA, S. 1987. Mouse embryonic stem cells exhibit indefinite proliferative potential. *J Cell Physiol,* 133**,** 197-201.

SUN, C., HOBOR, S., BERTOTTI, A., ZECCHIN, D., HUANG, S., GALIMI, F., COTTINO, F., PRAHALLAD, A., GRERNRUM, W., TZANI, A., SCHLICKER, A., WESSELS, L. F., SMIT, E. F., THUNNISSEN, E., HALONEN, P., LIEFTINK, C., BEIJERSBERGEN, R. L., DI NICOLANTONIO, F., BARDELLI, A., TRUSOLINO, L. & BERNARDS, R. 2014. Intrinsic resistance to MEK inhibition in KRAS mutant lung and colon cancer through transcriptional induction of ERBB3. *Cell Rep,* 7**,** 86-93.

SUZUKI, T., HIGGINS, P. J. & CRAWFORD, D. R. 2000. Control selection for RNA quantitation. *Biotechniques,* 29**,** 332-7.

SVEJSTRUP, J. Q. 2002. Mechanisms of transcription-coupled DNA repair. *Nat Rev Mol Cell Biol,* 3**,** 21-9.

SWEET, R. W., YOKOYAMA, S., KAMATA, T., FERAMISCO, J. R., ROSENBERG, M. & GROSS, M. 1984. The product of ras is a GTPase and the T24 oncogenic mutant is deficient in this activity. *Nature,* 311**,** 273-5.

SZEBERENYI, J., CAI, H. & COOPER, G. M. 1990. Effect of a dominant inhibitory Ha-ras mutation on neuronal differentiation of PC12 cells. *Mol Cell Biol,* 10**,** 5324-32.

TABIN, C. J., BRADLEY, S. M., BARGMANN, C. I., WEINBERG, R. A., PAPAGEORGE, A. G., SCOLNICK, E. M., DHAR, R., LOWY, D. R. & CHANG, E. H. 1982. Mechanism of activation of a human oncogene. *Nature,* 300**,** 143-9.

TAKAHASHI, K., MITSUI, K. & YAMANAKA, S. 2003. Role of ERas in promoting tumour-like properties in mouse embryonic stem cells. *Nature,* 423**,** 541-5.

TAM, P. P. 1981. The control of somitogenesis in mouse embryos. *J Embryol Exp Morphol,* 65 Suppl**,** 103-28.

TAM, P. P. & BEHRINGER, R. R. 1997. Mouse gastrulation: the formation of a mammalian body plan. *Mech Dev,* 68**,** 3-25.

TANG, F., BARBACIORU, C., NORDMAN, E., BAO, S., LEE, C., WANG, X., TUCH, B. B., HEARD, E., LAO, K. & SURANI, M. A. 2011. Deterministic and stochastic allele specific gene expression in single mouse blastomeres. *PLoS One,* 6**,** e21208.

TAPAROWSKY, E., SHIMIZU, K., GOLDFARB, M. & WIGLER, M. 1983. Structure and activation of the human N-ras gene. *Cell,* 34**,** 581-6.

TAPAROWSKY, E., SUARD, Y., FASANO, O., SHIMIZU, K., GOLDFARB, M. & WIGLER, M. 1982. Activation of the T24 bladder carcinoma transforming gene is linked to a single amino acid change. *Nature,* 300**,** 762-5.

TARTAGLIA, M. & GELB, B. D. 2010. Disorders of dysregulated signal traffic through the RAS-MAPK pathway: phenotypic spectrum and molecular mechanisms. *Ann N Y Acad Sci,* 1214**,** 99-121.

TENBAUM, S. P., ORDONEZ-MORAN, P., PUIG, I., CHICOTE, I., ARQUES, O., LANDOLFI, S., FERNANDEZ, Y., HERANCE, J. R., GISPERT, J. D., MENDIZABAL, L., AGUILAR, S., RAMON Y CAJAL, S., SCHWARTZ, S., JR., VIVANCOS, A., ESPIN, E., ROJAS, S., BASELGA, J., TABERNERO, J., MUNOZ, A. & PALMER, H. G. 2012. beta-catenin confers resistance to PI3K and AKT inhibitors and subverts FOXO3a to promote metastasis in colon cancer. *Nat Med,* 18**,** 892-901.

TESAR, P. J., CHENOWETH, J. G., BROOK, F. A., DAVIES, T. J., EVANS, E. P., MACK, D. L., GARDNER, R. L. & MCKAY, R. D. 2007. New cell lines from mouse epiblast share defining features with human embryonic stem cells. *Nature,* 448**,** 196-9.

THEILER, K. 1989. *The House Mouse. Atlas of Embryonic Development. ,* New York Berlin Heidelberg London Paris Tokyo, Springer-Verlag.

THELLIN, O., ZORZI, W., LAKAYE, B., DE BORMAN, B., COUMANS, B., HENNEN, G., GRISAR, T., IGOUT, A. & HEINEN, E. 1999. Housekeeping genes as internal standards: use and limits. *J Biotechnol,* 75**,** 291-5.

THEVATHASAN, J. V., TAN, E., ZHENG, H., LIN, Y. C., LI, Y., INOUE, T. & FIVAZ, M. 2013. The small GTPase HRas shapes local PI3K signals through positive feedback and regulates persistent membrane extension in migrating fibroblasts. *Mol Biol Cell,* 24**,** 2228-37.

THIERRY-MIEG, D. & THIERRY-MIEG, J. 2006. AceView: a comprehensive cDNA-supported gene and transcripts annotation. *Genome Biol,* 7 Suppl 1**,** S12 1-14.

THOMSON, J. A., ITSKOVITZ-ELDOR, J., SHAPIRO, S. S., WAKNITZ, M. A., SWIERGIEL, J. J., MARSHALL, V. S. & JONES, J. M. 1998. Embryonic stem cell lines derived from human blastocysts. *Science,* 282**,** 1145-7.

TIDYMAN, W. E. & RAUEN, K. A. 2008. Noonan, Costello and cardio-facio-cutaneous syndromes: dysregulation of the Ras-MAPK pathway. *Expert Rev Mol Med,* 10**,** e37.

TIDYMAN, W. E. & RAUEN, K. A. 2009. The RASopathies: developmental syndromes of Ras/MAPK pathway dysregulation. *Curr Opin Genet Dev,* 19**,** 230-6.

TO, M. D., WONG, C. E., KARNEZIS, A. N., DEL ROSARIO, R., DI LAURO, R. & BALMAIN, A. 2008. Kras regulatory elements and exon 4A determine mutation specificity in lung cancer. *Nat Genet,* 40**,** 1240-4.

TOETTCHER, J. E., WEINER, O. D. & LIM, W. A. 2013. Using optogenetics to interrogate the dynamic control of signal transmission by the Ras/Erk module. *Cell,* 155**,** 1422-34.

TOMMASI, S., DAMMANN, R., JIN, S. G., ZHANG, X. F., AVRUCH, J. & PFEIFER, G. P. 2002. RASSF3 and NORE1: identification and cloning of two human homologues of the putative tumor suppressor gene RASSF1. *Oncogene,* 21**,** 2713-20.

TONG, L. A., DE VOS, A. M., MILBURN, M. V., JANCARIK, J., NOGUCHI, S., NISHIMURA, S., MIURA, K., OHTSUKA, E. & KIM, S. H. 1989. Structural differences between a ras oncogene protein and the normal protein. *Nature,* 337**,** 90-3.

TRAHEY, M. & MCCORMICK, F. 1987. A cytoplasmic protein stimulates normal N-ras p21 GTPase, but does not affect oncogenic mutants. *Science,* 238**,** 542-5.

TRAVERSE, S., GOMEZ, N., PATERSON, H., MARSHALL, C. & COHEN, P. 1992. Sustained activation of the mitogen-activated protein (MAP) kinase cascade may be required for differentiation of PC12 cells. Comparison of the effects of nerve growth factor and epidermal growth factor. *Biochem J,* 288 (Pt 2)**,** 351-5.

TUCKER, K. L., MEYER, M. & BARDE, Y. A. 2001. Neurotrophins are required for nerve growth during development. *Nat Neurosci,* 4**,** 29-37.

TURKE, A. B., SONG, Y., COSTA, C., COOK, R., ARTEAGA, C. L., ASARA, J. M. & ENGELMAN, J. A. 2012. MEK inhibition leads to PI3K/AKT activation by relieving a negative feedback on ERBB receptors. *Cancer Res,* 72**,** 3228-37.

TUVESON, D. A., SHAW, A. T., WILLIS, N. A., SILVER, D. P., JACKSON, E. L., CHANG, S., MERCER, K. L., GROCHOW, R., HOCK, H., CROWLEY, D., HINGORANI, S. R., ZAKS, T., KING, C., JACOBETZ, M. A., WANG, L., BRONSON, R. T., ORKIN, S. H., DEPINHO, R. A. & JACKS, T. 2004. Endogenous oncogenic K-ras(G12D) stimulates proliferation and widespread neoplastic and developmental defects. *Cancer Cell,* 5**,** 375-87.

TUVESON, D. A., ZHU, L., GOPINATHAN, A., WILLIS, N. A., KACHATRIAN, L., GROCHOW, R., PIN, C. L., MITIN, N. Y., TAPAROWSKY, E. J., GIMOTTY, P.

A., HRUBAN, R. H., JACKS, T. & KONIECZNY, S. F. 2006. Mist1-KrasG12D knock-in mice develop mixed differentiation metastatic exocrine pancreatic carcinoma and hepatocellular carcinoma. *Cancer Res,* 66**,** 242-7.

UMANOFF, H., EDELMANN, W., PELLICER, A. & KUCHERLAPATI, R. 1995. The murine N-ras gene is not essential for growth and development. *Proc Natl Acad Sci U S A,* 92**,** 1709-13.

URANO, T., EMKEY, R. & FEIG, L. A. 1996. Ral-GTPases mediate a distinct downstream signaling pathway from Ras that facilitates cellular transformation. *EMBO J,* 15**,** 810-6.

VAN AELST, L., BARR, M., MARCUS, S., POLVERINO, A. & WIGLER, M. 1993. Complex formation between RAS and RAF and other protein kinases. *Proc Natl Acad Sci U S A,* 90**,** 6213-7.

VAN SCHAEYBROECK, S., KALIMUTHO, M., DUNNE, P. D., CARSON, R., ALLEN, W., JITHESH, P. V., REDMOND, K. L., SASAZUKI, T., SHIRASAWA, S., BLAYNEY, J., MICHIELI, P., FENNING, C., LENZ, H. J., LAWLER, M., LONGLEY, D. B. & JOHNSTON, P. G. 2014. ADAM17-dependent c-MET-STAT3 signaling mediates resistance to MEK inhibitors in KRAS mutant colorectal cancer. *Cell Rep,* 7**,** 1940-55.

VANDESOMPELE, J., DE PRETER, K., PATTYN, F., POPPE, B., VAN ROY, N., DE PAEPE, A. & SPELEMAN, F. 2002. Accurate normalization of real-time quantitative RT-PCR data by geometric averaging of multiple internal control genes. *Genome Biol,* 3**,** RESEARCH0034.

VANGUILDER, H. D., VRANA, K. E. & FREEMAN, W. M. 2008. Twenty-five years of quantitative PCR for gene expression analysis. *Biotechniques,* 44**,** 619-26.

VARTANIAN, S., BENTLEY, C., BRAUER, M. J., LI, L., SHIRASAWA, S., SASAZUKI, T., KIM, J. S., HAVERTY, P., STAWISKI, E., MODRUSAN, Z., WALDMAN, T. & STOKOE, D. 2013. Identification of mutant K-Ras-dependent phenotypes using a panel of isogenic cell lines. *J Biol Chem,* 288**,** 2403-13.

VASILEVA, A. & JESSBERGER, R. 2005. Precise hit: adeno-associated virus in gene targeting. *Nat Rev Microbiol,* 3**,** 837-47.

VETTER, I. R. & WITTINGHOFER, A. 2001. The guanine nucleotide-binding switch in three dimensions. *Science,* 294**,** 1299-304.

VILLALONGA, P., LOPEZ-ALCALA, C., BOSCH, M., CHILOECHES, A., ROCAMORA, N., GIL, J., MARAIS, R., MARSHALL, C. J., BACHS, O. & AGELL, N. 2001. Calmodulin binds to K-Ras, but not to H- or N-Ras, and modulates its downstream signaling. *Mol Cell Biol,* 21**,** 7345-54.

VITZTHUM, F., GEIGER, G., BISSWANGER, H., BRUNNER, H. & BERNHAGEN, J. 1999. A quantitative fluorescence-based microplate assay for the determination of double-stranded DNA using SYBR Green I and a standard ultraviolet transilluminator gel imaging system. *Anal Biochem,* 276**,** 59-64.

VOICE, J. K., KLEMKE, R. L., LE, A. & JACKSON, J. H. 1999. Four human ras homologs differ in their abilities to activate Raf-1, induce transformation, and stimulate cell motility. *J Biol Chem,* 274**,** 17164-70.

VOJTEK, A. B., HOLLENBERG, S. M. & COOPER, J. A. 1993. Mammalian Ras interacts directly with the serine/threonine kinase Raf. *Cell,* 74**,** 205-14.

VON AHSEN, N., WITTWER, C. T. & SCHUTZ, E. 2001. Oligonucleotide melting temperatures under PCR conditions: nearest-neighbor corrections for Mg(2+), deoxynucleotide triphosphate, and dimethyl sulfoxide concentrations with comparison to alternative empirical formulas. *Clin Chem,* 47**,** 1956-61.

VOS, M. D., ELLIS, C. A., BELL, A., BIRRER, M. J. & CLARK, G. J. 2000. Ras uses the novel tumor suppressor RASSF1 as an effector to mediate apoptosis. *J Biol Chem,* 275**,** 35669-72.

VOS, M. D., ELLIS, C. A., ELAM, C., ULKU, A. S., TAYLOR, B. J. & CLARK, G. J. 2003a. RASSF2 is a novel K-Ras-specific effector and potential tumor suppressor. *J Biol Chem,* 278**,** 28045-51.

VOS, M. D., MARTINEZ, A., ELLIS, C. A., VALLECORSA, T. & CLARK, G. J. 2003b. The pro-apoptotic Ras effector Nore1 may serve as a Ras-regulated tumor suppressor in the lung. *J Biol Chem,* 278**,** 21938-43.

WALSH, A. B. & BAR-SAGI, D. 2001. Differential activation of the Rac pathway by Ha-Ras and K-Ras. *J Biol Chem,* 276**,** 15609-15.

WANG, Q., CHAERKADY, R., WU, J., HWANG, H. J., PAPADOPOULOS, N., KOPELOVICH, L., MAITRA, A., MATTHAEI, H., ESHLEMAN, J. R., HRUBAN, R. H., KINZLER, K. W., PANDEY, A. & VOGELSTEIN, B. 2011. Mutant proteins as cancer-specific biomarkers. *Proc Natl Acad Sci U S A,* 108**,** 2444-9.

WANG, X. & SEED, B. 2003. A PCR primer bank for quantitative gene expression analysis. *Nucleic Acids Res,* 31**,** e154.

WANG, Y., LIU, Y., LU, J., ZHANG, P., WANG, Y., XU, Y., WANG, Z., MAO, J. H. & WEI, G. 2013. Rapamycin inhibits FBXW7 loss-induced epithelial-mesenchymal transition and cancer stem cell-like characteristics in colorectal cancer cells. *Biochem Biophys Res Commun,* 434**,** 352-6.

WANG, Y., YOU, M. & WANG, Y. 2001. Alternative splicing of the K-ras gene in mouse tissues and cell lines. *Exp Lung Res,* 27**,** 255-67.

WANG, Z., INUZUKA, H., ZHONG, J., WAN, L., FUKUSHIMA, H., SARKAR, F. H. & WEI, W. 2012. Tumor suppressor functions of FBW7 in cancer development and progression. *FEBS Lett,* 586**,** 1409-18.

WARBURTON, D. 2008. Developmental biology: order in the lung. *Nature,* 453**,** 733-5.

WARE, J. H., ZHOU, Z., GUAN, J., KENNEDY, A. R. & KOPELOVICH, L. 2007. Establishment of human cancer cell clones with different characteristics: a model for screening chemopreventive agents. *Anticancer Res,* 27**,** 1-16.

WARNE, P. H., VICIANA, P. R. & DOWNWARD, J. 1993. Direct interaction of Ras and the amino-terminal region of Raf-1 in vitro. *Nature,* 364**,** 352-5.

WELLS, J. M. & MELTON, D. A. 1999. Vertebrate endoderm development. *Annu Rev Cell Dev Biol,* 15**,** 393-410.

WILHELM, J. & PINGOUD, A. 2003. Real-time polymerase chain reaction. *Chembiochem,* 4**,** 1120-8.

WILHELM, S. M., CARTER, C., TANG, L., WILKIE, D., MCNABOLA, A., RONG, H., CHEN, C., ZHANG, X., VINCENT, P., MCHUGH, M., CAO, Y., SHUJATH, J., GAWLAK, S., EVELEIGH, D., ROWLEY, B., LIU, L., ADNANE, L., LYNCH, M., AUCLAIR, D., TAYLOR, I., GEDRICH, R., VOZNESENSKY, A., RIEDL, B., POST, L. E., BOLLAG, G. & TRAIL, P. A. 2004. BAY 43-9006 exhibits broad spectrum oral antitumor activity and targets the RAF/MEK/ERK pathway and receptor tyrosine kinases involved in tumor progression and angiogenesis. *Cancer Res,* 64**,** 7099-109.

WILLEMS, E., MATEIZEL, I., KEMP, C., CAUFFMAN, G., SERMON, K. & LEYNS, L. 2006. Selection of reference genes in mouse embryos and in differentiating human and mouse ES cells. *Int J Dev Biol,* 50**,** 627-35.

WILLIAMS, J. F. 1989. Optimization strategies for the polymerase chain reaction. *Biotechniques,* 7**,** 762-9.

WILLIAMS, R. L., HILTON, D. J., PEASE, S., WILLSON, T. A., STEWART, C. L., GEARING, D. P., WAGNER, E. F., METCALF, D., NICOLA, N. A. & GOUGH, N. M. 1988. Myeloid leukaemia inhibitory factor maintains the developmental potential of embryonic stem cells. *Nature,* 336**,** 684-7.

WILLINGHAM, M. C., PASTAN, I., SHIH, T. Y. & SCOLNICK, E. M. 1980. Localization of the src gene product of the Harvey strain of MSV to plasma membrane of transformed cells by electron microscopic immunocytochemistry. *Cell,* 19**,** 1005-14.

WINDER, T., MUNDLEIN, A., RHOMBERG, S., DIRSCHMID, K., HARTMANN, B. L., KNAUER, M., DREXEL, H., WENZL, E., DE VRIES, A. & LANG, A. 2009. Different types of K-Ras mutations are conversely associated with overall survival in patients with colorectal cancer. *Oncol Rep,* 21**,** 1283-7.

WITTINGHOFER, A. & HERRMANN, C. 1995. Ras-effector interactions, the problem of specificity. *FEBS Lett,* 369**,** 52-6.

WOLFMAN, J. C., PLANCHON, S. M., LIAO, J. & WOLFMAN, A. 2006. Structural and functional consequences of c-N-Ras constitutively associated with intact mitochondria. *Biochim Biophys Acta,* 1763**,** 1108-24.

WU, D., TADANO, M., EDAMATSU, H., MASAGO-TODA, M., YAMAWAKI-KATAOKA, Y., TERASHIMA, T., MIZOGUCHI, A., MINAMI, Y., SATOH, T. & KATAOKA, T. 2003. Neuronal lineage-specific induction of phospholipase Cepsilon expression in the developing mouse brain. *Eur J Neurosci,* 17**,** 1571-80.

WU, D. Y., UGOZZOLI, L., PAL, B. K., QIAN, J. & WALLACE, R. B. 1991. The effect of temperature and oligonucleotide primer length on the specificity and efficiency of amplification by the polymerase chain reaction. *DNA Cell Biol,* 10**,** 233-8.

WU, M., OBARA, Y., NOROTA, I., NAGASAWA, Y. & ISHII, K. 2014. Insulin suppresses IKs (KCNQ1/KCNE1) currents, which require beta-subunit KCNE1. *Pflugers Arch,* 466**,** 937-46.

XIONG, J. W., BATTAGLINO, R., LEAHY, A. & STUHLMANN, H. 1998. Large-scale screening for developmental genes in embryonic stem cells and embryoid bodies using retroviral entrapment vectors. *Dev Dyn,* 212**,** 181-97.

XU, C., ROSLER, E., JIANG, J., LEBKOWSKI, J. S., GOLD, J. D., O'SULLIVAN, C., DELAVAN-BOORSMA, K., MOK, M., BRONSTEIN, A. & CARPENTER, M. K. 2005. Basic fibroblast growth factor supports undifferentiated human embryonic stem cell growth without conditioned medium. *Stem Cells,* 23**,** 315-23.

YAMAUCHI, J., CHAN, J. R., MIYAMOTO, Y., TSUJIMOTO, G. & SHOOTER, E. M. 2005a. The neurotrophin-3 receptor TrkC directly phosphorylates and activates the nucleotide exchange factor Dbs to enhance Schwann cell migration. *Proc Natl Acad Sci U S A,* 102**,** 5198-203.

YAMAUCHI, J., MIYAMOTO, Y., TANOUE, A., SHOOTER, E. M. & CHAN, J. R. 2005b. Ras activation of a Rac1 exchange factor, Tiam1, mediates neurotrophin-3-induced Schwann cell migration. *Proc Natl Acad Sci U S A,* 102**,** 14889-94.

YAN, J., ROY, S., APOLLONI, A., LANE, A. & HANCOCK, J. F. 1998. Ras isoforms vary in their ability to activate Raf-1 and phosphoinositide 3-kinase. *J Biol Chem,* 273**,** 24052-6.

YARDEN, Y. & SCHLESSINGER, J. 1987a. Epidermal growth factor induces rapid, reversible aggregation of the purified epidermal growth factor receptor. *Biochemistry,* 26**,** 1443-51.

YARDEN, Y. & SCHLESSINGER, J. 1987b. Self-phosphorylation of epidermal growth factor receptor: evidence for a model of intermolecular allosteric activation. *Biochemistry,* 26**,** 1434-42.

YASHIRO, M., YASUDA, K., NISHII, T., KAIZAKI, R., SAWADA, T., OHIRA, M. & HIRAKAWA, K. 2009. Epigenetic regulation of the embryonic oncogene ERas in gastric cancer cells. *Int J Oncol,* 35**,** 997-1003.

YE, J., COULOURIS, G., ZARETSKAYA, I., CUTCUTACHE, I., ROZEN, S. & MADDEN, T. L. 2012. Primer-BLAST: a tool to design target-specific primers for polymerase chain reaction. *BMC Bioinformatics,* 13**,** 134.

YONEZAWA, K., ANDO, A., KABURAGI, Y., YAMAMOTO-HONDA, R., KITAMURA, T., HARA, K., NAKAFUKU, M., OKABAYASHI, Y., KADOWAKI, T., KAZIRO, Y. & ET AL. 1994. Signal transduction pathways from insulin receptors to Ras. Analysis by mutant insulin receptors. *J Biol Chem,* 269**,** 4634-40.

YOON, S. O., SHIN, S. & LIPSCOMB, E. A. 2006. A novel mechanism for integrin-mediated ras activation in breast carcinoma cells: the alpha6beta4 integrin regulates ErbB2 translation and transactivates epidermal growth factor receptor/ErbB2 signaling. *Cancer Res,* 66**,** 2732-9.

YOSHIDA-KOIDE, U., MATSUDA, T., SAIKAWA, K., NAKANUMA, Y., YOKOTA, T., ASASHIMA, M. & KOIDE, H. 2004. Involvement of Ras in extraembryonic endoderm differentiation of embryonic stem cells. *Biochem Biophys Res Commun,* 313**,** 475-81.

YUN, C. H., BOGGON, T. J., LI, Y., WOO, M. S., GREULICH, H., MEYERSON, M. & ECK, M. J. 2007. Structures of lung cancer-derived EGFR mutants and inhibitor complexes: mechanism of activation and insights into differential inhibitor sensitivity. *Cancer Cell,* 11**,** 217-27.

YUN, S., HONG, W. P., CHOI, J. H., YI, K. S., CHAE, S. K., RYU, S. H. & SUH, P. G. 2008. Phospholipase C-epsilon augments epidermal growth factor-dependent cell growth by inhibiting epidermal growth factor receptor down-regulation. *J Biol Chem,* 283**,** 341-9.

YUNXIA, Z., JUN, C., GUANSHAN, Z., YACHAO, L., XUEKE, Z. & JIN, L. 2010. Mutations in epidermal growth factor receptor and K-ras in Chinese patients with colorectal cancer. *BMC Med Genet,* 11**,** 34.

ZALZMAN, M., FALCO, G., SHAROVA, L. V., NISHIYAMA, A., THOMAS, M., LEE, S. L., STAGG, C. A., HOANG, H. G., YANG, H. T., INDIG, F. E., WERSTO, R. P. & KO, M. S. 2010. Zscan4 regulates telomere elongation and genomic stability in ES cells. *Nature,* 464**,** 858-63.

ZHANG, X., GUREASKO, J., SHEN, K., COLE, P. A. & KURIYAN, J. 2006. An allosteric mechanism for activation of the kinase domain of epidermal growth factor receptor. *Cell,* 125**,** 1137-49.

ZHANG, X. F., SETTLEMAN, J., KYRIAKIS, J. M., TAKEUCHI-SUZUKI, E., ELLEDGE, S. J., MARSHALL, M. S., BRUDER, J. T., RAPP, U. R. & AVRUCH, J. 1993. Normal and oncogenic p21ras proteins bind to the amino-terminal regulatory domain of c-Raf-1. *Nature,* 364**,** 308-13.

ZHU, K., HAMILTON, A. D. & SEBTI, S. M. 2003. Farnesyltransferase inhibitors as anticancer agents: current status. *Curr Opin Investig Drugs,* 4**,** 1428-35.

ZIPPER, H., BRUNNER, H., BERNHAGEN, J. & VITZTHUM, F. 2004. Investigations on DNA intercalation and surface binding by SYBR Green I, its structure determination and methodological implications. *Nucleic Acids Res,* 32**,** e103.

ZORN, A. M. 2008. Liver development. *StemBook.* Cambridge (MA).

ZWEIBAUM, A., TRIADOU, N., KEDINGER, M., AUGERON, C., ROBINE-LEON, S., PINTO, M., ROUSSET, M. & HAFFEN, K. 1983. Sucrase-isomaltase: a marker of foetal and malignant epithelial cells of the human colon. *Int J Cancer,* 32**,** 407-12.

Appendix

Name of construct:	pCR4-TOPO-mouseHRas cds+nc Mouse HRas coding sequences and 12 bp noncoding fragment
Origin of vector:	pCR4-TOPO
Origin of Insert:	Library: R1 Mouse embryonic stem cells cDNA; Primers: cmHRas F and R; Host: *DH10B TonA* (*E. coli*); Restriction sites: 5s: TA cloning, 3s: TA cloning
Vector size:	3956 bp
Insert size:	582 bp (BC119495 – HRas mRNA)
Date:	23/05/2012
Constructed by:	Anna Newlaczyl
Resistance:	ampicillin and kanamycin
Comments:	Dundee sequencing with M13 F and R primers

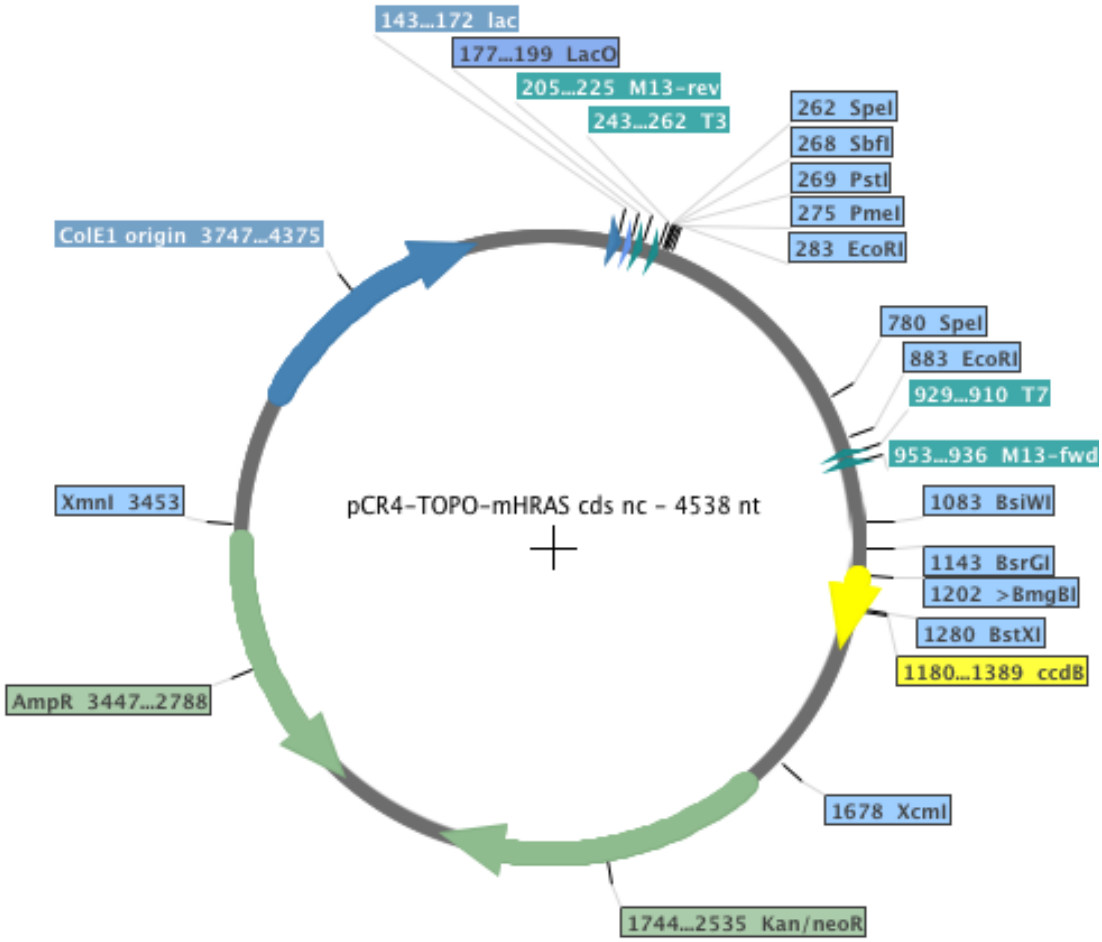

Fig. A3.1 pCR4-TOPO-mHRas plasmid. A schematic representation of pCR4-TOPO plasmid with the mouse HRas fragment insert with annotation and comments.

Name of construct:	pCR4-TOPO-mouseNRas cds+nc Mouse NRas coding sequences and noncoding fragment
Origin of vector:	pCR4-TOPO
Origin of Insert:	Library: R1 Mouse embryonic stem cells cDNA; Primers: cmNRas F and R; Host: *DH10B TonA* (*E. coli*); Restriction sites: 5s: TA cloning, 3s: TA cloning
Vector size:	3956bp
Insert size:	213 bp (NM_010937– NRas mRNA)
Date:	26/01/2012
Constructed by:	Anna Newlaczyl
Resistance:	ampicillin and kanamycin
Comments:	Dundee sequencing with M13 F and R primers

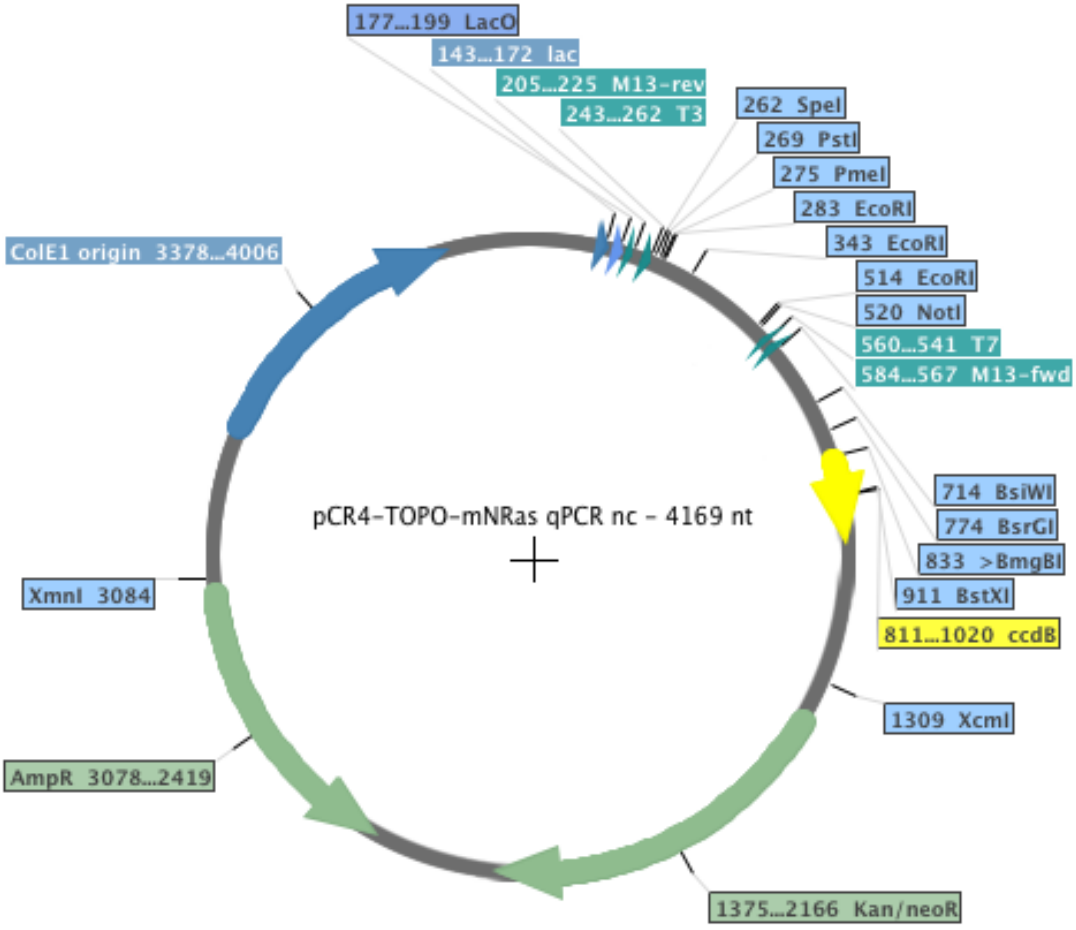

Fig. A3.2 pCR4-TOPO-mNRas plasmid. A schematic representation of pCR4-TOPO plasmid with the mouse NRas fragment insert with annotation and comments.

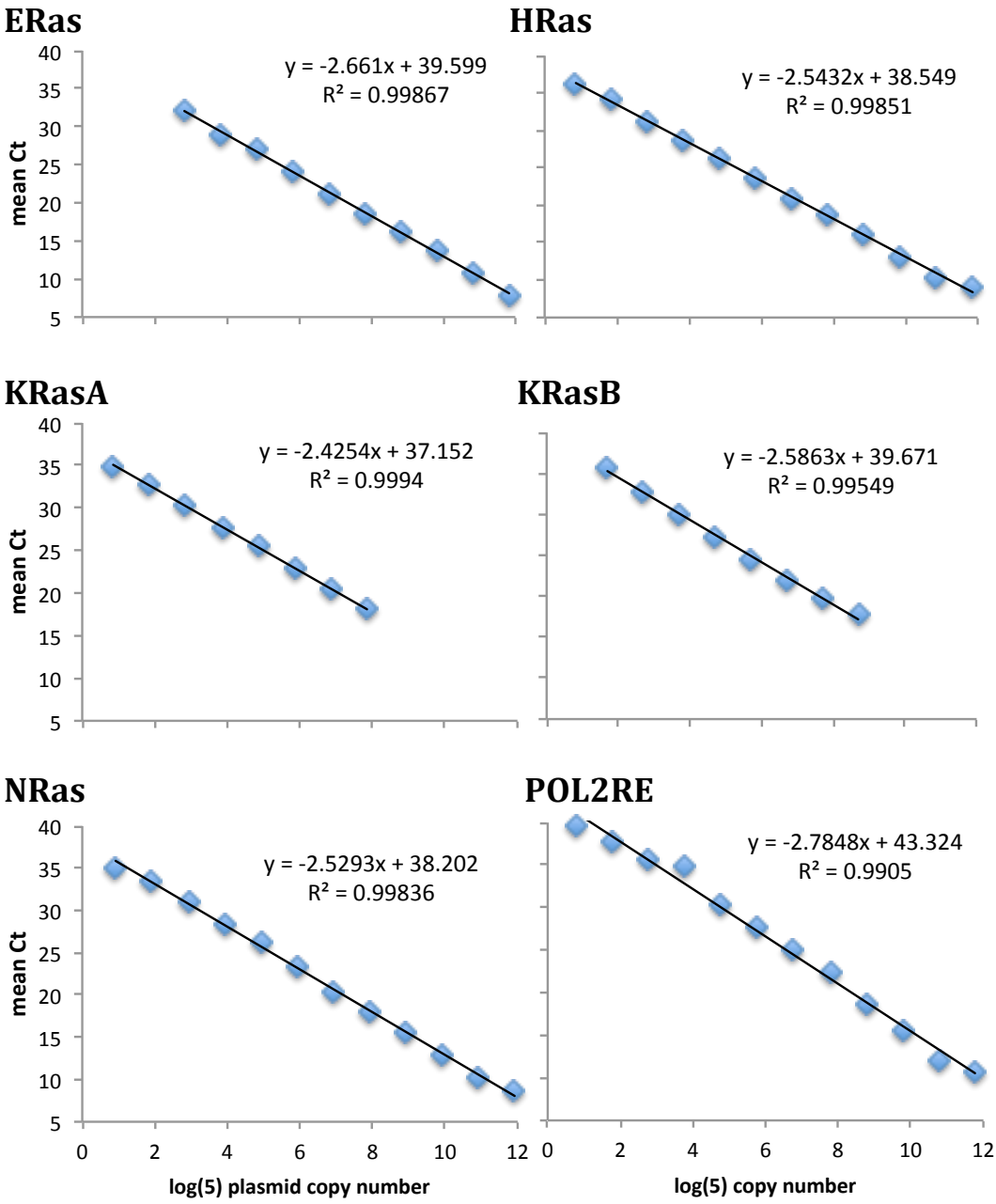

Plasmid	Standard curve equation	R^2	%E
ERas	-2.661x+39.599	0.99867	83.00
HRas	-2.5432x+38.549	0.99851	88.20
KRasA	-2.4254x+37.152	0.9994	94.07
KRasB	-2.5863x+39.671	0.99549	86.22
NRas	-2.5293+38.202	0.99836	88.85
POL2RE	-2.7848+43.324	0.9905	78.15

Fig. A4.1 Plasmid standard curves used in qRT-PCR for endoderm and mesoderm differentiation of mouse embryonic stem cells (ESCs). Graphs for standard curve equations and a summary table including coefficient of determination R^2 and calculated % efficiency (%E) used for data in Fig. 4.5-4.6.

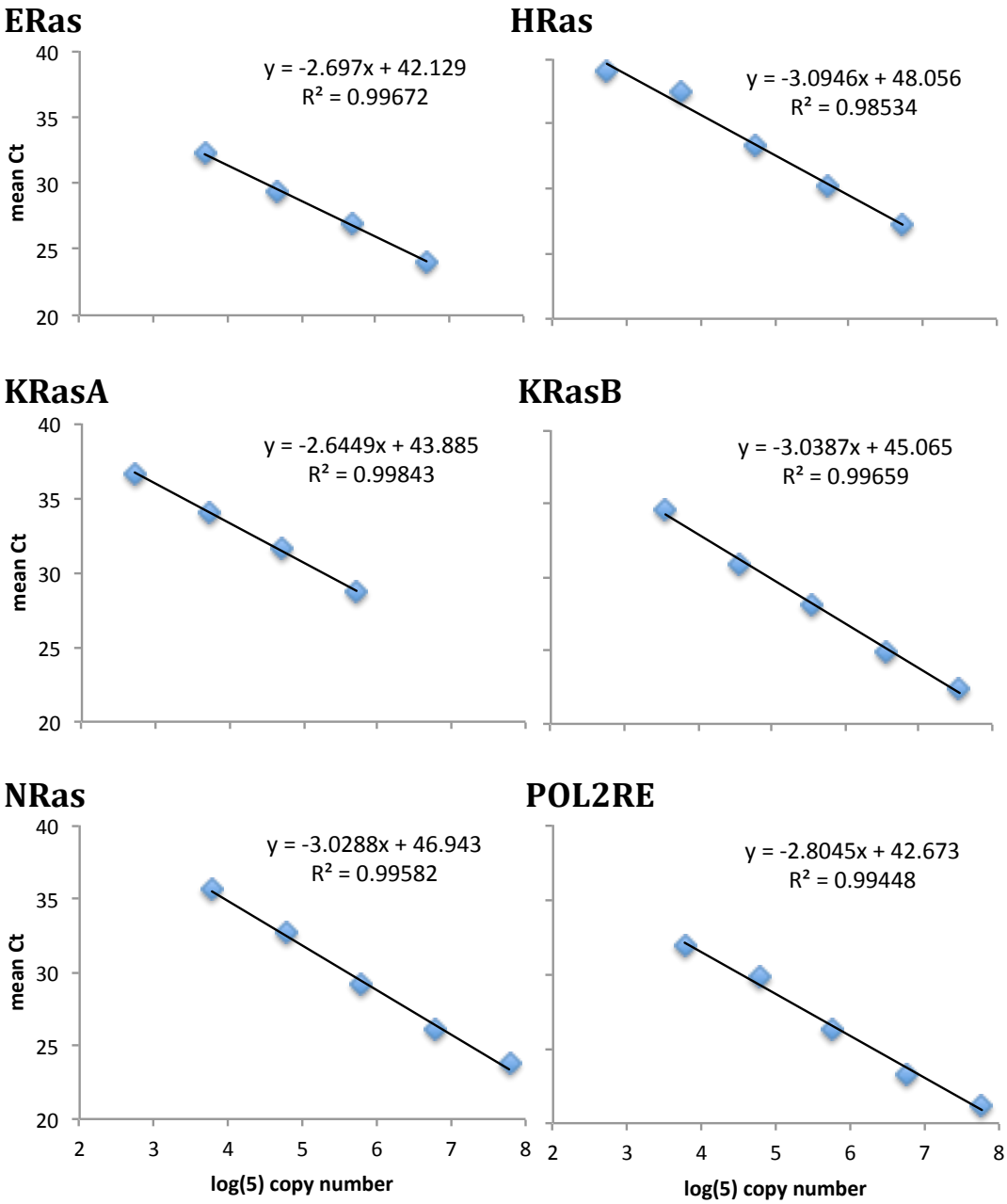

Plasmid	Standard curve equation	R^2	%E
ERas	-2.697x+42.129	0.99672	81.53
HRas	-3.0946x+48.056	0.98534	68.14
KRasA	-2.6449+43.885	0.99843	83.68
KRasB	-3.0387x+45.065	0.99659	69.76
NRas	-3.0288x+46.943	0.99582	70.05
POL2RE	-2.8045x+42.673	0.99448	77.43

Fig. A4.2 Plasmid standard curves used in qRT-PCR for mesoderm differentiation of mouse embryonic stem cells (ESCs). Graphs for standard curve equations and a summary table including coefficient of determination R^2 and calculated % efficiency (%E) used for data in Fig. 4.5 and 4.7.

A

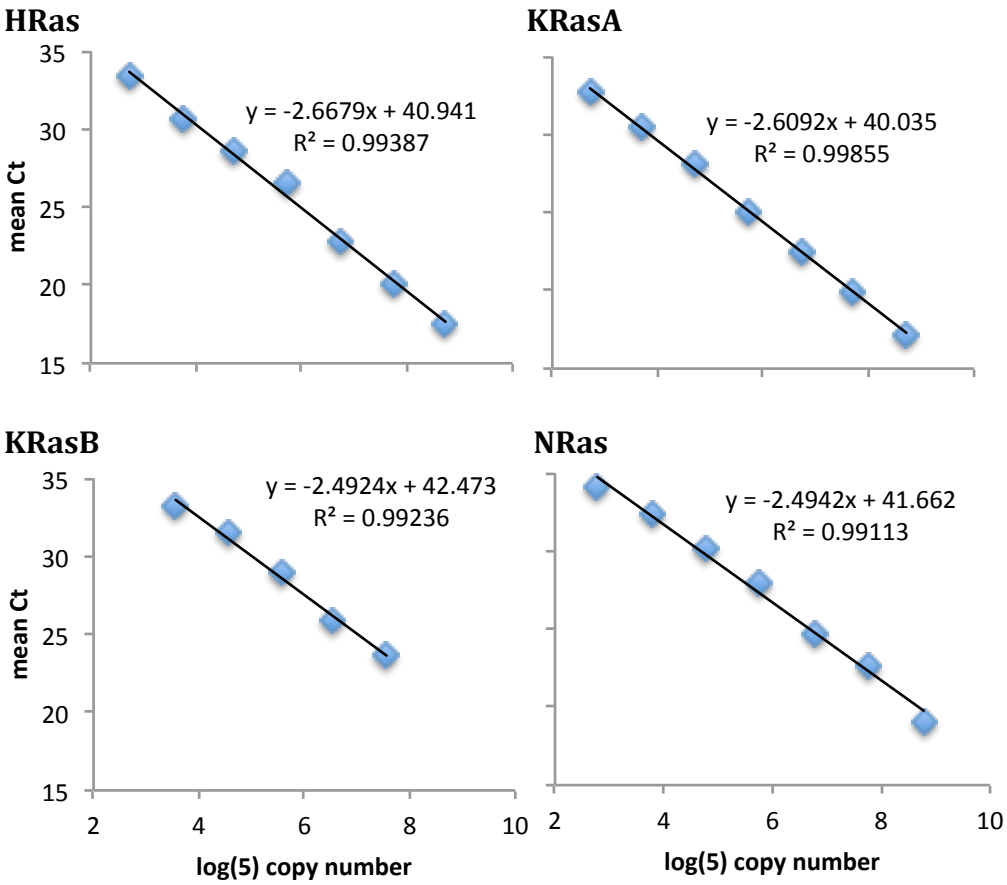

B

Ras isoform	Standard curve equation	R^2	%E
HRas	-2.6679x+40.941	0.99387	82.81
KRasA	-2.6092x+40.035	0.99855	85.30
KRasB	-2.4924x+42.473	0.99236	90.74
NRas	-2.4942+41.662	0.99113	90.65

Fig. A5.1 Ras isoform standard curves used for the qRT-PCR data from mouse tissues. Ras standard curves were based on isoform-specific plasmids in 5-fold serial dilutions for the calculation of transcript copy number. **A** Ras isoform standard curve graphs. **B** A summary table for Ras standard curve equations, the coefficient of determination R^2 and the calculated percentage efficiency %E of amplification. qRT-PCR conditions: 95˚C for 5 mins, 94˚C for 30 sec, 62˚C for 30 sec, 72˚C for 30 sec, 40 cycles.

Table A5.1 Ras isoform protein abundance in adult mouse tissues. Ras isoform ng protein per mg of total protein was estimated using standard-based mass spectrometry.

	Ras ng protein/mg total protein			
Mouse tissue	**HRas**	**KRasB**	**KRasA+NRas**	**panRas**
brain	424.00	263.55	83.07	770.61
lung	52.05	65.28	12.04	129.37
intestine	26.10	37.39	29.21	92.70
liver	13.79	0.00	58.64	72.43
pancreas	17.38	3.47	23.83	44.67